REPORT NO.
UC SESM 77-1

STRUCTURES AND MATERIALS RESEARCH
DEPARTMENT OF CIVIL ENGINEERING

NONLINEAR GEOMETRIC, MATERIAL AND TIME DEPENDENT ANALYSIS OF REINFORCED AND PRESTRESSED CONCRETE FRAMES

BY

Y. J. KANG

Report to
National Science Foundation
NSF Grant ENG 74-02658

JANUARY 1977

COLLEGE OF ENGINEERING
UNIVERSITY OF CALIFORNIA
BERKELEY CALIFORNIA

BIBLIOGRAPHIC DATA SHEET

1. Report No.

2.

3. Recipient's Accession No.

4. Title and Subtitle

Nonlinear Geometric, Material and Time Dependent Analysis of Reinforced and Prestressed Concrete Frames

5. Report Date

January 1977

6.

7. Author(s)

Young-Jin Kang

8. Performing Organization Rept. No. UC-SESM 77-1

9. Performing Organization Name and Address

Department of Civil Engineering
University of California
Berkeley, California 94720

10. Project/Task/Work Unit No.

11. Contract/Grant No.

ENG 74-02658

12. Sponsoring Organization Name and Address

National Science Foundation
Washington, D.C. 20550

13. Type of Report & Period Covered

Final Report

14.

15. Supplementary Notes

16. Abstracts An efficient numerical procedure for the material and geometric nonlinear analysis of planar reinforced and prestressed concrete frames including the time dependent effects due to load history, temperature history, creep, shrinkage and aging of concrete and relaxation of prestress is developed. The procedure, based on the finite element method, is capable of predicting the response of these structures throughout their service load history as well as throughout elastic, inelastic and ultimate load ranges.

In addition to reinforced concrete frames, pre-tensioned, post-tensioned bonded and unbonded concrete frames are analyzed distinguishing three distinct stages of loading; i.e., before, at and after the transfer of prestress.

A series of numerical examples are presented to study the validity and applicability of the present method. The results are compared with experimental results and the analytical results obtained by other investigators.

17. Key Words and Document Analysis. 17a. Descriptors

Structural engineering; Reinforced concrete; Prestressed concrete; Pre-tensioned; Post-tensioned; Nonlinear analysis; Material nonlinearities; Geometric nonlinearities; Creep; Shrinkage; Temperature; Load history; Cracking; Finite elements; Frames; Beams.

17b. Identifiers/Open-Ended Terms

17c. COSATI Field/Group

18. Availability Statement

Release Unlimited

19. Security Class (This Report) UNCLASSIFIED

20. Security Class (This Page) UNCLASSIFIED

21. No. of Pages 252

22. Price

Structures and Materials Research
Department of Civil Engineering
Division of Structural Engineering
and
Structural Mechanics

NONLINEAR GEOMETRIC, MATERIAL AND TIME DEPENDENT ANALYSIS OF REINFORCED AND PRESTRESSED CONCRETE FRAMES

by

Young-Jin Kang

Faculty Investigator: A. C. Scordelis

Prepared under the Sponsorship of
National Science Foundation
Grant ENG 74-02658

College of Engineering
Office of Research Services
University of California
Berkeley, California

January 1977

Nonlinear Geometric, Material and Time Dependent Analysis of Reinforced and Prestressed Concrete Frames

Doctor of Philosophy   Young-Jin Kang   Civil Engineering

Alex C. Scordelis
Chairman of Committee

ABSTRACT

An efficient numerical procedure for the material and geometric nonlinear analysis of planar reinforced and prestressed concrete frames including the time dependent effects due to load history, temperature history, creep, shrinkage and aging of concrete and relaxation of prestress is developed. The procedure is capable of predicting the response of these structures throughout their service load history as well as throughout elastic, inelastic and ultimate load ranges.

A step forward integration is performed by dividing the time domain into a discrete number of intervals for the quasi-static time dependent analysis. For each time interval nonlinear equilibrium equations which are valid for the current geometry and material properties are set up and solved by the finite element method based on the displacement formulation. An incremental load method combined with unbalanced load iterations for each load increment is used for the solution of the nonlinear equilibrium equations.

Time dependent variation of concrete properties is recognized. Concrete strain is assumed to consist of the

mechanical component and the non-mechanical component due to creep, shrinkage, aging and temperature variations. Parabolic-linear, bilinear and multilinear approximations of the stress-strain curves are utilized for concrete, reinforcing steel and prestressing steel, respectively. A simple model for the inelastic load reversal is incorporated.

Creep strain is evaluated by an efficient numerical procedure based on the age and temperature dependent integral formulation. In the procedure the history effect is incorporated by updating the values of only two variables instead of the storage of all the previous stress or strain histories. Nonlinear creep effect at high stress levels is also considered.

Varied material properties within a frame element is accounted for by the composite concrete and reinforcing steel layer system. Element properties are evaluated by a layer integration, and the contribution of prestressing steel is added directly.

Pre-tensioned, post-tensioned bonded and unbonded frames are analyzed distinguishing three distinct stages of loading ; i.e. before, at and after the transfer of prestress.

A series of numerical examples are presented to study the validity and applicability of the present method. The results are compared with experimental results and the analytical results obtained by other investigators.

ACKNOWLEDGEMENT

The author wishes to express his deepest appreciation and gratitude to Professor A.C. Scordelis for his constant guidance and encouragement throughout the course of this study. He would also like to thank Professors T.Y. Lin and A. Chorin for serving as members of his thesis committee. Various discussions with his colleague Dr. A.K. Kabir have been very helpful.

He also wishes to express his sincere appreciation to his wife Kyung Hee for her patience and support during the course of this work. She typed the entire manuscript of the thesis and drew part of the figures.

This research was sponsored by the National Science Foundation by Grant Eng 74-02658. The computer center at the University of California, Berkeley provided the facilities for the numerical work.

TABLE OF CONTENTS

Page

Page

1. INTRODUCTION

1.1 General Remarks

Reinforced and prestressed concrete structures are designed to satisfy the conditions of serviceability and safety. In order to ensure the serviceability requirements an accurate prediction of displacements, internal forces and deformations of the structure subjected to service loads throughout its service life is necessary. The service loads include not only the live load history the structure is subjected to, but also the loads imposed upon the structure due to environmental changes. To assess the safety of the structure against failure an accurate estimation of the ultimate load has to be made. And the prediction of the behavior of the structure throughout the elastic, inelastic and ultimate load ranges is desirable.

Analytical determination of the displacements, internal forces, stresses and deformations of reinforced and prestressed concrete structures throughout their load histories is complicated by a number of factors which include : nonhomogeneity of the material ; continuously changing topology of the structural system due to cracking of concrete under increasing load ; nonlinear stress-strain relationship of concrete, reinforcing and prestressing steels ; variation of concrete properties with time and the time dependent concrete deformations due to creep, shrinkage, load history and environmental changes ; difficulties in the analytical modelling of the dowel action of steel reinforcements, bond slip and aggregate interlock at cracks ; the effects of geometric nonlinearity on such structures as frames, plates and shells.

Due to the difficulties mentioned above engineers in the past have been relying heavily on empirical formulas derived from numerous experiments for the design of concrete structures. However, with the advent of digital computers and powerful modern numerical analysis methods such as the finite element method, numerous investigators in the past decade have been making efforts to develop analytical solutions which would hopefully obviate the needs for experiments. The present study is one of such continuing efforts, and concerns the analysis of reinforced and prestressed concrete planar frames.

1.2 Review of Previous Studies

In this section a brief review of previous studies on the application of the finite element method to reinforced concrete structures will be given. The theory and the application of the finite element method for the analysis of linear and nonlinear structures are treated comprehensively in the books by Zienkiewicz (1), Desai and Abel (2) and Gallagher (3).

Scordelis (4) presented a comprehensive review of the application of the finite element method for the analysis of reinforced concrete structures. He considered plane stress systems, plate bending systems, combined plane stress and plate bending systems, axisymmetric solid systems and general three dimensional solids for both short-time and long-time loadings. More recently, Schnobrich (5,6) and Wegner (7) presented similar surveys of the application of the finite element method for the study of reinforced concrete structures.

The earliest published application of the finite element method to reinforced concrete structures was by Ngo and Scordelis (8) at the University of California, Berkeley in 1967. Simple beams were analyzed in which concrete and steel reinforcements were represented by constant strain triangular elements, and special bond link elements were used to connect the steel to the concrete. A linear elastic analysis was performed on beams with predefined crack patterns to determine principal stresses in the concrete, stresses in the steel reinforcement and bond stresses. Ngo, Scordelis and Franklin (9) used the same approach to study shear in beams with diagonal tension cracks, considering the effects of stirrups, dowel shear, aggregate interlock and horizontal splitting along reinforcement near the support.

Nilson (10,11) introduced nonlinear material properties and a nonlinear bond-slip relationship into the analysis and used an incremental load method to account for these nonlinearities. He analyzed concentric and eccentric reinforced tensile members by using quadrilateral plane stress elements. Cracking was accounted for by stopping the solution when an element indicated a tensile failure and thence redefining a new cracked structure. Franklin (12) used an iterative procedure with incremental loading technique to trace the response of two-dimensional systems from initial loading to failure in one continuous computer analysis.

Plane stress elements were widely used by numerous investigators to study the behavior of reinforced concrete frame and wall systems. Zienkiewicz, et al (13,14) used an "initial stress" approach for two-dimensional stress studies including tensile cracking and elasto-plastic behavior in compression. Cervenka and Gerstle (15,16) analyzed shear walls and spandrel beams by using a similar approach and a constitutive relationship for the composite concrete-steel material properties. McCutcheon, Mirza, Mufti, et al (17,18) studied plane stress problems including cracking and bond failures. Plane stress problems have been also analyzed by other investigators (19,20,21,22,23,24) using similar approaches.

Reinforced concrete slabs were studied by Jofriet and McNiece (25) by using a bilinear moment-curvature relationship to account for progressive cracking. Bell and Elms (26, 27) used a similar approach to study slabs. Dotroppe et al (28) used a layered finite element procedure in which slab elements were divided into layers to account for the progressive cracking across the thickness of the slab. Berg, et al (29,30) used a similar approach and included geometric nonlinearity.

Lin (31,32) studied reinforced concrete shells utilizing layered triangular finite elements which take the coupling of the membrane action and the bending action into account. He included the tension stiffening effect of concrete due to steel reinforcements between cracks. Bell and Elms (33) analyzed shells by using reduced stiffness to account for the progressive cracking. Hand, et al (34) studied shells by using layered rectangular finite elements.

Use of three dimensional elements for reinforced concrete structures has been scarce due to the lack of knowledge regarding the behavior of concrete in general three-dimensional stress state. Suidan and Schnobrich (35) studied beams by using 20-node three-dimensional elements. Elastic-plastic concrete properties and the von Mises yield criterion were utilized. Sarne (37) analyzed prestressed concrete reactor vessels by using three-dimensional isoparametric elements. He included time dependent effects and material nonlinearity in his analysis.

Ngo (36) recently presented a method to predict the crack growth in concrete members by a network-topological approach. Bar elements, two-dimensional isoparametric elements, bond elements and link elements were used in his study.

Prestressed concrete reactor vessels were analyzed by Rashid (38,39) and Wahl and Kasiba (40) by utilizing axisymmetric elements. Further developments in the analysis of reactor vessels were presented by Zienkiewicz, et al (41), Argyris, et al (42) and Connor and Sarne (43).

The application of the finite element method for the analysis of concrete structures including the time dependent effects such as creep, shrinkage, load history and temperature has been made by a number of investigators. Selna (44, 45) analyzed planar reinforced concrete frames including cracking, creep and shrinkage by developing a time dependent constitutive relationship for concrete based on linear viscoelasticity. Aas-Jacobseh (46) studied slender reinforced concrete frames including creep and geometric nonlinearity. Aldstedt (47) analyzed reinforced concrete frames including the effects of bond slip, creep and geometric nonlinearity. Scanlon and Murray (48,49) studied the time dependent deflection of reinforced concrete slabs by utilizing Selna's (44,45) formulation of creep. Rashid (50) studied two-dimensional problems in concrete creep including the effects of temperature on creep. Sandhu, et al (51) analyzed plain concrete dams including the effects of creep and temperature.

1.3 Object and Scope of the Present Study

The object of the present study is to develop an efficient numerical procedure for the material and geometric nonlinear analysis of planar reinforced and prestressed concrete frames including the time dependent effects due to load history, temperature history, creep, shrinkage and aging of concrete and relaxation of prestress. An accurate prediction of the response of these structures throughout their service load history as well as throughtout elastic, inelastic and ultimate load ranges is aimed at.

A step forward integration is performed by dividing the time domain into a discrete number of intervals for the quasi-static time dependent analysis. For each time interval nonlinear equilibrium equations which are valid for the current geometry and material properties are set up and solved by the finite element method based on the displacement formulation. An incremental load method combined with the unbalanced load iteration for each load increment is used for the solution of the nonlinear equilibrium equations.

Concrete strain is assumed to consist of the mechanical component and the non-mechanical component due to creep, shrinkage, aging and temperature variations. Variation of the strength of concrete with time is recognized. Parabolic-linear, bilinear and multilinear approximations of the stress-strain curves are utilized for concrete, reinforcing steel and prestressing steel, respectively. A simple model for the inelastic load reversal is incorporated.

Creep strain is evaluated by an efficient numerical procedure based on the age and temperature dependent integral formulation. Nonlinear creep effect at high stress levels is also considered.

Varied material properties within a frame element is accounted for by the composite concrete and reinforcing steel layer system. Element properties are evaluated by a layer integration, and the contribution of prestressing steel is added directly.

Pre-tensioned, post-tensioned bonded and unbonded frames are analyzed distinguishing three distinct stages of loading ; i.e. before, at and after the transfer of prestress.

A series of numerical examples are presented to study the validity and applicability of the present method. The results are compared with experimental results and the analytical results obtained by other investigators.

2. MODELLING OF MATERIAL PROPERTIES

2.1 General Remarks

Reinforced and prestressed concrete structures consist of different materials, namely concrete, reinforcing steel and/or prestressing steel. Reinforcing and prestressing steels can be considered homogeneous materials, and their properties are generally well defined. On the other hand, concrete is a heterogeneous material consisting of cement mortar and aggregates. Mainly because of this heterogeneity the properties of concrete depend on many variables, and it is very difficult to define its properties accurately. However, concrete can be considered a homogeneous material in a macroscopic sense if we define its average properties on statistical grounds. For applications to civil engineering structures this assumption is generally accepted. Thus we can study the composite action of different homogeneous materials, concrete and steel.

Both concrete and steel exhibit various nonlinear material properties. The stress-strain relationship of concrete is not only nonlinear, but it differs in compression and tension. Tensile cracking is one of the most important factors which contribute to the nonlinear behavior of reinforced concrete structures. Furthermore, the properties of concrete are dependent on its age and environmental conditions such as temperature and ambient humidity. Reinforcing steel generally exhibits symmetrical nonlinear stress-strain relationships in tension and compression, and its properties are generally independent of time and environmental conditions encountered in most civil engineering applications. Prestressing steel is used exclusively in tension, and its stress-strain relationship is also nonlinear and the shape of its stress-strain curve is different from that of reinforcing steel.

Another nonlinear factor to be noted is the unloading and reloading characteristics of concrete and steel. Although the effects of dynamic loadings such as seismic load or wind load are not considered in this study, the effects of live load history and temperature history are considered in a static manner. Thus a simple mathematical model for unloading and reloading is developed to study the effects of load reversal.

The composite action of concrete and reinforcing steel in reinforced or prestressed concrete frames is studied utilizing a composite layer system. For this study it is assumed that perfect bond exists between concrete and reinforcing steel, then the displacement field within a reinforced concrete frame element can be considered continuous. The material properties of concrete and steel depend on the strain state of the material due to the effects of nonlinear stress-strain relationship, cracking, yielding and crushing of concrete and yielding of steel. In order to incorporate the varied material properties within a frame element in evaluating element properties such as element stiffness matrix or internal force vector, the element is divided into a discrete number of concrete and reinforcing steel layers. The integrations required to evaluate the element properties over the volume of the element is then performed layer by layer through the depth of the element. Each layer in a cross section is assumed to be in a state of uniaxial stress and the deformation due to shearing strain is neglected.

It is assumed that perfect bond also exists between concrete and prestressing steel in bonded prestressed concrete frames after the transfer of prestress as in pre-tensioned frames and post-tensioned bonded frames. Then the displacement field in an element of these frames can also be considered continuous. But the action of the prestressing steel is included in a different manner, as explained later in chapter 6, not using prestressing steel layers.
For post-tensioned unbonded frames in which the displacement field is not continuous within an element, an iterative method converging to the solution is utilized.

In subsequent sections important properties of three materials, namely concrete, reinforcing and prestressing steel, relevant to this study will be discussed briefly, but emphasis will be placed on mathematical modelling of their properties.

2.2 Concrete

2.2.1 Deformation of Concrete

One of the most important assumptions in studying the deformation of concrete is that the strain of concrete may be considered as being composed of strains caused by different phenomena. Davis (74,79,80) and Glanville (81) provided the experimental verification of this commonly accepted concept in their studies of creep and shrinkage of concrete. This concept is used by many investigators to study the behavior of concrete structures (4,44,47,52).

For the present investigation, total uniaxial concrete strain $\varepsilon(t)$ at any time t is assumed to be composed of the following contributions.

$$\varepsilon(t) = \varepsilon^m(t) + \varepsilon^{nm}(t) \quad (2.1)$$

$$\varepsilon^{nm}(t) = \varepsilon^c(t) + \varepsilon^s(t) + \varepsilon^a(t) + \varepsilon^t(t) \quad (2.2)$$

$\varepsilon^m(t)$ is the mechanical strain or instantaneous strain caused by a short-time loading, and is the independent variable in the following functional of the stress-strain relationship,

$$\sigma(t) = f(\varepsilon^m(t)) \quad (2.3)$$

where $\sigma(t)$ is the uniaxial concrete stress at time t. Non-mechanical strain $\varepsilon^{nm}(t)$ consists of creep strain $\varepsilon^c(t)$, shrinkage strain $\varepsilon^s(t)$, aging strain $\varepsilon^a(t)$ and thermal strain $\varepsilon^t(t)$. Among these strains, $\varepsilon^m(t)$, $\varepsilon^c(t)$, $\varepsilon^a(t)$ are stress produced strains, and $\varepsilon^s(t)$ and $\varepsilon^t(t)$ are non-stress produced strains.

The meaning of each of these strain components is illustrated in Fig. 2.1 (53) except for the thermal strain which is produced by temperature changes. Fig. 2.1.a shows shrinkage strain of an unloaded concrete specimen. Shrinkage of con-

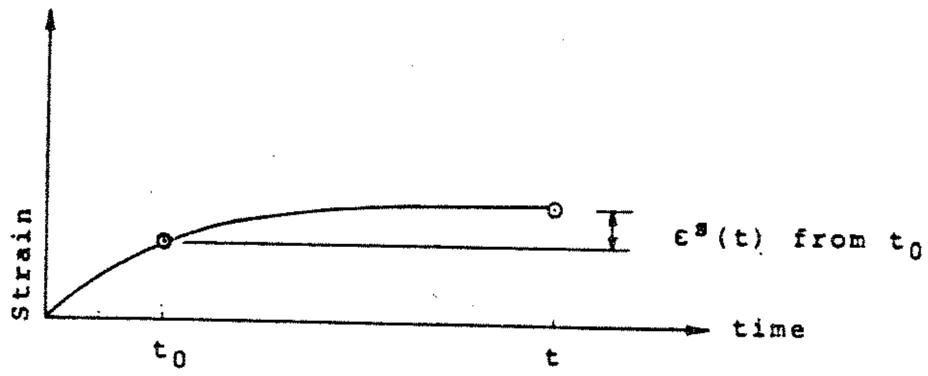

(a) Strain of an Unloaded Specimen

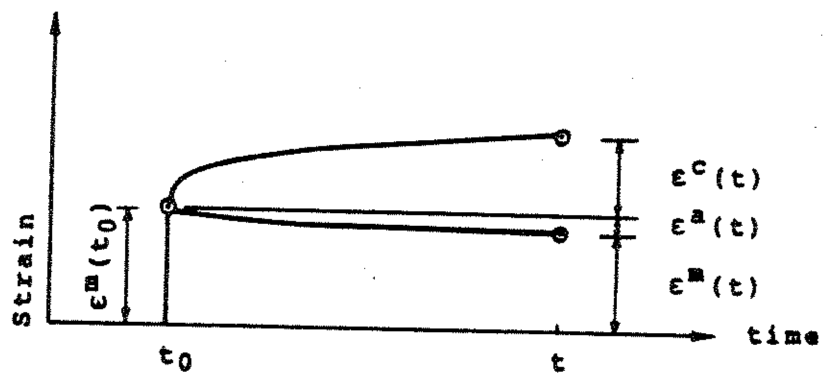

(b) Strain of a Loaded Specimen in Hygral Equilibrium with the Ambient Medium

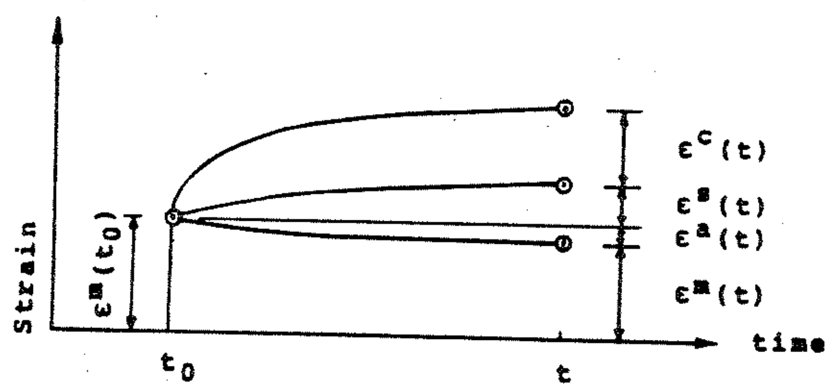

(c) Strain of a Loaded and Drying Specimen

Fig. 2.1. Definitions of Strain Components

crete is defined as the volume change which occurs independently of imposed stresses and of temperature changes. Fig. 2.1.b shows the strain history of a concrete specimen in hygral equilibrium with the ambient medium, subjected to sustained axial compression. We note that the strain at time t is increased by $\varepsilon^{c}(t)$ compared to the strain at time t_0. This increase in strain under a sustained stress, whether it is external or internal, is defined as creep. We also note that the mechanical strain at time t is smaller than that at time t_0. This is caused by the fact that the strength and modulus of concrete increase as time elapses. This phenomenon is called the aging of concrete, and the decrease in the mechanical strain due to the aging of concrete is called aging strain. Fig. 2.1.c shows the strain history of a loaded and drying specimen in which all the strain components except thermal strain are present.

In this study, for the time dependent analysis, the time domain is divided into a discrete number of intervals each of which may not be of the same length in time. The junctions of these intervals are called time steps. Thus we have a finite number of time steps t_n ; $n = 1,2,\cdots,N$, where N is the total number of time steps considered in the analysis. Then a step forward integration is performed by adding the results obtained for each time step successively, starting from the first time step, to arrive at the final solution. The calculation of concrete strains and stresses at a typical time step, t_n is performed as followes.

(1) Total strain ε_n at time step t_n is obtained by adding the increment of total strain $\Delta\varepsilon_n$ occurring during time interval t_{n-1} to t_n, to the total strain ε_{n-1} at time step t_{n-1}.

$$\varepsilon_n = \varepsilon_{n-1} + \Delta\varepsilon_n \tag{2.4}$$

(2) The increment of non-mechanical strain $\Delta\varepsilon_n^{nm}$ occurring between time steps t_{n-1} and t_n is obtained by adding contributions due to creep, shrinkage, aging and temperature changes.

$$\Delta\varepsilon_n^{nm} = \Delta\varepsilon_n^{c} + \Delta\varepsilon_n^{s} + \Delta\varepsilon_n^{a} + \Delta\varepsilon_n^{t} \tag{2.5}$$

(3) Non-mechanical strain ε_n^{nm} at time step t_n is then obtained by adding the increment $\Delta\varepsilon_n^{nm}$ to the previous total.

$$\varepsilon_n^{nm} = \varepsilon_{n-1}^{nm} + \Delta\varepsilon_n^{nm} \tag{2.6}$$

(4) Mechanical strain ε_n^{m} at time step t_n is obtained by subtracting non-mechanical strain ε_n^{nm} from total strain ε_n.

$$\varepsilon_n^{m} = \varepsilon_n - \varepsilon_n^{nm} \tag{2.7}$$

(5) Stress σ_n at time step t_n is then obtained from the stress-strain relationship valid at time step t_n.

$$\sigma_n = f_n(\varepsilon_n^{m}) \tag{2.8}$$

2.2.2 Short-Time Deformation and the Stress-Strain Relationship

Response of a structure under load depends to a large degree on the stress-strain relationship of the material from which it is made, and the type of stress to which the material is subjected. Concrete is used mostly in compression, so that its compressive stress-strain curve is of primary interest. Such a curve can be obtained by cylinder tests or appropriate strain measurements on the compression side in beams. Fig. 2.2.a shows two such curves, obtained at moderate testing speeds on an axially loaded concrete cylinder having two different compressive strengths (53).

The curves consist of an initial relatively straight elastic portion in which stress and strain are closely proportional, followed by a curve with a decreasing slope, reaching zero slope and maximum stress σ_{max} at a strain ε_0 which has the value of approximately 0.002 in. per in., and finally show a descending branch, reaching the maximum strain ε_{max}. The initial linearly elastic part extends to about 30 percent of the maximum stress. The initial slope of the curve is called the initial modulus of concrete.

The shape of the compressive stress-strain curve of concrete is largely determined by its compressive strength. We note in Fig. 2.2.a that the initial modulus of concrete having higher strength is larger than that of concrete having lower strength. It is also seen that concrete of lower strength is less brittle, i.e. fracture occurs at a larger maximum strain, than for high-strength concrete. The shape of the curve is also affected by the rate of application of stress, as shown in Fig. 2.2.b (54).

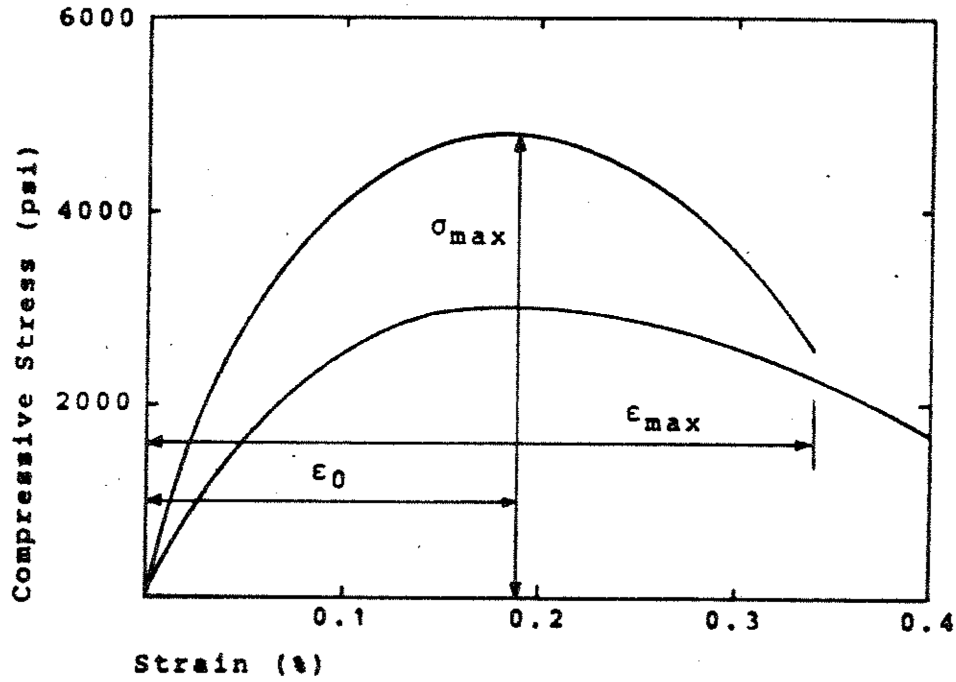

(a) Typical Compressive Stress-Strain Curve of Concrete (53)

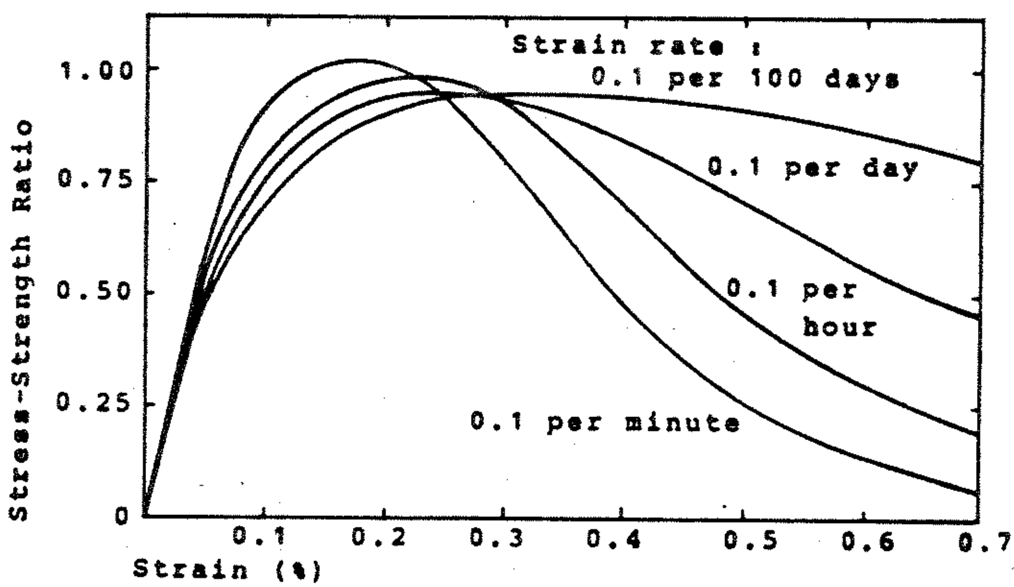

(b) Influence of the Rate of Application of Strain on the Shape of the Stress-Strain Curve (54)

Fig. 2.2. Compressive Stress-Strain Curve of Concrete

The compressive strength of concrete is usually defined as the maximum average stress obtained from the testing of concrete specimens such as cylinders, cubes and prisms, subjected to uniaxial compression. The compressive strength of a 6 x 12 in. cylinder, denoted by f'_c, is most commonly used in the United States. The compressive strength of concrete is influenced by many factors, among which water-cement ratio, size of aggragate and gain of strength with time are often mentioned. The increase in the strength of concrete with time is well known, but it is not often fully taken into consideration in design practice. A typical compressive strength-time curve is shown in Fig. 2.3 (55), in which considerable gain in strength can be noted. Since the stress-strain relationship of concrete is largely determined by the magnitude of its compressive strength, it is essential to consider this variation in strength with time in order to analyze concrete structures for long-time loading more accurately.

ACI Committee 209 (56) recommends the following form of equation for predicting compressive strength at any time.

$$(f'_c)_t = \frac{t}{a+bt}(f'_c)_{28d} \qquad (2.9)$$

where, $(f'_c)_{28d}$ is 28-day strength, t is time in days after casting of concrete, and a and b are constants. The values of a and b depend on the type of cement and curing method used for the particular concrete. Following approximate average values determined from some 88 test specimens are

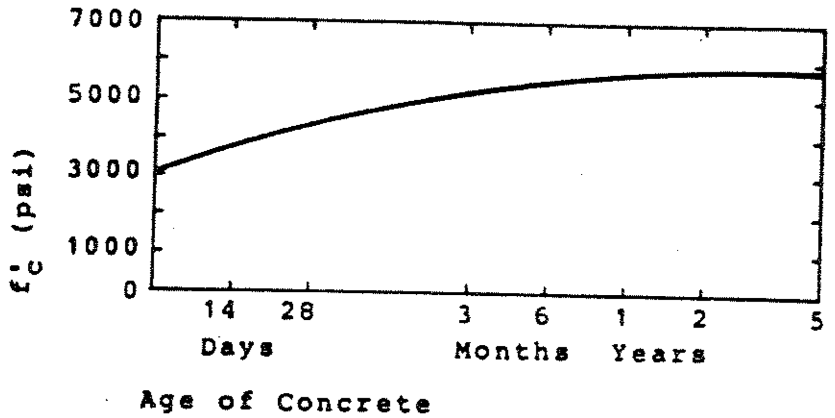

Fig. 2.3. Effect of Age on Compressive Strength (55)

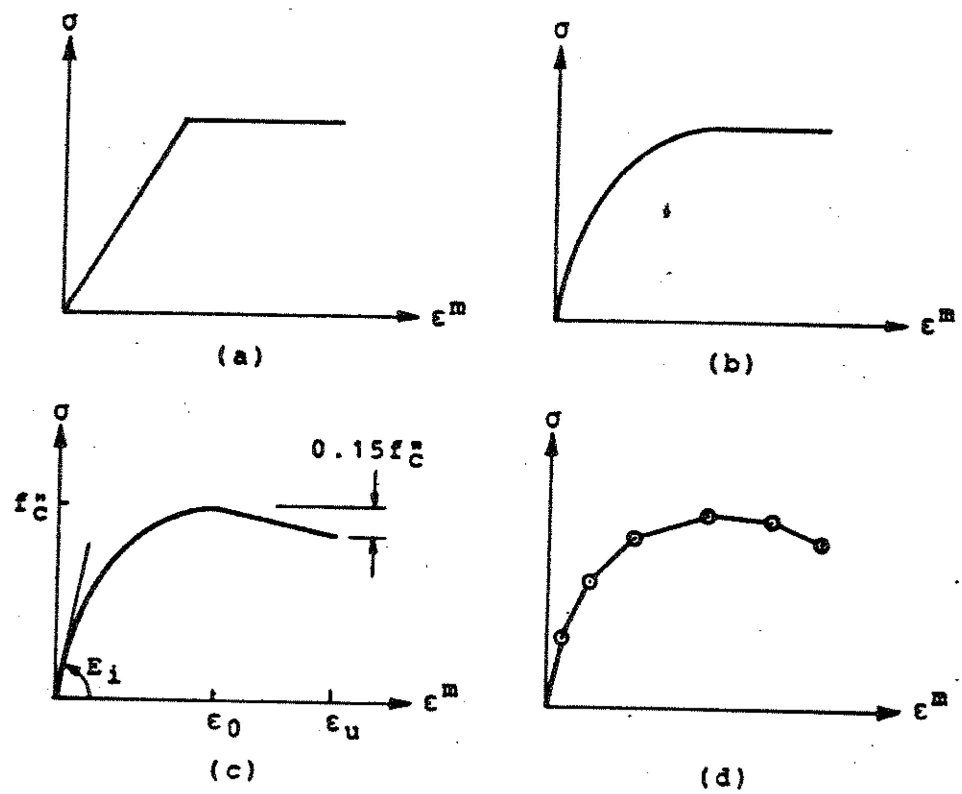

Fig. 2.4. Idealizations of Stress-Strain Curve

recommended.

Moist cured concrete, type I cement : a=4.00, b=0.85

Moist cured concrete, type III cement : a=2.30, b=0.92

Steam cured concrete, type I cement : a=1.00, b=0.95

Steam cured concrete, type III cement : a=0.70, b=0.98

As a basis for the analysis of concrete structures, a mathematical formula for the stress-strain relationship of concrete is a convenient and necessary tool. Many empirical formulas developed are summarized by Popovics (58). Some of the frequently utilized mathematical idealizations are shown in Fig. 2.4.

Fig. 2.4.a shows a linearly elastic-perfectly plastic model. This is the simplest of nonlinear models. This model was used by Lin (31) in his study of reinforced concrete slabs and shells.

Fig. 2.4.b shows an inelastic-perfectly plastic model proposed by the European Concrete Committee (59), consisting of a parabola and a horizontal line.

Fig. 2.4.d shows a piecewise linear model in which the curve is approximated by a series of straight line segments. Franklin (12) and Aldstedt (47) used this model in their studies of reinforced concrete frames. Although this is the most versatile model capable of representing wide variety of stress-strain curves, the use of this model is restricted to the special cases in which the experimental data for the particular concrete used is available.

A model which represents the stress-strain curve of wide variety of concretes in a mathematical formula was suggested by Hognestad (60), and is shown in Fig. 2.4.c. For the present investigation this model is utilized with minor modifications. This model has been widely used by many investigators ; Kroenke, et al (61) in their study of slender concrete columns, Wilhelm, et al (52) and Aroni (63,64) in their studies of prestressed concrete columns, to name a few.

The ascending part of the curve is described by the equation,

$$\sigma = f''_c \frac{\varepsilon^m}{\varepsilon_0}\left(2 - \frac{\varepsilon^m}{\varepsilon_0}\right) \qquad (2.10)$$

in which the strain ε_0 corresponding to the maximum compressive stress f''_c is given by

$$\varepsilon_0 = \frac{2f''_c}{E_i} \qquad (2.11)$$

where E_i is the initial tangent modulus. By differentiating Eq.(2.10), the tangent modulus, E_t is obtained.

$$E_t = \frac{d\sigma}{d\varepsilon^m} = E_i\left(1 - \frac{\varepsilon^m}{\varepsilon_0}\right) \qquad (2.12)$$

Observing the three equations given above, we note that : the ascending branch of the stress-strain curve is a parabola ; the initial tangent modulus E_i has twice the magnitude of the secant modulus at the peak point ; the tangent modulus E_t varies linearly from the origin where it has the maximum value E_i to the peak point where the value reduces to zero.

The descending part of the compressive stress-strain curve is a straight line. In this study, the tangent modulus of this part is assumed to be zero. But the decrease in stress with the increase in the mechanical strain is accounted for as unloading. The equation of this part can be written,

$$\sigma = -0.15 f_c'' \frac{\varepsilon^m - \varepsilon_0}{\varepsilon_u - \varepsilon_0} + f_c'' \; ; \; E_t = 0. \quad (2.13)$$

Maximum compressive stress, f_c'' is given by a fraction of the compressive strength f_c' in this study as follows.

$$f_c'' = r_c \; f_c' \quad (2.14)$$

Hognestad suggested to use $r_c = 0.85$ for prismatic members based on numerous tests of concentrically loaded columns, but many investigators also use $r_c = 1$. For this study r_c is considered an input parameter for a particular problem, decided by the analyzer.

There are numerous empirical formulas for the evaluation of the initial tangent modulus, E_i. They are summarized by Aldstedt (47). ACI Committee 209 (56) recommends the following formula,

$$E_i = 33 w^{1.5} \sqrt{f_c'} \text{ psi} \quad (2.15)$$

where f_c' the compressive strength in psi, and w is the unit weight of the concrete in pcf.

Tensile strength of concrete has the magnitude of about

10 percent of the compressive strength (65). It is usually measured in the flexure test of a plain concrete beam. The computed flexural tensile stress at which the test beam would fracture is called the modulus of rupture. The tensile strength is also measured by applying pure tensile axial force to a specimen or by a split-cylinder test. For this study, the maximum tensile stress in the stress-strain curve of concrete is assumed to have the value of the modulus of rupture, and will be denoted by f_t'. ACI Committee 209 (56) recommends the following value.

$$f_t' = r_t \sqrt{w f_c'} \text{ psi} \qquad (2.16)$$

where f_c' is the compressive strength in psi, w is the unit weight in pcf, parameter r_t has the value of 0.6 to 1.0.

The slope of the tensile stress-strain curve is assumed to be constant, and the same as the initial tangent modulus E_i. Then the tensile stress-strain relationship can be written as follows.

$$\sigma = E_i \, \varepsilon^m \; ; \; E_t = E_i \qquad (2.17)$$

Tension stiffening of concrete after cracking due to reinforcing steel is neglected in this study. The effect of tension stiffening was incorporated by Scanlon (48) and Lin (31) in their studies of reinforced concrete slabs and shells.

2.2.3 Long-Time Deformation - Creep, Shrinkage and Aging

Concrete is unique among structural materials in that its deformations and properties are time dependent under practical conditions of service. Thus it is important to incorporate the time dependent effects of creep, shrinkage and aging in the study of concrete structures throughout their service lives.

Creep is defined as the increase in strain under a sustained stress, whether the stress is produced by external loading or any other cause such as temperature changes. The nature of creep is illustrated in Fig. 2.5 (53). After the application of the load the strain increases with time due to creep at a decreasing rate. At 120 days after sustained load the strain becomes more than twice the strain on loading. When the sustained load is removed the strain decreases immediately by an amount equal to the instantaneous strain at that age, which is smaller than the instantaneous strain at the initial loading. This instantaneous recovery is followed by a gradual decrease in strain, called creep recovery. The shape of the creep recovery curve is similar to that of the creep curve, but the recovery reaches its maximum value more rapidly.

The mechanism of creep is still not completely understood. And there are many theories attempting to explain it, for example, mechanical deformation theory (66), plastic theory (67), viscous flow theory (68), and seepage of gel water theory (69).

There are many factors influencing creep of concrete. Some of the important factors are discussed below.

(1) Age at loading

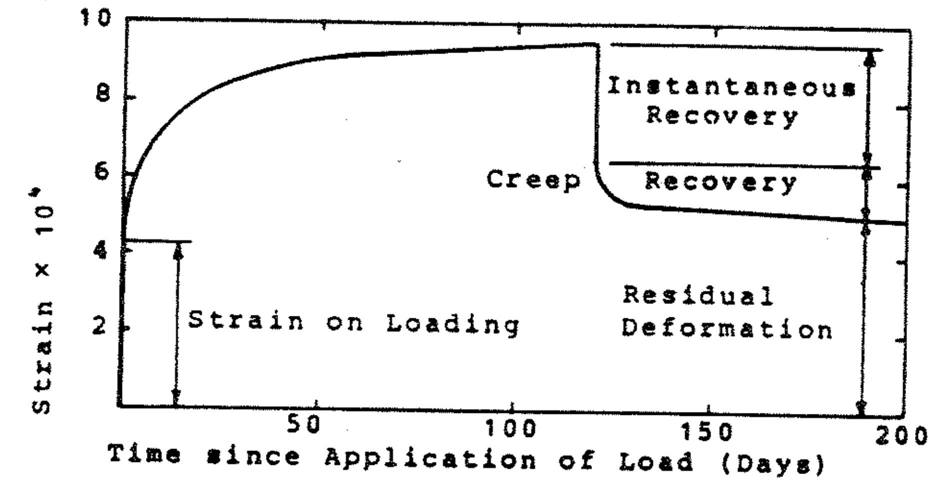

Fig. 2.5. Creep and Creep Recovery of a Mortar Specimen Stored in Air at a Relative Humidity of 95%, Subjected to a Compressive Stress of 2150 psi And Then Unloaded. (53)

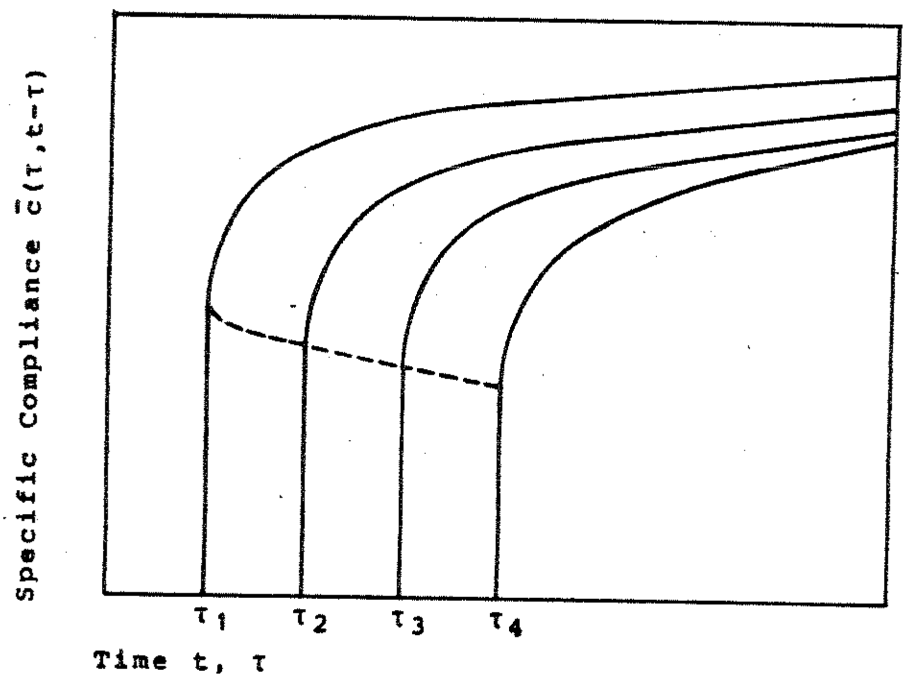

Fig. 2.6. Specific Compliance Curves for Different Loading Ages

In Fig. 2.6 typical specific compliance curves for different ages at loading are shown. Specific compliance is defined as the total stress-produced strain, instantaneous and creep, due to a unit sustained stress. We note first that the creep strain of the specimen loaded at later age is generally smaller than that of the specimen loaded at earlier ages after the same time interval following initial loading. We also note that the instantaneous strain of the specimen loaded at a later age is smaller due to the increase in the modulus of elasticity with time. This decrease in creep strain and instantaneous strain with increasing age at loading can be attributed to the degree of hydration and the development of strength of concrete.

(2) Intensity of stress

Creep is proportional to the applied stress within the range of working stress. At higher stress-strength ratios, about 0.4 to 0.6, creep increases at an increasing rate. Above a stress-strength ratio of 0.8 to 0.9, creep produces failure in time. This dependency of creep on the intensity of stress is shown in Fig. 2.7 (54). Manuel and McGregor (70) developed an empirical formula evaluating creep as a function of time and stress-strength ratio based on Rüsch's study. To account for this nonlinear creep effect in the linear creep formulation used in the present study, which is based on the assumption that creep strain is proportional to stress intensity, the effective stress concept explained in chapter 3 is used.

(3) Aggregate content

Maximum size of the aggregate, its grading and shape influence the aggregate content, and consequently influence creep by the restraining effect of the aggregate on the free creep of cement paste. Generally creep decreases with the increase of the volume and the modulus of elasticity of the aggregate (74).

(4) Compressive strength

For a constant cement paste content and the same applied stress, creep is generally inversely proportional to the strength of concrete (53). Gain of strength with time also causes the decrease in creep as shown in Fig. 2.6.

(5) Size of the member

Creep decreases with an increase in the size of the specimen, but when the specimen thickness exceeds about 3 ft, no furthur effect is apparent. It is also noted that beyond several weeks after the application of the load, the rate of creep is the same regardless of the size of the specimen (75).

(6) Ambient humidity

Creep generally decreases with an increase in the ambient relative humidity. But creep is not affected by the relative humidity if concrete has reached hygral equilibrium prior to loading.

(7) Temperature

Creep generally increases proportionally to temperature ranging from 0 deg. F to 180 deg. F (76,77). But beyond 180 deg. F the rate of creep decreases up to about 300 deg.

F, and then increases again up to 500 deg. F (78).

Prediction of creep is a difficult task because of various factors influencing creep, and any formula attempting to predict the creep of concrete is bound to be approximate. Based on hundreds of experiments by many investigators, ACI Committee 209 (56) suggests following form of equation for the prediction of creep.

$$C_{t-\tau} = \frac{(t-\tau)^{0.6}}{10 + (t-\tau)^{0.6}} C_u \qquad (2.18)$$

where, $C_{t-\tau}$ is the creep coefficient defined as the ratio of creep strain at $(t-\tau)$ days after loading to initial strain at loading ; C_u is the ultimate creep coefficient defined as the ratio of creep strain at infinite time after loading to initial strain at loading ; t is the current observation time from the casting of concrete measured in days ; and τ is the age of concrete in days at loading. The ultimate creep coefficient C_u is computed as follows.

$$C_u = 2.35\, K_\tau^c\, K_H^c\, K_T^c\, K_S^c\, K_F^c\, K_A^c \qquad (2.19)$$

where K_τ^c, K_H^c, K_T^c, K_S^c, K_F^c and K_A^c are creep correction factors due to loading age, humidity, minimum thickness of member, slump, percent fines and air content respectively. All of these creep correction factors have the value of unity, i.e. $C_u = 2.35$, for the following standard conditions ; 4 in. or less slump, 40 percent ambient relative humidity, minimum thickness of member 6 in. or less, loading age 7 days for moist cured concrete and 1-3 days for steam cured concrete. For conditions which differ from the standard conditions, the following creep correction factors are used.

$$K_\tau^c = 1.25\tau^{-0.118} \quad \text{for moist cured concrete} \qquad (2.20)$$

$$= 1.13\tau^{-0.095} \quad \text{for steam cured concrete}$$

$$K_H^c = 1.27 - 0.0067H, \quad H \geq 40\%$$

$$K_T^c = 1.14 - 0.023T \quad \text{for} \leq 1 \text{ yr loading}$$

$$= 1.10 - 0.017T \quad \text{for ultimate value}$$

$$K_S^c = 0.82 + 0.067S$$

$$K_F^c = 0.88 + 0.0024F$$

$$K_A^c = 1.00 \quad \text{for } A \leq 6\%$$

$$= 0.46 + 0.090A \quad \text{for } A > 6\%$$

where τ is the loading age in days, H is the ambient relative humidity in percent, T is the minimum thickness in inches, S is the slump in inches, F is the percent of fine aggregate by weight, and A is the air content in percent.

Shrinkage of concrete is defined as non-stress and non-thermal produced time dependent volume change. As can be seen in Fig. 2.1.a, shrinkage reaches its maximum value asymptotically with time similarly to creep. Shrinkage of concrete is generally considered to arise from loss of water on drying and volume changes on carbonation. Shrinkage generally increases with the increase of water-cement ratio, and decreases with the increase of aggregate volume, size of the member and ambient relative humidity.

It is preferable to have experimental shrinkage strain-time curves for the time dependent analysis of concrete structures. But in most cases such experimental data are not available, so that a mathematical formula for predicting shrinkage has to be used. ACI Committee 209 (56) suggests the use of the following equation for the prediction of shrinkage.

$$\varepsilon^s_{t-t_0} = \frac{(t-t_0)}{f + (t-t_0)} \varepsilon^s_u \quad (2.21)$$

where, $\varepsilon^s_{t-t_0}$ is the shrinkage strain after $(t-t_0)$ days from the completion of curing, ε^s_u is the ultimate shrinkage strain after infinite time, t is time in days after casting of concrete, t_0 is the age of concrete in days at the completion of curing, and f is a constant depending on the type of curing. The following values of f and t_0 are recommended by the Committee.

$f = 35$; $t_0 = 7$ for moist cured concrete (2.22)

$f = 55$; $t_0 = 1\text{-}3$ for steam cured concrete

The ultimate shrinkage coefficient ε^s_u is computed as follows.

$$\varepsilon^s_u = 800 \times 10^{-6} K^s_H K^s_T K^s_S K^s_B K^s_F K^s_A \quad (2.23)$$

for moist cured concrete

$$\varepsilon^s_u = 730 \times 10^{-6} K^s_H K^s_T K^s_S K^s_B K^s_F K^s_A$$

for steam cured concrete

where K^s_H, K^s_T, K^s_S, K^s_B, K^s_F and K^s_A are shrinkage correction factors due to humidity, minimum thickness of member, slump, cement content, percent fines and air content respectively. All of these shrinkage correction factors have the value of unity for the following standard conditions ; 4 in. or less slump, 40 percent ambient relative humidity, minimum thickness of member 6 in. or less. For conditions which differ from the standard conditions, the following shrinkage correction factors are used.

$$
\begin{aligned}
K_H^s &= 1.40 - 0.010H, \quad 40\% \leq H \leq 80\% \\
&= 3.00 - 0.030H, \quad 80\% \leq H \leq 100\% \\
K_T^s &= 1.23 - 0.038T, \quad \text{for} \leq 1 \text{ yr loading} \\
&= 1.17 - 0.029T, \quad \text{for ultimate value} \\
K_S^s &= 0.89 + 0.041S \\
K_B^s &= 0.75 + 0.034B \\
K_F^s &= 0.30 + 0.0140F \quad \text{for } F \leq 50\% \\
&= 0.90 + 0.0020F \quad \text{for } F \geq 50\% \\
K_A^s &= 0.95 + 0.0080A
\end{aligned}
\tag{2.24}
$$

where H is the ambient relative humidity in percent, T is the minimum thickness in inches, S is the slump in inches, B is the number of 94-lb sacks of cement per cu yd. of concrete, F is the percent of fine aggregate by weight, and A is the air content in percent.

Aging strain of concrete can be defined as the decrease in the mechanical strain with time due to the aging of concrete. If a concrete prism is subjected to a constant sustained stress at time t_0, the strain at some time t after loading would be the same as the strain at t_0 if we exclude creep and shrinkage strains, as shown in Fig. 2.1.c. But, due to the increase in the modulus of concrete with time, the mechanical strain at time t corresponding to the constant stress would be reduced. Thus we can consider the aging strain as a correction factor for the calculation of the current stress as a function of the current mechanical strain at any time, rather than actual physical straining.

The increment of aging strain $\Delta\varepsilon_n^a$ occurring between time steps t_{n-1} and t_n, assuming that the stress remains constant at σ_{n-1}, can be calculated as follows.

$$\Delta\varepsilon_n^a = g_{n-1}(\sigma_{n-1}) - g_n(\sigma_{n-1}) \qquad (2.25)$$

where, g is a time dependent function for computing mechanical strain in terms of stress, i.e. an inverse function of f defined in Eq. (2.3), and subscripts (n-1) and n represent time steps. Explicitly, function g can be expressed as follows.

$$\varepsilon^m = \sigma/E_i \text{ in tension} \qquad (2.26)$$

$$\varepsilon^m = \varepsilon_0(1 - \sqrt{1-\sigma/f_c''}) \text{ in compression} \qquad (2.27)$$

where, currently valid values of time dependent variables E_i, ε_0 and f_c'' have to be used.

2.2.4 Deformation Due to Temperature Changes

Concrete structures are subjected to temperature changes during their service lives not only due to changes in environmental conditions, but also due to artificial heating or cooling. Stresses induced by temperature changes in statically indeterminate concrete structures are often substantial and damaging to the structures. Therefore the effect of temperature changes has to be incorporated in the analysis.

Uniaxial thermal strain, ε^t may be expressed as follows.

$$\varepsilon^t = \int_{T_0}^{T} \alpha(T)\,dT \qquad (2.28)$$

where T_0 is reference temperature, T is current temperature, and $\alpha(T)$ is the coefficient of thermal expansion which may be temperature dependent. But below 600 deg. F, the coefficient of thermal expansion of concrete is almost constant (82), and the magnitude depends on the composition of the concrete mix and its hygral state at the time of the temperature change. For this study α is assumed to be constant at all temperature levels. Then Eq. (2.28) can be rewritten as follows.

$$\varepsilon^t = \alpha(T-T_0) = \alpha\,\Delta T \qquad (2.29)$$

Creep strain of concrete is influenced by temperature, as discussed previously. The effect is taken into account in the present investigation, and will be discussed in detail in chapter 3.

2.2.5 Load Reversal and Complete Stress-Strain Curve

The effects of dynamic cyclic loading such as seismic load or wind load are not considered in this study. But unloading and reloading due to live load history and temperature history are accounted for by a simple load reversal model of the stress-strain curve. Even under a constant sustained load unloading could take place in reinforced concrete frames due to creep and shrinkage of concrete.

The load reversal model utilized in this study is shown in Fig. 2.8. Blakeley and Park (83) utilized a similar model for their study of prestressed concrete sections with cyclic flexure. The following assumptions are made in this model.

(1) The slope of the load reversal path in the stress-strain curve is the same as the initial tangent modulus E_i.

(2) Tensile failure or cracking of concrete occurs when the tensile stress exceeds its maximum tensile stress f'_t.

(3) Compressive failure of crushing of concrete occurs when the compressive mechanical strain exceeds its maximum compressive strain ε_u.

(4) Once concrete is cracked, it cannot take any tensile stress again. But it can take compressive stress upon closing of the crack and reloading. Thus the crack is assumed to close in compression and reopen in tension without any resistance.

In the computer program developed for this study the concrete material state is classified into 11 different states, as shown in Fig. 2.8, for the purpose of tracing primary loading, unloading and reloading paths in the stress-strain curve and evaluating the stress and the tangent modulus E_t. In the following description of the 11 different concrete material states, concrete is defined as yielded when its compressive mechanical strain exceeds ε_0, the strain corresponding to the maximum compressive stress, f''_c.

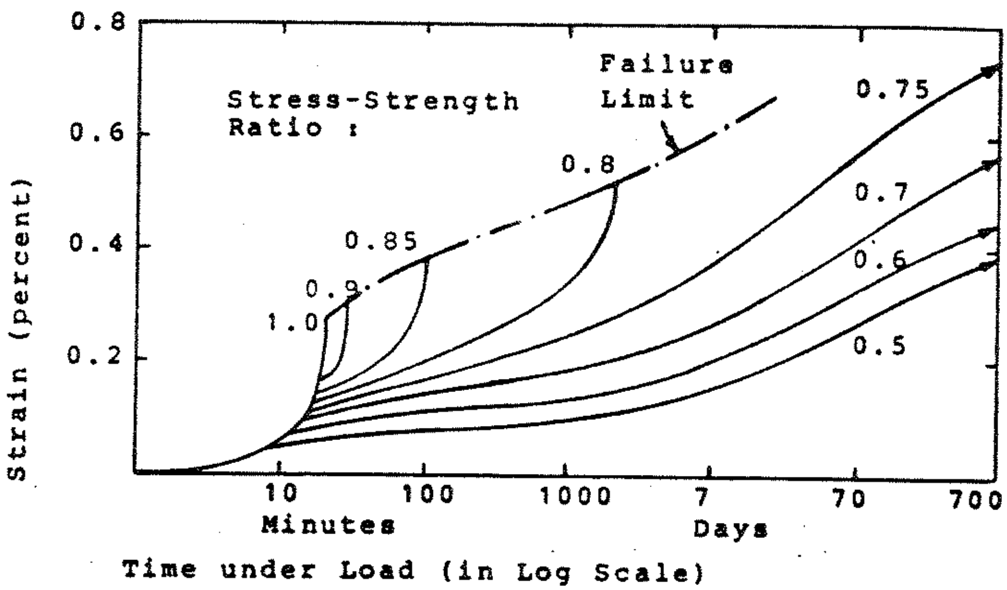

Fig. 2.7. The Strain-Time Relation for Different Stress-Strength Ratios (54)

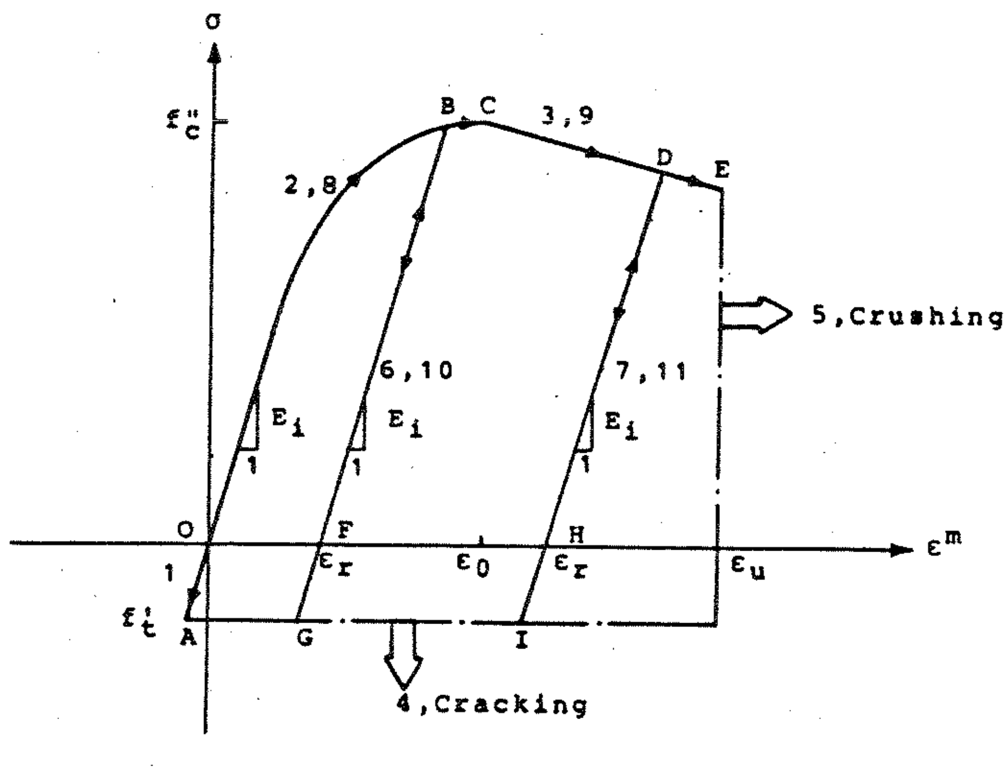

Fig. 2.8. Stress-Strain Curve of Concrete Assumed in the Present Study (Numbers Represent the Material State of Concrete)

(1) In primary tension (path OA or AO)

(2) In compression, not yielded (path OC)

(3) In compression, yielded (path CE)

(4) Cracked (beyond points A, G, I)

(5) Crushed (beyond point E)

(6) In load reversal path from state 2 (path BG or GB)

(7) In load reversal path from state 3 (path DI or ID)

(8) In compression, not yielded and once cracked (path OC or BC)

(9) In compression, yielded and once cracked (path CE or DE)

(10) In load reversal path from state 2 and once cracked (path BF or FB)

(11) In load reversal path from state 3 and once cracked (path DH or HD)

The complete stress-strain relationship of concrete used in this study can now be summarized in the following Eqs.

For state 1,

$$\sigma = E_i \varepsilon^m \; ; \; E_t = E_i \qquad (2.30)$$

For states 2 and 8,

$$\sigma = f_c'' \frac{\varepsilon^m}{\varepsilon_0}\left(2 - \frac{\varepsilon^m}{\varepsilon_0}\right) \; ; \; E_t = E_i\left(1 - \frac{\varepsilon^m}{\varepsilon_0}\right) \qquad (2.31)$$

For states 3 and 9,

$$\sigma = -0.15 f_c'' \frac{\varepsilon^m - \varepsilon_0}{\varepsilon_u - \varepsilon_0} + f_c'' \; ; \; E_t = 0. \qquad (2.32)$$

For states 6, 7, 10 and 11,

$$\sigma = E_i(\varepsilon^m - \varepsilon_r) \ ; \ E_t = E_i \qquad (2.33)$$

where ε_r is the residnal strain due to unloading as shown by points F and H in Fig. 2.8.

2.2.6 Specification of Time Dependent Concrete Properties

In the computer program developed for this study, time dependent properties of concrete are specified in the following ways. Complete input instruction for the program is provided in the Appendix.

In order to determine the stress-strain relationship at any time after casting of concrete two options are provided for the specification of necessary parameters.

When experimental data for the time dependent properties of the particular concrete used in the structure to be analyzed are available, four parameters, i.e. maximum compressive stress f_c'', initial tangent modulus, E_i, maximum tensile stress, f_t' and ultimate compressive strain, ε_u are specified at each time step. Strain corresponding to f_c'', ε_0 is computed by Eq. (2.11).

When experimental data are not available, seven parameters which do not vary with time, i.e. 28 day compressive strength $(f_c')_{28d}$, unit weight w, ultimate compressive strain ε_u, and coefficients a, b, r_c and r_t are specified. Then the following parameters are computed within the program recommended by ACI Committee 209.

(1) Compressive strength $(f_c')_t$ is computed by Eq. (2.9).

(2) Maximum compressive stress f_c'' is computed by Eq. (2.14).

(3) Maximum tensile stress f_t' is computed by Eq. (2.16).

(4) Initial tangent modulus E_i is computed by Eq. (2.15).

(5) Compressive strain corresponding to f_c'', ε_0 is computed by Eq. (2.11).

Once the values of f_c'', f_t', E_i, ε_0 and ε_u at any time step are determined, the stress-strain relationship at that time step is defined by Eq. (2.30) to (2.33).

Shrinkage strain and temperature histories are specified in a similar manner. Increments of shrinkage strain and temperature are specified at each time step. Both uniform distribution over the whole structure and nonuniform distribution through the depth of each frame element can be specified. Either experimental data for the particular concrete used or ACI Eqs. (2.21) to (2.24) may be used for the shrinkage strain history.

Specification of concrete creep properties will be discussed in chapter 3.

2.3 Reinforcing Steel

The properties of reinforcing steel, unlike concrete, generally are not dependent on environmental conditions or time. Thus specification of its stress-strain relationship is sufficient to define its properties relevant in the analysis of reinforced concrete structures. In this study a bilinear model which is symmetrical about origin, as shown in

Fig. 2.9, is used. The only non-mechanical strain considered is thermal strain ε^t, which is computed by Eq. (2.33) as in concrete. The coefficient of thermal expansion, α of steel (about 6.5×10^{-6} per deg. F) is only slightly different from that of concrete (about 5.5×10^{-6} per deg. F). The mechanical strain ε^m is then computed by subtracting thermal strain ε^t from total strain ε.

The slope of the load reversal path is assumed to be the same as the initial modulus, and the load reversal path is assumed to stay within the envelope shown with dotted lines in Fig. 2.9. Four different material states can be identified in the stress-strain curve. Their equations can be written as follows.

(1) In primary tension or compression

$$\sigma = E_1 \varepsilon^m \; ; \; E_t = E_1 \tag{2.34}$$

where E_1 is the initial modulus up to yielding.

(2) Yielded

$$\sigma = E_2 \varepsilon^m \pm (\sigma_y - E_2 \sigma_y) \; ; \; E_t = E_2 \tag{2.35}$$

where, E_2 is the second modulus after yielding, σ_y and ε_y are yield stress and yield strain respectively.

(3) In load reversal path

$$\sigma = E_1 (\varepsilon^m - \varepsilon_r) \; ; \; E_t = E_1 \tag{2.36}$$

where ε_r is the residual strain due to load

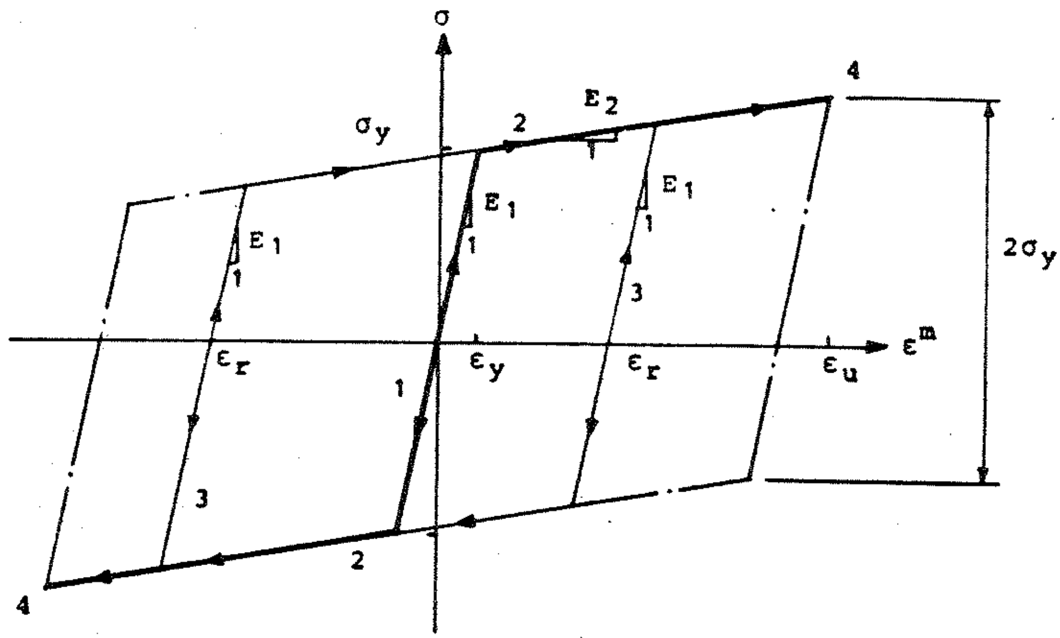

Fig. 2.9. Stress-Strain Curve of Reinforcing Steel Assumed in the Present Study (Numbers Represent the Material State of Reinforcing Steel)

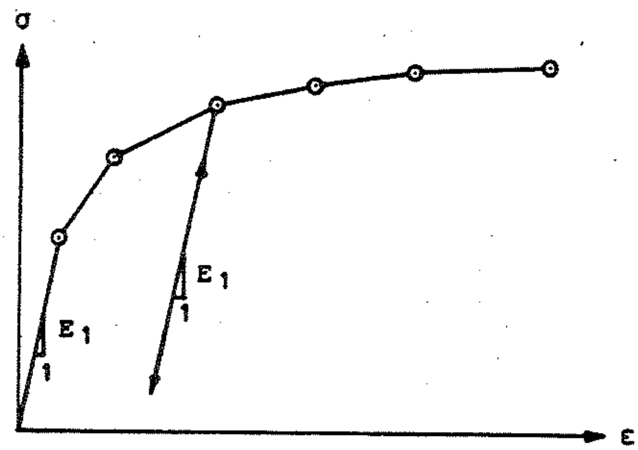

Fig. 2.10. Stress-Strain Curve of Prestressing Steel Assumed in the Present Study

reversal as shown in Fig. 2.9.

(4) Failed

Failure is assumed to occur when the mechanical strain ε^m exceeds the ultimate strain ε_u.

2.4 Prestressing Steel

Besides a large difference in the magnitude of the tensile strength, the stress-strain curve of prestressing steel is different from that of reinforcing steel in that there is no definite yield plateau for prestressing steel. Yielding develops more gradually, and in the inelastic range the stress-strain curve continues to rise smoothly until the tensile strength is reached. To accomodate this different shape a multilinear stress-strain curve, as shown in Fig. 2.10, is adopted for prestressing steel in this study. The slope of the unloading and reloading path is assumed to be the same as the initial modulus. Since prestressing steel is never subjected to compressive stress, the compressive stress-strain curve is not considered. Also temperature strain is not considered for prestressing steel.

Another important factor in the properties of prestressing steel is the relaxation of stress with time. Relaxation can be defined as the decrease in stress with time under a constant strain. Relaxation is just another manifestation of creep in prestressing steel, i.e. increase in strain with time under a constant stress. But relaxation is more often used as a basis of measurement for time dependent properties of prestressing steel because of its similarity to the actual conditions in prestressed concrete structures. The incorporation of relaxation in the analysis of prestressed concrete frames is treated in detail in chapter 6.

Friction properties of prestressing steel are also discussed in chapter 6 in conjunction with the tensioning operation of post-tensioned structures.

2.5 Composite Layer System

A composite layer system consisting of concrete and reinforcing steel layers is constructed in order to account for varied material properties within a frame element, as shown in Fig. 2.11. Each concrete or steel layer in a cross section is assumed to be in a state of uniaxial stress, and for each layer the cross sectional area and distance from the reference plane are specified as geometric properties.

Since concrete and reinforcing steel are assumed to be perfectly bonded together, the displacement field of the reinforced concrete frame element is continuous. Then any integral involving varying material properties over the volume of a frame element, such as the integral required to evaluate element stiffness matrix or internal force vector, can be performed layer by layer as follows.

$$\int_V \phi\psi dV = \sum_{i=1}^{n_c} \int_V \phi\psi_i dV + \sum_{i=1}^{n_s} \int_V \phi\psi_i dV \qquad (2.37)$$

where, ϕ is a function of space, ψ is a function of varying material properties such as tangent modulus, stress or various time dependent strains, n_c is the number of concrete lay-

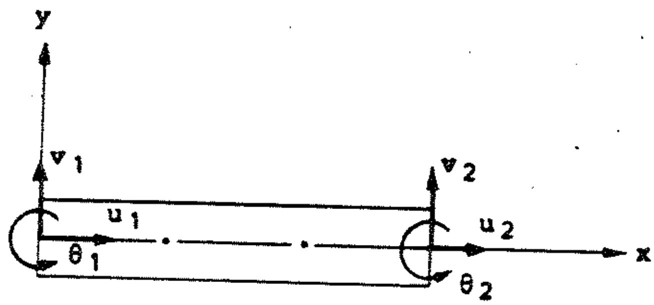

(a) Frame Element in Local Coordinates

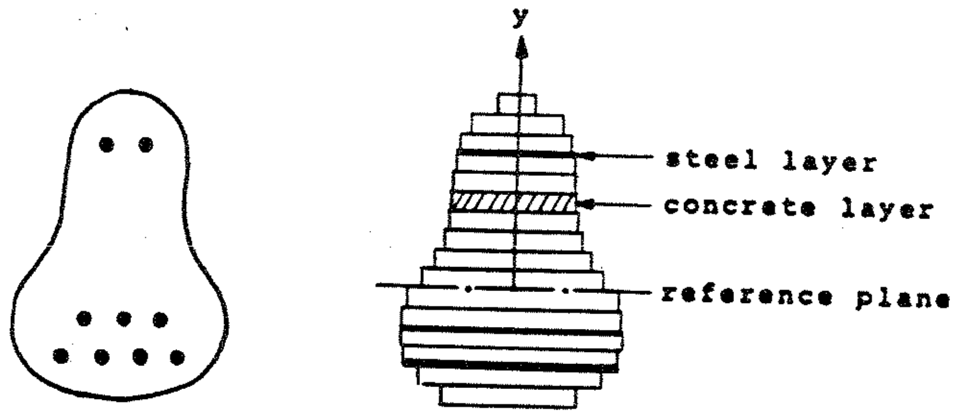

(b) Actual and Idealized Cross Section

Fig. 2.11. Composite Layer System of a Reinforced Concrete Frame Element

ers, n_s is the number of steel layers. Integration along the length of a frame element is performed by three point Gaussian quadrature as explained in chapter 5.

The composite action due to prestressing steel in concrete frames is discussed in detail in chapter 6, distinguishing bonded structures in which the displacement field of the frame element is assumed to be continuous, and unbonded structures in which the displacement field is not continuous.

3. MATHEMATICAL FORMULATION OF CREEP

3.1 Review of the Analytical Methods

Various analytical methods evaluating creep strain for the time dependent analysis of concrete structures have been developed by many investigators. Most of these methods are based on the linear creep law which may be defined as a law in which the principle of superposition is valid. In the linear creep law the creep strain is assumed to be proportional to the stress. This assumption is demonstrated by experiments to be valid up to the compressive stress level of about $0.4f'_c$ (71,72).

Thus the strain history of a concrete specimen subjected to a unit sustained stress, as shown in Fig. 3.1, is of importance. Fig. 3.1.a shows a specific compliance curve, and Fig. 3.1.b shows a specific creep curve. Specific compliance $\bar{c}(t)$ is defined as the total stress produced strain at time t due to a unit sustained stress applied at time $t = 0$. Specific creep $c(t)$ is defined as the creep strain at time t due to a unit sustained stress applied at time $t = 0$.

Bazant and Najjar (84), Ross (85) and England (86) presented comprehensive reviews of available linear creep methods. The analytical methods can be classified into two categories, namely approximate methods and general methods. In approximate methods, aim is taken at finding an approximate solution with the least amount of computational effort by using some simplifying assumptions. The effective modulus

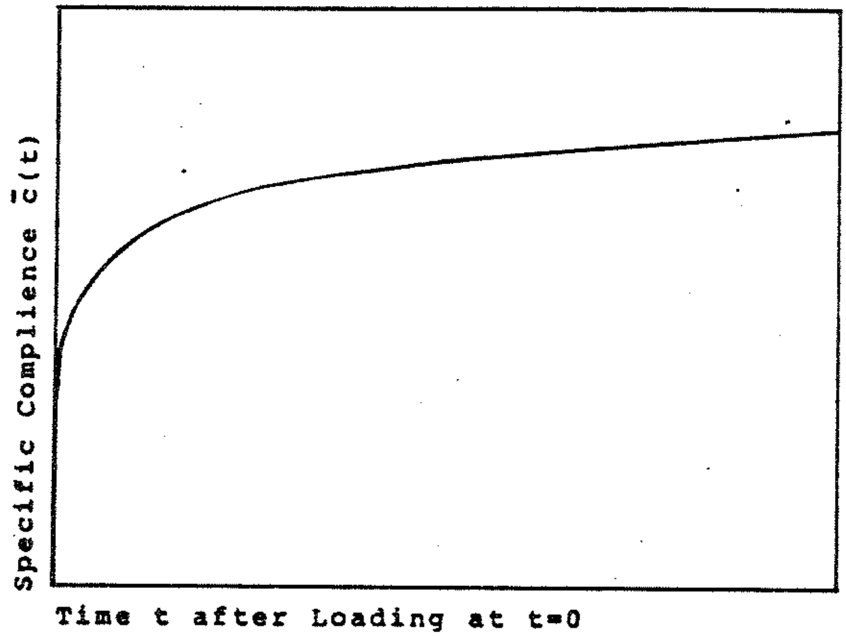

(a) Specific Compliance Curve

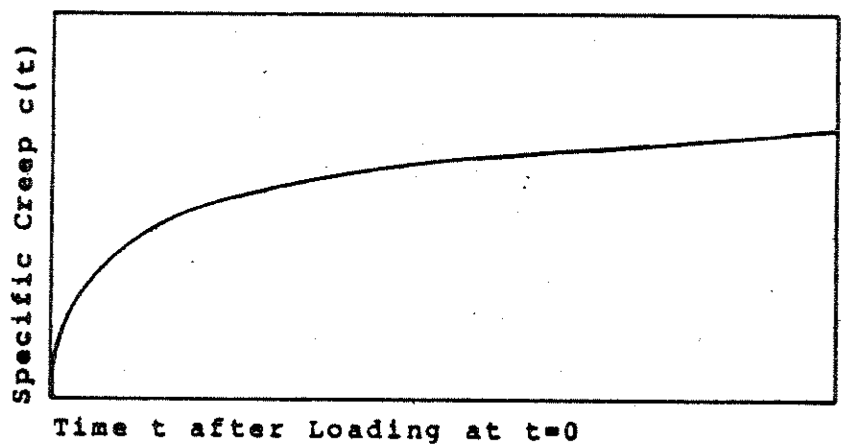

(b) Specific Creep Curve

Fig. 3.1. Strain History of a Concrete Specimen Subjected to a Unit Sustained Stress

method and the rate of creep method will be mentioned from this category. More accurate solutions are aimed at in general methods by defining the time dependent constitutive relationship of concrete either in differential form or in integral form.

The effective modulus method, initially presented by Faber (87), is the oldest and simplest method. It consists of a single elastic solution using the effective modulus $E'(t)$ defined as follows.

$$E'(t) = 1/\bar{c}(t) \tag{3.1}$$

where $\bar{c}(t)$ is the specific compliance at time t, defined previously. Total strain $\varepsilon(t)$ is then computed by

$$\varepsilon(t) = \sigma(t)/E'(t) \tag{3.2}$$

This method does not take the stress histories and aging of concrete into account. Thus, strains due to stress changes after the initial loading are overestimated because the decrease of specific compliance with aging, as shown in Fig. 2.6, is neglected. Also complete strain recovery is predicted by this method if the stress is reduced to zero, which is not true as shown in Fig. 2.5.

The rate of creep method, due to Glanville (81), is based on the assumption that the creep strain rate is a function of the current stress $\sigma(t)$ and the time elapsed since loading. Specifically,

$$\frac{d\varepsilon^c(t)}{dt} = \sigma(t)\frac{dc(t)}{dt} \tag{3.3}$$

where c(t) is the specific creep. Then the creep strain is evaluated by the integration,

$$\varepsilon^c(t) = \int_0^t \sigma(x)\frac{dc(x)}{dx}\,dx \tag{3.4}$$

This method does not include the effects of aging and strain history, thus no creep recovery is accounted for. Varying stresses with time is included, but the history effect on creep strain is disregarded.

In the differential formulation of the linear creep law, total stress produced strain is expressed in terms of the stress with linear differential operator,

$$\varepsilon^\sigma(t) = \frac{\alpha_n D^n + \alpha_{n-1} D^{n-1} + \cdots + \alpha_0}{\beta_m D^m + \beta_{m-1} D^{m-1} + \cdots + \beta_0}\,\sigma(t) \tag{3.5}$$

where, D is a differential operator, d/dt. Separating the instantaneous elastic strain from the total strain, Zienkiewicz (88) expressed the creep strain with a series of partial fractions obtained from the expansion of Eq. (3.5)

$$\varepsilon^c(t) = \sum_{i=1}^{n} \frac{a_i}{D + b_i}\,\sigma(t) \tag{3.6}$$

This can be interpreted as a response of a series of n Kelvin elements. But, difficulties in the experimental determination of the coefficients a_i and b_i which may represent the effects of aging and temperature variations restrict the use of this method for concrete. Sarne (37) used this formulation in his three dimensional time dependent analysis of concrete structures.

In the integral formulation of the linear creep law, the total stress produced strain is represented as a Volterra functional of stress.

$$\varepsilon^{\sigma}(t) = \int_0^t \bar{c}(\tau, t-\tau)\frac{\partial\sigma(\tau)}{\partial\tau}d\tau \qquad (3.7)$$

where $\bar{c}(\tau, t-\tau)$ is the specific compliance at time $(t-\tau)$ after loading, τ is the age of concrete at loading, and t is the observation time after casting of concrete. Specific compliance $\bar{c}(\tau, t-\tau)$ can be divided into two parts ; an instantaneous elastic part and a creep part.

$$\bar{c}(\tau, t-\tau) = \frac{1}{E(\tau)} + c(\tau, t-\tau) \qquad (3.8)$$

where $E(\tau)$ is the modulus of elasticity at age τ, and $c(\tau, t-\tau)$ is the specific creep at time $(t-\tau)$ after loading. Then, Eq. (3.7) can be rewritten,

$$\varepsilon^{\sigma}(t) = \int_0^t \left[\frac{1}{E(\tau)} + c(\tau, t-\tau)\right]\frac{\partial\sigma}{\partial\tau}d\tau \qquad (3.9)$$

Effects of stress history are accounted for by the linear superposition method. This method asserts that the strain at a given time can be obtained by adding independent strains caused by stresses with different durations of time. This implies that each stress is independent and does not affect the strain histories caused by other stresses. The application of the linear superposition method is illustrated in Fig. 3.2 with an axially loaded prism.

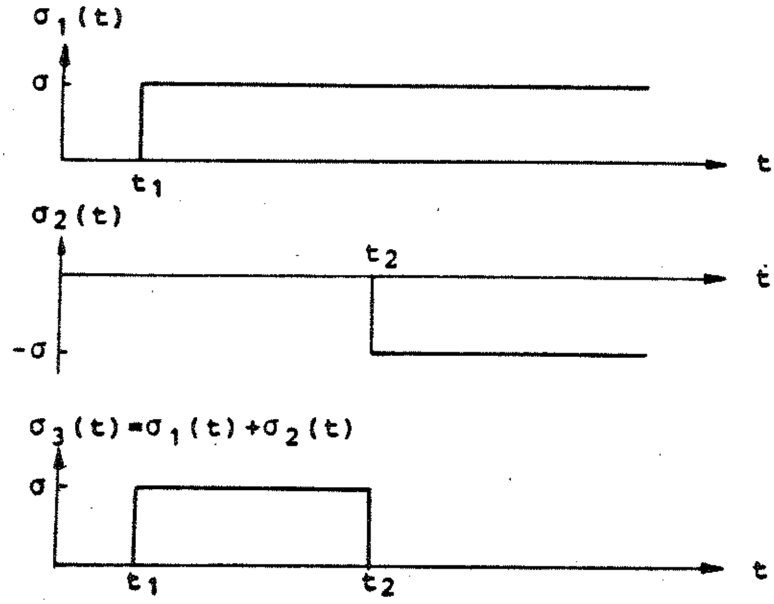

(a) Stress History of a Prism

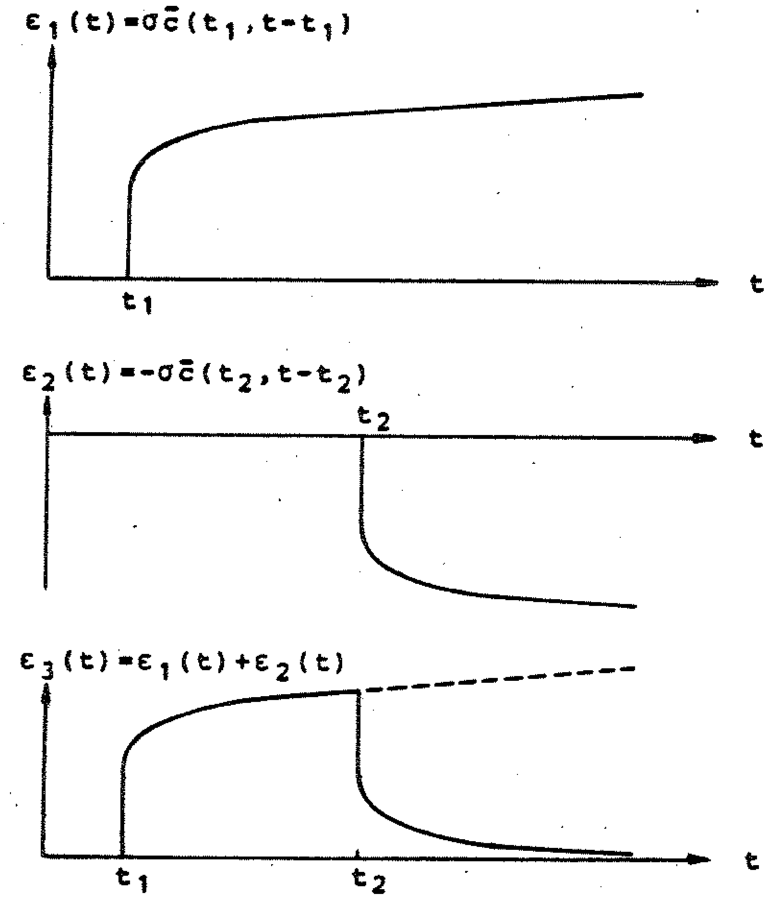

(b) Strain History of a Prism

Fig. 3.2. Application of the Linear Superposition Method

We want to find the strain history of a prism due to the stress history $\sigma_3(t)$ shown in Fig. 3.2.a. $\sigma_3(t)$ is obtained by superposing $\sigma_1(t)$ in which a constant sustained stress σ is applied at time t_1, and $\sigma_2(t)$ in which a constant sustained stress $-\sigma$ is applied at time t_2. The strain history $\varepsilon_1(t)$ due to $\sigma_1(t)$ can be computed by

$$\varepsilon_1(t) = \sigma\ \bar{c}(t_1, t-t_1) \tag{3.10}$$

The strain history $\varepsilon_2(t)$ due to $\sigma_2(t)$ is

$$\varepsilon_2(t) = -\sigma\ \bar{c}(t_2, t-t_2) \tag{3.11}$$

Then the strain history $\varepsilon_3(t)$ due to $\sigma_3(t)$ is obtained by superposing $\varepsilon_1(t)$ and $\varepsilon_2(t)$ as shown in Fig. 3.2.b.

$$\varepsilon_3(t) = \varepsilon_1(t) + \varepsilon_2(t) \tag{3.12}$$

From Eq. (3.9), creep strain $\varepsilon^c(t)$ may be written

$$\varepsilon^c(t) = \int_0^t c(\tau, t-\tau) \frac{\partial \sigma(\tau)}{\partial \tau} d\tau \tag{3.13}$$

For the numerical evaluation of creep strain, the specific creep $c(\tau, t-\tau)$ has to be approximated by some analytical function. Proper choice of the analytical function for the specific creep is very important in creep analysis because the form of the function often influences the efficiency of the numerical procedure for the solution of Eq. (3.13). The function also has to be selected such that it fits the experimental data as closely as possible.

McHenry (89), who first utilized the superposition principle for the concrete creep analysis, suggested the following form for the specific creep function.

$$c(\tau,t-\tau) = \alpha\,[1-e^{-\gamma(t-\tau)}] + \beta e^{-p\tau}[1-e^{-m(t-\tau)}] \qquad (3.14)$$

where α, β, γ, p, m are parameters used to fit the experimental data.

Arutyunyan (90) suggested the form

$$c(\tau,t-\tau) = (a+b/\tau)\sum_{k=0}^{m} B_k e^{-\gamma_k(t-\tau)} \qquad (3.15)$$

where a, b, B_k, γ_k, m are coefficients for fitting the experimental data.

Selna (44,45) proposed the following form in his time dependent analysis of reinforced concrete frames.

$$c(\tau,t-\tau) = \sum_{i=1}^{3}\sum_{j=1}^{4}\alpha_i a_j \tau^{-0.1(j-i)}[1-e^{-K_i(t-\tau)}] \qquad (3.16)$$

where α_i, K_i, a_j are coefficients to be determined from experimental data. In Selna's creep formulation, current total strain is determined from the quantities stored from two previous time steps instead of the entire history. Scanlon (48) used Selna's formulation of creep for his study of time dependent deflection of reinforced concrete slabs.

Mukaddam and Bresler (91) proposed a specific creep function in which the effects of both age and temperature variations are taken into account with the time-shift principle.

$$c(\tau,t-\tau,T) = \sum_{i=1}^{n} a_i e^{-\lambda_i \phi(T)\psi(\tau)(t-\tau)} \qquad (3.17)$$

in which a_i, λ_i are coefficients determined from experimental data, $\phi(T)$ is the temperature shift function and $\psi(\tau)$ is the age shift function.

However the application of their formulation of creep is restricted to relatively simple structures because all the previous stress histories have to be stored to evaluate current strains.

Zienkiewicz and Watson (92) proposed to use the form

$$c(\tau, t-\tau, T) = \sum_{i=1}^{n} C_i(\tau, T)\,[1-e^{-p_i(t-\tau)}] \tag{3.18}$$

where age and temperature dependent function $C_i(\tau,T)$ and parameters n, p_i are determined from experimental data. By using this form of the specific creep function, they showed that the storage of only a vector and the stress increment at a time step immediately preceding the current time step is required to evaluate the creep strain increment at any time step. But they did not suggest a specific form of both age and temperature dependent function $C_i(\tau,T)$.

3.2 Age and Temperature Dependent Integral Formulation of Creep

In the present study an efficient numerical procedure for the evaluation of creep strain at any time is developed with an integral formulation which takes into account both age and temperature variations. The following assumptions are used for this formulation.

(1) Total stress produced strain $\varepsilon^{\sigma}(t)$ at any time t consists of three components.

$$\varepsilon^{\sigma}(t) = \varepsilon^{m}(t) + \varepsilon^{a}(t) + \varepsilon^{c}(t) \tag{3.19}$$

Each component of the strain has been defined in section 2.2.1, and illustrated in Fig. 2.1.b. Creep strain $\varepsilon^{c}(t)$ is expressed with a superposition integral

$$\varepsilon^{c}(t) = \int_{0}^{t} c(\tau, t-\tau, T) \frac{\partial \sigma(\tau)}{\partial \tau} d\tau \tag{3.20}$$

in which the kernel function $c(\tau, t-\tau, T)$ is the specific creep function dependent on age and temperature variations.

(2) Creep strain is assumed to be proportional to applied stress, both in tension and compression. And Eq. (3.20) is used both in compression and tension.

(3) Principle of superposition is assumed to be valid for the evaluation of creep strain. Thus, total creep strain at any time t can be obtained as the sum of independent creep strains produced by stress changes at different ages with different durations of time up to t.

(4) Concrete is assumed to be a thermorheologically simple material (91). Such a material is defined as a material which obeys the time-shift principle for the temperature variation, as illustrated in Fig. 3.3. Let T_0 be a fixed reference temperature, and T a constant temperature such that $T > T_0$. The specific creep versus logarithmic time curves at temperatures T_0 and T are identical in shape, but shifted horizontally with a distance $\psi(T)$.
This relationship can be written

$$c_T(\ell nt) = c_{T_0}(\ell nt + \psi(T)) \tag{3.21}$$

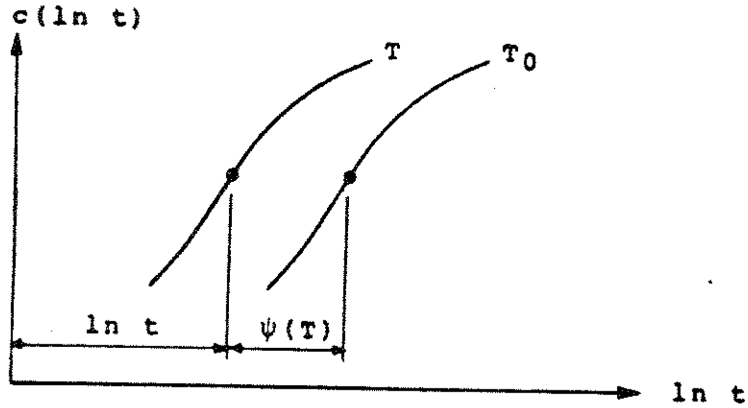

Fig. 3.3. Specific Creep vs. Logarithmic Time Curve of a Thermorheologically Simple Material

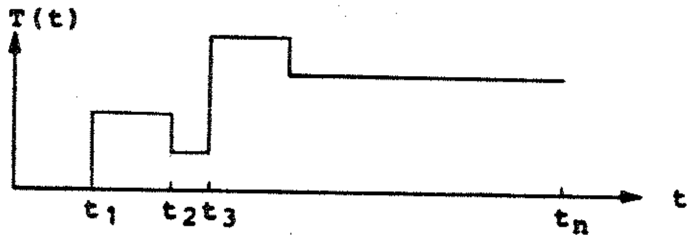

(a) Temperature History

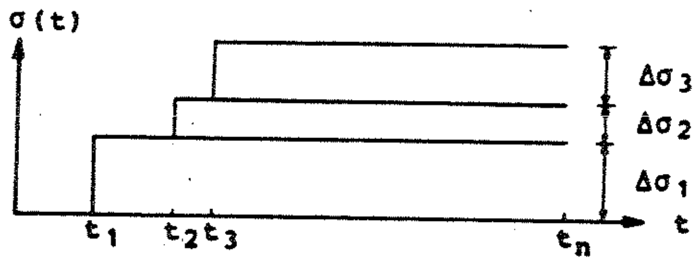

(b) Stress History

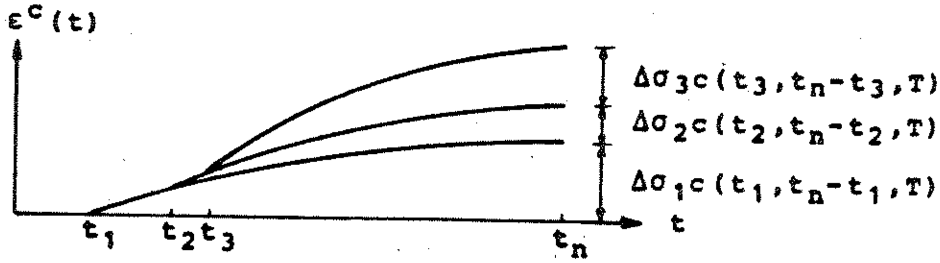

(c) Creep Strain History

Fig. 3.4. Superposition of Creep Strains

where C_T, C_{T_0} are the specific creep curves for temperatures T and T_0 respectively. Since both sides of the equation represent the same curve, taking the exponential of the arguments on both sides and noting that $e^{\ell n t} = t$ and $e^{\ell n t + \psi(T)} = te^{\psi(T)}$,

$$c_T(t) = c_{T_0}(te^{\psi(T)}) = c_{T_0}(t\phi(T)) \;;\; \phi(T) = e^{\psi(T)} \qquad (3.22)$$

where $\phi(T)$ is called a temperature shift function. Then the specific creep curve for any temperature T is obtained by replacing the time t by $t \cdot \phi(T)$ in the specific creep curve for the reference temperature T_0. The validity of this time-shift principle for concrete was demonstrated by Mukaddam and Bresler (91) using temperature dependent creep data obtained by Ross, et al (76,71), Browne (93), and Hannant (94).

(5) Stress changes are assumed to occur only at distinct time steps t_n ; $n = 1,2,\cdots,N$ (see section 2.2.1). And, for the calculation of creep strain increment during some time interval, the stress is assumed to remain constant during that interval.

The following form of age and temperature dependent specific creep function is used in this study.

$$c(\tau,t-\tau,T) = \sum_{i=1}^{m} a_i(\tau)[1-e^{-\lambda_i\phi(T)(t-\tau)}] \qquad (3.23)$$

in which m, $a_i(\tau)$, λ_i, $\phi(T)$ are to be determined from experimental creep data.

The principle of superposition for the creep strain is illustrated in Fig. 3.4 with given temperature and stress histories. The following definitions for incremental quantities of time steps, stresses and creep strains are used.

$$\Delta t_n = t_n - t_{n-1} \tag{3.24}$$

$$\Delta\sigma_n = \sigma_n - \sigma_{n-1} \equiv \sigma(t_n) - \sigma(t_{n-1}) \tag{3.25}$$

$$\Delta\varepsilon_n = \varepsilon_n^c - \varepsilon_{n-1}^c \equiv \varepsilon^c(t_n) - \varepsilon^c(t_{n-1}) \tag{3.26}$$

Total creep strain ε_n^c at typical time step t_n can be obtained by

$$\varepsilon_n^c = \Delta\sigma_1 \cdot c(t_1, t_n - t_1, T) + \Delta\sigma_2 \cdot c(t_2, t_n - t_2, T) + \cdots + \Delta\sigma_{n-1} \cdot c(t_{n-1}, t_n - t_{n-1}, T) \tag{3.27}$$

Total creep strain ε_{n-1}^c at time step t_{n-1} can be obtained by

$$\varepsilon_{n-1}^c = \Delta\sigma_1 \cdot c(t_1, t_{n-1} - t_1, T) + \Delta\sigma_2 \cdot c(t_2, t_{n-1} - t_2, T) + \cdots + \Delta\sigma_{n-2} \cdot c(t_{n-2}, t_{n-1} - t_{n-2}, T) \tag{3.28}$$

And the creep strain increment $\Delta\varepsilon_n^c$ occurring during time steps t_{n-1} and t_n is obtained by Eq. (3.26). On inspection of Eq. (3.26) to (3.28) it is evident that knowledge of all previous stress increments are required to evaluate the creep strain increment at any time step. This presents a considerable difficulty in computational procedures, and would require a substantial storage space and computational time for a computer even for moderately sized problems. It will be shown that this difficulty can be avoided by using the form of the specific creep function expressed by Eq. (3.23).

Eq. (3.27) can be written as follows substituting the specific creep function expression given in Eq. (3.23) and taking the temperature history into account.

$$\begin{aligned} \varepsilon^c_n = \; & \Delta\sigma_1 \Sigma a_i(t_1)[1-e^{-\lambda_i(\phi(T_1)\Delta t_2+\phi(T_2)\Delta t_3+\cdots+\phi(T_{n-1})\Delta t_n)}] \\ & + \Delta\sigma_2 \Sigma a_i(t_2)[1-e^{-\lambda_i(\phi(T_2)\Delta t_3+\phi(T_3)\Delta t_4+\cdots+\phi(T_{n-1})\Delta t_n)}] \\ & + \cdots \\ & + \Delta\sigma_{n-1} \Sigma a_i(t_{n-1})[1-e^{-\lambda_i\phi(T_{n-1})\Delta t_n}] \end{aligned} \qquad (3.29)$$

where summation is made on $i = 1,2,\cdot\cdot,m$.

Similarly Eq. (3.28) may be written

$$\begin{aligned} \varepsilon^c_{n-1} = \; & \Delta\sigma_1 \Sigma a_i(t_1)[1-e^{-\lambda_i(\phi(T_1)\Delta t_2+\phi(T_2)\Delta t_3+\cdots+\phi(T_{n-2})\Delta t_{n-1})}] \\ & + \Delta\sigma_2 \Sigma a_i(t_2)[1-e^{-\lambda_i(\phi(T_2)\Delta t_3+\phi(T_3)\Delta t_4+\cdots+\phi(T_{n-2})\Delta t_{n-1})}] \\ & + \cdots \\ & + \Delta\sigma_{n-2} \Sigma a_i(t_{n-2})[1-e^{-\lambda_i\phi(T_{n-2})\Delta t_{n-1}}] \end{aligned} \qquad (3.30)$$

Then the creep strain increment $\Delta\varepsilon^c_n$ is obtained by subtracting Eq. (3.30) from Eq. (3.29).

$$\begin{aligned} \Delta\varepsilon^c_n = \; & \Delta\sigma_1 \Sigma a_i(t_1) e^{-\lambda_i(\phi(T_1)\Delta t_2+\cdots+\phi(T_{n-2})\Delta t_{n-1})}[1-e^{-\lambda_i\phi(T_{n-1})\Delta t_n} \\ & + \Delta\sigma_2 \Sigma a_i(t_2) e^{-\lambda_i(\phi(T_2)\Delta t_3+\cdots+\phi(T_{n-2})\Delta t_{n-1})}[1-e^{-\lambda_i\phi(T_{n-1})\Delta t_n} \\ & + \cdots \end{aligned}$$

$$+ \Delta\sigma_{n-2}\Sigma a_i(t_{n-2})e^{-\lambda_i\phi(T_{n-2})\Delta t_{n-1}}[1-e^{-\lambda_i\phi(T_{n-1})\Delta t_n}]$$

$$+ \Delta\sigma_{n-1}\Sigma a_i(t_{n-1})[1-e^{-\lambda_i\phi(T_{n-1})\Delta t_n}] \quad (3.31)$$

Eq. (3.31) can be simply written

$$\Delta\varepsilon^c_n = \sum_{i=1}^{m} A_{i,n}[1-e^{-\lambda_i\phi(T_{n-1})\Delta t_n}] \quad (3.32)$$

where $A_{i,n}$ is expressed by

$$A_{i,n} = \Delta\sigma_1 a_i(t_1)e^{-\lambda_i(\phi(T_1)\Delta t_2+\phi(T_2)\Delta t_3+\cdots+\phi(T_{n-2})\Delta t_{n-1}}$$

$$+ \Delta\sigma_2 a_i(t_2)e^{-\lambda_i(\phi(T_2)\Delta t_3+\phi(T_3)\Delta t_4+\cdots+\phi(T_{n-2})\Delta t_{n-1}}$$

$$+ \cdots$$

$$+ \Delta\sigma_{n-2}a_i(t_{n-2})e^{-\lambda_i\phi(T_{n-2})\Delta t_{n-1}} + \Delta\sigma_{n-1}a_i(t_{n-1}) \quad (3.33)$$

Using the general description of $A_{i,n}$, we note that

$$A_{i,n-1} = \Delta\sigma_1 a_i(t_1)e^{-\lambda_i(\phi(T_1)\Delta t_2+\phi(T_2)\Delta t_3+\cdots+\phi(T_{n-3})\Delta t_{n-2})}$$

$$+ \Delta\sigma_2 a_i(t_2)e^{-\lambda_i(\phi(T_2)\Delta t_3+\phi(T_3)\Delta t_4+\cdots+\phi(T_{n-3})\Delta t_{n-2})}$$

$$+ \cdots$$

$$+ \Delta\sigma_{n-2}a_i(t_{n-2}) \quad (3.34)$$

Inspection of Eq. (3.33) and (3.34) leads us to the following expression which enables us to evaluate $A_{i,n}$ from the previous value $A_{i,n-1}$ successively.

$$A_{i,n} = A_{i,n-1}\cdot e^{-\lambda_i\phi(T_{n-2})\Delta t_{n-1}} + \Delta\sigma_{n-1}a_i(t_{n-1}) \quad (3.35)$$

$$A_{i,2} = \Delta\sigma_1 a_i(t_1) \quad (3.36)$$

We note that, by using Eq. (3.32), (3.35) and (3.36), storage of only $\Delta\sigma_{n-1}$ and $A_{i,n-1}$ at time step t_{n-1} is required to evaluate the creep strain increment $\Delta\varepsilon_n^c$ at time step t_n instead of the entire stress history. Thus, the present formulation of creep saves a considerable amount of storage space and computational time for a computer compared to other formulations in which part or all of the previous stress histories have to be stored, and enables us to efficiently analyze complex concrete structures.

3.3 Creep at High Stress Levels

In the present formulation, the analysis of creep is based on the assumption that the creep strain is proportional to stress intensity. But this assumption is valid only up to a stress level of approximately $0.4f_c'$ for concrete. As shown in Fig. 2.7 (54), creep strain generally increases at an increasing rate at higher stress levels. To account for this nonlinear creep effect in the present linear formulation of creep the effective stress concept suggested by Becker and Bresler (73) is used in this study.

The effective stress is obtained by multiplying the actual stress by an appropriate magnifying factor such that the creep strain calculated by the effective stress on the basis of the linear creep law would be the same as that produced by the actual stress. The following equations are used for the calculation of the effective stress σ_e in this study.

$$\sigma_e = \sigma \qquad \text{if} \quad \sigma \le r_1 f''_c \tag{3.37}$$

$$\sigma_e = c_1 + c_2 f''_c \qquad \text{if} \quad r_1 f''_c < \sigma \le f''_c \tag{3.38}$$

$$\sigma_e = r_2 \sigma \qquad \text{if} \quad \sigma = f''_c \tag{3.39}$$

where, r_1 is the stress-strength ratio up to which creep strain is proportional to stress intensity, and r_2 is the magnifying factor when the stress equals the maximum compressive stress f''_c. With given values of r_1 and r_2, c_1 and c_2 can be calculated from the three equations given above.

$$c_1 = \frac{r_2 - r_1}{1 - r_1} \; ; \; c_2 = r_1(1 - c_1) \tag{3.40}$$

Becker and Bresler used the values of $c_1 = 2.33$ and $c_2 = -0.465$ with $r_1 = 0.35$ and $r_2 = 1.865$, based on the study of Roll (71,72).

3.4 Determination of Specific Creep Coefficients

Coefficients m, $a_i(\tau)$, λ_i ; $i = 1,2,\cdots,m$ and temperature shift function $\phi(T)$ in the specific creep function expressed by Eq. (3.23) are determined from experimental creep data at some loading age τ and reference temperature T_0. And assume that parameter m is known. Then the specific creep function in Eq. (3.23) can be written

$$c(x) = \sum_{i=1}^{m} a_i (1 - e^{-\lambda_i x}) \tag{3.41}$$

where $x = t - \tau$ represents the time elapsed since the loading age τ. The determination of a_i, λ_i ; $i = 1,2,\cdots,m$ is discussed by Fröberg (95) using Prony's method in which solutions of mth degree polynomial equation and systems of simultaneous linear equations are required. By using this method and comparing the results obtained using different values of m, it was found that the use of following fixed values enables us to fit the experimental creep data to the assumed specific creep function with a sufficient degree of accuracy.

$$m = 3, \ \lambda_i = 10^{-i} \ ; \ i = 1,2,3. \qquad (3.42)$$

Then, at any given loading age and reference temperature, the determination of a_i ; $i = 1,2,3$ are required. Suppose the experimental creep data are given at discrete points in time, so that we have N pairs of the value (x_j, y_j) ; $j = 1, 2, \cdots, N$ in which y_j is the experimental specific creep at time x_j, and N is the total number of time steps. Then the a_i's can be determined by setting up the following equations.

$$\sum_{i=1}^{3} a_i (1 - e^{-10^{-i} x_j}) = y_j \ ; \ j = 1,2,\cdots,N \qquad (3.43)$$

Eq. (3.43) represent N sets of linear equations in 3 unknown coefficients a_1, a_2 and a_3 in which N is much larger than 3. These equations are solved by the least-square method (95, 96) in which the sum of the squares of errors are minimized.

Determination of a_i's for different loading ages is performed similarly, and for intermediate loading ages, where the experimental data are not given, linear interpolation is used to determine a_i's.

Experimental creep data for the particular concrete used in the structure to be analyzed are not always available. In such a case the creep data recommended by ACI Committee

209 (56) and summarized in Eqs. (2.18) to (2.20) may be used. Since Eq. (2.18) expresses creep data as the ratio of creep strain to initial strain at loading, specific creep, which is the creep strain due to a unit stress, can be obtained by dividing Eq. (2.18) by the initial modulus $E_i(\tau)$ at loading age τ.

If we use the ACI creep data, the determination of the coefficients a_i's by the least-square method may be performed only for one loading age because the ACI equations of the creep curves for different loading ages differ only by a constant multiplying factor C_u. The ultimate creep coefficient C_u for different loading ages can be computed by Eqs. (2.19) and (2.20). Thus, assuming all the other conditions are identical except for the loading age, once $a_i(\tau_o)$ at some loading age τ_o are determined by the least-square method, $a_i(\tau)$ for any other loading age τ may be determined as follows for moist cured concrete from Eq. (2.20).

$$a_i(\tau) = a_i(\tau_o)\cdot\frac{E(\tau_o)}{E(\tau)}\cdot\left(\frac{\tau}{\tau_o}\right)^{-0.118} \quad ; \; i = 1,2,3 \qquad (3.44)$$

where $E(\tau_o)$, $E(\tau)$ are initial moduli at loading age τ_o and τ respectively. This equation may also be used in case the experimental creep data is available only at one loading age.

The following standard values of the coefficients a_i's obtained by the least-square method for the standard conditions defined in section 2.2.3 may be used for the creep analysis.

$$\tau_o = 28 \text{ days} \; ; \; E_o = 3.834 \times 10^6 \text{ psi}$$
$$a_1 = 2.02565 \times 10^{-7} \qquad (3.45)$$
$$a_2 = 1.85702 \times 10^{-7}$$
$$a_3 = 1.37290 \times 10^{-7}$$

For loading ages other than $\tau_o = 28$, Eq. (3.44) may be used to evaluate a_i's for moist cured concrete. And for conditions which differ from standard conditions, the a_i's are multiplied by corrction factors K_H^c, K_T^c, K_S^c, K_F^c and K_A^c defined in Eq. (2.20).

The temperature shift function $\phi(T)$ can be obtained by plotting specific creep versus logarithmic time curves for different temperatures as shown in Fig. 3.3. Then the function $\psi(T)$ or the temperature shift function $\phi(T)$ may be approximated by a polynomial function.

The effectiveness of present specific creep function expression to simulate the experimental creep data is demonstrated in Fig. 3.5 in which Browne's (93) experimental creep curves at different loading ages can be seen to be almost exactly simulated by the creep curves generated by present analytical model, maximum discrepancy between the two curves being less than 2 percent.

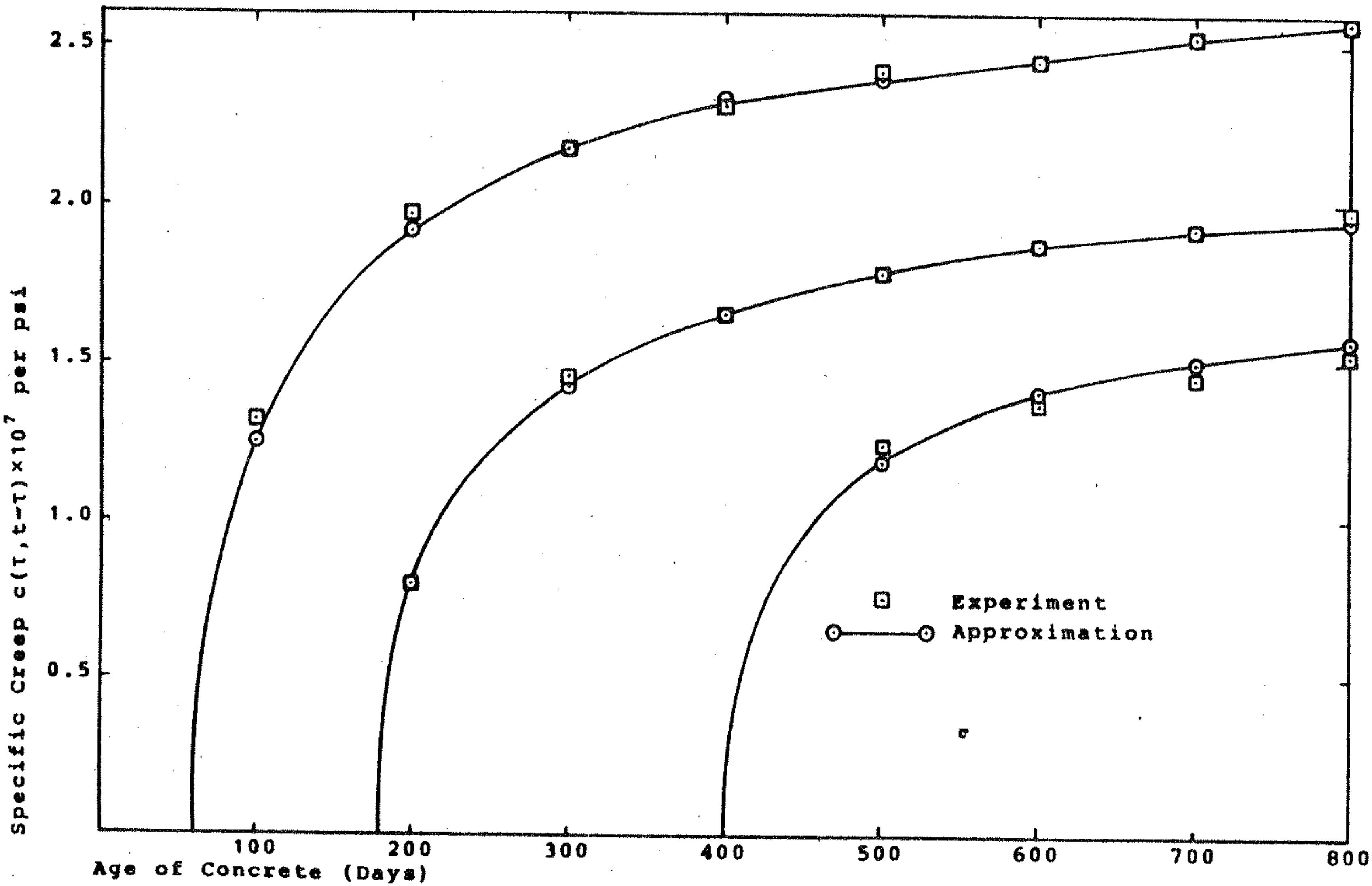

Fig. 3.5. Comparison of Browne's (93) Experimental Specific Creep Curves and Their Approximations by the Present Analysis

4. SOLUTION STRATEGY FOR THE TIME DEPENDENT NONLINEAR FRAME PROBLEM

4.1 Problem Statement

Suppose we want to analyze a planar concrete frame shown in Fig. 4.1.a. The structure is idealized as an assemblage of finite elements interconnected by joints with given boundary conditions as shown in Fig. 4.2.b. The external loads are assumed to be applied only at joints. Distributed loads may be converted into equivalent joint loads either by the consistent load method or a lumped formulation (2). The joint load history, temperature history of every part of the structure and the stress-strain curve valid at any instant of time are given. Also creep and shrinkage characteristics of the concrete are given. Then we want to find out joint displacements, support reactions, internal forces for each element, strains and stresses of every part of the structure at any instant of time.

We note that the load-displacement ($\underset{\sim}{R}-\underset{\sim}{r}$) relationship of this structure would be nonlinear for the following reasons.

(1) The stress-strain ($\sigma-\varepsilon^m$) relationship is nonlinear.

(2) The strain-displacement ($\varepsilon-\underset{\sim}{r}$) relationship is nonlinear because of the large displacement effects.

(3) Time dependent effects of load history, temperature history, creep, shrinkage and aging of concrete are present.

In order to incorporate these time dependent nonlinear-

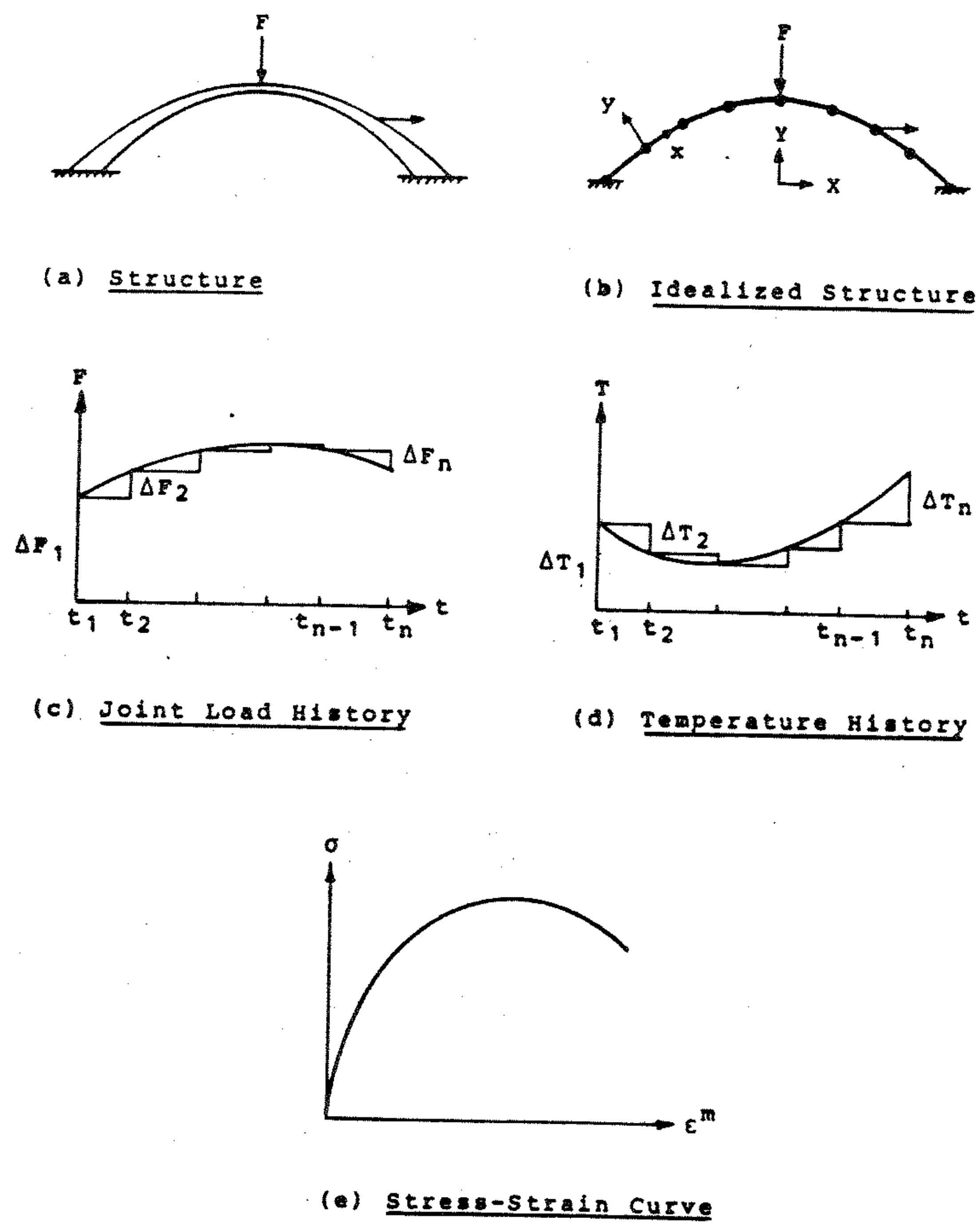

Fig. 4.1. A Planar Concrete Frame

ities the time domain is divided into a discrete number of intervals, and a step forward integration is performed in which increments of displacements and strains are successively added to the previous total as we march forward in the time domain.

At each time step a direct stiffness finite element method based on the displacement formulation is used for the analysis in the space domain. Here, we need to set up an equilibrium equation which is necessarily nonlinear to be valid for the current state of geometry and material properties.

To account for the geometric nonlinearity, an "Updated Lagrangian" formulation (97,98,99,47) for the description of motion is used in this study. For each element a local rectangular Cartesian coordinate system x, y is defined as shown in Fig. 4.1.b. The direction of this local coordinate system varies continuously as the structure deforms. Internal forces and stiffnesses are calculated in the local coordinate system for each element, and then transformed to a fixed global coordinate system X, Y shown in Fig. 4.1.b, where the equilibrium equations for the entire structure are set up and solved. Thus, the continuously changing displacement transformation matrix for each element represents the effect of geometric nonlinearity along with nonlinear form of strain-displacement (ε-$\underset{\sim}{r}$) relationship.

4.2 Solution Methods for Nonlinear Equilibrium Equations

Various methods for the solution of the total equilibrium equations

$$\underline{K}\,\underset{\sim}{r} = \underset{\sim}{R} \tag{4.1}$$

or the tangential equilibrium equations

$$\underline{K}_t\, d\underset{\sim}{r} = d\underset{\sim}{R} \tag{4.2}$$

in which stiffness matrices $\underline{K}$ and $\underline{K}_t$ are functions of displacements $\underset{\sim}{r}$ and material properties are available (1,2,31, 100,101). These methods can be generally classified into three categories as follows.

(1) Incremental Load Method (Fig. 4.2.a)

Total load $\underset{\sim}{R}$ is subdivided into load increments $\Delta\underset{\sim}{R}$. For each load increment $\Delta\underset{\sim}{R}$, displacement increment $\Delta\underset{\sim}{r}$ is obtained using tangent stiffness, and total displacement $\underset{\sim}{r}$ is obtained by adding displacement increments.

(2) Iterative Method (Fig. 4.2.b)

Total load is applied in one step in the iterative method, and the unbalanced load iteration is performed until the equilibrium is reached to a desired degree. Unbalanced load is obtained by subtracting internal resisting load from external joint load, thus it represents the magnitude of discrepancy from the equilibrium state. Depending on the stiffness used for the iterations, the iterative method can be classified into three methods ; initial stiffness method, secant stiffness method and tangent stiffness method.

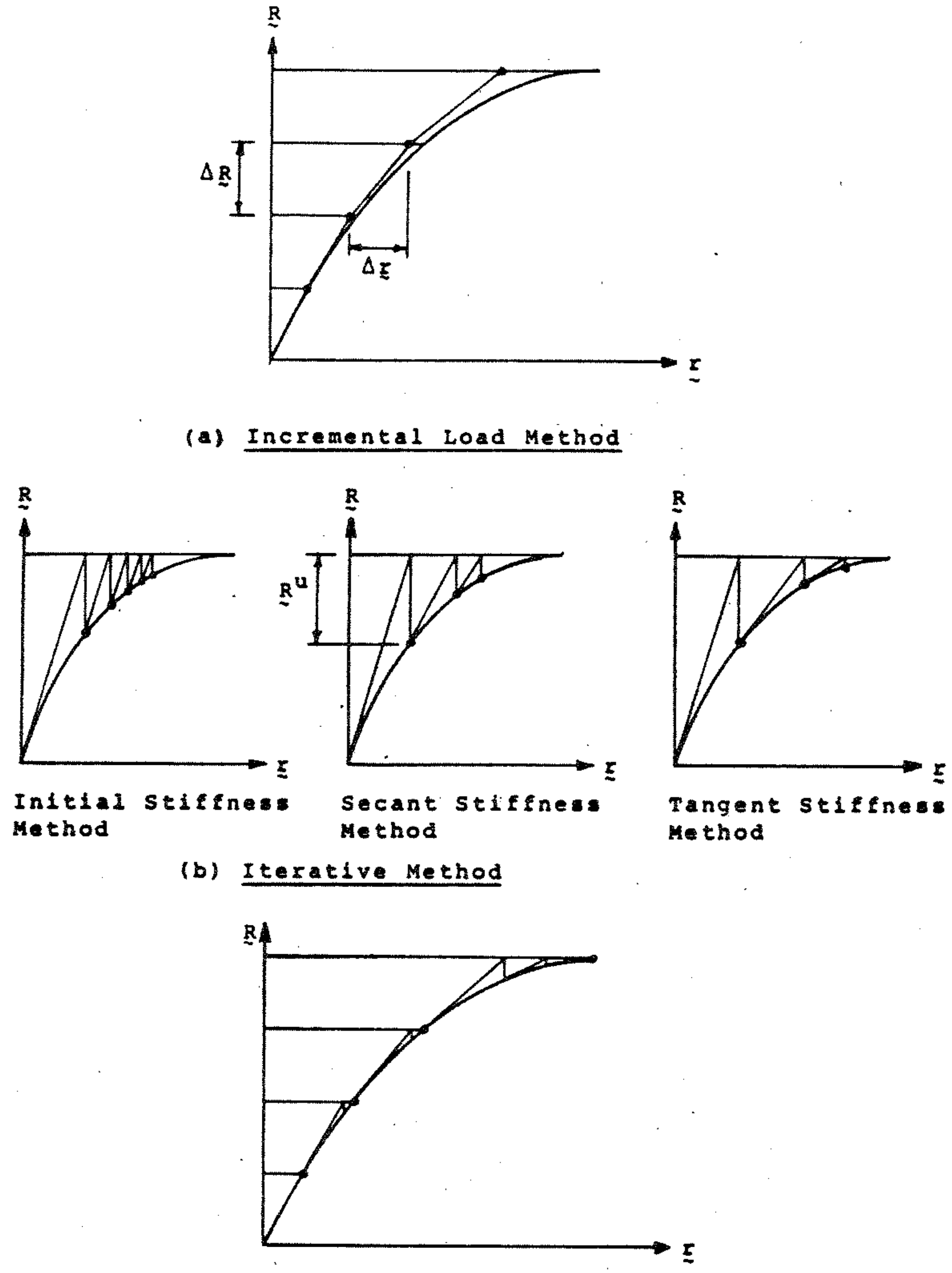

(a) Incremental Load Method

(b) Iterative Method

(c) Combined Method

Fig. 4.2. Solution Methods for Nonlinear Equilibrium Equations

Tangent stiffness method requires the fewest number of iterations to arrive at the solution, but it has the disadvantage that the tangent stiffness has to be formed and triangularized for the Gaussian elimination, for each iteration. On the other hand, initial stiffness method requires the largest number of iterations, but it has the advantage that the same stiffness which is formed and triangularized initially can be used for all the iterations.

(3) Combined Method (Fig. 4.2.c)

This method combines the two methods described above. Thus, total load is divided into load increments, and for each load increment one of the three iterative methods are used for better accuracy.

The incremental load method generally gives good approximations to the intermediate and final solutions while iterative methods yield the final solution to the desired degree of accuracy. For concrete structures, the solution is generally path-dependent mainly due to the progressive cracking in tensile regions, so that it is desirable to use the incremental method. For this study, the combined method is used to enhance the accuracy of the solution. An option is provided to use either tangent stiffness or constant stiffness during iterations.

4.3 Outline of the Nonlinear Time Dependent Analysis Procedure

For the time dependent analysis, the time domain is divided into a discrete number of time intervals each of which may not have the same duration in time, as already explained in section 2.2.1. The junctions of these time intervals are defined as time steps. Thus we have a discrete number of time steps t_n ; $n = 1,2,\cdots,N$, where N is the total number of time steps considered in the analysis. Then a step forward integration is performed in which incremental solutions are successively added to the previous total to obtain the solution at the current time step, as follows.

At time step t_{n-1}, we know all the joint displacements $\tilde{r}$, total strains ε, total non-mechanical strains ε^{nm}, and stresses σ of every part of the structure. Evaluate the increments of non-mechanical strains $\Delta\varepsilon_n^{nm}$ due to creep and shrinkage of concrete and temperature changes occurring during time steps t_{n-1} and t_n by the mechod described in chapters 2 and 3. Then calculate the equivalent joint load increments ΔR_n^{nm} at time step t_n which would produce the non-mechanical strain increments $\Delta\varepsilon_n^{nm}$ by treating them as initial strains (1). As shown in chapter 5, ΔR_n^{nm} for each element can be calculated by the equation

$$\Delta R_n^{nm} = \int_V \underline{B}^T E_t \, \Delta\varepsilon_n^{nm} \, dV \tag{4.3}$$

where $\underline{B}$ is the strain-displacement matrix, and E_t is the tangent modulus.

Physically, ΔR_n^{nm} can be obtained by the following procedure (4).

(1) Lock all the joints against displacements at time step t_{n-1}.

(2) Calculate the loads required at time step t_n to maintain all the joints locked by integrating the stresses produced by the restraint of the non-mechanical strains due to creep, shrinkage and temperature changes which would have occured during time steps t_{n-1} and t_n if the joints were free to displace.

(3) At time step t_n release all the joints and apply the opposite of the joint locking loads calculated above. In computing ΔR_n^{nm} by Eq. (4.3) the aging strain increment $\Delta\varepsilon_n^a$ should be excluded from $\Delta\varepsilon_n^{nm}$ since the aging strain does not cause actual physical straining, and can be considered as a correction factor for the calculation of the stress, as explained in section 2.2.3.

At time step t_n, load increment $\Delta \underset{\sim}{R}_n$ is obtained by adding external joint load increment ΔR_n^j and unbalanced load R_{n-1}^u left over from time step t_{n-1}, to the equivalent joint load increment ΔR_n^{nm} due to non-mechanical strains.

$$\Delta \underset{\sim}{R}_n = \Delta \underset{\sim}{R}_n^j + \Delta \underset{\sim}{R}_n^{nm} + \underset{\sim}{R}_{n-1}^u \qquad (4.4)$$

Then $\Delta \underset{\sim}{R}_n$ is divided into load increments $\Delta \underset{\sim}{R}$, each of which may not be of equal magnitude, for incremental load analysis and the unbalanced load iteration is performed for each load step as follows.

(1) Form tangent stiffness for each element based on current geometry and material properties. Assemble structure tangent stiffness $\underline{K}_t$ in global coordinates using current displacement transformation matrix for each element.

(2) Solve $\underline{K}_t \, \Delta \tilde{r} = \Delta \tilde{R}$ for displacement increments $\Delta \tilde{r}$ and transform into local coordinates to obtain element end displacement increments.

(3) Compute strain increment $\Delta\varepsilon$ from element end displacement increments by using nonlinear incremental strain-displacement relationship, and add to previous total to obtain current total strain ε.

(4) Add displacements $\Delta \tilde{r}$ to previous total to get current total joint displacements $\tilde{r}$. Based on current total displacements $\tilde{r}$, update member geometry, i.e. update element length and displacement transformation matrix.

(5) Subtract current total non-mechanical strain ε^{nm} due to creep, shrinkage and aging of concrete and temperature changes from current total strain ε to obtain current total mechanical strain ε^{m}. Compute current stress σ from nonlinear stress-strain (σ-ε^{m}) law valid for the present time step t_n, taking load reversals into account.

(6) Compute element end forces by integrating current total stresses for each element in local coordinates, and transform into global coordinates using updated displacement transformation matrices to assemble for the internal resisting loads $\tilde{R}^{i}$.

(7) Subtract internal resisting loads $\tilde{R}^{i}$ from current total external joint loads $\tilde{R}^{j}$ to obtain unbalanced loads $\tilde{R}^{u}$.

$$\tilde{R}^{u} = \tilde{R}^{j} - \tilde{R}^{i} \qquad (4.5)$$

(8) Set $\Delta \tilde{R} = \tilde{R}^{u}$, and go back to step (1). Steps (1)

to (8) are continued until unbalanced loads $\tilde{R}^u$ are within allowable tolerances. At this point the current unbalanced loads $\tilde{R}^u$ are added to the load increment $\Delta\tilde{R}$ for the next load step and the iterative procedure (1) to (8) is performed again. At the end of the final load step we proceed to next time step t_{n+1}.

4.4 Convergence Criteria

In solving the nonlinear equilibrium equations by iterative methods, the convergence at the end of an iteration can be measured by two criteria. The first criterion is the magnitude by which equilibrium is violated. This can be measured by the magnitude of the unbalanced loads. The second criterion is the accuracy of the total displacements. This can be measured by the magnitudes of additional displacement increments.

For this study the displacement criterion is used as a primary convergence criterion. But to guard against the excessive violation of equilibrium, the unbalanced load criterion is also provided. Two kinds of displacement tolerances are provided for this study. The first is the displacement ratio tolerance and the second is the displacement increment tolerance.

Displacement ratio to be compared with the displacement ratio tolerance is defined as follows. For each load step, search for two components of the displacement vector $\tilde{r}$, one with maximum absolute value of the displacement increment (here, the word displacement is used meaning translational displacement only), the other with maximum absolute value of the rotation increment, after the first iteration. Suppose jth component has the maximum displacement increment and kth component has the maximum rotation increment. Let r_j^i be the total displacement increment of the jth component after ith iteration and Δr_j^{i+1} be the displacement increment of the jth component for (i+1)th iteration (see Fig. 4.3.1). r_k^i and Δr_k^{i+1} are defined similarly for rotation increments. Calculate following ratios for displacement and rotation.

$$\rho_d = \left|\frac{\Delta r_j^{i+1}}{r_j^i}\right| \quad , \quad \rho_r = \left|\frac{\Delta r_k^{i+1}}{r_k^i}\right| \tag{4.6}$$

Then the displacement ratio ρ is defined by

$$\rho = \text{the larger of } \rho_d \text{ and } \rho_r \tag{4.7}$$

The displacement ratio ρ is compared with three convergence tolerances as follows.

(1) t_f (for final load step)

If $\rho \le t_f$, proceed to next time step.

If $\rho > t_f$, continue iteration.

(2) t_i (for intermediate load steps)

If $\rho \le t_i$, proceed to next load step

If $\rho > t_i$, continue iteration

(3) t_c (for changing stiffness)

If $\rho \le t_c$, use previously formed and triangularized stiffness for next iteration.

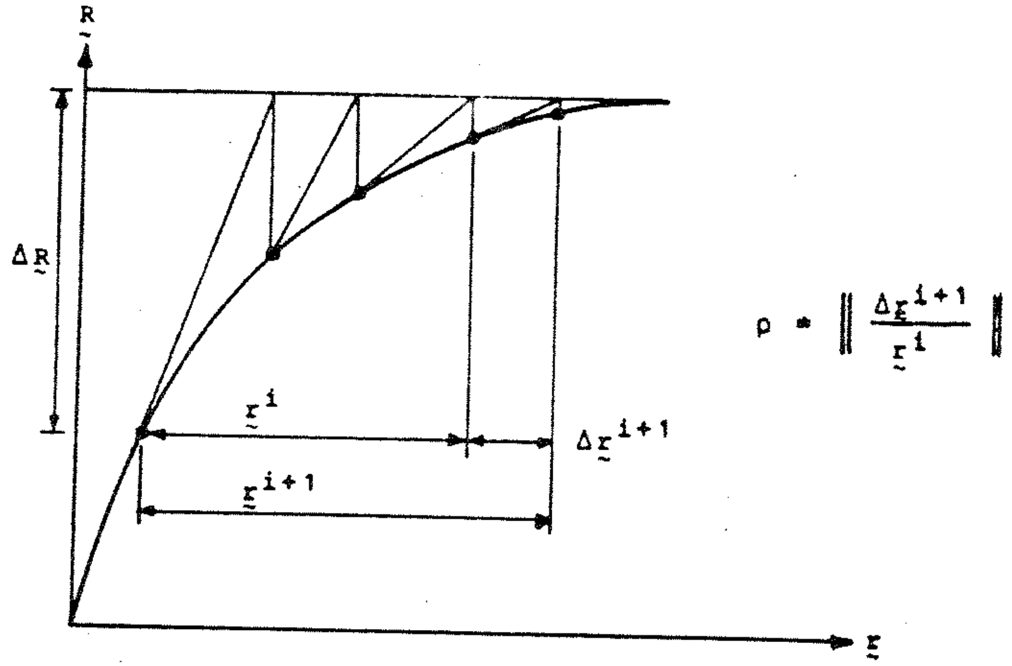

(a) Displacement Ratio Tolerance

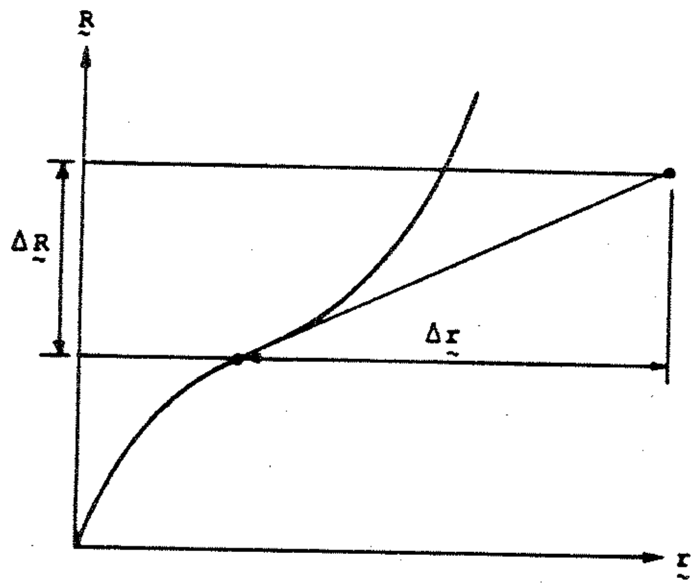

(b) Overshoot Due to Geometric Nonlinearity

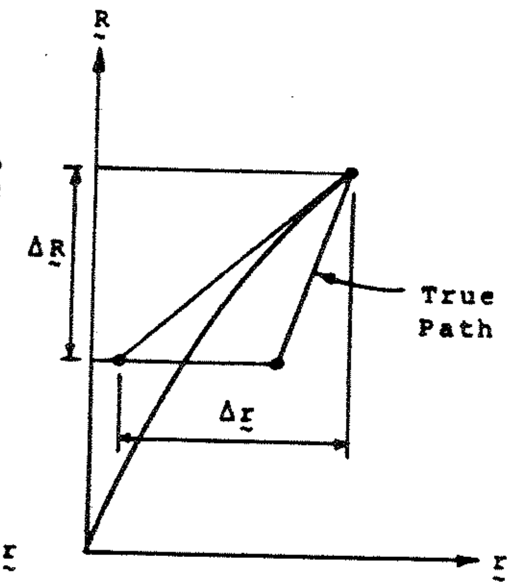

(c) Overshoot Due to Load Reversal

Fig. 4.3. Convergence Tolerances

If $\rho > t_c$, form new stiffness for next iteration.

By providing appropriate values of displacement ratio tolerances, we can obtain intermediate and final results to the desired degree of accuracy. And an appropriate choice of t_c allows us to use either the initial stiffness method or the tangent stiffness method for iterations.

To guard against unfavorable situations of the displacement overshoot which may occur in geometric nonlinear analysis (Fig. 4.3.b) or load reversal analysis with material nonlinearities (Fig. 4.3.c), maximum allowed values of the displacement increment (t_d) and the rotation increment (t_r) for each iteration are provided. Suppose the jth component of the displacement vector $\underset{\sim}{r}$ has the maximum displacement increment Δr_j, and kth component has the maximum rotation increment Δr_k for the current iteration.

(1) If $|\Delta r_j| > t_d$ and $|\Delta r_k| \leq t_r$, set

$\Delta r_i = \Delta r_i \times \left|\frac{t_d}{\Delta r_j}\right|$; $i = 1,2,\cdots,n$, where n is the number of degrees of freedom in the structure.

(2) If $|\Delta r_j| \leq t_d$ and $|\Delta r_k| > t_r$, set

$\Delta r_i = \Delta r_i \times \left|\frac{t_r}{\Delta r_k}\right|$; $i = 1,2,\cdots,n$

(3) If $|\Delta r_j| > t_d$ and $|\Delta r_k| > t_r$, set

$\Delta r_i = \Delta r_i \times$ (the smaller of $\left|\frac{t_d}{\Delta r_j}\right|$ and $\left|\frac{t_r}{\Delta r_k}\right|$) ; $i = 1,2,\cdots,n$

There is a possibility that equilibrium may be violated excessively even though the displacement convergence criterion is satisfied. To guard against such a case, a ceiling is provided for the maximum unbalanced load allowed for each iteration. t_l is the maximum unbalanced force, and t_m is the maximum unbalanced moment allowed for each iteration.

In addition to the convergence tolerances described above, a ceiling is provided to limit the number of iterations performed for each load step in case convergence tolerance provided are too stringent. n_i is the maximum number of iterations allowed for intermediate load steps, and n_f is the maximum number of iterations allowed for the final load step.

4.5 Numerical Examples

4.5.1 Time Dependent Analysis of a Concrete Prism

In order to demonstrate the time dependent analysis procedure a concrete prism having only one degree of freedom, shown in Fig. 4.4, is analyzed with simple numerical data. Joint load history and temperature history are given. Concrete is assumed linearly elastic both in compression and tension but the modulus is assumed to vary with time. shrinkage strain history and specific compliance curves for different loading ages are given. Four time steps are considered ; $t_1 = 10$, $t_2 = 20$, $t_3 = 30$, and $t_4 = 60$.

Creep is assumed to be temperature independent for simplicity in computations. Specific creep curves given in Fig. 4.4.e can be evaluated by

$$c(\tau,t-\tau) = \sum_{i=1}^{3} a_i(\tau)\,[1-e^{-10^{-i}(t-\tau)}]$$

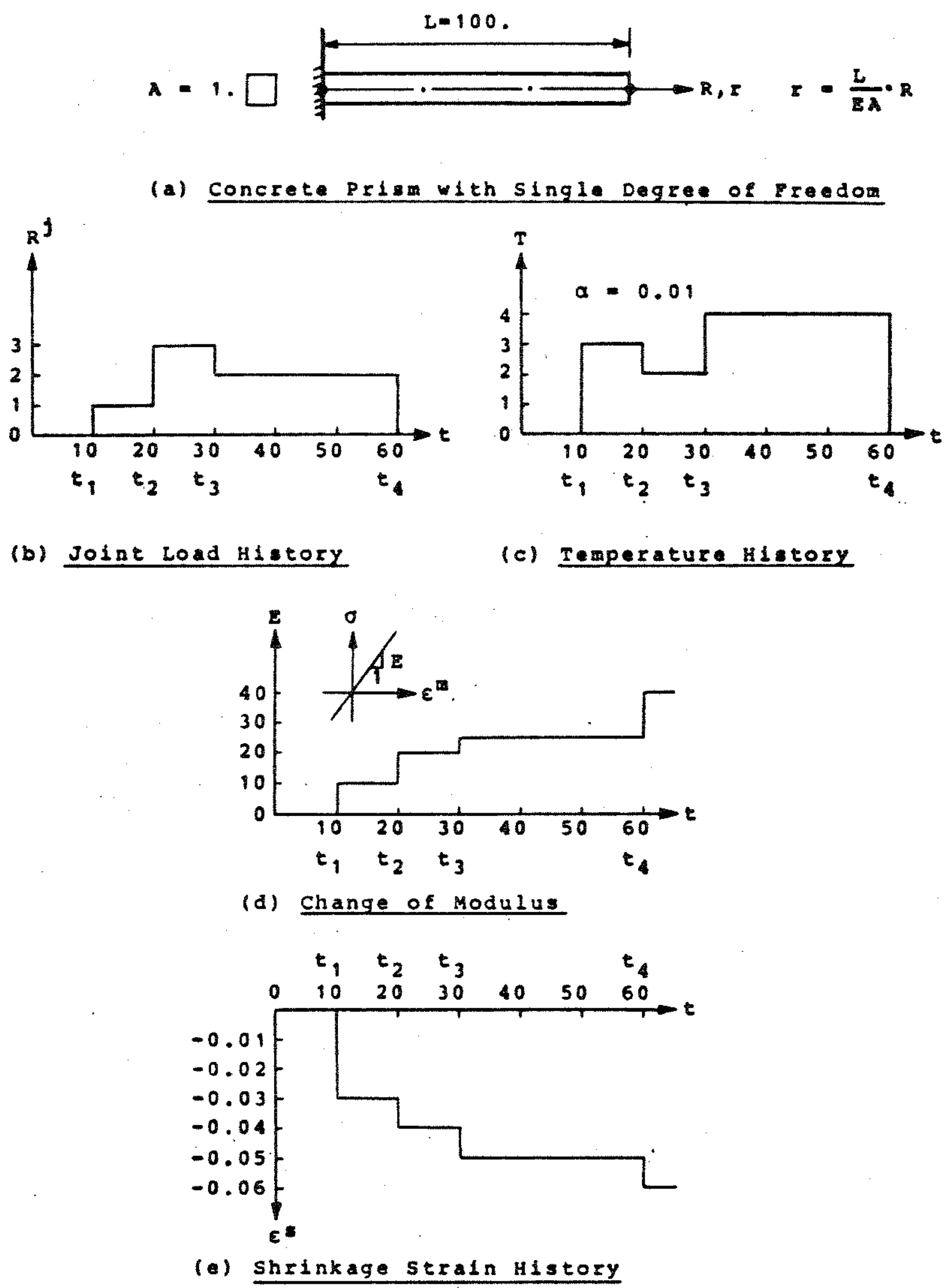

Fig. 4.4. Time Dependent Analysis of a Concrete Prism

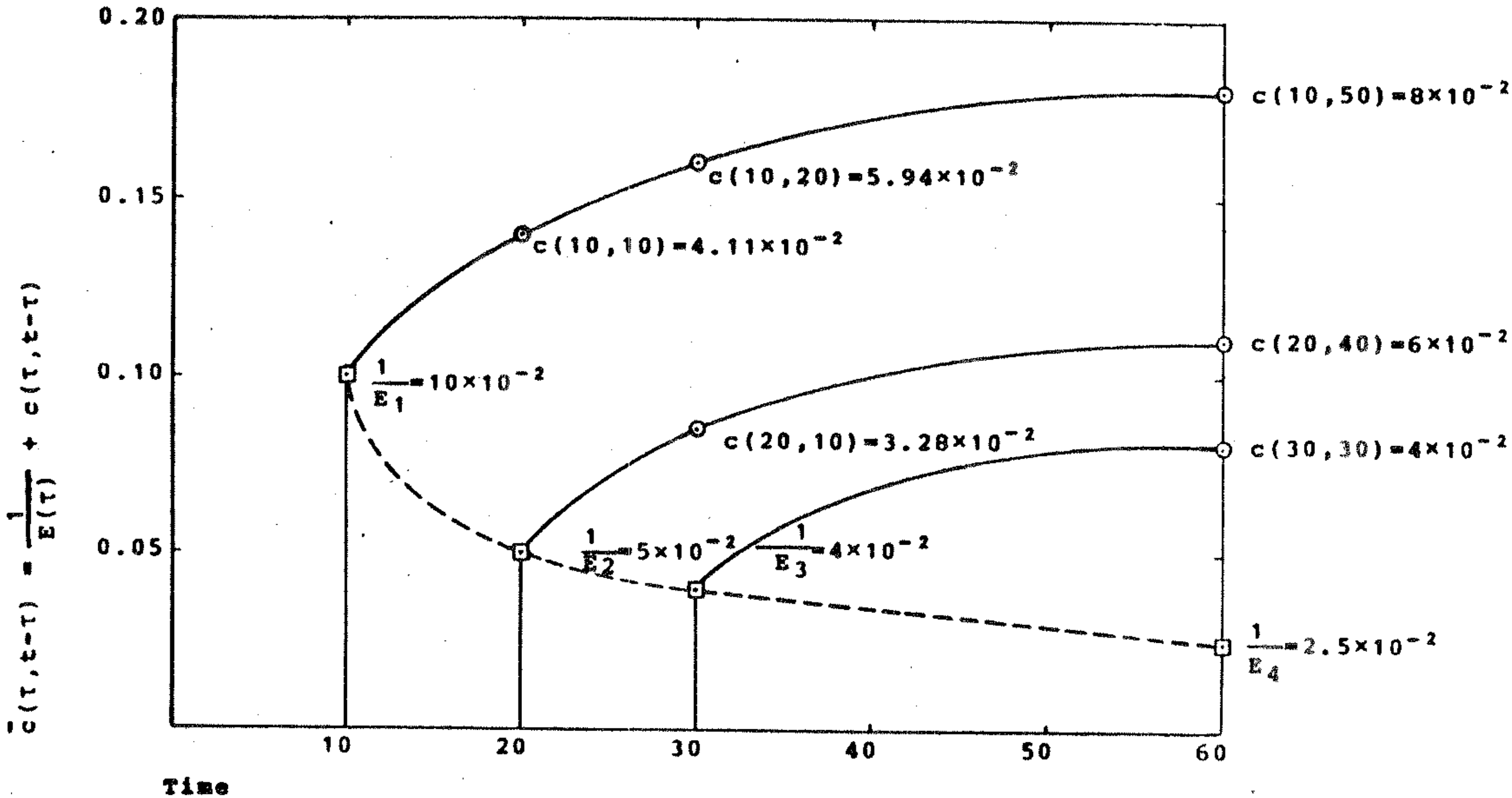

(f) Specific Compliance Curves for Different Ages

Fig. 4.4. Time Dependent Analysis of a Concrete Prism

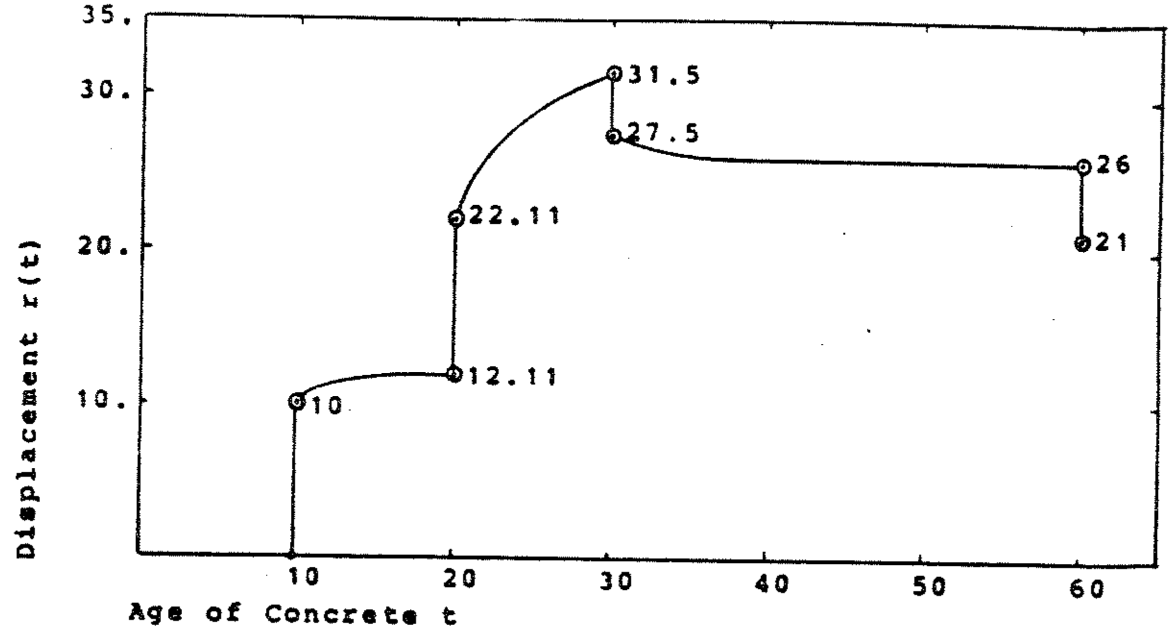

(a) Total Displacement

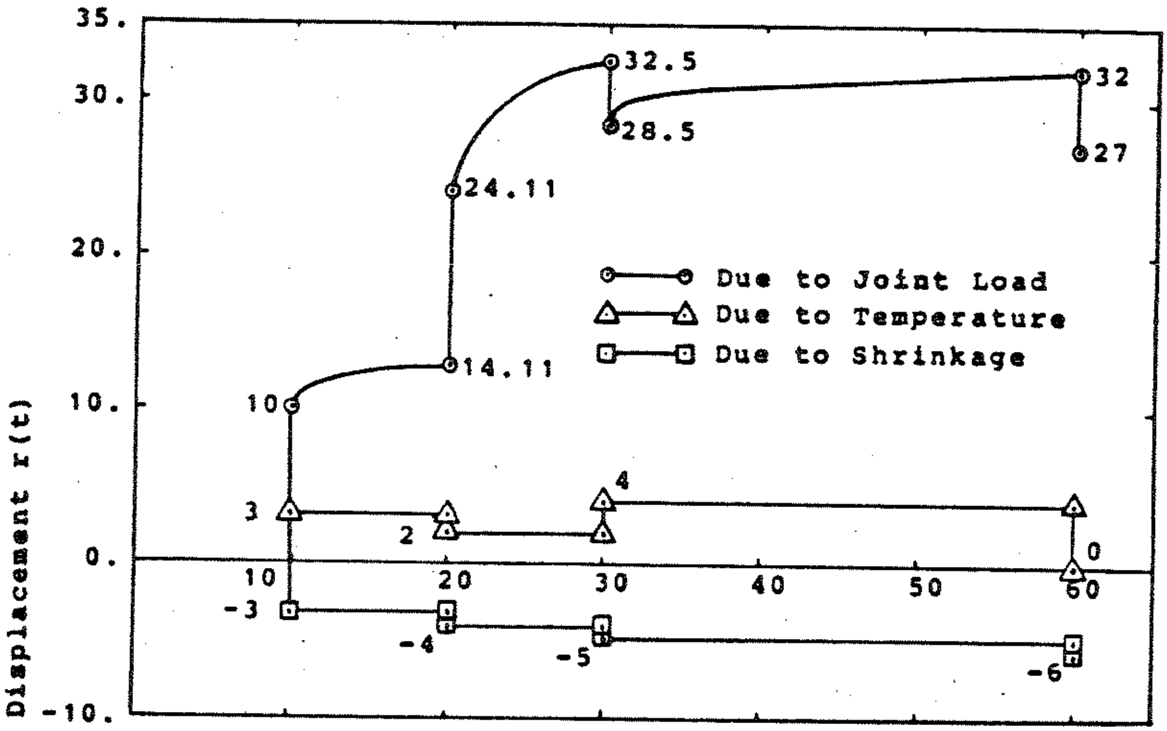

(b) Displacements Due to Joint Load, Temperature and Shrinkage

Fig. 4.5. Displacement History of a Concrete Prism

For this example it is assumed that $a_1 = a_2 = a_3$ at each loading age τ, and these values are chosen such that we can have simple numerical creep values at the last time step t_4. The values used are ; $a_i(10) = 5.57296 \times 10^{-2}$, $a_i(20) = 4.44255 \times 10^{-2}$, $a_i(30) = 3.22854 \times 10^{-2}$. Creep strains are evaluated by using Eq. (3.26) to (3.28) directly instead of using Eq. (3.32), (3.35) and (3.36) with $\phi(T) = 1$, which would give the same result.

The following sequence of computations are performed for each time step.

a. Calculate the incremental and total values of non-mechanical strains.

b. Calculate the load increment.

c. Calculate the incremental and total values of the displacement and the strain.

d. Calculate the stress.

(1) Analysis at time step 1, $t_1 = 10$.

a. $\varepsilon_1^c = 0.$; $\varepsilon_1^s = -3 \times 10^{-2}$; $\varepsilon_1^t = 3 \times 10^{-2}$; $\varepsilon_1^a = 0.$

$\varepsilon_1^{nm} = \varepsilon_1^c + \varepsilon_1^s + \varepsilon_1^t + \varepsilon_1^a = 0.$

b. $R_1^{nm} = E_1 A(\varepsilon_1^c + \varepsilon_1^s + \varepsilon_1^t) = 0.$; $R^j = 1.$

$R_1 = R_1^j + R_1^{nm} = 1.$

c. $r_1 = (L/E_1 A) \cdot R_1 = 10.$; $\varepsilon_1 = r_1/L = 10 \times 10^{-2}$

d. $\sigma_1 = E_1(\varepsilon_1 - \varepsilon_1^{nm}) = 1.$

(2) Analysis at time step 2, $t_2 = 20$.

a. $\varepsilon_2^c = \Delta\varepsilon_2^c = \sigma_1 \cdot c(t_1, t_2 - t_1) = 4.11 \times 10^{-2}$;

$\Delta\varepsilon_2^s = -1 \times 10^{-2}$; $\Delta\varepsilon_2^t = -1 \times 10^{-2}$

$\varepsilon_2^a = \Delta\varepsilon_2^a = \sigma_1(1/E_1 - 1/E_2) = 5 \times 10^{-2}$

$\Delta\varepsilon_2^{nm} = \Delta\varepsilon_2^c + \Delta\varepsilon_2^s + \Delta\varepsilon_2^t + \Delta\varepsilon_2^a = 7.11 \times 10^{-2}$

$\varepsilon_2^{nm} = \varepsilon_1^{nm} + \Delta\varepsilon_2^{nm} = 7.11 \times 10^{-2}$

b. $\Delta R_2^{nm} = E_2 A(\Delta\varepsilon_2^c + \Delta\varepsilon_2^s + \Delta\varepsilon_2^t) = 0.422$; $\Delta R_2^j = 2.$

$\Delta R_2 = \Delta R_2^j + \Delta R_2^{nm} = 2.422$

c. $\Delta r_2 = (L/E_2 A)\Delta R_2 = 12.11$; $r_2 = r_1 + \Delta r_2 = 22.11$

$\Delta\varepsilon_2 = \Delta r_2/L = 12.11 \times 10^{-2}$; $\varepsilon_2 = \varepsilon_1 + \Delta\varepsilon_2 = 22.11 \times 10^{-2}$

d. $\sigma_2 = E_2(\varepsilon_2 - \varepsilon_2^{nm}) = 3.$; $\Delta\sigma_2 = \sigma_2 - \sigma_1 = 2.$

(3) Analysis at time step 3, $t_3 = 30.$

a. $\varepsilon_3^c = \sigma_1 c(t_1, t_3 - t_1) + \Delta\sigma_2 c(t_2, t_3 - t_2) = 12.5 \times 10^{-2}$

$\Delta\varepsilon_3^c = \varepsilon_3^c - \varepsilon_2^c = 8.39 \times 10^{-2}$; $\Delta\varepsilon_3^s = -1 \times 10^{-2}$;

$\Delta\varepsilon_3^t = 2 \times 10^{-2}$

$\Delta\varepsilon_3^a = \sigma_2(1/E_2 - 1/E_3) = 3 \times 10^{-2}$

$\Delta\varepsilon_3^{nm} = \Delta\varepsilon_3^c + \Delta\varepsilon_3^s + \Delta\varepsilon_3^t + \Delta\varepsilon_3^a = 12.39 \times 10^{-2}$

$\varepsilon_3^{nm} = \varepsilon_2^{nm} + \Delta\varepsilon_3^{nm} = 19.5 \times 10^{-2}$

b. $\Delta R_3^{nm} = E_3 A(\Delta\varepsilon_3^c + \Delta\varepsilon_3^s + \Delta\varepsilon_3^t) = 2.3475$; $\Delta R_3^j = -1.$

$\Delta R_3 = \Delta R_3^j + \Delta R_3^{nm} = 1.3475$

c. $\Delta r_3 = (L/E_3 A)\Delta R_3 = 5.39$; $r_3 = r_2 + \Delta r_3 = 27.5$

$\Delta\varepsilon_3 = \Delta r_3/L = 5.39 \times 10^{-2}$; $\varepsilon_3 = \varepsilon_2 + \Delta\varepsilon_3 = 27.5 \times 10^{-2}$

d. $\sigma_3 = E_3(\varepsilon_3 - \varepsilon_3\ ) = 2.$; $\Delta\sigma_3 = \sigma_3 - \sigma_2 = -1.$

(4) Analysis at time step 4, $t_4 = 60.$

a. $\varepsilon_4^c = \sigma_1 \cdot c(t_1, t_4 - t_1) + \Delta\sigma_2 c(t_2, t_4 - t_2)$

$+ \Delta\sigma_3 c(t_3, t_4 - t_3) = 16 \times 10^{-2}$

$\Delta\varepsilon_4^c = \varepsilon_4^c - \varepsilon_3^c = 3.5 \times 10^{-2}$; $\Delta\varepsilon_4^s = -1 \times 10^{-2}$;

$\Delta\varepsilon_4^t = -4 \times 10^{-2}$

$\Delta\varepsilon_4^a = \sigma_3(1/E_3 - 1/E_4) = 3 \times 10^{-2}$

$\Delta\varepsilon_4^{nm} = \Delta\varepsilon_4^c + \Delta\varepsilon_4^s + \Delta\varepsilon_4^t + \Delta\varepsilon_4^a = 1.5 \times 10^{-2}$

$\varepsilon_4^{nm} = \varepsilon_3^{nm} + \Delta\varepsilon_4^{nm} = 21 \times 10^{-2}$

b. $\Delta R_4^{nm} = E_4 A(\Delta\varepsilon_4^c + \Delta\varepsilon_4^s + \Delta\varepsilon_4^t) = -0.6 \;;\; \Delta R_4^j = -2.$

$\Delta R_4 = \Delta R_4^j + \Delta R_4^{nm} = -2.6$

c. $\Delta r_4 = (L/E_4 A)\ R_4 = -6.5 \;;\; r_4 = r_3 + r_4 = 21.$

$\Delta\varepsilon_4 = \Delta r_4/L = -6.5 \times 10^{-2} \;;\; \varepsilon_4 = \varepsilon_4 + \Delta\varepsilon_4 = 21 \times 10^{-2}$

d. $\sigma_4 = E_4(\varepsilon_4 - \varepsilon_4^{nm}) = 0.$

Displacement histories due to the combined and separate effects of joint load, temperature and shrinkage are plotted in Fig. 4.5.

The results are checked with the solution obtained by the computer program developed for this study, RCFRAME. In the computer analysis the creep strain increment $\Delta\varepsilon_n^c$ is computed according to the procedure developed in section 3.3 using the Eq. (3.32), (3.35) and (3.36).

4.5.2 Geometric and Material Nonlinear Analysis of a Truss

A simple hypothetical truss structure is analyzed to demonstrate the combined effects of geometric and material nonlinearities by the computer program NTRUSS developed during the course of this investigation to study the nonlinear behavior of truss structures.

The truss consists of three elements, as shown in Fig. 4.6 and 4.7, among which only the middle element has nonlinear material properties like concrete, i.e. it cracks in tension and yields and crushes in compression as shown in the stress-strain diagram. The outer two elements have the same modulus as the middle element, but they behave linearly elastically both in compression and tension.

In Fig. 4.6 the load-deflection curve of the truss subjected to tension is plotted. After the middle element is cracked we notice the stiffening of the truss due to geometric nonlinearity.

Load-deflection curve of the truss subjected to compression is plotted in Fig. 4.7. After the middle element yields and crushes, the structure can be seen to be softening due to geometric nonlinearity.

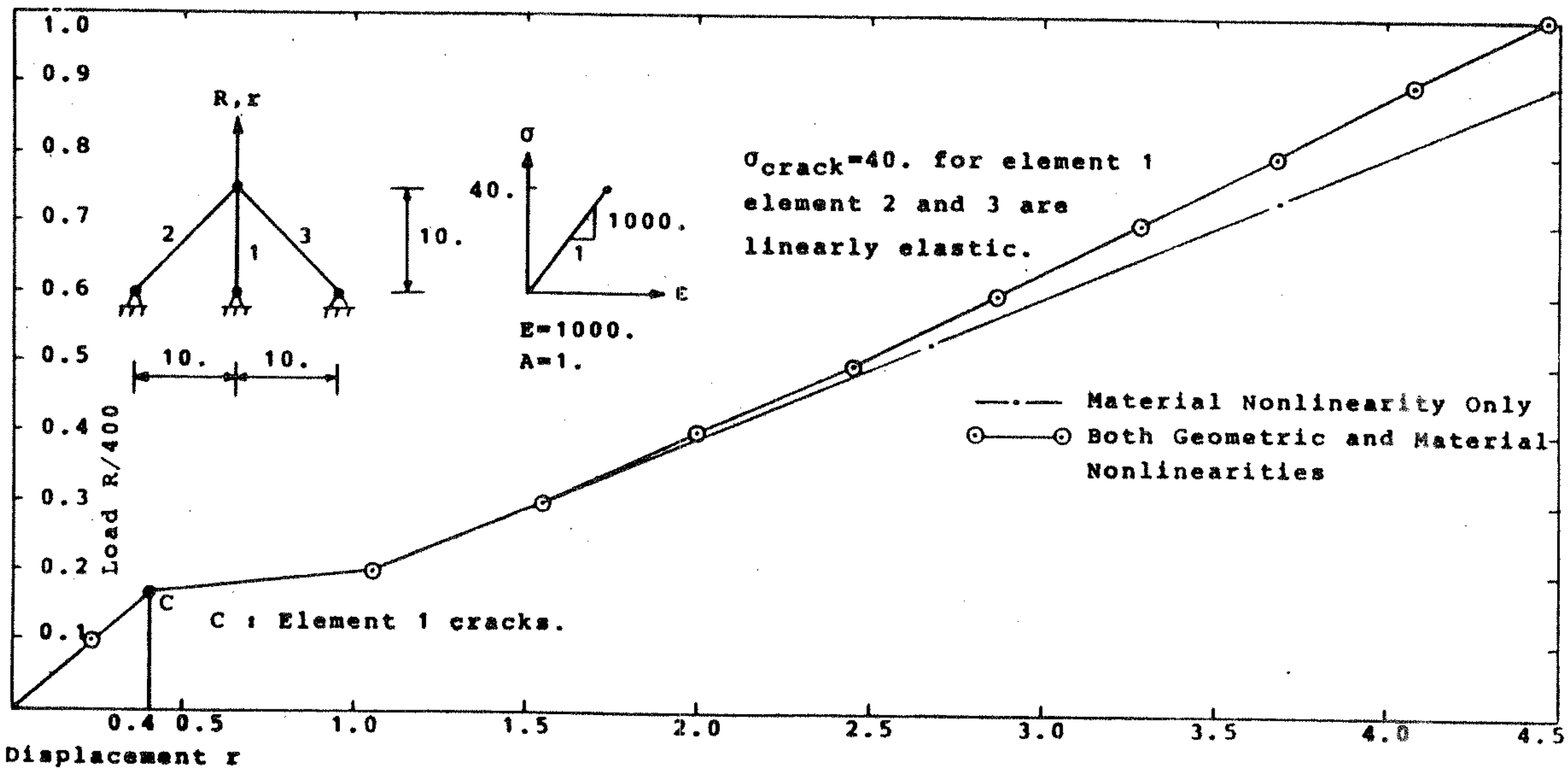

Fig. 4.6. A Truss Subjected to Tension

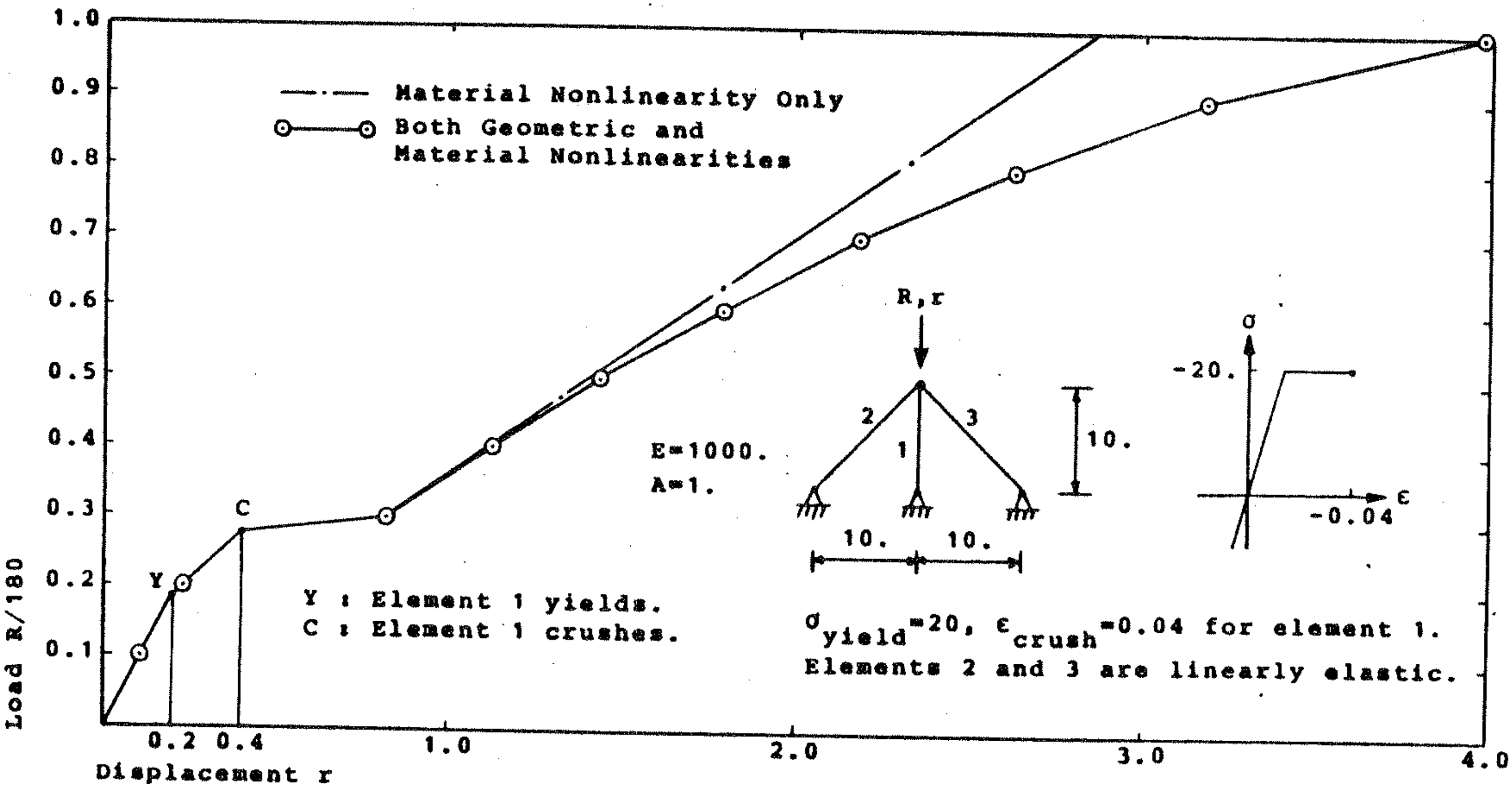

Fig. 4.7. A Truss Subjected to Compression

5. REINFORCED CONCRETE FRAMES

5.1 General Remarks

A general procedure for the geometric and material non-linear analysis of planar reinforced concrete frames including the time dependent effects of load history, temperature history, creep, shrinkage and aging of concrete was discussed in chapter 4 utilizing the mathematical model for material properties developed in chapters 2 and 3.

Detailed descriptions for the derivation of equilibrium equations, evaluation of tangent stiffness matrix and the calculation of internal forces will be given in this chapter based on the displacement formulation of the finite element method.

5.2 Definitions and Assumptions Regarding Geometry and Deformation

A typical planar reinforced concrete framed structure is shown in Fig. 5.1. The structure consists of elements interconnected by joints.

Each element is assumed to have a prismatic cross section which has an axis of symmetry. But the shape of the cross section may differ element by element.

Local coordinates x, y for each element are defined as follows. Let the two joints at the ends of an element be i and j. Joint i is the origin of the local coordinate system. Then the axis connecting the two joints i, j defines the x axis, and the axis perpendicular to the x axis in the plane

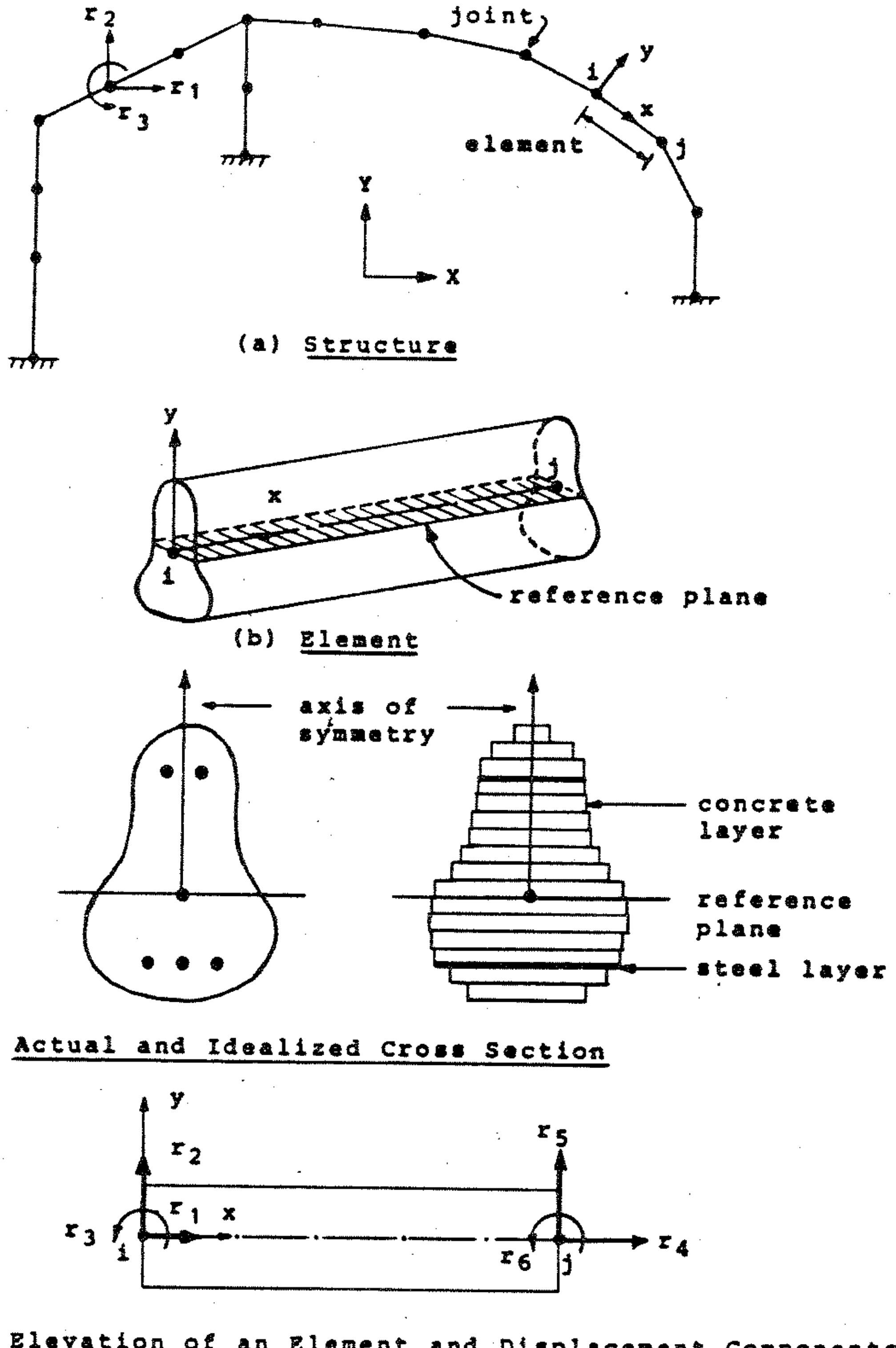

(a) Structure

(b) Element

(c) Actual and Idealized Cross Section

(d) Elevation of an Element and Displacement Components

Fig. 5.1. Geometry of a Planar Reinforced Concrete Frame

of the frame defines the y axis. The x axis need not coincide with the centroidal axis of the frame element. The reference plane of the element is defined as the plane containing the x axis and is also perpendicular to x-y plane. The y axis coincides with the axis of symmetry of the cross section.

Each element is divided into a discrete number of concrete and reinforcing steel layers. The geometry of each layer is defined by its cross sectional area and the distance from the reference plane.

Each joint has three degrees of freedom, i.e. two translational degrees of freedom and one rotational degree of freedom. The displacements of each joint can be defined either in the global coordinate system or the local coordinate system.

The global coordinate system X, Y is fixed in space, and is common for all elements. Equilibrium equations for the structure are set up and solved in this coordinate system.

Element properties such as the element stiffness matrix and the internal forces are formed in local coordinates for each element. However, the origin and the direction of this coordinate system are continuously changing according to the current locations of the two joints which vary as the structure deforms.

The cross section of an element is assumed to remain plane at all stages of loading and time. This implies that the deformation due to shearing stress is neglected.

Concrete and the reinforcing steel are assumed to be perfectly bonded together. This assumption makes the displacement field of the frame element continuous.

5.3 Derivation of Equilibrium Equations Including Geometric and Material Nonlinearities and Non-mechanical Strains

Displacement components of a frame element having six degrees of freedom are defined in Fig. 5.2.a in its local coordinate system. x-displacements, y-displacements and rotations of the two end joints, and all components of the joint displacements are represented by vectors $\underset{\sim}{u}$, $\underset{\sim}{v}$, and $\underset{\sim}{r}$ respectively.

$$\underset{\sim}{u} = \begin{Bmatrix} u_1 \\ u_2 \end{Bmatrix} \; ; \; \underset{\sim}{v} = \begin{Bmatrix} v_1 \\ v_2 \end{Bmatrix} \; ; \; \underset{\sim}{\theta} = \begin{Bmatrix} \theta_1 \\ \theta_2 \end{Bmatrix} \; ; \; \underset{\sim}{r} = \begin{Bmatrix} \underset{\sim}{u} \\ \underset{\sim}{v} \\ \underset{\sim}{\theta} \end{Bmatrix} \tag{5.1}$$

A non-dimensional parameter p is defined which represents the position along the axis of the frame element as follows.

$$p = x/L \tag{5.2}$$

Let $u_0(x)$ and $v(x)$ be the x-displacement and the y-displacement of any point along the frame axis respectively. Assume a linear variation of $u_0(x)$ and cubic variation of $v(x)$, then we can write

$$u_0(x) = \underline{\phi}\, \underset{\sim}{u} \tag{5.3}$$

$$\underline{\phi} = \langle (1-p), p \rangle \tag{5.4}$$

$$v(x) = \underline{\psi} \begin{Bmatrix} \underset{\sim}{v} \\ \underset{\sim}{\theta} \end{Bmatrix} \tag{5.5}$$

$$\underline{\psi} = \langle (1-3p^2+2p^3), (3p^2-2p^3), L(p-2p^2+p^3), L(-p^2+p^3) \rangle \tag{5.6}$$

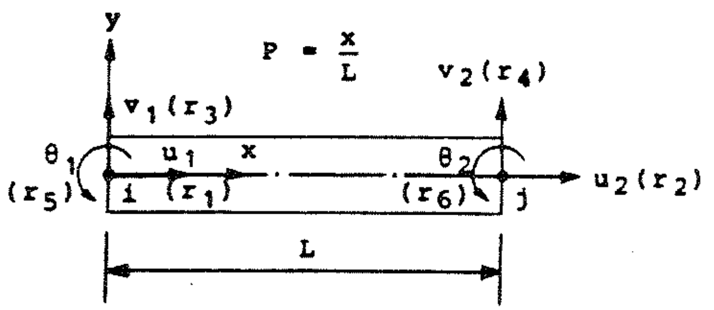

$$\underset{\sim}{u} = \langle u_1,\ u_2 \rangle^T$$

$$\underset{\sim}{v} = \langle v_1,\ v_2 \rangle^T$$

$$\underset{\sim}{\theta} = \langle \theta_1,\ \theta_2 \rangle^T$$

$$\underset{\sim}{r} = \begin{Bmatrix} \underset{\sim}{u} \\ \underset{\sim}{v} \\ \underset{\sim}{\theta} \end{Bmatrix}$$

(a) Displacements of a Frame Element

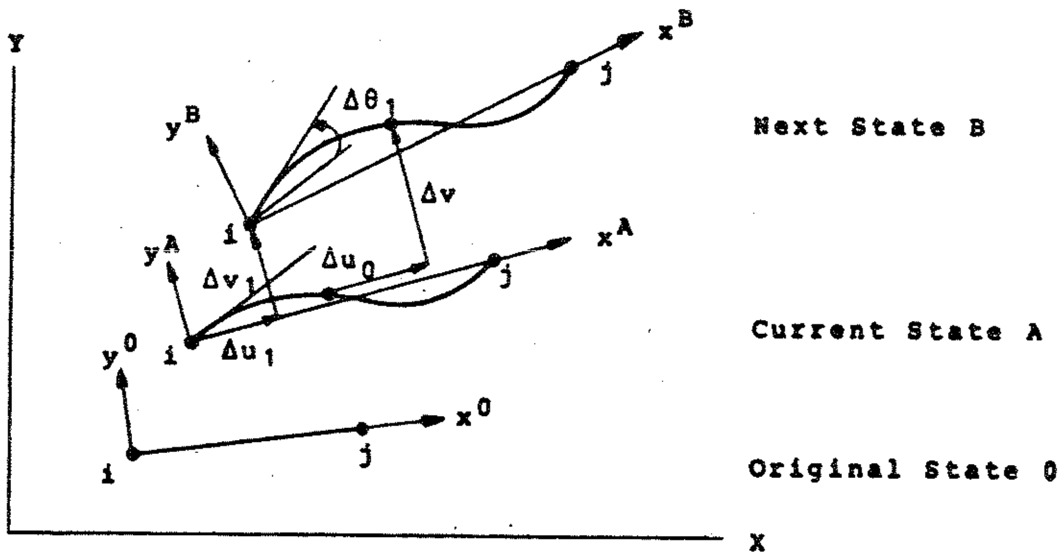

(b) Frame Element in Various States of Deformation

Fig. 5.2. Displacements and Deformations of a Frame Element

in which $\underline{\phi}$ and $\underline{\psi}$ are shape functions for $u_0(x)$ and $v(x)$ respectively.

Let $u(x,y)$ be the x-displacement of any point in the frame element. Then by the plane section assumption we can express $u(x,y)$ in terms of joint displacements as follows.

$$u(x,y) = u_0(x) - y\frac{dv(x)}{dx} = \underline{\phi}\,\underset{\sim}{u} - y\underline{\psi}_{,x}\begin{Bmatrix}\underset{\sim}{v}\\ \underset{\sim}{\theta}\end{Bmatrix} \tag{5.7}$$

$u(x,y)$ and $v(x)$ may be expressed in terms of $\underset{\sim}{r}$.

$$u(x,y) = \langle\underline{\phi}, -y\underline{\psi}_{,x}\rangle\,\underset{\sim}{r} \tag{5.8}$$

$$v(x) = \langle\underline{0}, \underline{\psi}\rangle\,\underset{\sim}{r} \tag{5.9}$$

Axial strain $\varepsilon(x,y)$ is defined by (102)

$$\varepsilon(x,y) = \frac{du(x,y)}{dx} + \frac{1}{2}\left(\frac{dv(x)}{dx}\right)^2 \tag{5.10}$$

in which the second term represents the nonlinear displacement effect.

In Fig. 5.2.b a frame element is shown in its various states of deformation. State O represents the original undeformed state. State A represents the current deformed state. And state B represents the next state from the current state A with the displacement increments $\Delta\underset{\sim}{r}$ and the deformation increments Δu and Δv. As the frame element deforms, we note that the origin and the direction of the local coordinates x,y, and the length of the element are continuously changing. Total, incremental and tangential equilibrium equations which are valid at the current state A will be developed. All the state variables are referred to the current state A, so that joint displacements, deformations, loads and internal forces are referred to the current local coordinates, and integrations are performed over the current element volume.

Consider a finite change in the joint displacements $\Delta\underset{\sim}{r}$ from the current state A, with corresponding changes in deformations Δu, Δv and the strain $\Delta\varepsilon$. From Eq. (5.8) to (5.10) the following expressions can be derived by replacing the total values with the incremental values.

$$\Delta u = \langle \underline{\phi},\ -y\underline{\psi}_{,x} \rangle\ \Delta\underset{\sim}{r} \tag{5.11}$$

$$\Delta v = \langle \underline{0},\ \underline{\psi} \rangle\ \Delta\underset{\sim}{r} \tag{5.12}$$

$$\frac{d\Delta u}{dx} = \langle \underline{\phi}_{,x},\ -y\underline{\psi}_{,xx} \rangle\ \Delta\underset{\sim}{r} \tag{5.13}$$

$$\frac{d\Delta v}{dx} = \langle \underline{0},\ \underline{\psi}_{,x} \rangle\ \Delta\underset{\sim}{r} \tag{5.14}$$

$$\Delta\varepsilon = \langle \underline{\phi}_{,x},\ -y\underline{\psi}_{,xx} \rangle\ \Delta\underset{\sim}{r} + \frac{1}{2}\Delta\underset{\sim}{r}^T \langle \underline{0},\ \underline{\psi}_{,x} \rangle^T \langle \underline{0},\ \underline{\psi}_{,x} \rangle\ \Delta\underset{\sim}{r} \tag{5.15}$$

The incremental strain-displacement relationship at the current state A represented by Eq. (5.15) may be rewritten

$$\Delta\varepsilon = \underline{B}\Delta\underset{\sim}{r} + \frac{1}{2}\Delta\underset{\sim}{r}^T\underline{c}^T\underline{c}\Delta\underset{\sim}{r}, \text{ where} \tag{5.16}$$

$$\underline{B} = \langle \underline{\phi}_{,x},\ -y\underline{\psi}_{,xx} \rangle \tag{5.17}$$

$$= \langle -\frac{1}{L}, \frac{1}{L}, \frac{6}{L^2}y(1-2p), \frac{6}{L^2}y(-1+2p), \frac{2}{L}y(2-3p), \frac{2}{L}y(1-3p) \rangle$$

$$\underline{c} = \langle \underline{0},\ \underline{\psi}_{,x} \rangle \tag{5.18}$$

$$= \langle 0, 0, \frac{6}{L}(-p+p^2), \frac{6}{L}(p-p^2), (1-4p+3p^2), (-2p+3p^2) \rangle$$

From Eq. (5.16), the tangential strain-displacement relationship at the state A is

$$d\varepsilon = \underline{B}d\underset{\sim}{r} \tag{5.19}$$

The virtual work equations at the state A can be written

$$d\bar{\underset{\sim}{r}}^T \underset{\sim}{R}^j = \int_V d\bar{\varepsilon}\sigma dV \tag{5.20}$$

where $\underset{\sim}{R}^j$ is the external joint load vector, $d\bar{\underset{\sim}{r}}$ and $d\bar{\varepsilon}$ are the virtual displacement vector and the corresponding virtual strain respectively, and σ is the current stress of the element. Note that the integration must be performed over the current volume of the element. By substituting Eq. (5.19) into Eq. (5.20), noting that $d\bar{\varepsilon} = d\bar{\underset{\sim}{r}}^T \underline{B}^T$, we obtain the total equilibrium equations at the state A.

$$\underset{\sim}{R}^j = \int_V \underline{B}^T \sigma dV \tag{5.21}$$

The tangential strain-displacement retationship at the next state B can be obtained by taking the differential from Eq. (5.16).

$$\begin{aligned} d\varepsilon &= \underline{B}d\underset{\sim}{r} + d\underset{\sim}{r}^T \underline{c}^T \underline{c}\Delta\underset{\sim}{r} \\ &= d\underset{\sim}{r}^T(\underline{B}^T + \underline{c}^T\underline{c}\Delta\underset{\sim}{r}) \end{aligned} \tag{5.22}$$

The virtual work equations at the state B can be written

$$d\bar{\underset{\sim}{r}}^T(\underset{\sim}{R}^j + \Delta\underset{\sim}{R}^j) = \int_V d\bar{\varepsilon}(\sigma+\Delta\sigma)dV \tag{5.23}$$

in which, as the joint displacements change by $\Delta\underset{\sim}{r}$, the stresses change to $(\sigma+\Delta\sigma)$ and the joint loads required to maintain the equilibrium change to $(R^j+\Delta R^j)$. By substituting Eq. (5.22) into Eq. (5.23) we obtain the total equilibrium equations at the state B.

$$\underset{\sim}{R}^j + \Delta \underset{\sim}{R}^j = \int_V (\underline{B}^T + \underline{c}^T \underline{c} \Delta \underset{\sim}{r})(\sigma + \Delta\sigma)\, dV \tag{5.24}$$

The incremental equilibrium equations at the state A are then obtained by subtracting Eq. (5.21) from Eq. (5.24) and neglecting the higher order term $\int_V \underline{c}^T \Delta\sigma \underline{c}\, dV \cdot \Delta \underset{\sim}{r}$.

$$\Delta \underset{\sim}{R}^j = \int_V \underline{B}^T \Delta\sigma\, dV + \int_V \underline{c}^T \sigma \underline{c}\, dV \cdot \Delta \underset{\sim}{r} \tag{5.25}$$

The tangential equilibrium equations can be obtained from Eq. (5.25) by replacing $\Delta \underset{\sim}{r}$ by $d\underset{\sim}{r}$, $\Delta \underset{\sim}{R}^j$ by $d\underset{\sim}{R}^j$ and $\Delta\sigma$ by $d\sigma$. The tangential stress-strain relationship for both concrete and the reinforcing steel can be written

$$d\sigma = E_t d\varepsilon^m = E_t (d\varepsilon - d\varepsilon^{nm}) \tag{5.26}$$

where $d\varepsilon^m$, $d\varepsilon$ and $d\varepsilon^{nm}$ are the infinitesimal increments of the mechanical strain, the total strain and the non-mechanical strain respectively, and E_t is the tangent modulus as defined in chapter 2. By substituting Eq. (5.19) for $d\varepsilon$ into Eq. (5.26),

$$d\sigma = E_t \underline{B} d\underset{\sim}{r} - E_t d\varepsilon^{nm} \tag{5.27}$$

Substitution of Eq. (5.27) into Eq. (5.25), after replacing the incremental operator Δ by the differential operator d, gives us the following tangential equilibrium equations at the current state A.

$$d\tilde{R}^{j} = \left(\int_V \underline{B}^T E_t \underline{B}\, dV + \int_V \underline{c}^T \underline{\sigma}\, \underline{c}\, dV\right) \cdot d\tilde{r} - \int_V \underline{B}^T E_t d\varepsilon^{nm} dV \qquad (5.28)$$

By defining the following terms

$$d\tilde{R}^{nm} = \int_V \underline{B}^T E_t d\varepsilon^{nm} dV \qquad (5.29)$$

$$d\tilde{R} = d\tilde{R}^{j} + d\tilde{R}^{nm} \qquad (5.30)$$

$$\underline{K}_e = \int_V \underline{B}^T E_t \underline{B}\, dV \qquad (5.31)$$

$$\underline{K}_g = \int_V \underline{c}^T \underline{\sigma}\, \underline{c}\, dV \qquad (5.32)$$

$$\underline{K}_t = \underline{K}_e + \underline{K}_g \qquad (5.33)$$

we can rewrite the Eq. (5.28)

$$d\tilde{R} = \underline{K}_t d\tilde{r} \qquad (5.34)$$

This is the desired form of the tangential equilibrium equations which are valid for the current geometry and material properties. $d\tilde{R}^{nm}$ is the equivalent load increment vector due to non-mechanical strains. The tangent stiffness $\underline{K}_t$ consists of the elastic stiffness $\underline{K}_e$ and the geometric stiffness $\underline{K}_g$. The elastic stiffness $\underline{K}_e$ represents the material nonlinearity and the geometric stiffness $\underline{K}_g$ represents the geometric nonlinearity since it originates from the nonlinear strain-displacement relationship in Eq. (5.10). But both of these stiffnesses are dependent on the current geometry because the integrations are performed over the current volume of the element.

5.4 Evaluation of the Tangent Stiffness Matrix

Numerical evaluation of the tangent stiffness $\underline{K}_t$, consisting of the elastic stiffness $\underline{K}_e$ and the geometric stiffness $\underline{K}_g$, and its transformation from the local element coordinates to the global coordinates will be discussed in this section.

To evaluate the elastic stiffness $\underline{K}_e$, decompose the strain-displacement matrix $\underline{B}$ into two parts, one associated with the axial force action, the other associated with the bending action, as follows.

$$\underline{B} = \langle \underline{\phi}_{,x},\ -y\underline{\psi}_{,xx} \rangle = \langle \underline{B}_a,\ -y\underline{B}_b \rangle \tag{5.35}$$

$$\underline{B}_a = \langle \underline{\phi}_{,x} \rangle = \frac{1}{L} \langle -1,\ 1 \rangle \tag{5.36}$$

$$\underline{B}_b = \langle \underline{\psi}_{,xx} \rangle = \frac{2}{L} \langle \frac{3}{L}(-1+2p), \frac{3}{L}(1-2p), (-2+3p), (-1+3p) \rangle \tag{5.37}$$

Then, from Eq. (5.31)

$$K_e = \int_V B^T E_t \underline{B} dV = \int_V \begin{bmatrix} \underline{B}_a^T E_t \underline{B}_a & -y\underline{B}_a^T E_t \underline{B}_b \\ -y\underline{B}_b E_t \underline{B}_a & y^2 \underline{B}_b^T E_t \underline{B}_b \end{bmatrix} dV = \begin{bmatrix} \underline{K}_{aa} & \underline{K}_{ab} \\ \underline{K}_{ba} & \underline{K}_{bb} \end{bmatrix} \tag{5.38}$$

Note that $\underline{B}_a$ is a constant matrix, $\underline{B}_b$ is a function of x only, while the tangent modulus E_t is a function of both x and y since the value of E_t varies along the length of the frame element as well as through its depth according to the strain state. Thus it is necessary to perform the integration in both x and y directions. However, if we assume that the values of E_t at the mid-length of the frame element represent the average value along its length, the integrations in Eq. (5.38) can be separated as follows.

$$\underline{K}_{aa} = \int_V \underline{B}_a^T E_t \underline{B}_a dV = \int_V E_t dA \cdot \int_0^L \underline{B}_a^T \underline{B}_a dx \tag{5.39}$$

$$\underline{K}_{ab} = \underline{K}_{ba}^T = \int_V -y \underline{B}_a^T E_t \underline{B}_b dV = -\int_V E_t y dA \cdot \int_0^L \underline{B}_a^T \underline{B}_b dx \tag{5.40}$$

$$\underline{K}_{bb} = \int_V y^2 \underline{B}_b^T E_t \underline{B}_b dV = \int_A E_t y^2 dA \cdot \int_0^L \underline{B}_b^T \underline{B}_b dx \tag{5.41}$$

Note that the exact evaluation of the tangent stiffness matrix is not a necessary requirement for the solution of the nonlinear equilibrium equations as discussed in chapter 4. Savings in the computation time due to this approximation well compensates the increased computation time for the increased number of iterations required to arrive at the equilibrium state.

The first integrals are evaluated at the mid-length of the frame element by a layer integration as follows.

$$EA = \int_A E_t dA = \sum_{i=1}^{n_c} E_{ci} A_{ci} + \sum_{i=1}^{n_s} E_{si} A_{si} \tag{5.42}$$

$$ES = -\int_A E_t y dA = -\sum_{i=1}^{n_c} E_{ci} y_{ci} A_{ci} - \sum_{i=1}^{n_s} E_{si} y_{si} A_{si} \tag{5.43}$$

$$EI = \int_A E_t y^2 dA = \sum_{i=1}^{n_c} E_{ci} y_{ci}^2 A_{ci} + \sum_{i=1}^{n_s} E_{si} y_{si}^2 A_{si} \tag{5.44}$$

where n_c and n_s are the number of concrete layers and reinforcing steel layers respectively, and the subscripts c and s represent the concrete and the reinforcing steel respectively.

The second integrals are evaluated analytically by integrating the shape functions.

$$\int_0^L \underline{B}_a^T \underline{B}_a dx = \frac{1}{L} \begin{bmatrix} 1 & -1 \\ -1 & 1 \end{bmatrix} \tag{5.45}$$

$$\int_0^L \underline{B}_a^T \underline{B}_b dx = \frac{1}{L} \begin{bmatrix} 0 & 0 & 1 & -1 \\ 0 & 0 & -1 & 1 \end{bmatrix} \tag{5.46}$$

$$\int_0^L \underline{B}_b^T \underline{B}_b dx = \frac{2}{L^3} \begin{bmatrix} 6 & -6 & 3L & 3L \\ & 6 & -3L & -3L \\ \text{sym.} & & 2L^2 & L^2 \\ & & & 2L^2 \end{bmatrix} \tag{5.47}$$

The elastic stiffness $\underline{K}_e$ can be expressed explicitly as follows combining Eqs. (5.38) to (5.47).

$$\underline{K}_e = \begin{bmatrix} \frac{EA}{L} & -\frac{EA}{L} & 0 & 0 & \frac{ES}{L} & -\frac{ES}{L} \\ & \frac{EA}{L} & 0 & 0 & -\frac{ES}{L} & \frac{ES}{L} \\ & & \frac{12EI}{L^3} & -\frac{12EI}{L^3} & \frac{6EI}{L^2} & \frac{6EI}{L^2} \\ & & & \frac{12EI}{L^3} & -\frac{6EI}{L^2} & -\frac{6EI}{L^2} \\ \text{sym.} & & & & \frac{4EI}{L} & \frac{2EI}{L} \\ & & & & & \frac{4EI}{L} \end{bmatrix} \tag{5.48}$$

The geometric stiffness $\underline{K}_g$ can be evaluated similarly at the mid-length of the frame element as follows.

$$\underline{K}_g = \int_V \underline{C}^T \sigma \underline{C} dV = \int_A \sigma dA \cdot \int_0^L \underline{C}^T \underline{C} dx = p \int_0^L \underline{C}^T \underline{C} dx \tag{5.49}$$

where p is the axial force of the frame element. By integrating the shape functions the geometric stiffness $\underline{K}_g$ is expressed explicitly as follows.

$$\underline{K}_g = \begin{bmatrix} 0 & 0 & 0 & 0 & 0 & 0 \\ & 0 & 0 & 0 & 0 & 0 \\ & & \frac{6p}{5L} & -\frac{6p}{5L} & \frac{p}{10} & \frac{p}{10} \\ & & & \frac{6p}{5L} & -\frac{p}{10} & -\frac{p}{10} \\ & \text{sym.} & & & \frac{2pL}{15} & -\frac{pL}{30} \\ & & & & & \frac{2pL}{15} \end{bmatrix} \qquad (5.50)$$

The same result has been derived by other investigators (103 ,104).

The element tangent stiffness matrix $\underline{K}_t$ is then obtained by adding $\underline{K}_e$ and $\underline{K}_g$. In order to form the structure tangent stiffness matrix, element tangent stiffness matrices have to be transformed from the local element coordinates to the global coordinates. For the assemblage of the structure stiffness matrix the numbering system for the displacement components shown in Fig. 5.1.c is used instead of that shown in Fig. 5.2.a. Then the transformation can be performed with the following equation.

$$\underline{K}_t^G = \underline{A}^T \underline{K}_t \underline{A} \qquad (5.51)$$

in which $\underline{K}_t$ is the element tangent stiffness in local coordinates, $\underline{K}_t^G$ is the element tangent stiffness in global coordinates and the coordinate transformation matrix $\underline{A}$ can be written as follows.

$$\underset{\sim}{A} = \begin{bmatrix} c & s & 0 & & & \\ -s & c & 0 & & 0 & \\ 0 & 0 & 1 & & & \\ & & & c & s & 0 \\ & 0 & & -s & c & 0 \\ & & & 0 & 0 & 1 \end{bmatrix} \qquad (5.52)$$

where $c = \cos\theta$, $s = \sin\theta$, and θ is the angle between the global and local coordinates, measured from the global X-axis to the local x-axis. It should be noted that the angle θ for the current state A has to be used here for each element.

After all the element tangent stiffnesses are transformed to the global coordinates, the structure tangent stiffness is assembled in a standard manner utilized in the direct stiffness method (1,2).

5.5 Calculation of Strains and Stresses

For each iteration in the course of the solution procedure discussed in chapt. 4, tangential equilibrium equations are solved for global displacement increments. For this study a symmetric banded equation solver utilizing Gaussian elimination procedure is used. The procedure for the calculation of the strain and the stress at any point in the frame element is outlined. In the following description all the state variables should be referred to the current state A in which displacement increments $\Delta\underset{\sim}{r}$ are not added yet.

(1) Transform global displacement increments $\Delta\underset{\sim}{r}^G$ to

local displacement increments $\tilde{\Delta r}$ for each element. The transformation is performed by the following equation.

$$\Delta \tilde{r} = \underline{A} \Delta \tilde{r}^G \tag{5.53}$$

where the transformation matrix $\underline{A}$ was defined by Eq. (5.52).

(2) Strain increment $\Delta\varepsilon$ at any point in the element is calculated by Eq. (5.16). Total strain ε is then obtained by adding $\Delta\varepsilon$ to the previous total.

(3) Mechanical strain ε^m is calculated by subtracting non-mechanical strain ε^{nm} from total strain ε. Non-mechanical strain ε^{nm} is due to the combined effects of creep, shrinkage, aging and temperature changes for concrete, and due to the effect of temperature changes for reinforcing steel.

(4) Stress σ is calculated by the nonlinear σ-ε^m curve given in chapter 2. For concrete, Eqs. (2.30) to (2.33) are used, and for reinforcing steel, Eqs. (2.34) to (2.36) are used.

The computation of strains and stresses described above is performed for each concrete and steel layer at 3 Gaussian quadrature points along the length of the element as explained in the next section.

5.6 Calculation of Internal Resisting Loads and the Equivalent Loads Due to Non-mechanical Strains

Internal resisting loads $\tilde{R}^i$, which can be defined as the loads required to hold the structure in equilibrium, is calculated by the total equilibrium Eq. (5.21) for each element.

$$\underset{\sim}{R}^{i} = \int_V \underline{B}^T \sigma dV \tag{5.54}$$

Equivalent load increments $\Delta\underset{\sim}{R}^{nm}$ due to the increments of non-mechanical strain $\Delta\varepsilon^{nm}$ are calculated by Eq. (5.29).

$$\Delta\underset{\sim}{R}^{nm} = \int_V \underline{B}^T E_t \Delta\varepsilon^{nm} dV \tag{5.55}$$

Unlike tangent stiffnesses, internal resisting loads have to be calculated as accurately as possible because the comparison between the internal resisting loads and the external joint loads form the basis of the equilibrium correction for the iterative nonlinear analysis procedure. For this reason both $\underset{\sim}{R}^{i}$ and $\Delta\underset{\sim}{R}^{nm}$ are evaluated by a 3-point Gaussian quadrature (95,96) combined with the layer integration.

Each component of the vector $\underset{\sim}{R}^{i}$ or $\Delta\underset{\sim}{R}^{nm}$ contains a function f(x) which is dependent on x only and a function g(x,y) which is dependent on both x and y, to be integrated over the volume of the element. The integration can be performed as follows.

$$\int_0^L f(x) \int_A g(x,y)\, dA dx = \frac{L}{2}\int_0^1 f(p) \int_A g(p,y)\, dA dp \tag{5.56}$$

$$= \frac{L}{2}\sum_{k=1}^{3} w_k f(p_k) h(p_k)$$

$$h(p_k) = \int_A g(p_k,y)\, dA \tag{5.57}$$

where three Gaussian integration points p_k are ; $p_1 = 0.5$, $p_2 = 0.112701665379258$, $p_3 = 0.887298334620742$, and the weights w_k are ; $w_1 = 8/9$, $w_2 = w_3 = 5/9$.

Six components of the internal resisting load vector $\underset{\sim}{R}^i$ or the equivalent load vector $\Delta\underset{\sim}{R}^{nm}$ due to non-mechanical strains shown in Fig. 5.3.a. Since these components of the load vector form a self equilibrating system of forces there are only three independent internal force components as shown in Fig. 5.3.b. S_1 is the moment at joint i, S_2 is the moment at joint j and S_3 is the axial force. Thus only these three components need to be calculated, and the other components are computed by the equilibrium requirements. The functions f(p) and g(p,y) for the calculation of the three internal forces S_1, S_2 and S_3 are tabulated below.

S	f(p)	g(p,y)	
		for $\underset{\sim}{R}^i$	for $\Delta\underset{\sim}{R}^{nm}$
S_1	$\frac{2}{L}(2-3p)$	$y\sigma$	$yE_t\Delta\varepsilon^{nm}$
S_2	$\frac{2}{L}(1-3p)$	$y\sigma$	$yE_t\Delta\varepsilon^{nm}$
S_3	$\frac{1}{L}$	σ	$E_t\Delta\varepsilon^{nm}$

The function $h(p_k)$ defined by Eq. (5.57) is evaluated by the layer integration for each Gaussian integration point p_k. For example,

$$\int_A y\sigma dA = \sum_{i=1}^{n_c} y_{ci}\sigma_{ci}A_{ci} + \sum_{i=1}^{n_s} y_{si}\sigma_{si}A_{si}$$

where n_c is the number of concrete layers, n_s is the number of steel layers.

Internal resisting load vector $\underset{\sim}{R}^i$ and the equivalent load vector $\Delta\underset{\sim}{R}^{nm}$ for each element are transformed to the

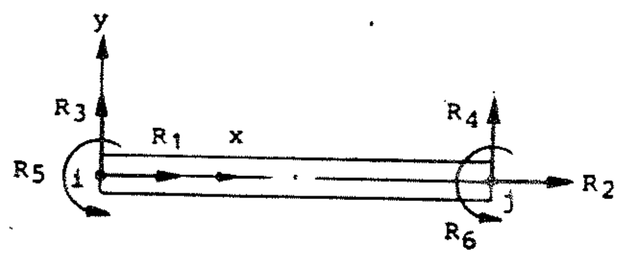

(a) Components of the Element Load Vector

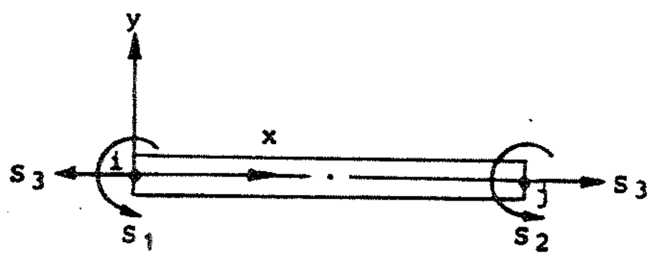

(b) Three Independent Internal Forces

Fig. 5.3. Internal Loads of a Frame Element

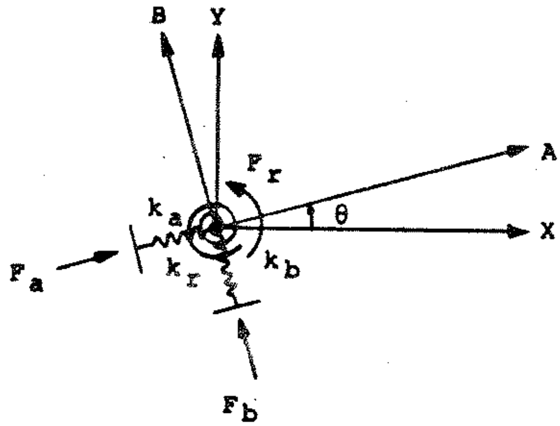

Fig. 5.4. Support Springs and Reactions

global coordinates by multiplying the transformation matrix $\underline{A}^T$ defined in Eq. (5.52), and assembled for the structure.

5.7 Treatment of Boundary Conditions and Calculation of Reactions

Boundary conditions at the support are specified by means of support springs. Two translational springs in orthogonal directions A and B and a rotational spring are provided for each support as shown in Fig. 5.4. Spring axes A and B form a rectangular Cartesian coordinate system which is rotated by an angle θ from the global coordinate system.

Spring stiffnesses k_a, k_b and k_r associated with these three springs are specified to simulate the boundary conditions at the support. For a zero displacement in the specific direction, a large value of spring stiffness corresponding to that direction is specified, and for a free displacement, zero value is specified for the spring stiffness.

Support spring stiffness matrix $\underline{K}_s$ may be written in A-B coordinates as follows.

$$K_s = \begin{bmatrix} k_a & 0 & 0 \\ 0 & k_b & 0 \\ 0 & 0 & k_r \end{bmatrix} \qquad (5.58)$$

spring stiffness matrix $\underline{K}_s^G$ in global coordinates can be obtained by

$$\underline{K}_s^G = \underline{A}^T \underline{K}_s \underline{A} \qquad (5.59)$$

in which the transformation matrix $\underset{\sim}{\Lambda}$ is given by

$$\underline{A} = \begin{bmatrix} c & s & 0 \\ -s & c & 0 \\ 0 & 0 & 1 \end{bmatrix} \tag{5.60}$$

where $c = \cos\theta$ and $s = \sin\theta$.

$\underline{K}_s^G$ for each support is added to the structure stiffness to solve for the displacements at each joint. The reactions $\underset{\sim}{F} = \langle F_a, F_b, F_r \rangle^T$ are then calculated by the equation

$$\underset{\sim}{F} = -\underline{K}_s \underset{\sim}{r} \tag{5.61}$$

in which $\underset{\sim}{r}$ is the displacement vector at the support in A-B coordinates.

In calculating the unbalanced load vector $\underset{\sim}{R}^u$ by Eq. (4.5), the support reactions have to be subtracted from the internal resisting load vector $\underset{\sim}{R}^i$ since the external joint load vector $\underset{\sim}{R}^j$ does not include the reactions.

5.8 Summary

Based on the nonlinear time dependent analysis procedure for planar frames described in chapter 4, detailed derivation of the equilibrium equations, tangent stiffness matrix and the procedure to compute strains, stresses, internal resisting loads, the equivalent loads due to non-mechanical strains and reactions is described in this chapter.

Total, incremental and tangential forms of equilibrium equations including material and geometric nonlinearities and the effects of non-mechanical strains are developed based on the "Updated Lagrangian" formulation for the description of motion. The expression for the tangential stiffness matrix, consisting of elastic and geometric components, which is valid for the current geometry and material properties is derived.

Numerical evaluation of the tangent stiffness matrix by the integration over concrete and steel layers at the center of each element is discussed. The integration is performed over the current length of the element using the current material properties of each concrete and steel layer. The transformation of the tangent stiffness matrix to the global coordinates is performed using current displacement transformation matrix for each element.

Computation of strains and stresses for each concrete and steel layer at 3 Gaussian quadrature points along the length of each element is discussed. Total strain ε is computed by accumulating the strain increments $\Delta\varepsilon$ for each iteration. $\Delta\varepsilon$ is computed by a nonlinear strain-displacement relationship from joint displacement increments $\Delta \tilde{r}$. Total non-mechanical strain ε^{nm} is computed by accumulating the increments $\Delta\varepsilon^{nm}$ for each time step. Total mechanical strain ε^{m} is obtained by subtracting ε^{nm} from ε. Stress σ is then computed by the currently valid stress-strain (σ-ε^{m}) relationship.

Internal resisting loads and the equivalent loads due to non-mechanical loads are evaluated by a layer integration through the depth of an element and 3 point Gaussian quadrature along the length of the element.

Finally the treatment of boundary conditions and the calculation of reactions by providing support springs are discussed.

6. PRESTRESSED CONCRETE FRAMES

6.1 General Remarks

Depending on the method of applying the prestress, prestressed concrete structures are classified into pre-tensioned and post-tensioned structures. In pre-tensioned structures the prestressing steel is tensioned against some abutments before the concrete is placed, and the prestress is transferred to the concrete after it has set by the bond between the concrete and the prestressing steel. In post-tensioned structures the prestress is transferred gradually to the concrete while the prestressing steel is tensioned against the hardened concrete, and anchored against it immediately after the tensioning operation. And depending on whether the prestressing steel is grouted or ungrouted after the tensioning operation, post-tensioned structures are further classified into bonded and unbonded structures.

In the analysis of prestressed concrete structures the variation of the stress in the prestressing steel during various stages of loading is an important factor since the behavior of prestressed concrete structures is largely dependent on the effective amount of prestress acting on them.
In pre-tensioned structures the prestress loss takes place before the transfer of prestress due to the shrinkage of concrete and the relaxation of prestressing steel ; at the transfer due to the elastic shortening of concrete ; and after the transfer due to the creep and shrinkage of concrete, the relaxation of prestressing steel and the effects of load history

and temperature history. In post- tensioned structures the prestress loss takes place during the tensioning operation due to the friction between the prestressing steel and the duct, and the anchorage slip ; and after the transfer of prestress due to the creep and shrinkage of concrete, the relaxation of prestressing steel and the effects of load history and temperature history.

In this study aim is taken at finding all the displacements, internal forces, stresses and strains for the concrete, reinforcing steel and the prestressing steel in the planar prestressed concrete frames subjected to load history and temperature history, at any time during their service lives by one complete analysis which includes both geometric and material nonlinearities and the time dependent effects of the creep, shrinkage and aging of concrete and the relaxation of prestressing steel. The nonlinear time dependent analysis procedure developed previously for reinforced concrete frames is employed with some modifications due to the distinct features present in prestressed concrete frames. In this chapter only those features distinct in prestressed concrete frames are discussed.

6.2 Definitions and Assumptions Regarding Geometry and Deformation

A typical planar prestressed concrete frame is shown in Fig. 6.1.a. In addition to the definitions and assumptions regarding the geometry and deformation of reinforced concrete frames given in chapter 5 the following definitions and as-

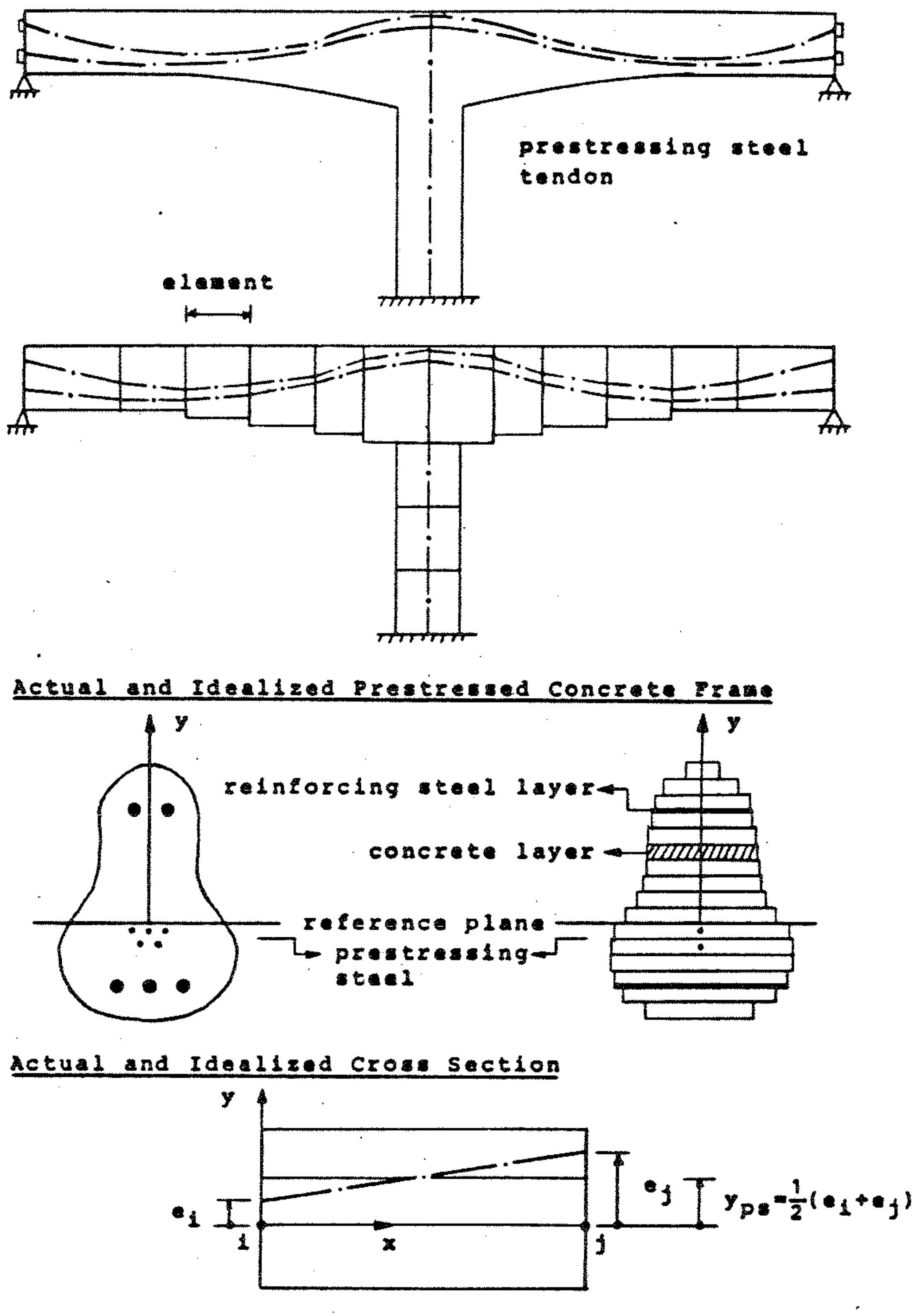

(a) Actual and Idealized Prestressed Concrete Frame

(b) Actual and Idealized Cross Section

(c) A Prestressing Steel Segment in an Element

Fig. 6.1. Geometry of a Planar Prestressed Concrete Frame

sumptions are used for prestressed concrete frames.

There is a discrete number of prestressing steel tendons in the frame. Each of these prestressing steel tendons has a given profile, initial tensioning force and a constant cross-sectional area along its length.

A prestressing steel tendon consists of a discrete number of prestressing steel segments each of which is straight, spans a frame element and assumed to have a constant force. The locations of the two end points of a prestressing steel segment in a frame elenent are defined by the eccentricities e_i and e_j as shown in Fig. 6.1.c. e_i and e_j are the distances of the two end points from the joints i and j respectively measured in the local y coordinate.

Perfect bond between the concrete and the prestressing steel is assumed for pre-tensioned structures and post-tensioned bonded structures. Thus the displacement field within an element of these structures is assumed to be continuous. The stiffness of the prestressing steel segment in an element for these structures is calculated as follows and added to the element stiffness. Assume the prestressing steel segment in an element is located at the depth of the mid-length of the segment parallel to the x-axis of the element and calculate its stiffness as if the segment is a steel layer having the distance from the reference plane, $y_{ps} = (e_i+e_j)/2$ as shown in Fig. 6.1.c.

6.3 Analysis of Pre-tensioned Frames

6.3.1 Analysis at the Transfer of Prestress

After the initial prestressing force is applied to the prestressing steel which is anchored to the abutments the concrete is formed and cured. Before the prestress is transferred to the concrete the following events occur.

(1) The stress in the prestressing steel is relaxed.

(2) The concrete and the prestressing steel are bonded together as the concrete hardens.

(3) Shrinkage of concrete takes place gradually.

To analyze the structure for these events assume that all the shrinkage of concrete take place at the time of the transfer after the stress in the prestressing steel is relaxed and the concrete and the prestressing steel is completely bonded together.

The analysis procedure is illustrated by a simple example shown in Fig. 6.2.a in which a concentrically pre-tensioned concrete prism with linearly elastic material properties is given. Let P_r be the force in the prestressing steel remaining just before the transfer after the relaxation has taken place from the initial prestressing force P_0. Let ε_c^s be the total free shrinkage of concrete up to transfer, then the equivalent load P^s acting on the composite prism due to ε_c^s is

$$P^s = E_c A_c \varepsilon_c^s \tag{6.1}$$

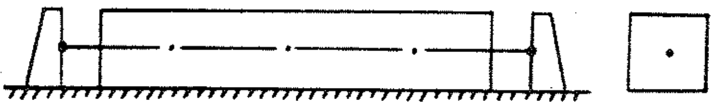

P_o = 180 kips

P_r = $0.97P_o$ = 174.6 kips

$E_c = 5\times10^3$ ksi

$E_s = 30\times10^3$ ksi

$A_c = 225$ in^2

$A_s = 1.2$ in^2

$$m = \frac{E_sA_s}{E_cA_c} = 0.032$$

$\varepsilon_c^s = -2\times10^{-4}$ up to transfer

(a) <u>Concentrically Pre-tensioned Concrete Prism with Given Data</u>

(b) <u>Equivalent Load Due to Shrinkage and Free Body Diagram</u>

$P^s = E_cA_c\varepsilon_c^s$

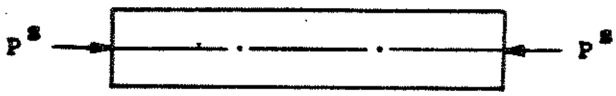

$$\Delta\varepsilon_1^s = \frac{P^s}{E_cA_s+E_sA_s} = \frac{1}{1+m}\,\varepsilon_c^s$$

$\Delta P_1^s = -E_sA_s\Delta\varepsilon_1^s$

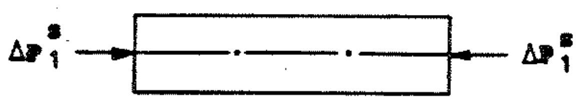

$$\Delta\varepsilon_2^s = \frac{\Delta P_1^s}{E_cA_c+E_sA_s} = -\frac{m}{(1+m)^2}\,\varepsilon_c^s$$

$\Delta P_2^s = -E_sA_s\Delta\varepsilon_2^s$

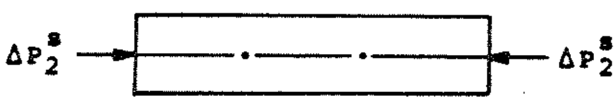

$$\Delta\varepsilon_3^s = \frac{\Delta P_2^s}{E_cA_c+E_sA_s} = -\frac{m^2}{(1+m)^3}\,\varepsilon_c^s$$

(c) <u>Iterative Method of Solution</u>

Fig. 6.2. <u>Shrinkage Analysis of a Concentrically Pre-tensioned Concrete Prism Before the Transfer of Prestress</u>

Let $\Delta\varepsilon^s$ be the amount of change in the strain of the composite concrete and steel prism due to the shrinkage ε_c^s. Then the corresponding decrease in the force for the prestressing steel embedded in the prism is

$$\Delta P^s = -E_s A_s \Delta\varepsilon^s \tag{6.2}$$

The force in the prestressing steel embedded in the prism is decreased by the amount ΔP^s, and the force in the prestressing steel between the prism and the abutments is increased by the amount ΔP^s as shown in the free body diagram in Fig. 6.2.b.

Then, the change in the strain of the composite prism, $\Delta\varepsilon^s$ can be calculated by applying the forces P^s and ΔP^s on the composite prism.

$$\Delta\varepsilon^s = \frac{P^s + \Delta P^s}{E_c A_c + E_s A_s} = \frac{E_c A_c \varepsilon_c^s - E_s A_s \Delta\varepsilon^s}{E_c A_c + E_s A_s} \tag{6.3}$$

Solving Eq. (6.3) for $\Delta\varepsilon^s$,

$$\Delta\varepsilon^s = \frac{\varepsilon_c^s}{1 + 2m} \tag{6.4}$$

in which $m = E_s A_s / E_c A_c$.

The axial force P_c for the concrete can be computed by

$$P_c = E_c A_c (\Delta\varepsilon^s - \varepsilon_c^s) = 2\Delta P^s \tag{6.5}$$

in which $\Delta\varepsilon^s$ represents the total strain and ε_c^s represents the non-mechanical strain due to shrinkage. By using Eq.

(6.4) and (6.2) P_c can be shown to be equal to $2\Delta P^s$ which checks the statics as shown in Fig. 6.2.b.

The analysis for the shrinkage is based on the solution of Eq. (6.3). However, for complex structures with nonlinear material properties it is generally impossible to set up such a nonlinear force-displacement relationship. In this case we may use the following iterative procedure as shown in Fig. 6.2.c.

(1) Apply $P^s = E_c A_c \varepsilon_c^s$ on the composite prism and calculate the corresponding strain $\Delta\varepsilon_1^s$.

(2) Since the prestressing steel connected to abutments is stretched by $-\Delta\varepsilon_1^s$, apply the corresponding force $\Delta P^s = -E_s A_s \Delta\varepsilon_1^s$ and calculate the corresponding strain increment $\Delta\varepsilon_2^s$.

(3) Now the prestressing steel connected to abutments is shortened by $-\Delta\varepsilon_2^s$, so apply the corresponding force $\Delta P_2^s = -E_s A_s \Delta\varepsilon_2^s$ and calculate the corresponding strain increment $\Delta\varepsilon_3^s$.

The desired strain $\Delta\varepsilon^s$ can be calculated by adding the increments obtained in the iterative process. By adding the results shown in Fig. 6.2.c

$$\Delta\varepsilon^s = \Delta\varepsilon_1^s + \Delta\varepsilon_2^s + \Delta\varepsilon_3^s + \cdots \tag{6.6}$$

$$= \frac{1}{1+m}\left[1 - \frac{m}{1+m} + \left(\frac{m}{1+m}\right)^2 - \cdots\right]\varepsilon_c^s$$

Note that the expression in brackets is a Taylor series expansion of $1/(1 + 1/(1+m)) = (1+m)/(1+2m)$, thus Eq. (6.6) converges to Eq. (6.4) which is the exact solution.

The first term in Eq. (6.6) represents the first order approximation to the exact solution, and the rest of the terms represent successive corrections. With numerical data given in Fig. 6.2.a the exact value of the loss of prestress ΔP^s due to shrinkage can be calculated by Eq. (6.2) and (6.4), which gives us $\Delta P^s = 6.767^k$. This represents the loss of 3.76% of the initial prestress $P_0 = 180^k$. The first order approximation which is obtained by applying P^s gives the value $\Delta P_1^s = 6.977^k$ which represents the loss of 3.88%. Note that the error involved by using the first order approximation represents only 0.12% of the initial prestress force. Thus it can be concluded that the first order approximation without subsequent corrections gives us an acceptable solution.

Then the analysis at the transfer of prestress can be performed in a single step by applying the following loads on the composite frame in which the stiffness of the prestressing steel is included.

(1) Joint loads due to the prestressing force P_r existing at the time of the transfer after the relaxation has taken place. The calculation of P_r is discussed in section 6.6 and the calculation of the joint loads due to P_r is discussed in section 6.5.

(2) Joint loads due to the shrinkage of concrete up to the time of the transfer.

(3) Dead load of the frame. Dead load is applied at transfer since most of the frames are eccentrically

prestressed and will hog upward at transfer.

6.3.2 Analysis after the Transfer of Prestress

After the transfer of prestress the composite frame, in which the stiffness due to the prestressing steel is included, is analyzed for various time dependent loads due to live load history, temperature history, and the creep, shrinkage and aging of concrete by the procedure developed previously for reinforced concrete frames. Calculation of the strain and the stress for the prestressing steel and the contribution of the prestressing steel to the element loads are discussed in section 6.7.

6.4 Analysis of Post-tensioned Frames

6.4.1 Analysis at the Transfer of Prestress

For post-tensioned structures the prestress is transferred to the concrete gradually during the tensioning operation. As the prestressing force is applied from the tensioning end with the initial force P_0 as shown in Fig. 6.3.a friction takes place between the prestressing steel and the duct, resulting in the gradual decrease in the prestressing force away from the tensioning end. The decrease in the prestressing steel force due to the friction can be calculated by the formula (105)

$$P_2 = P_1 e^{-(\mu\theta+KL)} \qquad (6.7)$$

Referring to Fig. 6.3.b

P_1 = Prestressing force at point 1

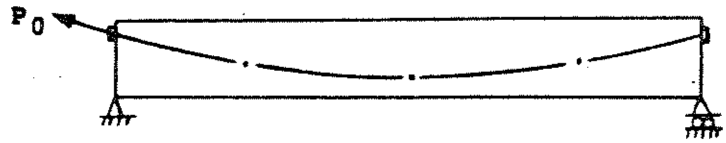

(a) Post-tensioned Beam with Initial Prestressing Force P_0

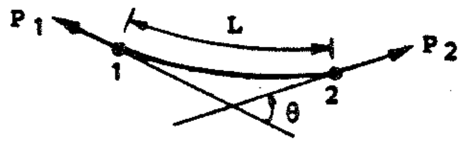

(b) Variation of the Prestressing Steel Force Due to Friction

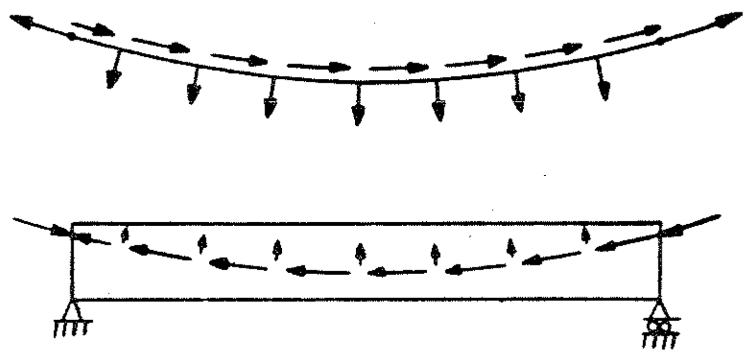

(c) Free Body Diagrams of the Prestressing Steel and the Concrete Beam

Fig. 6.3. Analysis of a Post-tensioned Beam at Transfer

P_2 = Prestressing force at point 2

L = Length of the prestressing steel segment

θ = Change in the slope of the prestressing steel segment in radians assumed to be uniformly distributed over the length L

μ = Curvature friction coefficient

K = Wobble friction coefficient

With Eq. (6.7) we can calculate the prestressing force at any point along the tendon by starting from the tensioning end with given initial tensioning force P_0.

Since each prestressing steel segment is assumed to be straight and have a constant force, the force in a specific prestressing steel segment is taken as the average of the forces at the two end points of the segment.

When there is an anchorage slip by an amount ΔL at the tensioning end, it is assumed that uniform decrease in the strain by the amount of $\Delta L/L$, where L is the length of the prestressing steel tendon, takes place throughout the tendon, and the force in each of the prestressing steel segments is subtracted by the corresponding decrease in the force $EA\Delta L/L$.

Fig. 6.3.c shows free body diagrams of the prestressing steel tendon and the concrete frame at transfer, in which interacting forces between the prestressing steel and the concrete can be observed. Then the analysis procedure at transfer can be summarized as follows.

(1) Calculate the prestressing segment end forces by Eq. (6.7) by starting from the tensioning end with

given initial tensioning force for each prestressing steel tendon.

(2) Calculate each prestressing steel segment force by averaging two segment end forces.

(3) Subtract the loss due to anchorage slip from each of the prestressing steel segment forces.

(4) Calculate the joint loads due to prestress by a procedure described in section 6.5.

(5) Analyze the plain or reinforced concrete frame, in which the stiffness of the prestressing steel is not included, for the joint loads due to prestress and the dead load.

6.4.2 Analysis after the Transfer of Prestress for Bonded and Unbonded Frames

After the transfer of prestress the prestressing steel in the duct is grouted for bonded frames and left ungrouted for unbonded frames.

For bonded frames the displacement field in a frame element is continuous, so that the composite structure, in which the stiffness of the prestressing steel is included, is analyzed for various time dependent loads after transfer.

For unbonded structures the displacements and strains of the concrete and the prestressing steel are independent except at anchorage points, and there is an interaction between the concrete and the prestressing steel due to friction. To illustrate the basic procedure for the analysis of unbonded structures a simple beam with an unbonded straight eccentric prestressing steel shown in Fig. 6.4.a is analyzed. The material properties are assumed to be linearly elastic and no friction is taken into account for simplicity.

Let ΔP be the increase in the prestressing steel force due to the live load w. The corresponding increase in the steel strain is $\Delta P/E_sA_s$ assuming that the steel strain increase is uniform throughout the tendon and the effect of the friction between the prestressing steel and the duct is neglected. This strain increase for the steel is equal to the strain increase for the concrete at the steel level which is obtained by applying the following end moments and forces to the concrete beam as shown in Fig. 6.4.a.

(1) Average bending moment of $\frac{2}{3}M_o$ where M_o is the maximum bending moment at the midspan due to w.

(2) Eccentric compression Δp at the steel level.

Equating the strain increase for the steel and the concrete at the steel level

$$\frac{\Delta P}{E_sA_s} = \frac{2}{3}M_o \cdot \frac{e}{E_cI_c} - \frac{\Delta P}{E_cA_c} - \frac{\Delta Pe^2}{E_cI_c} \qquad (6.8)$$

Solving for ΔP

$$\Delta P = \frac{2}{3}M_o \cdot \frac{me}{r^2} \cdot \frac{1}{1+m(1+e^2/r^2)} \qquad (6.9)$$

in which the parameter m and the radius of gyration r are defined in Fig. 6.4.a.

However, we cannot always set up the equation for ΔP for

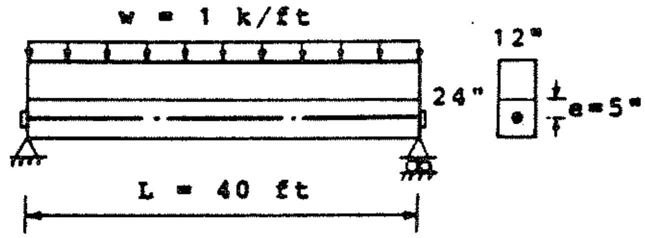

$E_c = 5 \times 10^3$ ksi

$E_s = 30 \times 10^3$ ksi

$A_c = 288$ in^2

$A_s = 2.5$ in^2

$I_c = 13{,}824$ in^4

$r^2 = I_c/A_c = 48$ in^2

$m = \dfrac{E_s A_s}{E_c A_c} = 0.052$

P = 300 kips after transfer

$M_0 = wL^2/8 = 200$ ft·k at midspan

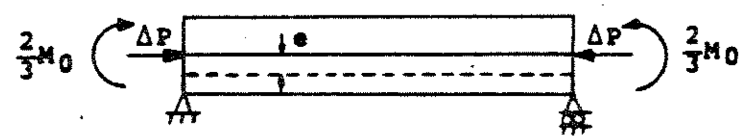

(a) An Unbonded Simple Beam Example with Given Data

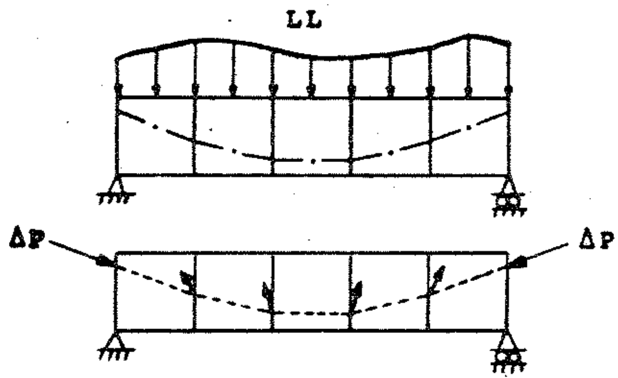

(b) Analysis of an Unbonded Frame Neglecting Friction

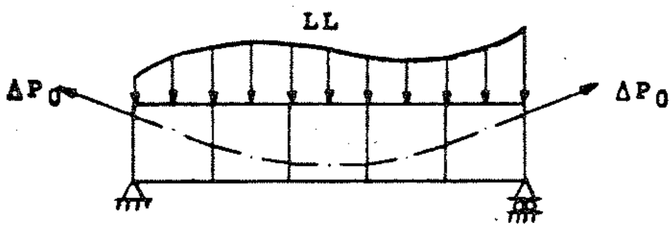

(c) Analysis of an Unbonded Frame Including Friction

Fig. 6.4. Analysis of Unbonded Frames

complex structures with nonlinear material properties. The following iterative procedure, similar to the procedure for the shrinkage analysis of pre-tensioned frames before transfer, in which the solution is given by a series each term of which represents a successive correction to the previous solution, can be used for general structures.

(1) Apply w on the concrete beam. The average strain increase at the steel level is

$$\Delta\varepsilon_1 = \frac{2}{3}M_o \cdot \frac{e}{E_c I_c} = \frac{2}{3}M_o \cdot \frac{me}{r^2 E_s A_s}$$

The corresponding increase in the steel force is

$\Delta P_1 = E_s A_s \Delta\varepsilon_1$.

(2) Apply $-\Delta P_1$ on the concrete beam at the steel level. The resulting strain change is

$$\Delta\varepsilon_2 = -\left(\frac{\Delta P_1}{E_c A_c} + \frac{\Delta P_1 e^2}{E_c I_c}\right) = -\frac{\Delta P_1 m}{E_s A_s}\left(1+\frac{e^2}{r^2}\right)$$

The corresponding change in the steel force is

$\Delta P_2 = E_s A_s \Delta\varepsilon_2$.

(3) We could go on by applying the next correction force $-\Delta P_2$, and so forth for a more rigorous solution.

The change in the steel force ΔP is obtained by

$$\Delta P = \Delta P_1 + \Delta P_2 + \Delta P_3 + \cdots \quad (6.10)$$

$$= \frac{2}{3}M_o \cdot \frac{me}{r^2}\left[1 - m\left(1+\frac{e^2}{r^2}\right) + m^2\left(1+\frac{e^2}{r^2}\right)^2 - \cdots\right]$$

Eq. (6.10) represents a Taylor series expansion of Eq. (6.9). Thus step (1) in the iterative procedure represents a first order approximation and step (2) represents a second order approximation to the true solution. With the numerical values given in Fig. 6.4.a

$\Delta P = 8.032^k = 2.68$ percent of P

$\Delta P_1 = 8.667^k = 2.89$ percent of P

$\Delta P_1 + \Delta P_2 = 7.982^k = 2.66$ percent of P

The error for taking ΔP_1 is 0.21 percent of the total prestressing force P and that for taking $\Delta P_1 + \Delta P_2$ is only 0.02% of P. Thus we can conclude that it is quite acceptable to take the first order approximation and taking the second order approximation may be too rigorous.

The procedure described above can be generalized to analyze general unbonded frames for any time dependent load assuming that the changes in the strain and the force for the prestressing steel are uniform throughout the tendon by neglecting the friction between the prestressing steel and the duct. Refer to Fig. 6.4.b.

(1) Analyze the concrete frame excluding the stiffness of the prestressing steel for any live load LL. The average change in the steel strain $\Delta\varepsilon$ can be calculated by $\Delta\varepsilon = \Sigma\Delta L/\Sigma L$ where the summation is made for each prestressing steel segment. The corresponding average increase in the prestressing steel force is given by $\Delta P = E_s A_s \Delta\varepsilon$. This step represents the first order approximation.

(2) Analyze the concrete frame for the forces induced by the increase in the steel force ΔP and calculate

the corresponding changes in the steel strain and force.

(3) Superpose the results of steps (1) and (2) for the second order approximation.

If we want to take the friction between the unbonded steel and the duct into account we can proceed as follows. Refer to Fig. 6.4.c.

(1) Analyze the concrete frame for the live load LL and calculate the total elongation ΔL of the tendon. The problem here lies in the fact that the distribution of the steel force increase along the tendon cannot be determined easily. Assume that this distribution can be determined by applying the equivalent tensioning force ΔP_o at both anchorage points A and B. The equivalent tensioning force ΔP_o can be determined by an iterative method such that it produces the total elongation ΔL for the tendon including the effect of friction as in the tensioning operation. Once ΔP_o is determined we can calculate the distribution of the steel forces along the tendon.

(2) For the second order approximation, analyze the concrete for the forces induced by the increase in the steel force and calculate the corresponding changes in the steel strain and force, and superpose the results obtained in step (1).

It can be shown that the difference between the results obtained by including and excluding the effect of the friction is very small.

6.5 Calculation of the Load Vector Due to Prestress at Transfer

For pre-tensioned frames the prestressing steel tendon is usually straight and has a constant force. In this case the transfer of prestress takes place by the concentrated compression at the two end points of the tendon. But sometimes harped tendons are used to get the desired eccentricity. At harped points the tendon is connected to the prestressing bed and the connection is removed at transfer. Thus concentrated forces are applied to the concrete at the harped points.

In post-tensioned frames the prestressing steel tendon generally has a curved profile. This profile is approximated by a series of straight prestressing steel segments each of which is assumed to have a constant force.

The assumption that each prestressing steel segment has a constant force implies that the interaction between the prestressing steel and the concrete takes place only at the end points of the prestressing steel segments. Fig. 6.5 shows a typical frame element in which a prestressing steel segment AB with a force P is embedded. Application of the opposite of the prestressing force P at two end points A and B represents the interaction between the prestressing steel and the concrete.

The components of P in local element coordinates are : $P_x = P\cos\alpha$, $P_y = P\sin\alpha$, where α is the angle between the lo-

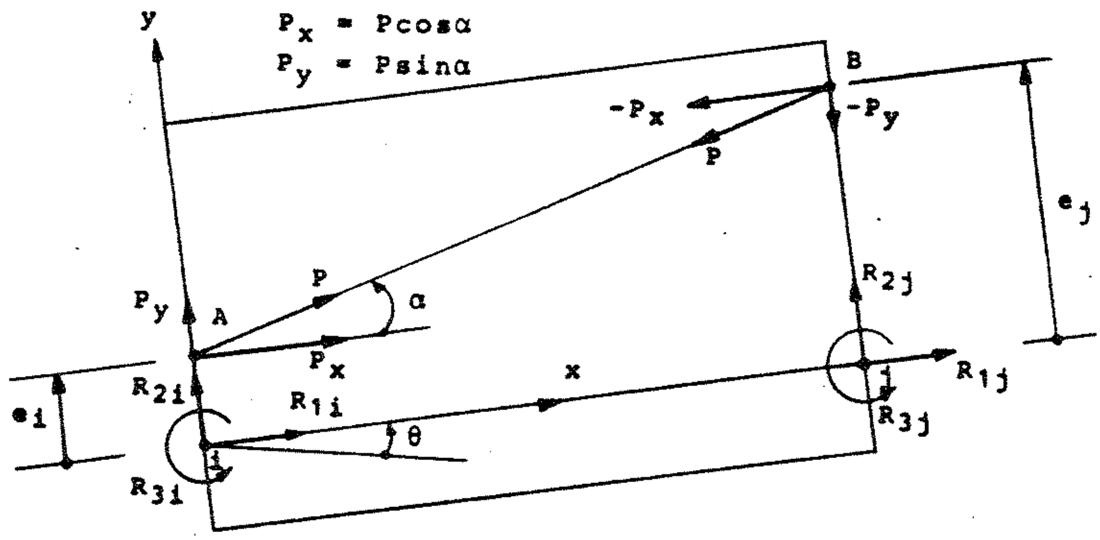

Fig. 6.5. Calculation of the Joint Load Vector Due to Prestress at Transfer

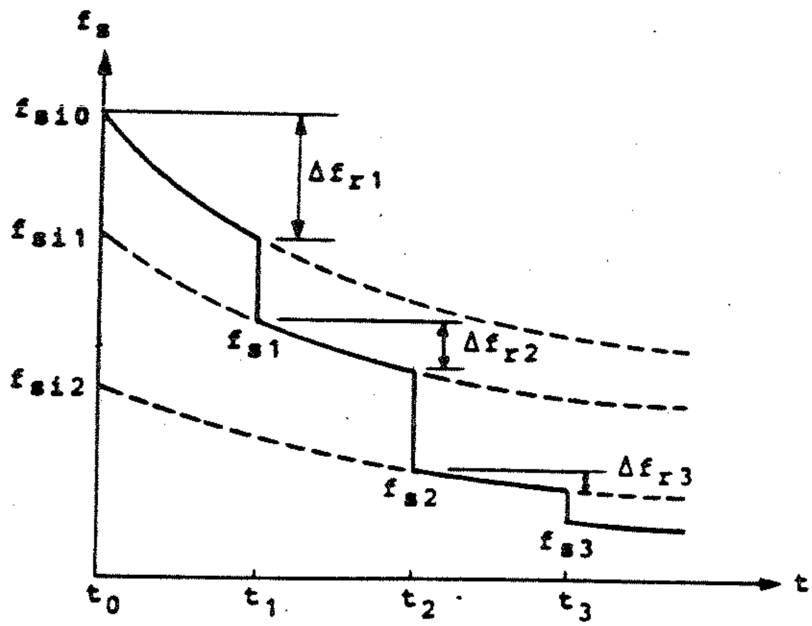

Fig. 6.6. Calculation of the Stress Relaxation

cal x axis and the prestressing steel segment AB. Then the equivalent joint load vectors $\underset{\sim}{R}_i$ and $\underset{\sim}{R}_j$ at joints i and j of the element are

$$\underset{\sim}{R}_i = \langle R_{1i}, R_{2i}, R_{3i} \rangle^T = \langle P_x, P_y, -P_x e_i \rangle^T \qquad (6.11)$$

$$\underset{\sim}{R}_j = \langle R_{1j}, R_{2j}, R_{3j} \rangle^T = \langle -P_x, -P_y, P_x e_j \rangle^T \qquad (6.12)$$

These load vectors are transformed into the global coordinates by multiplying the transformation matrix $\underset{\sim}{A}^T$ defined by Eq. (5.60). By assembling these load vectors for each element the total joint load vector for the structure due to prestress at transfer can be obtained.

An identical procedure can be used to calculate the equivalent joint loads due to correction forces in the prestressing steel for the second order analysis of unbonded frames described in section 6.4.2.

6.6 Stress Relaxation in Prestressing Steel

The nature of the stress relaxation in prestressing steel was discussed in section 2.4. Magura, Sozen and Siess (106) developed the following equation for the calculation of the stress relaxation in prestressing steel based on numerous experimental data for a wide variety of prestressing steels.

$$\frac{f_s}{f_{si}} = 1 - \frac{\log t}{10}\left(\frac{f_{si}}{f_y} - 0.55\right) \; ; \; \frac{f_{si}}{f_y} \geq 0.55 \qquad (6.13)$$

in which f_s is the stress at time t, f_{si} is the initial stress immediately after stressing, f_y is 0.1 percent offset yield stress and t is time in hours after stressing.

Eq. (6.13) is developed on the condition that the strain remains constant and the initial prestress is the only stress applied. In reality various changes in the prestress take place due to other causes. One example is the loss of prestress due to elastic shortening of concrete at transfer for pre-tensioned structures, and after transfer the amount of prestress varies due to various time dependent loads. In order to take these variations in prestress into account in the calculation of the relaxation, Hernandez and Gamble (107) suggested the following procedure. Ghali, Sisodiya and Tadros (108) utilized a similar procedure.

Referring to Fig. 6.6, let f_{sio} be the initial prestress applied at time t_o. At time t_1, in addition to the stress relaxation Δf_{r1} from the initial prestress f_{sio}, the prestress drops to f_{s1} due to other causes. Calculate a fictitious initial prestress f_{si1} by Eq. (6.13) such that the initial prestress f_{si1} applied at t_o would be relaxed to f_{s1} at t_1. Then, on the basis of the initial prestress f_{si1}, calculate the stress relaxation Δf_{r2} occurring during t_1 and t_2. Δf_{r3} is calculated similarly after calculating a fictitious initial prestress f_{si2} which would relax to f_{s2} at t_2. By continuing this process the total stress relaxation f_{rn} at time t_n can be calculated by

$$f_{rn} = \sum_{i=1}^{n} \Delta f_{ri} \tag{6.14}$$

6.7 Calculation of Prestressing Steel Strains and Stresses and Internal Element Forces Due to Prestress

In order to calculate the prestressing steel strains and stresses, the current length of each of the prestressing steel segments at each stage of the iteration process is calculated by first calculating the global coordinates of the two end points. Fig. 6.7 shows a procedure to calculate the current global coordinates (X,Y) of the end point corresponding to joint i which have the original global coordinates (X_o, Y_o). In the figure, θ_o is the original angle of the element axis from the global coordinate axis, r_1, r_2 and r_3 are the components of the current total displacement vector of the joint i.

For pre-tensioned and post-tensioned bonded frames the strain and the stress for each prestressing steel segment are evaluated as follows.

(1) Calculate the strain increment by

$$\Delta\varepsilon = (L_c - L_p)/L_o \qquad (6.15)$$

where, L_c is the segment length for the current iteration, L_p is the previous length and L_o is the original length. L_o is calculated on the basis of the original locations of the two end points in the frame element.

(2) Add $\Delta\varepsilon$ to the previous total to obtain the current total strain ε.

(3) Calculate the stress corresponding to ε from the

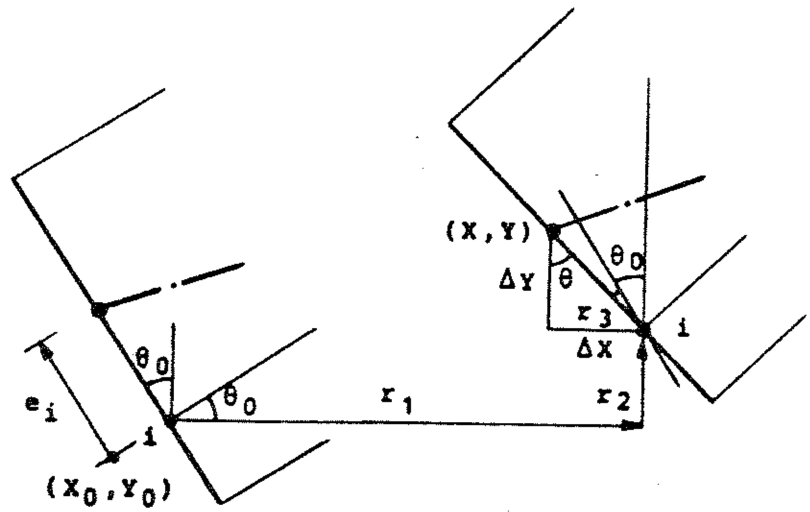

$$\theta = \theta_0 + r_3$$
$$\Delta X = -e_i \sin\theta$$
$$\Delta Y = e_i \cos\theta$$
$$X = X_0 + r_1 + \Delta X$$
$$Y = Y_0 + r_2 + \Delta Y$$

Fig. 6.7. <u>Calculation of the Current Global Coordinates of an End Point of the Prestressing Steel Segment</u>

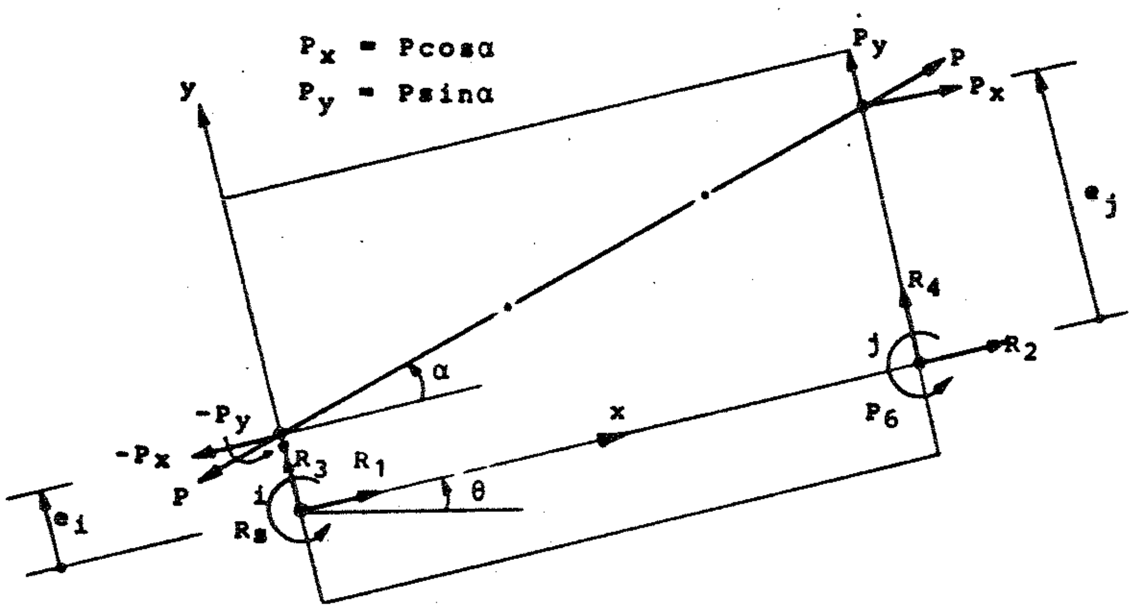

Fig. 6.8. <u>Internal Resisting Loads Due to Prestress</u>

nonlinear stress-strain curve shown in Fig. 2.10.

(4) Subtract the stress relaxation f_{rn} calculated by the procedure described in section 6.6 from the stress obtained in step (3) to calculate the current stress σ.

For post-tensioned unbonded frames, average strain increment $\Delta\varepsilon$ for the entire prestressing steel tendon is first calculated by a similar expression as the Eq. (6.15) in which L represents the length of the tendon. Then the steps (2) to (4) are followed for each prestressing steel segment.

Internal resisting load vector $\underset{\sim}{R}_p^i$ due to prestress can be expressed as follows for each element. Refer to Fig. 6.8

$$\underset{\sim}{R}_p^i = \langle -P_x,\ P_x,\ -P_y,\ P_y,\ P_x e_i,\ -P_x e_j \rangle^T \qquad (6.16)$$

in which relevant terms are defined in section 6.5. For geometric nonlinear analysis, current values of θ and α should be used.

$\underset{\sim}{R}_p^i$ is transformed to global coordinates and added to the internal resisting load vector due to internal forces for the concrete and the reinforcing steel, and then assembled for all the elements to form the internal resisting load vector $\underset{\sim}{R}^i$ for the structure.

6.8 Summary

The procedure for the nonlinear time dependent analysis of prestressed concrete frames is similar to that for the analysis of reinforced concrete frames developed in preceeding chapters except for some additional steps which result from the features distinct in prestressed concrete frames.

The analysis is performed distinguishing pre-tensioned and post-tensioned structures for three distinct stages of loading in prestressed concrete structures ; namely before, at and after the transfer of prestress.
Bonded and unbonded post-tensioned structures are distinguished for the analysis after the transfer of prestress.

For each type of structure, and for each stage of loading a method for the evaluation of the stiffness and loading due to prestress is developed. For pre-tensioned and post-tensioned bonded structures the approximate stiffness due to prestressing steel is added directly to the element stiffness assuming that the displacement field within an element is continuous. For unbonded post-tensioned structures an iterative method is developed to account for the displacement incompatibility. A procedure for the determination of the stress for the prestressing steel including the time dependent effects is discussed.

7. COMPUTER PROGRAMS

7.1 General Remarks

During the course of the present investigation 4 computer programs had been written in FORTRAN language for the CDC 6400 computer at the University of California, Berkeley. Two programs, NTRUSS and NFRAME were written in the earlier stage of this investigation to study and verify various time dependent nonlinear analysis procedures.

In the program NTRUSS a procedure for the nonlinear time dependent analysis of planar concrete trusses is incorporated. Elastic-perfectly plastic stress-strain relationship is assumed. Geometric nonlinearity and the time dependent effects due to creep, shrinkage and aging of concrete and temperature variations are included. Example 4.5.2 was analyzed by this program.

The program NFRAME was written to verify the geometric nonlinear analysis procedure for planar frames. Linearly elastic material properties were assumed. Example 8.2.1 was analyzed by this program.

In the programs RCFRAME and PCFRAME the present analytical procedures are incorporated for planar reinforced and prestressed concrete frames, respectively. The input instructions for these programs are given in the Appendix.

7.2 Flow Chart of the Programs RCFRAME and PCFRAME

A brief flow chart of the programs RCFRAME and PCFRAME is given in the following page.

FLOW CHART

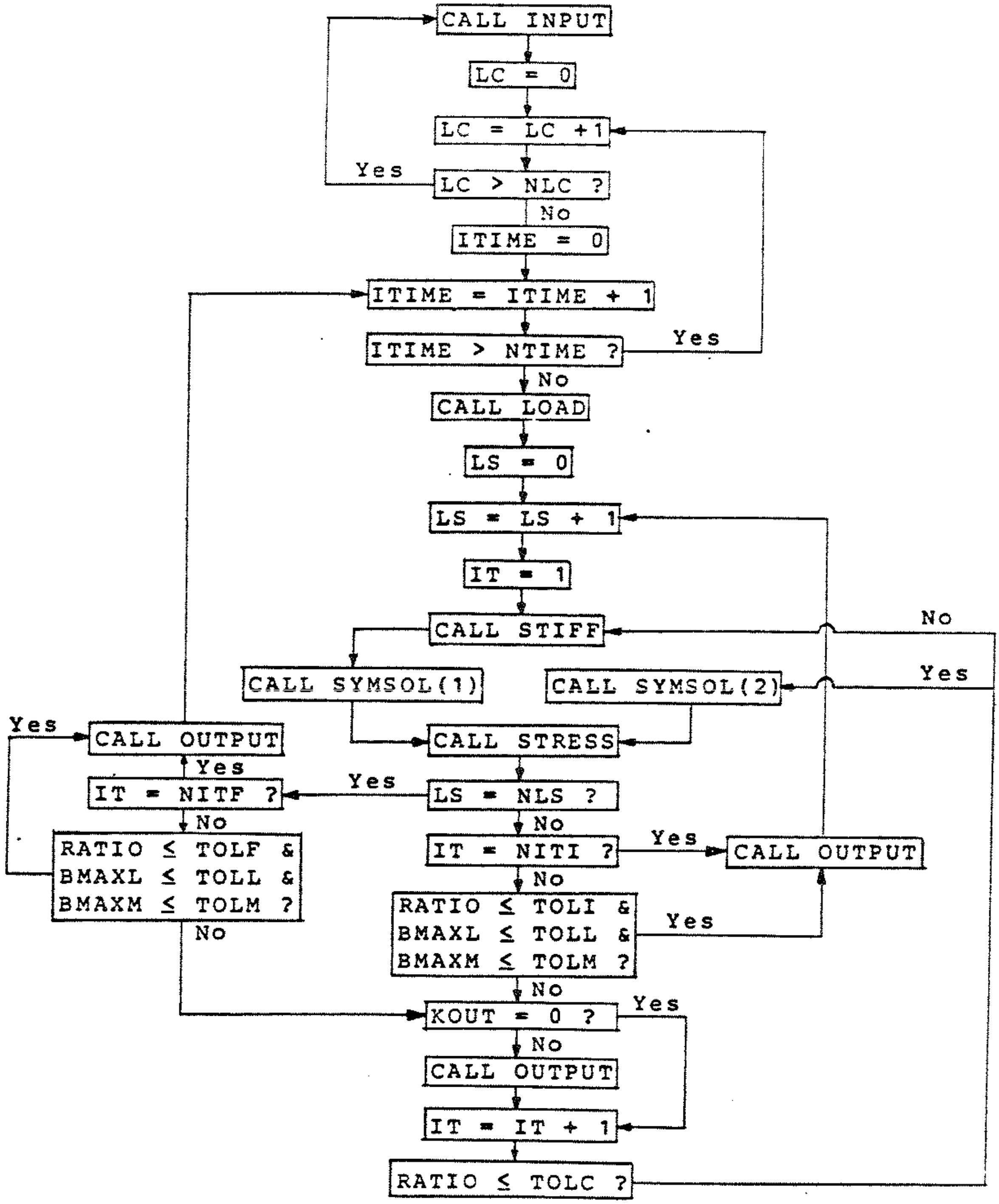
CALL INPUT
LC = 0
LC = LC +1
LC > NLC ?
Yes
No
ITIME = 0
ITIME = ITIME + 1
ITIME > NTIME ?
Yes
No
CALL LOAD
LS = 0
LS = LS + 1
IT = 1
CALL STIFF
No
CALL SYMSOL(1)
CALL SYMSOL(2)
Yes
CALL STRESS
CALL OUTPUT
Yes
IT = NITF ?
Yes
LS = NLS ?
Yes
No
RATIO ≤ TOLF &
BMAXL ≤ TOLL &
BMAXM ≤ TOLM ?
No
IT = NITI ?
Yes
CALL OUTPUT
No
RATIO ≤ TOLI &
BMAXL ≤ TOLL &
BMAXM ≤ TOLM ?
Yes
No
KOUT = 0 ?
Yes
No
CALL OUTPUT
IT = IT + 1
RATIO ≤ TOLC ?

The variables in the flow chart are defined as follows.

LC : Load case counter

NLC : Total number of load cases

ITIME : Time step counter

NTIME : Total number of time steps

LS : Load step counter

NLS : Total number of load steps for the current time step

IT : Iteration counter

NITF : Maximum number of iterations allowed for the final load step

NITI : Maximum number of iterations allowed for intermediate load steps

RATIO : Displacement ratio defined in section 4.4, to be compared with the following convergence tolerances

TOLI : Tolerance for intermediate load steps

TOLC : Tolerance for changing stiffness

TOLF : Tolerance for the final load step

BMAXL : Maximum unbalanced force

BMAXM : Maximum unbalanced moment

TOLL : Maximum allowed unbalanced force

TOLM : Maximum allowed unbalanced moment

KOUT : Iteration output code (Output is given for each iteration if KOUT is not zero.)

Main functions of the subroutines listed are as follows.

1. INPUT

The geometry, boundary conditions, material properties and element data are read in.

2. LOAD

Load vector for the current time step including the equivalent loads due to creep, shrinkage and aging of concrete and temperature changes is computed.

3. STIFF

Tangent stiffness matrix is formed based on the current geometry and material properties.

4. SYMSOL

Displacement increments are solved by this symmetric banded equation solver. SYMSOL(1) triangularizes the newly formed stiffness matrix while SYMSOL(2) utilizes already triangularized and stored stiffness matrix.

5. STRESS

Strains, stresses, element forces and unbalanced loads are computed.

6. OUTPUT

The following informations are printed out for each load step, and for each iteration if KOUT is not zero.

(a) Joint displacement and rotations.

(b) Support reaction forces and moments.

(c) Unbalanced loads and moments.

(d) Element forces and moments (Moments at two end joints and the axial force).

(e) Strains, stresses and forces for each prestressing steel segment for prestressed concrete frames.

(f) Material state number defined in chapter 2, stresses and strains for each concrete and reinforcing steel layer.

8. NUMERICAL STUDIES

8.1 General Remarks

A number of reinforced and prestressed concrete frames has been analyzed by the computer programs RCFRAME and PCFRAME described in chapter 7. The purpose of these numerical studies can be stated as follows.

(1) To verify the validity of the theoretical procedure developed in this study for the nonlinear time dependent analysis of reinforced and prestressed concrete frames ;

(2) To demonstrate the accuracy and the capability of the computer programs RCFRAME and PCFRAME to predict the nonlinear time dependent behavior of reinforced and prestressed concrete frames.

In section 8.2, theoretical studies on the effects of geometric and material nonlinearities and the load reversal on concrete beams are presented. In sections 8.3 and 8.4, reinforced and prestressed concrete frames studied experimentally by previous investigators are analyzed by the computer programs RCFRAME and PCFRAME, and the experimental and the analytical results are compared.

8.2 Theoretical Studies

8.2.1 Timoshenko Beam - Test on Geometric Nonlinear Analysis

In order to test the accuracy of geometric nonlinear analysis procedure a simply supported beam, restrained axially and loaded uniformly, as shown in Fig. 8.1.a is analyzed. The

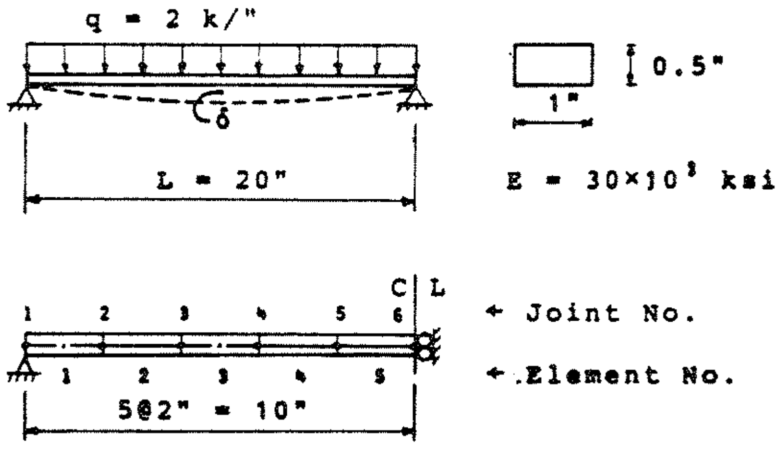

Fig. 8.1.a. Example 8.2.1 - Timoshenko Beam

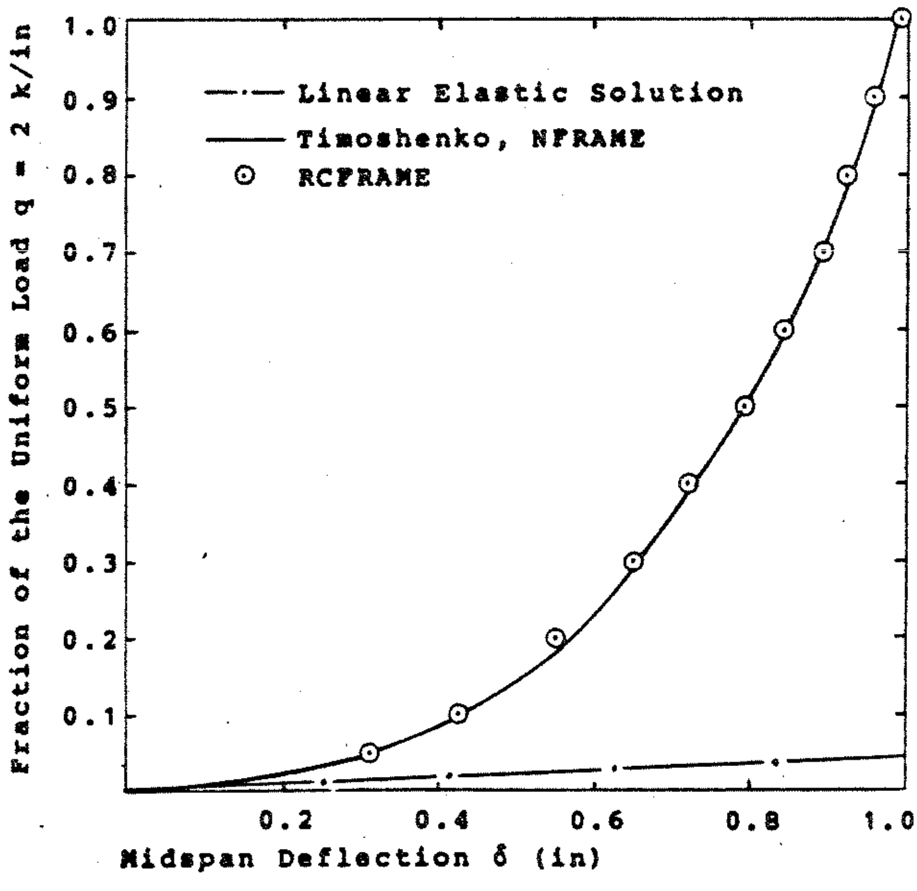

Fig. 8.1.b. Example 8.2.1 - Load vs. Midspan Deflection

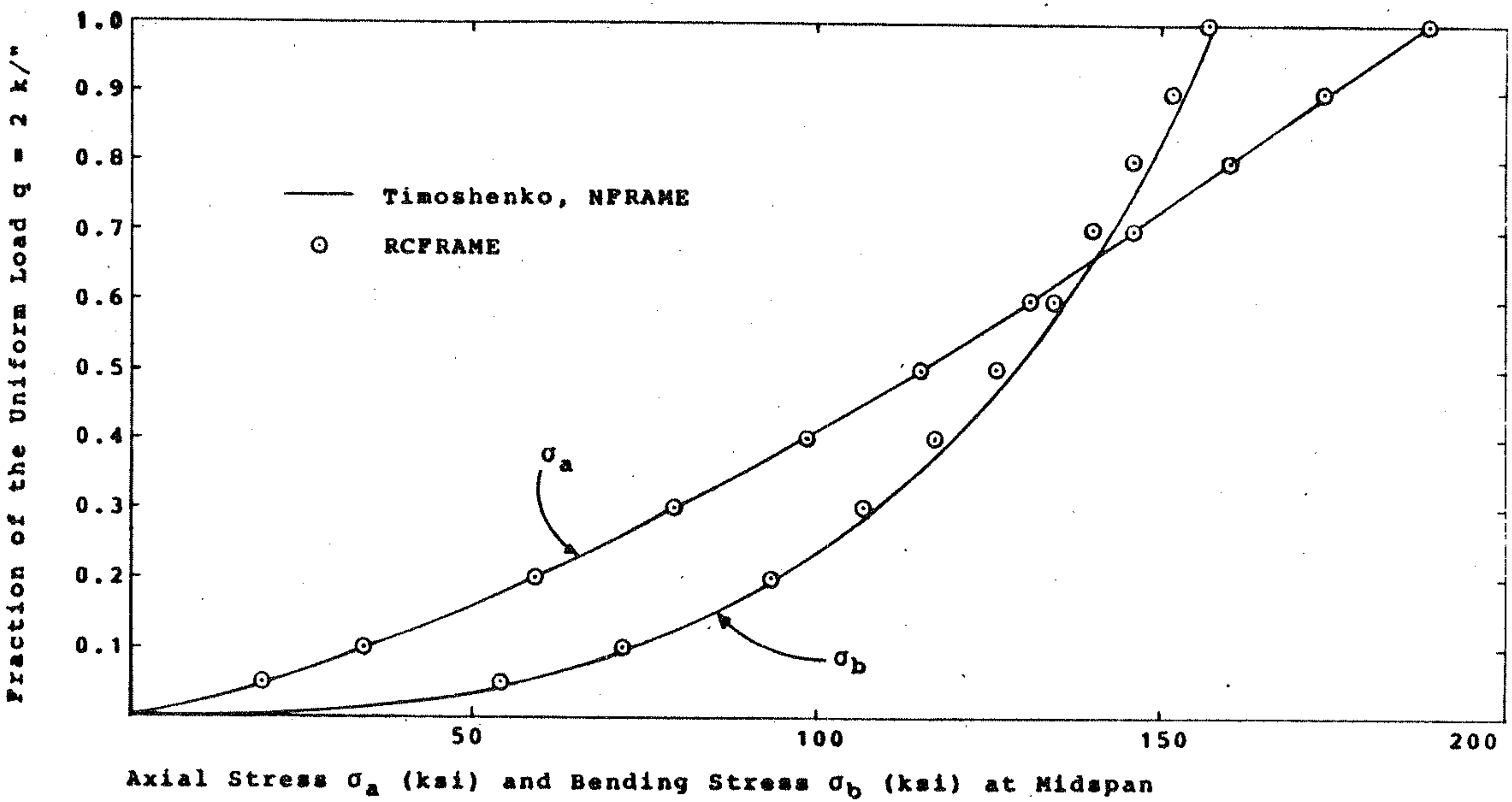

Fig. 8.1.c. Example 8.2.1 - Load vs. Midspan Stress Curve

material is assumed to be linearly elastic. However, due to the presence of axial force, if we consider the equilibrium in the deformed configuration, the structure becomes stiffer as the applied load is increased.

Timoshenko (109) has presented an analytical solution to this problem treating the structure as an elemental strip cut out from a long rectangular plate bending into a cylindrical surface.

Since the structure and the loading are symmetric about midspan, one half of the structure, divided into 5 equal elements, was analyzed by the programs NFRAME and RCFRAME with 11 load steps up to $q = 2$ k/in. The cross section of the beam was divided into 10 equal layers for the analysis by RCFRAME. The results for the midspan deflection are shown in Fig. 8.1.b, and those for the axial and bending stress at midspan are shown in Fig. 8.1.c. It can be seen that the comparison between Timoshenko's solution and the present analytical solution is very good. A small error in the solution by RCFRAME can be attributed to the error involved in layering of the cross section. This problem was also analyzed by Yeh (100) and Aldstedt (47).

8.2.2 Reinforced Concrete Timoshenko Beam - Test on Geometric and Material Nonlinear Analysis

An axially restrained reinforced concrete simple beam, similar to that analyzed in section 8.2.1, is analyzed to study both separate and combined effects of geometric and material nonlinearities.

In Fig. 8.2.a, the geometry and material properties of the structure are summarized. Due to the symmetry only half of the structure divided into 10 elements is analyzed. The cross section is divided into 10 concrete layers and a steel layer. In order to increase the ultimate load capacity of the cross section the compressive strength of the concrete is arbitrarily increased.

The structure is analyzed up to $q = 140$ lb/in with 10 load steps. Fig. 8.2.b shows load-deflection curves at mid-span for 4 different cases. Case 1 represents linearly elastic response. Only geometric nonlinearity is considered in case 2. We notice a distinct stiffening of the load-deflection curve due to nonlinear geometry effects as discussed in the preceeding section. In case 3 only material nonlinearity is considered. Beyond the cracking load the structure softens as the load is increased due to the gradual decrease of the modulus of elasticity of concrete until it fails. In case 4 both geometric and material nonlinearities are considered. Beyond the cracking load the structure can be seen softening initially as the load is increased. However, as the load is increased further, we notice that the structure stiffens gradually due to the effects of geometric nonlinearity. We note from Fig. 8.2.b that the single most important source of nonlinearity is the cracking of concrete at relatively low load level which reduces the structure stiffness in a sudden manner. The gradual softening and stiffening of the structure stiffness due to the yielding of concrete and the effects

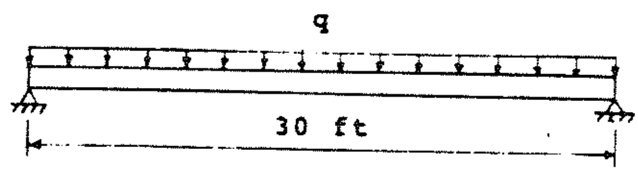

Structure and Loading

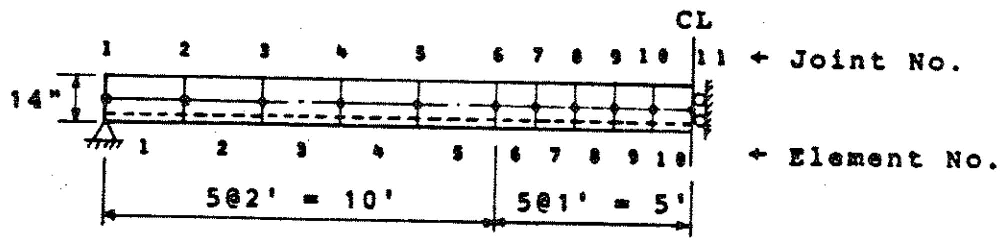

Finite Element Mesh Layout

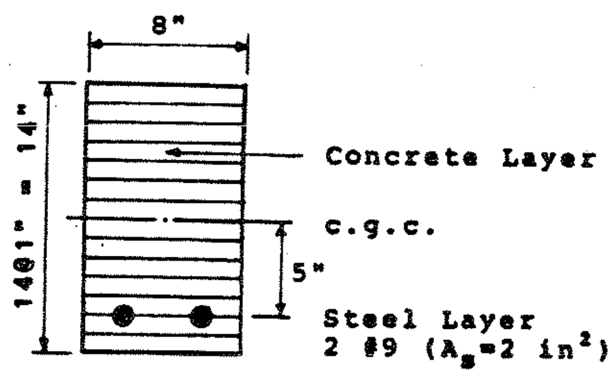

Cross Section

Concrete Properties

f'_c = 8000 psi $\quad$ f'_t = 775 psi

E_i = 3.834×10^6 psi $\quad$ ε_u = 3.8×10^{-4}

Steel Properties

f_{sy} = 60×10^3 psi $\quad$ ε_{su} = 0.13

E_{s1} = 29×10^6 psi $\quad$ E_{s2} = 3.46×10^5 psi

Fig. 8.2.a. Example 8.2.2 - Geometry and Material Properties

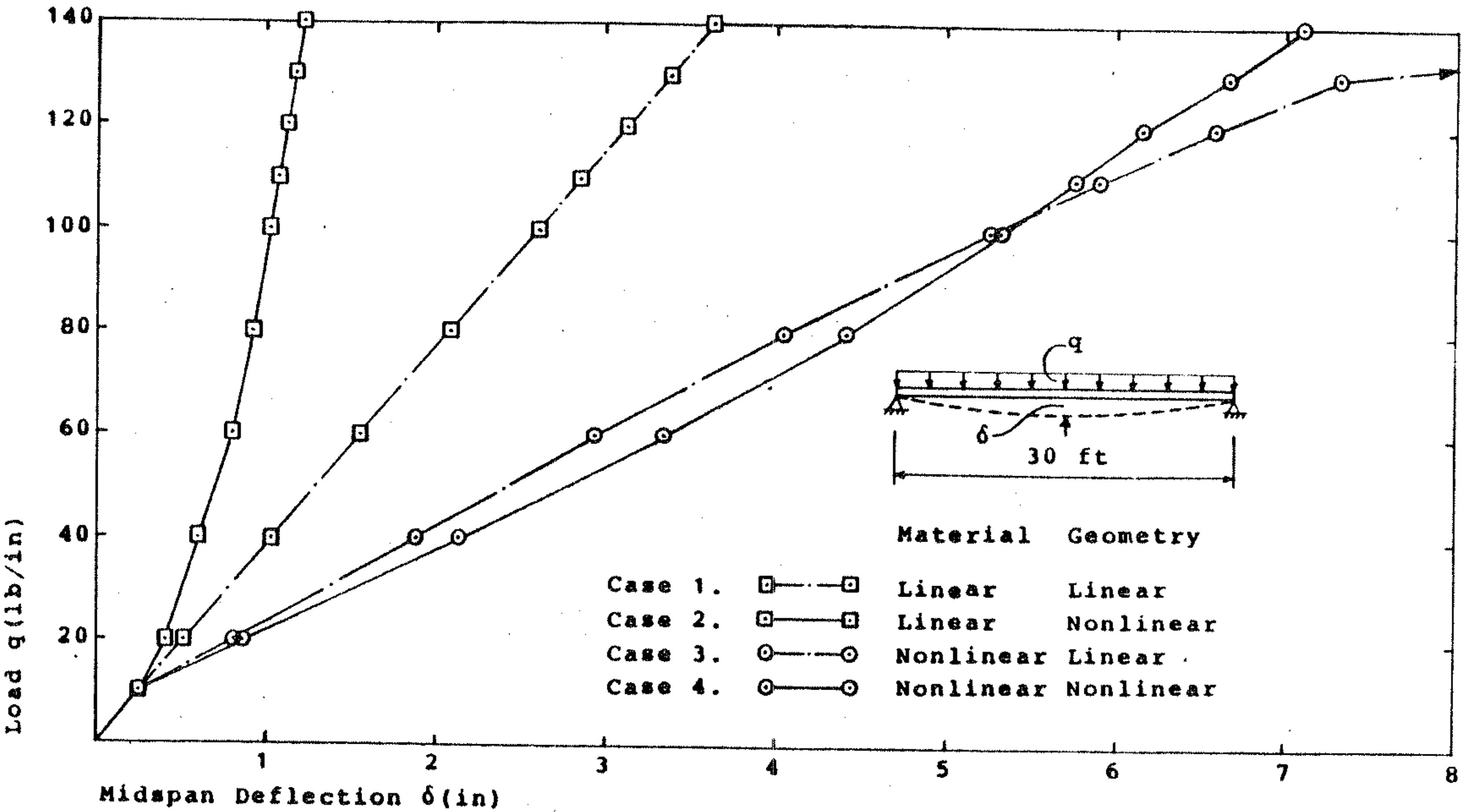

Fig. 8.2.b. Example 8.2.2 - Comparison of Midspan Deflection

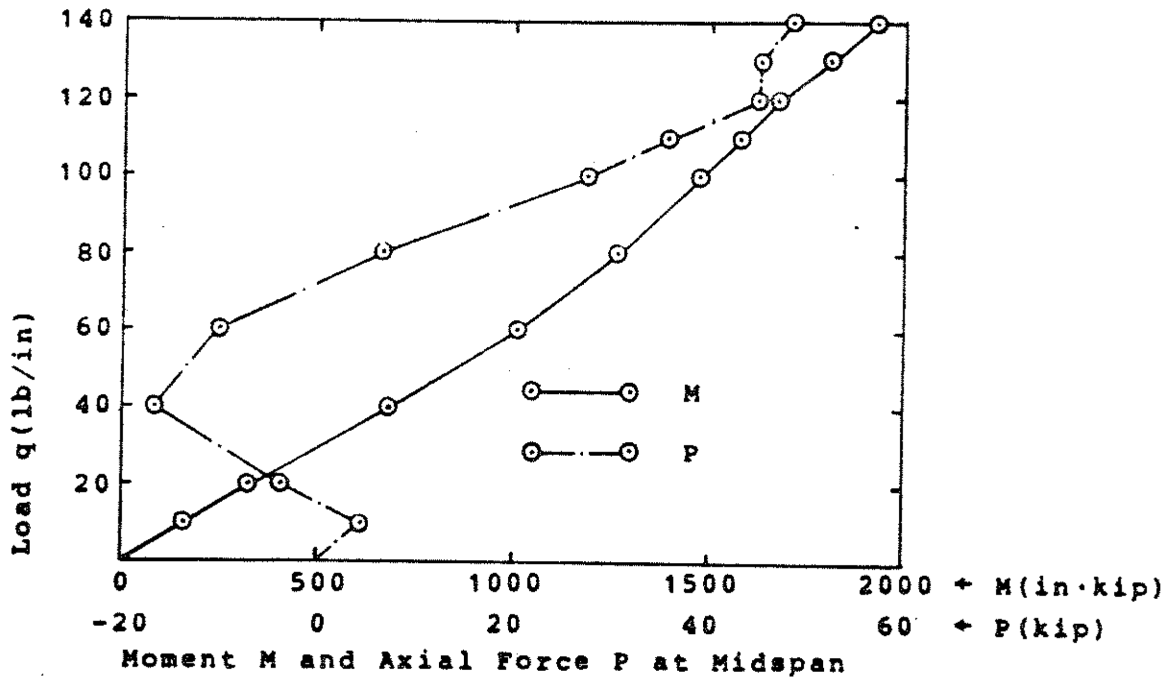

Fig. 8.2.c. Example 8.2.2 - Bending Moment and Axial Force at Midspan for Case 4.

q	δ(in)		P(kip)		M(in·kip)	
(lb/in)	Case 3	Case 4	Case 3	Case 4	Case 3	Case 4
10	0.26	0.26	3.8	4.4	162.	161.
20	0.82	0.86	-7.2	-3.7	324.	327.
40	1.88	2.14	-33.3	-16.4	648.	683.
60	2.94	3.34	-54.0	-10.0	972.	1005.
80	4.05	4.41	-70.8	6.5	1296.	1267.
100	5.26	5.31	-86.3	27.7	1620.	1472.
110	5.90	5.75	-92.7	35.7	1782.	1576.
120	6.58	6.15	-97.9	44.8	1944.	1668.
130	7.32	6.66	-102.3	45.1	2106.	1805.
140	—	7.12	—	48.3	—	1924.

Table 8.1. Example 8.2.2 - Comparison of Deflection δ, Axial Force P and Bending Moment M at Midspan for Case 3 and Case 4.

of geometric nonlinearity can be noted at higher load level.

For cases 3 and 4, displacement ratio tolerance ρ defined in section 4.4 was taken 0.01. The average number of iterations per load step was 4 for case 3 and 5 for case 4. The results for cases 3 and 4 are summarized in Table 8.1. In addition to the deflection δ, the axial force P and the bending moment M at midspan corresponding to each load step are tabulated.

In case 3, the equilibrium equations are solved in undeformed state. Thus in calculating the bending moment M at midspan, the effect of the axial force P is neglected, and the value of M is proportional to the applied load q as can be seen in Table 8.1. The bending moment M can be computed by $M = qL^2/8$ in this case. However, in case 4, the equilibrium equations are solved in deformed state, and the effect of the axial force P is included in computing the bending moment M at midspan. The bending moment M can be computed by $M = qL^2/8 - P\delta$. The bending moment M and the axial force P at midspan are plotted in Fig. 8.2.c. We note that as the load q is increased, the portion of the moment resisted by the axial force P is increased.

8.2.3 Load Reversal Analysis of a Reinforced Concrete Simple Beam

A hypothetical reinforced concrete simple beam shown in Fig. 8.3.a is analyzed to study the behavior of reinforced concrete structures subjected to load reversal. One half of the structure is divided into six elements. The cross section is divided into 10 equal concrete layers and two steel layers, each representing 2 #9 bars at the top and bottom of the cross section.

The concentrated load P applied at midspan is first increased from 0 to 40 kips, then the direction of the load is reversed and increased up to -40 kips, and then the direction of the load is again reversed and increased up to 40 kips. With the load increment of 10 kips, 20 load steps are required to analyze for this sequence. For each load step, the displacement ratio tolerance ρ is taken 0.01. The average number of iterations per load step is 11. The effects of geometric nonlinearities are not included in this analysis.

The results at midspan are tabulated in Table 8.2. δ represents the deflection at midspan. However, σ_1, ε_1 and σ_2, ε_2 represent the stress, strain values of the bottom and the top concrete layer, respectively, at the middle of the element No. 6, i.e., 6 inches apart from the midspan. The material codes, representing various material states in the concrete stress-strain curve, are defined in section 2.2.5. Fig.8.3.d shows the stress-strain curves of the bottom fiber (σ_1-ε_1) and the top fiber (σ_2-ε_2), respectively, at midspan corresponding to each load step. In Fig. 8.3.e, the stress distribution through the depth of the cross section, as well as along the length of the beam, is shown for each load step distinguishing the compressive stress zone, the tensile stress zone and the cracked zone.

The behavior of the beam for each load step will be discussed briefly by dividing the 20 load steps into 5 groups each of which consists of 4 load steps.

(1) Steps 1 to 4 ($P = 0^k$ to $P = 40^k$)

The beam exhibits almost linearly elastic behavior up to step 2. Between steps 2 and 3, cracking takes place in bottom fibers, and the midspan deflection at step 3^k is mardedly increased as shown in Fig. 8.3.b. The neural axis of the beam at midspan has moved up as shown in Fig. 8.3.e. The slope of the load-deflection curve at midspan between steps 3 and 4 shows the cracked stiffness.

(2) Steps 4 to 8 ($P = 40^k$ to $P = 0^k$)

Cracked regions remain cracked during the unloading to zero load as shown in Fig. 8.3.e since the cracks cannot be closed as long as the strain states remain positive. The structure stiffness during this unloading remain almost constant. However, we note that this stiffness is increased compared to the stiffness between steps 3 and 4. This can be explained by examining the stress-strain curve of the top fiber at midspan shown in Fig. 8.3.d. In an unloading path the modulus of elasticity is the same as the initial modulus which is greater than the secant modulus between steps 3 and 4. Accordingly, the stiffness is increased. We also note in the figure that there is some residual strain at step 8 ($P = 0^k$) due to the unloading path with the initial modulus. A small amount of residual stress present may be considered as a numerical error. However, total axial force at midspan computed by the layer integration is zero.

(3) Steps 8 to 12 ($P = 0^k$ to $P = -40^k$)

As the upward load P is applied up to 40^k, we first note that the cracks formed previously in bottom fibers of the beam are now closed, and the fibers participate in resisting compression as shown in Fig. 8.3.c and Fig. 8.3.e. We also note in Fig. 8.3.b that cracking of the top fibers takes place between steps 9 and 10, instead of between steps 10 and 11 corresponding to the cracking load for downward P. The reason for this lower cracking load for upward P can be explained by the presence of compressive residual strain in top fibers as shown in Fig. 8.3.d. The cracking is assumed to take place when the stress reaches the tensile strength f'_t. Due to the residual compressive strain, the tensile strain corresponding to f'_t is reduced compared to the value for the initial downward loading. Hence the cracking load is also reduced. As a consequence of this low cracking load, displacements are increased compared to those in steps 1 to 4 as shown in Fig. 8.3.b. Structure stiffness after cracking becomes softer compared to that for the downward loading since the value of the tangent modulus becomes lower for higher compressive stresses. Also, crack propagates to a wider region as shown in Fig. 8.3.e.

(4) Steps 12 to 16 ($P = -40^k$ to $P = 0^k$)

Crack patterns for steps 13 to 15 remain essentially the same as those for step 12, and the structure stiffness becomes stiffer for the same reason as explained for steps 4 to 8. Load reversal path of the bottom fiber at midspan in

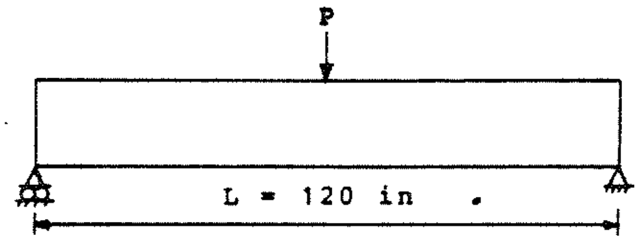

Structure and Loading

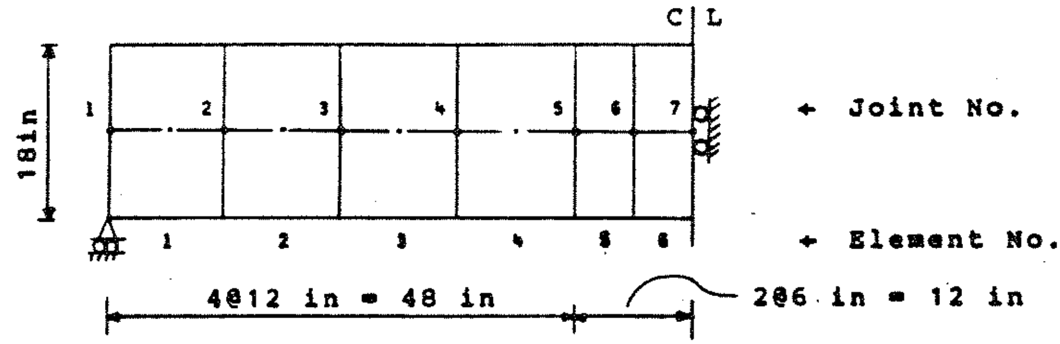

Finite Element Mesh Layout

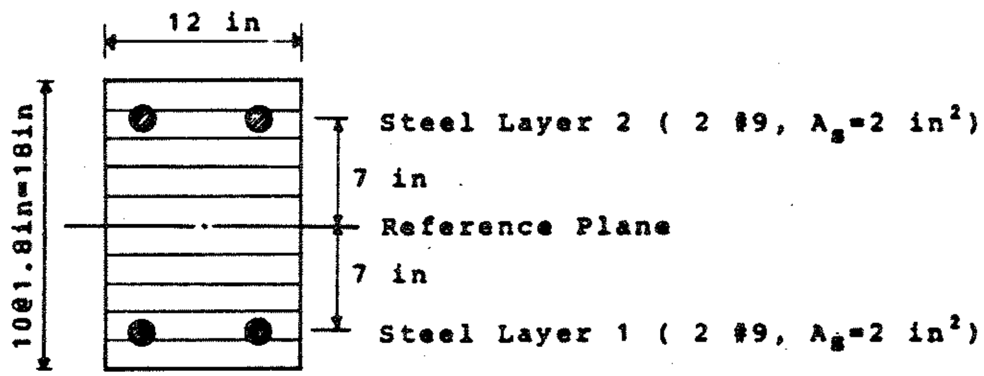

Cross Section

Concrete Properties

$f_c'' = 5.5$ ksi $\quad f_t' = 0.77$ ksi

$E_i = 4150$ ksi $\quad \varepsilon_u = 3.8\times10^{-3}$

Steel Properties

$f_{sy} = 45$ ksi $\quad \varepsilon_{su} = 0.17$

$E_{s1} = 29\times10^{3}$ ksi $\quad E_{s2} = 176$ ksi

Fig. 8.3.a. Example 8.2.3 - Geometry and Material Properties

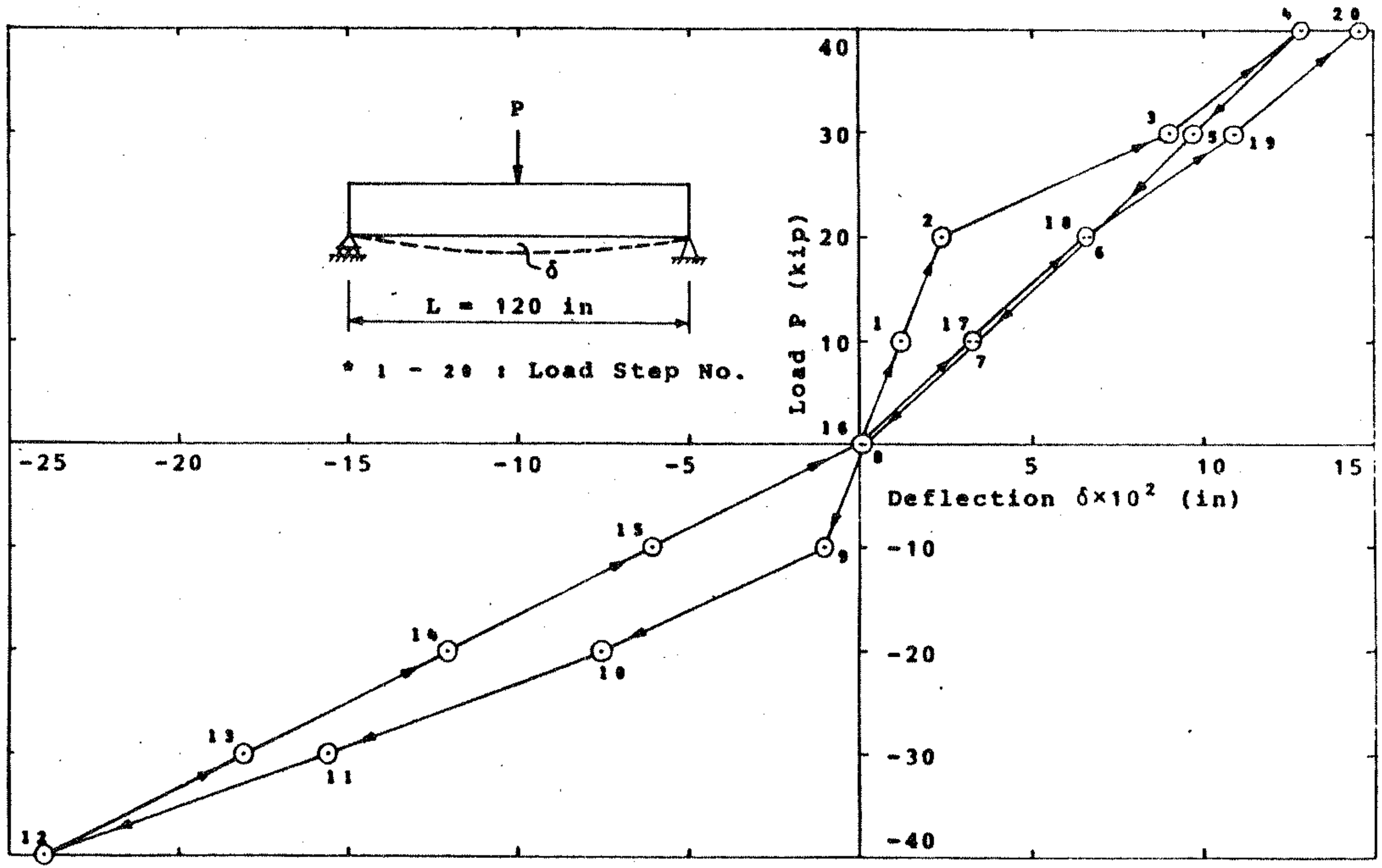

Fig. 8.3.b. Example 8.2.3 - Load-Deflection Curve at Midspan

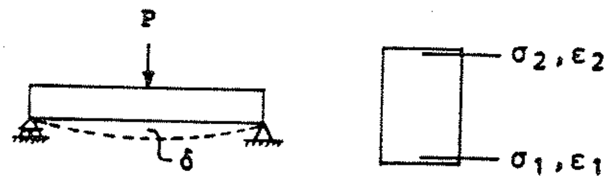

				Bottom Fiber			Top Fiber		
Load Step	ΔP (k)	P (k)	$\delta \times 10^2$ (in)	Mat. Code	σ_1 (ksi)	$\epsilon_1 \times 10^4$	Mat. Code	σ_2 (ksi)	$\epsilon_2 \times 10^4$
1	10	10	1.22	1	0.32	0.78	2	-0.32	-0.78
2	10	20	2.45	1	0.65	1.57	2	-0.64	-1.58
3	10	30	8.98	4	0.	9.60	2	-1.47	-3.83
4	10	40	12.93	4	0.	14.45	2	-1.85	-4.93
5	-10	30	9.74	4	0.	10.87	6	-1.36	-3.74
6	-10	20	6.56	4	0.	7.29	6	-0.87	-2.56
7	-10	10	3.37	4	0.	3.71	6	-0.38	-1.38
8	-10	0	0.18	4	0.	0.13	6	0.11	-0.20
9	-10	-10	-1.08	8	-0.30	-0.73	6	0.44	0.60
10	-10	-20	-7.64	8	-2.83	-8.04	4	0.	8.13
11	-10	-30	-15.64	8	-3.89	-12.15	4	0.	12.19
12	-10	-40	-23.98	8	-4.67	-16.23	4	0.	16.25
13	10	-30	-18.08	10	-3.03	-12.27	4	0.	12.18
14	10	-20	-12.09	10	-1.36	-8.23	4	0.	8.11
15	10	-10	-6.07	4	0.	-4.11	4	0.	4.05
16	10	0	-0.01	4	0.	-0.01	4	0.	-0.02
17	10	10	3.22	4	0.	3.75	10	-0.38	-1.36
18	10	20	6.50	4	0.	7.61	10	-0.82	-2.43
19	10	30	10.44	4	0.	11.37	10	-1.28	-3.55
20	10	40	14.65	4	0.	15.12	10	-1.74	-4.66

Table 8.2. Example 8.2.3 - Summary of Results at Midspan

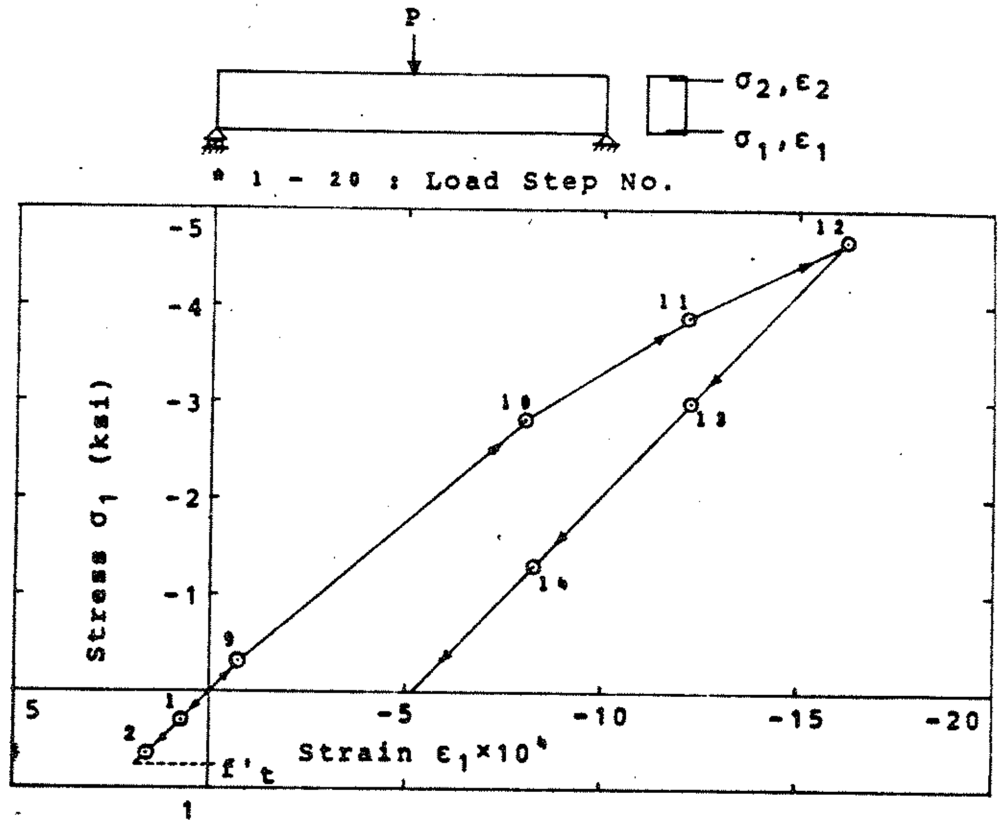

Fig. 8.3.c. Example 8.2.3 - Stress-Strain Curve of Bottom Fiber at Midspan

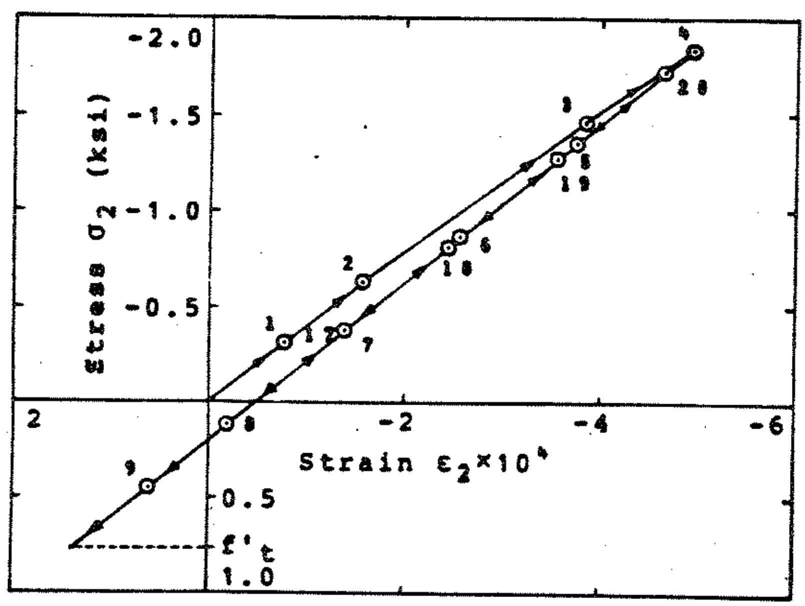

Fig. 8.3.d. Example 8.2.3 - Stress-Strain Curve of Top Fiber at Midspan

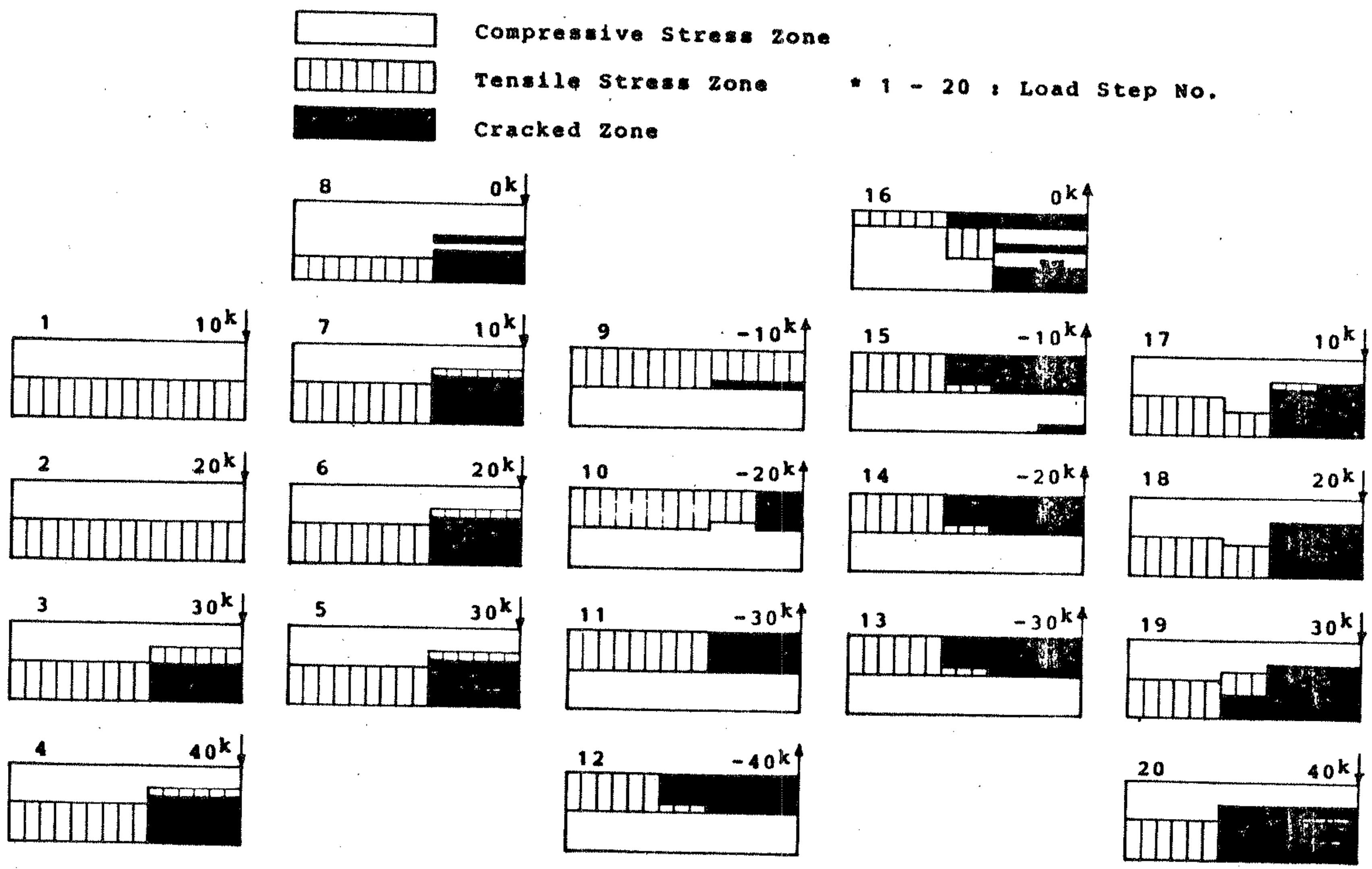

Fig. 8.3.e. Example 8.2.3 - Stress Distribution for Each Load Step

the stress-strain curve is shown in Fig. 8.3.c. We note that the bottom fiber is cracked at step 15 although the strain shows a negative value of -4.11×10^{-4} (see Table 8.2). This confirms the assumption that previously cracked fibers cannot resist any tensile stress. At step 16 ($P = 0^k$) we again note some residual stresses due to numerical error.

(5) Steps 16 to 20 ($P = 0^k$ to $P = 40^k$)

As the downward load is again applied, cracks reopen in the previously cracked bottom fibers as soon as they are subjected to tensile stresses. As the load is increased, crack propagates to a wider region and the displacement is also increased accordingly compared to that corresponding to the initial downward loading.

8.3 Reinforced Concrete Frames

8.3.1 Bresler-Scordelis Beam - Ultimate Load Analysis of a Simple Beam

Bresler and Scordelis (110,111) have conducted numerous tests on a series of reinforced concrete beams to study the failure modes of these beams. A simple beam, failing in a flexural mode and designated by beam B3, is selected for this study.

One half of the beam loaded at midspan, with its reinforcement details is shown in Fig. 8.4.a. One half of the beam is divided into 16 elements, and the cross section is divided into 19 concrete layers and 4 steel layers for the analysis. Web reinforcements are not included in the analytical model. Lin (31) also analyzed this beam with layered plate elements for his study of reinforced concrete slabs and shells. The element division and the layering of the cross section are similar to those used by Lin.

Material properties are also shown in Fig. 8.4.a. The secant modulus of concrete measured at the stress of 1. ksi was 4640 ksi. Since parabolic stress-strain curve is utilized in this study, the initial modulus E_i of concrete can be computed as follows. From Eq. (2.10), with σ = 1 ksi, ε^m = 1/4640, and f''_c = 5.62 ksi, solve for ε_0. Then solve for E_i from Eq. (2.11). The results are : $\varepsilon_0 = 2.309\times10^{-3}$, and E_i = 4867 ksi.

In the present analysis, 9 load steps were required to reach the ultimate load. Only material nonlinearity was included. With the displacement ratio tolerance of 0.01, the average number of iterations was 6 per load step.

In Fig. 8.4.b, load-deflection curves at midspan are plotted. Experimental and analytical results, both by present analysis and Lin's analysis, are shown together for comparison. In the experiment, about 30 percent of the ultimate load was first applied and removed. And then the beam was loaded again up to the ultimate load. The load-deflection curve shown in Fig. 8.4.b corresponds to the second cycle of loading. In both analyses, the midspan load was applied in one cycle. The difference between the experimental and the analytical results in lower load level can be attributed to the effects of load reversal. Both analyses predict the ultimate load of 80 kips compared to the experimental value of 79.5 kips. Although the load-deflection curves for both analyses follow that for the experiment fairly closely, the result by present analysis can be seen closer to the experimental result compared to the result by Lin's analysis. This can be attributed to the fact that present analysis approximates concrete stress-strain curve with a parabola as opposed to Lin's analysis in which elastic-perfectly plastic stress-strain curve for concrete is assumed.

In table 8.3 the strain and stress distributions through the depth of the cross section at the center of element 16 at ultimate load ($P = 80k$) are tabulated. Strain distribution is linear as assumed, and layer stresses are computed by the parabolic stress-strain law for concrete and the bilinear law for reinforcing steel. Also, statics check for the cross section is presented. Total axial force, which should be zero, is -0.018 kips, and the bending moment, which should be $40\ k \times (126-4.5/2)\ in = 4950\ k\cdot in$, is $4950.21\ k\cdot in$. Small errors present result from not carrying enough significant digits in the computation. In the computer output, the axial force and the bending moment at midspan, evaluated by the numerical integration of Eq. (5.54), are 6.80×10^{-4} kips and $5040\ k\cdot in$ ($40\ k \times 126\ in$) respectively.

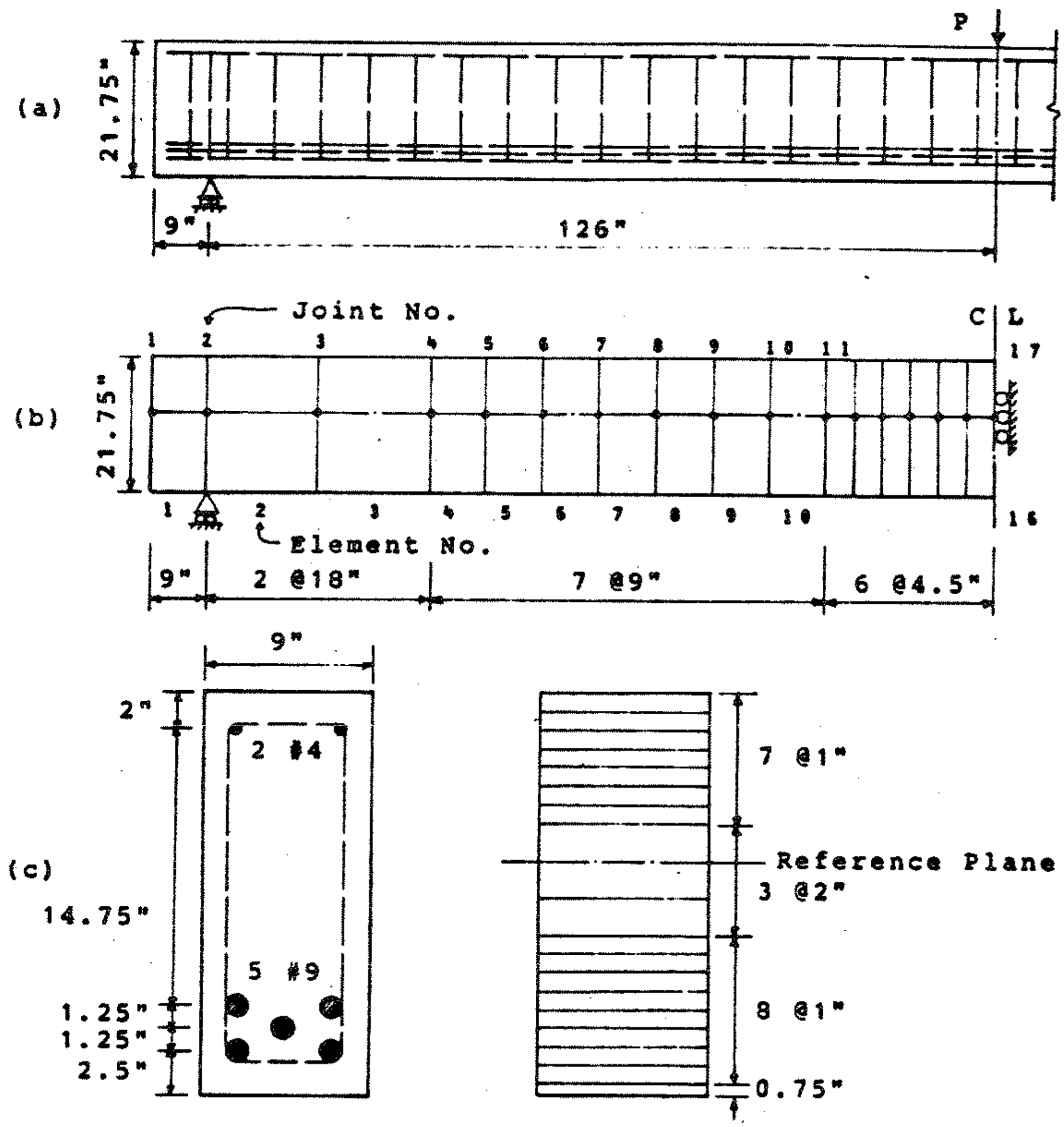

(d) Concrete : f''_c = 5.62 ksi $\quad$ f'_t = 0.611 ksi
E_i = 4.867×10^3 ksi $\quad$ ε_u = 3.8×10^{-3}

#4 Bars : f_{sy} = 50.1 ksi $\quad$ ε_{su} = 0.2
E_{s1} = 29.2×10^3 ksi $\quad$ E_{s2} = 144 ksi

#9 Bars : f_{sy} = 80.1 ksi $\quad$ ε_{su} = 0.139
E_{s1} = 30.7×10^3 ksi $\quad$ E_{s2} = 418 ksi

Fig. 8.4.a. Example 8.3.1 - Bresler-Scordelis Beam
(a) Structure and Loading
(b) Finite Element Mesh Layout
(c) Cross Section
(d) Material Properties

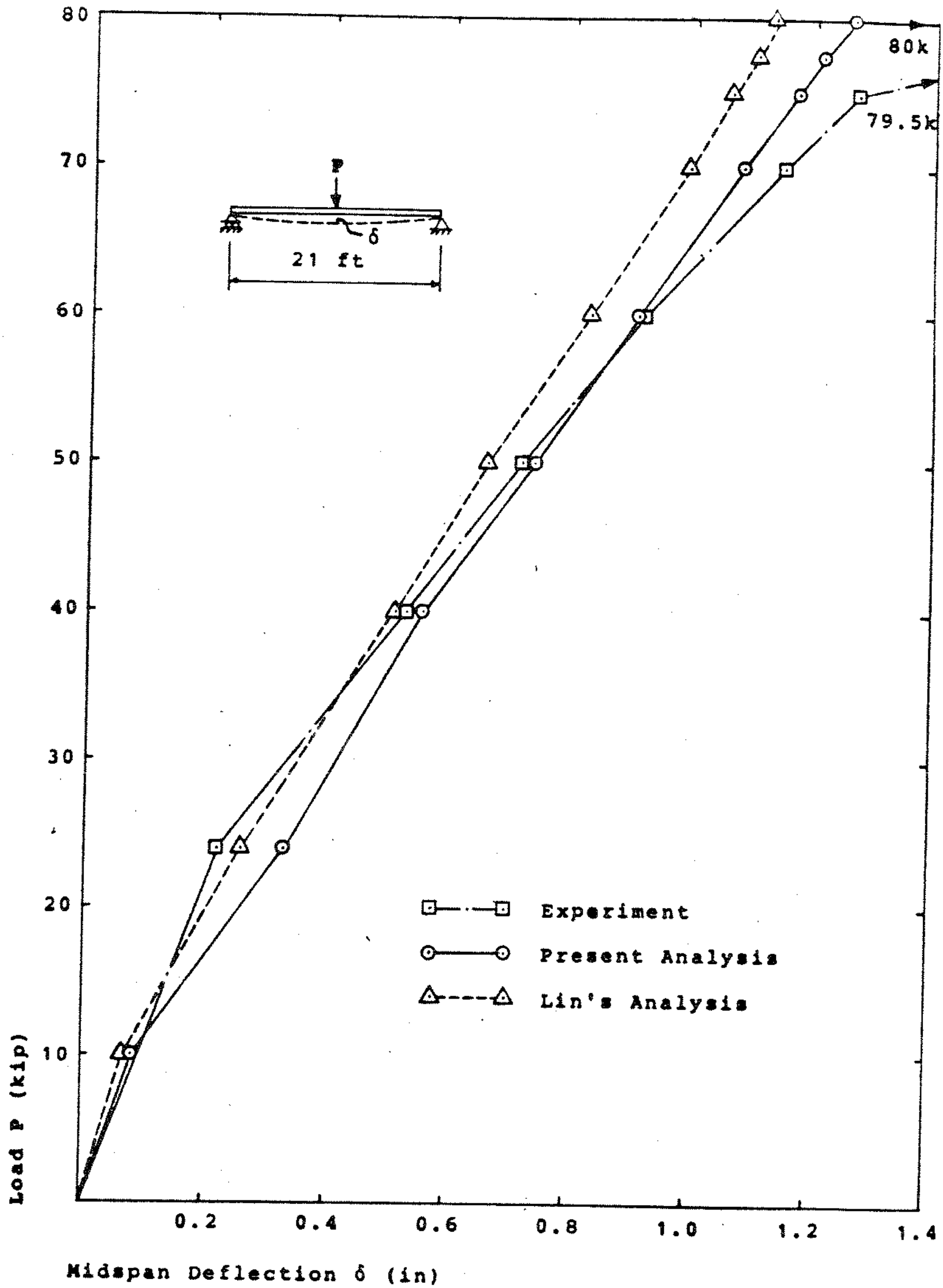

Fig. 8.4.b. Example 8.3.1 - Comparison of Midspan Deflection

Layer	No.	Area A (in^2)	y (in)	Strain $\varepsilon \times 10^3$	Stress σ (ksi)	$\sigma \times A$ (k)	$-\sigma \times A \times y$ (k·in)
Concrete Layers	1	9.	8.5	-2.208	-5.609	-50.481	429.09
	2	9.	7.5	-1.959	-5.491	-49.419	370.64
	3	9.	6.5	-1.710	-5.241	-47.169	306.60
	4	9.	5.5	-1.461	-4.861	-43.749	240.62
	5	9.	4.5	-1.211	-4.349	-39.141	176.13
	6	9.	3.5	-0.962	-3.707	-33.363	116,77
	7	9.	2.5	-0.713	-2.933	-26.397	65.99
	8	18.	1.	-0.339	-1.528	-27.504	27.50
	9	18.	-1.	0.160	0.	0.	0.
	10	18.	-3.	0.658	0.	0.	0.
	11	9.	-4.5	1.032	0.	0.	0.
	12	9.	-5.5	1.282	0.	0.	0.
	13	9.	-6.5	1.531	0.	0.	0.
	14	9.	-7.5	1.780	0.	0.	0.
	15	9.	-8.5	2.030	0.	0.	0.
	16	9.	-9.5	2.279	0.	0.	0.
	17	9.	-10.5	2.528	0.	0.	0.
	18	9.	-11.5	2.777	0.	0.	0.
	19	6.75	-12.375	2.996	0.	0.	0.
Steel Layers	1	0.3907	7.	-1.835	-50.12	-19.582	137.07
	2	2.037	-7.75	1.843	56.57	115.233	893.06
	3	1.0185	-9.	2.154	66.13	67.353	606.18
	4	2.037	-10.25	2.466	75.70	154.201	1580.56
					Total →	-0.018	4950.21

Table 8.3. Example 8.3.1 - Stress Distribution and Statics Check at the Center of Element 16 at Ultimate Load (P = 80k)

8.3.2 Washa-Fluck Beam - Time Dependent Analysis of a Continuous Beam

Washa and Fluck (112) conducted tests on a series of two-span reinforced concrete continuous beams to study their behavior under sustained load up to 2½ years after loading. This test followed their earlier test (113) in which they studied time dependent behavior of a series of reinforced concrete simple beams.

Among the continuous beams tested, two beams, designated by X1 and X3, were selected for the present analytical study. Their geometric properties are shown in Fig. 8.5.a. Each beam consists of two 20 ft spans loaded uniformly with w = 190 lb/ft. The uniform load which includes the dead load of the beam is applied 14 days after casting of concrete, and then sustained up to 2½ years after loading. Both beams, 6" × 8" in cross section, have tensile and compressive reinforcements in the negative moment region. In the positive moment region, Beam X3 has tensile reinforcements only while Beam X1 has both tensile and compressive reinforcements. The cross section originally designed with ACI specifications was that of Beam X3. Compressive reinforcements in the positive moment region for Beam X1 were added to study the effects of these reinforcements in reducing the effects of creep and shrinkage.

Since the structure and loading are both symmetric about the midlength support, one half of the beam was analyzed by dividing into 15 beam elements. Locations D, P and N, corresponding to the locations of maximum deflection, maximum positive moment and maximum negative moment, respectively are predetermined although their exact locations vary slightly due to the redistribution of internal forces. The cross section is generally divided into 15 concrete layers and 2 or 3 steel layers.

Material properties used in the analysis are summarized in Fig. 8.5.b. Formulas for time dependent concrete properties, recommended by ACI Committee 209 (56) and described in detail in chapter 2, are used. The numerical values are based on the experimental values of the strength, f'_c = 3230 psi and the secant modulus, E = 2835 ksi at σ = 1575 psi which represent the average values of type X beams at 14 days after casting of concrete. The weight of the concrete w = 146 pcf is assumed. The increase of the strength and modulus of concrete with time are shown in Fig. 8.5.b.

Experimental creep and shrinkage data are not given in the reference 112. However, in the earlier test on simple beams by Washa and Fluck (113), the cross sectional properties and the span length of the beams were identical to those of the present continuous beams. Both experiments were conducted with similar concrete mixes and under similar laboratory conditions. Thus it was decided that the creep and shrinkage data measured in the simple beam test be used for the present analysis. Utilizing the expression for the specific creep function developed in chapter 3, i. e.

$$c(\tau,t-\tau) = \sum_{i=1}^{3} a_i(\tau)[1 - e^{-10^{-i}(t-\tau)}] \qquad (8.1)$$

the following values of creep coefficients $a_i(\tau_0)$ at $\tau_0 = 14$ days were obtained by the least-square method ; $a_1 = 6.8308 \times 10^{-7}$, $a_2 = 8.9356 \times 10^{-7}$, $a_3 = 0.1120 \times 10^{-7}$. However, the creep data was obtanied by applying the compressive stress of 1575 psi to the concrete prism. Using the values of $r_1 = 0.35$ and $r_2 = 1.865$ in Eqs. (3.37) to (3.39), the effective stress corresponding to 1575 psi is 2165 psi. Thus the creep coefficients a_i's were reduced by a factor of 1575/2165 = 0.727. Creep coefficients for loading ages later than the initial loading age of 14 days are computed by Eq. (3.44). Based on the experimental data, hyperbolic shrinkage function is used. Specific creep curves for different loading ages and the shrinkage curve used in the analysis are shown in Fig. 8.5.c.

In the experiment, measurements of deflections, reactions and strains were taken 3, 7, 28, 90, 180, 270, 365, 545, 730, and 910 days after loading. In the analysis, 19 time steps were used after loading, i.e. 1, 3, 7, 12, 17, 22, 28, 40, 60, 90, 120, 150, 180, 210, 270, 365, 545, 730, and 910 days after loading. Since most of the creep and shrinkage takes place prior to 6 months after loading, closer time intervals were used during the earlier period. At each time step, including the first time step when the load was applied, analysis was performed with one load step with the displacement ratio tolerance of 0.01. For the initial loading 14 and 19 iterations were required to arrive at the equilibrium for Beam X1 and X3, respectively. The average number of iterations for each time step after initial loading was 2 for Beam X1 and 3 for Beam X3.

In table 8.4, a summary of experimental and theoretical results for the changes in deflections, reactions and strains due to creep and shrinkage are given. And in Figs. 8.5.d to 8.5.g, variations of deflections, strains, reactions and bending moments due to creep and shrinkage with time are plotted up to 2½ years after loading. The following facts can be observed.

(1) All the changes due to creep and shrinkage occur at a decreasing rate as time elapses after loading. By 6 months after loading most of the changes takes place.

(2) The effects of creep and shrinkage are reduced markedly by the presence of compressive reinforcements in the positive moment region.

(3) Deflection due to creep and shrinkage 2½ years after loading are greater than the immediate deflection at loading.

(4) Midlength reaction is increased due to the redistribution of internal forces. As a result, the bending moment at the maximum negative moment location N is increased while the moment at the maximum positive moment location P is decreased.

(5) Compressive strain of the beam increases due to creep and shrinkage much more than tensile strain does. The increase of the compressive strain in the positive moment region is greater than the increase in the negative moment region.

(6) Theoretical results from the present analysis are

generally lower than experimental results at loading, and the reverse is true for the increase due to creep and shrinkage. The average discrepancies between experimental and theoretical results for the deflection, the midlength reaction, the strain at compressive steel level at the maximum positive moment location and at the maximum negative moment location, respectively are ; 3%, 1%, 37% and 38% at loading ; 6%, 32%, 13% and 23% for the increase due to creep and shrinkage at 2½ years after loading ; 4%, 2%, 2% and 5% for the total value 2½ years after loading. The discrepancy of the results at loading might have been resulted from not taking sufficient number of elements in the analytical model. The discrepancy of results due to creep and shrinkage is expected since approximate creep and shrinkage data are used. The degree of accuracy for the present analytical model to predict the effects of creep and shrinkage cannot be measured directly in this example because of the absence of the experimental creep and shrinkage data. However, present model predicts the time dependent behavior of a reinforced concrete continuous beam fairly well qualitatively, and considering the uncertainties inherent in the creep and shrinkage data, the quantitative results are also quite satisfactory.

The effects of creep on the time dependent behavior of the present continuous beam will be briefly discussed qualitatively. Fig. 8.5.h shows total strain distributions between the compressive steel level and the tensile steel level at maximum positive and negative moment locations P and N, respectively at loading and 2½ years after loading for beams X1 and X3. Analytical stress distributions at loading and 2½ years after loading at locations P and N are shown in Fig. 8.5.i. We first note that the neutral axis of the beam cross section is located between the c.g.c. and the compressive steel level at loading. The portion of the concrete on the tension side beyond the c.g.c. is cracked, hence most of the tensile force is carried by the tensile steel. Since most of the concrete creep takes place on the compression side due to the sustained compressive stress on concrete, and only small amount of the tensile creep takes place, it can be expected that strain increase with time will occur mainly on compression side. This can be observed to be true in Fig. 8.5.h. As a result of this difference in the change of strain at compression and tension side, the neutral axis shifts toward the c.g.c. At 2½ years after loading the neutral axis almost coincides with the c.g.c. except for the Beam X3 at location P where no compressive steel is present.

We also note in Fig. 8.5.i that the concrete stress distribution at 2½ years after loading is drastically changed. The amount of compressive stress is markedly reduced and the resultant compressive and tensile forces for concrete are almost identical. The reduction of the compressive concrete stress can be explained as follows. Tensile force in the cross section is mostly carried by the tensile steel, and the tensile force is increased only slightly with time since the tensile strain is increased by a small amount as already mentioned. Compressive force is carried by both compressive steel and concrete. Since the compressive force carried by the compressive steel is increased by a large amount due to the large increase of compressive strain, the compressive stress of concrete has to be reduced to maintain the horizontal equilibrium of forces in the cross section. The reduction of the compressive stress in concrete with time is shown in Fig. 8.5.j for Beam X1. The reduction of the concrete stress was assumed to follow the straight-line load reversal path with the initial modulus as shown in Fig. 2.8. The fact that the resultant compressive and tensile forces for concrete are almost identical is consistent with the fact that the neutral axis is located almost at the c.g.c. As a result of this redistribution of the internal forces, the bending moment in negative moment region is increased and the moment in positive moment region is decreased accompanied by the increase of the midlength reaction.

Another point worth noting in Fig. 8.5.j is the nonlinear stress distribution at 2½ years after loading despite the fact that the stress distribution at loading is almost linear. This is a result of the nonlinear creep effect, i.e. concrete creep at higher stress levels is no longer proportional to stress intensity, but increases at an increasing rate. The incorporation of this nonlinear creep effect in the present analytical study was discussed in section 3.3. The concrete stress is computed as a function of the mechanical strain $\varepsilon^m(t)$, obtained by subtracting the non-mechanical

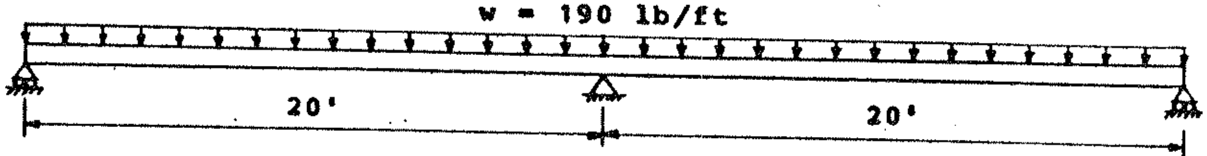

Structure and Loading

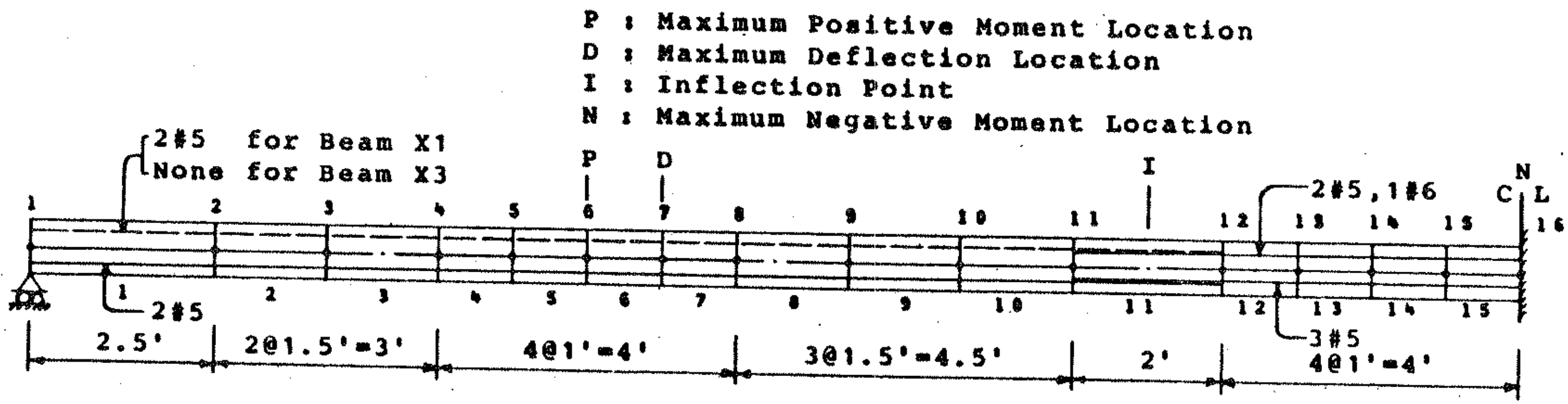

Finite Element Mesh Layout

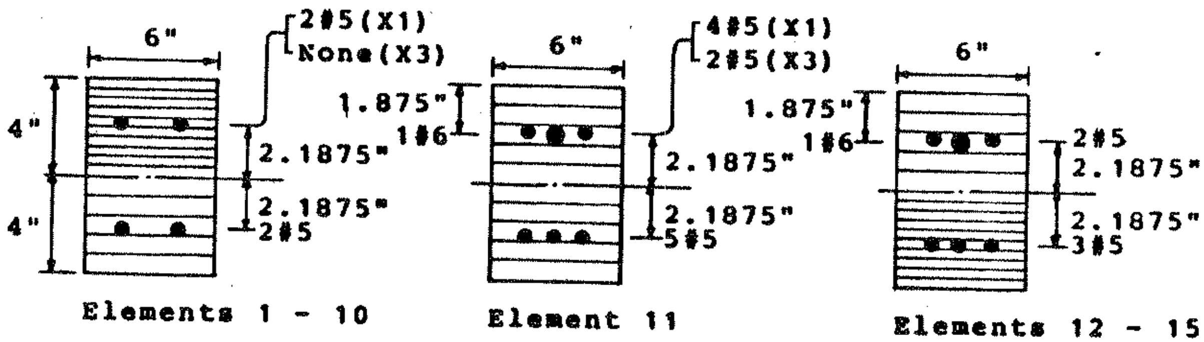

Cross Sections

Fig. 8.5.a. Example 8.3.2 - Washa-Fluck Beam

(a) Concrete Properties

$$f'_c(\tau) = \frac{\tau}{a + b\tau} \cdot f'_c(28) \;;\; f'_c(28) = 3668 \text{ psi}, \; a = 4., \; b = 0.85$$

$$E_i(\tau) = 33 \cdot w^{1.5}\sqrt{f'_c(\tau)} \text{ psi} \;;\; w = 146 \text{ pcf}$$

$$f''_c(\tau) = f'_c(\tau)$$

$$f'_t(\tau) = \sqrt{w \cdot f'_c(\tau)}$$

$$c(\tau, t-\tau) = \sum_{i=1}^{3} a_i(\tau)\left[1 - e^{-10^{-i}(t-\tau)}\right]$$

$$a_i(\tau) = a_i(\tau_o) \cdot \frac{E_i(\tau_o)}{E_i(\tau)} \cdot \left(\frac{\tau}{\tau_o}\right)^{-0.118} \;;\; \tau_o = 14 \text{ days}$$

$$\left.\begin{aligned} a_1(\tau_o) &= 4.9660 \times 10^{-7} \\ a_2(\tau_o) &= 6.4962 \times 10^{-7} \\ a_3(\tau_o) &= 0.8142 \times 10^{-7} \end{aligned}\right\} \text{per psi}$$

$r_1 = 0.35$, $r_2 = 1.865$ in Eqs. (3.37) to (3.39)

$$\varepsilon^s(\tau) = \frac{\tau}{35 + \tau} \cdot \varepsilon^{su} \;;\; \varepsilon^{su} = 7.71 \times 10^{-4}$$

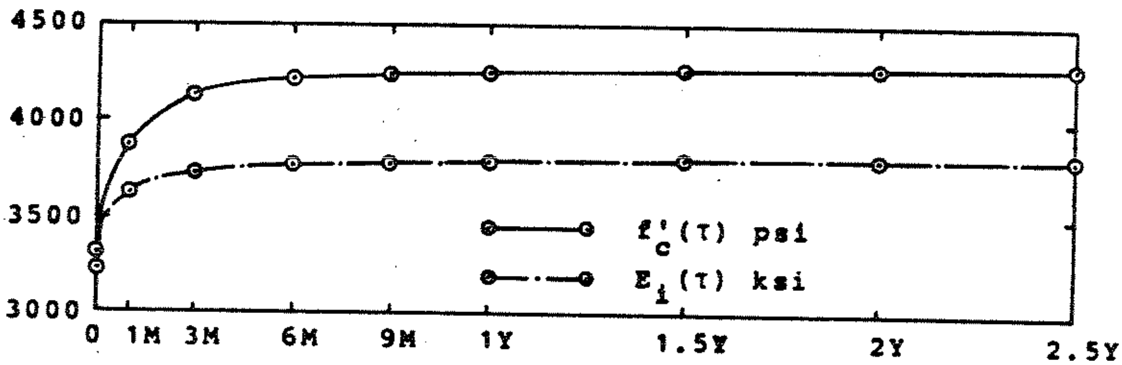

(b) Steel Properties

Steel	f_{sy} (psi)	E_{s1} (psi)	E_{s2} (psi)	ε_{su}
#5 Bars	62.0×10^3	30.0×10^6	3.53×10^5	0.14
#6 Bars	56.2×10^3	30.0×10^6	2.01×10^5	0.18

Fig. 8.5.b. Example 8.3.2 - Material Properties

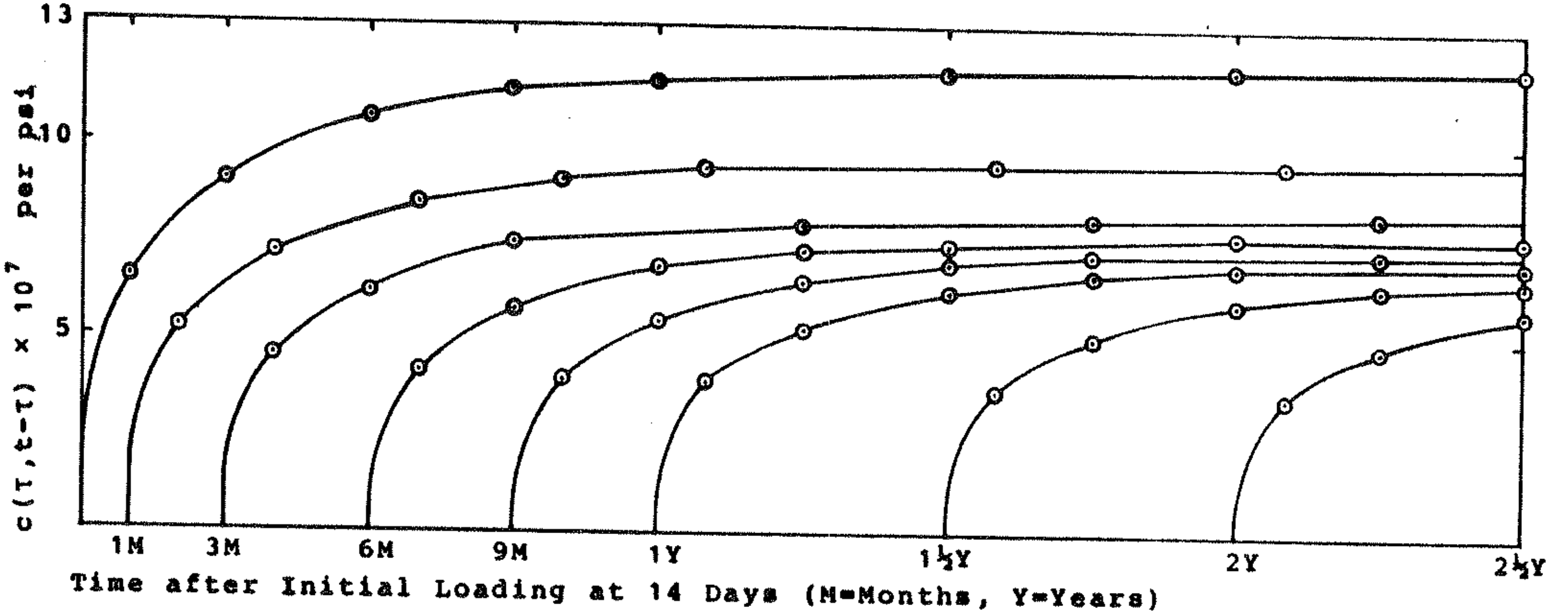

(a) Specific Creep Curves at Different Loading Ages

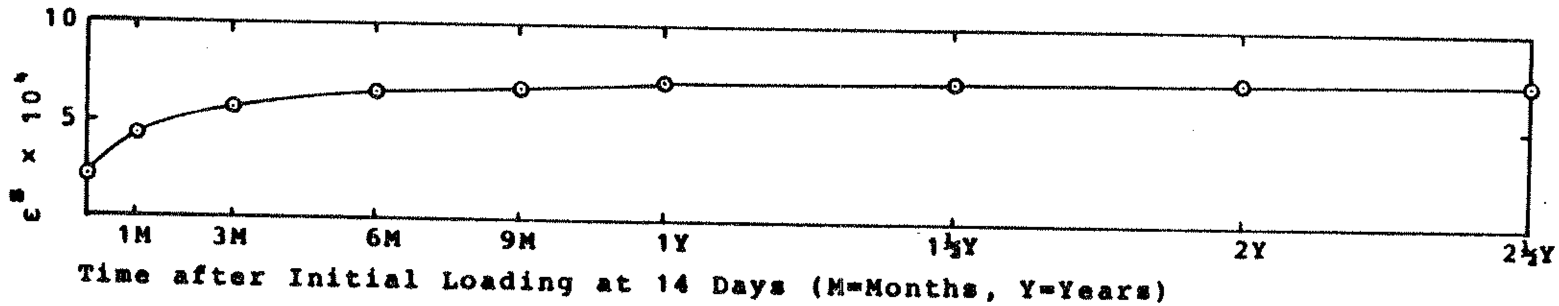

(b) Shrinkage Curve

Fig. 8.5.c. Example 8.3.2 - Creep and Shrinkage Properties of Concrete

Beam Type		At Loading	After 6 Months		After 2½ Years	
			δ	$\delta^c+\delta^s$	δ	$\delta^c+\delta^s$
X1	Exp.	0.56	1.06	0.50	1.14	0.58
	Th.	0.59	1.14	0.55	1.18	0.59
X3	Exp.	0.62	1.32	0.70	1.49	0.87
	Th.	0.61	1.47	0.86	1.57	0.96

(a) Deflection δ(in) at Max. Deflection Location D

Beam Type		At Loading	After 6 Months		After 2½ Years	
			R	% Inc.	R	% Inc.
X1	Exp.	4880	4990	2.2	4960	1.6
	Th.	4828	4872	0.9	4872	0.9
X3	Exp.	4850	5050	4.1	5070	4.6
	Th.	4836	5084	5.1	5118	5.8

(b) Reaction R(lbs) at Midlength Support

Beam Type		Comp. Steel Level			Tens. Steel Level		
		At Loading	After 2½ Years		At Loading	After 2½ Years	
			ε	$\varepsilon^c+\varepsilon^s$		ε	$\varepsilon^c+\varepsilon^s$
X1	Exp.	-2.2	-6.7	-4.5	4.1	5.1	1.0
	Th.	-1.40	-6.70	-5.30	5.65	6.50	0.85
X3	Exp.	-2.8	-12.4	-9.6	4.6	4.8	0.2
	Th.	-1.76	-12.17	-10.41	5.60	4.99	-0.61

(c) Strain $\varepsilon \times 10^4$ at Max. Positive Moment Location P

Beam Type		Comp. Steel Level			Tens. Steel Level		
		At Loading	After 2½ Years		At Loading	After 2½ Years	
			ε	$\varepsilon^c+\varepsilon^s$		ε	$\varepsilon^c+\varepsilon^s$
X1	Exp.	-3.9	-9.3	-5.4	7.0	8.0	1.0
	Th.	-2.47	-8.59	-6.12	6.78	8.00	1.22
X3	Exp.	-4.2	-9.8	-5.6	6.7	9.0	2.3
	Th.	-2.50	-9.99	-7.49	6.84	10.01	3.17

(d) Strain $\varepsilon \times 10^4$ at Max. Negative Moment Location N

Table 8.4. Example 8.3.2 - Summary of Experimental and Theoretical Results

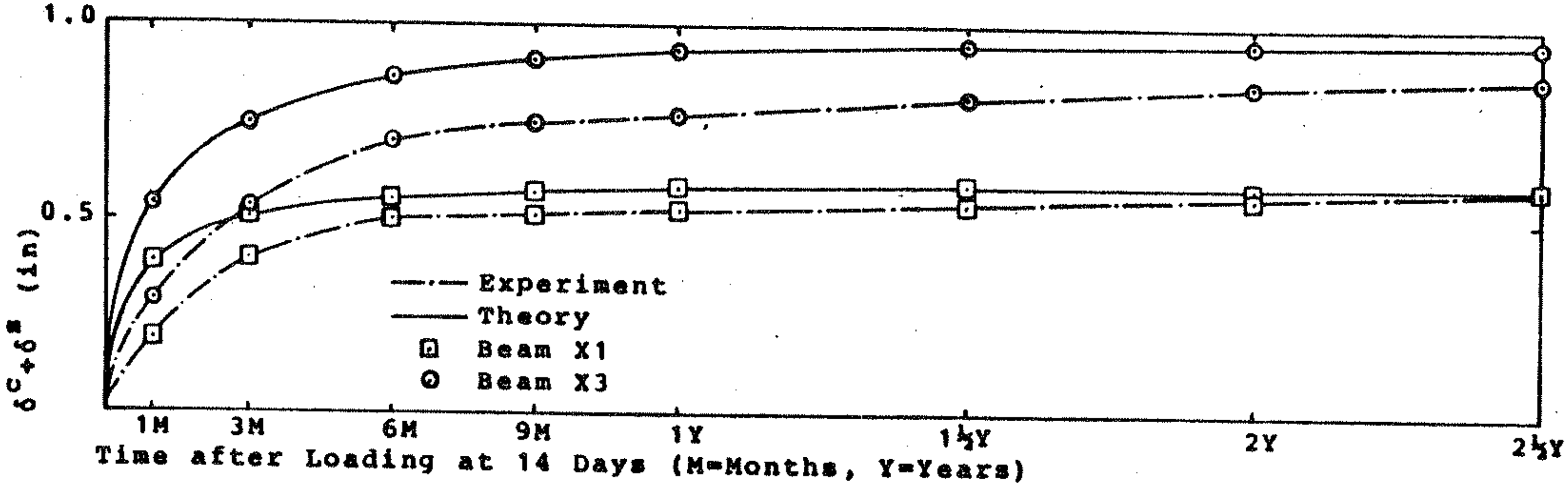

Fig. 8.5.d. Example 8.3.2 - Comparison of Deflection Due to Creep and Shrinkage at Maximum Deflection Location D

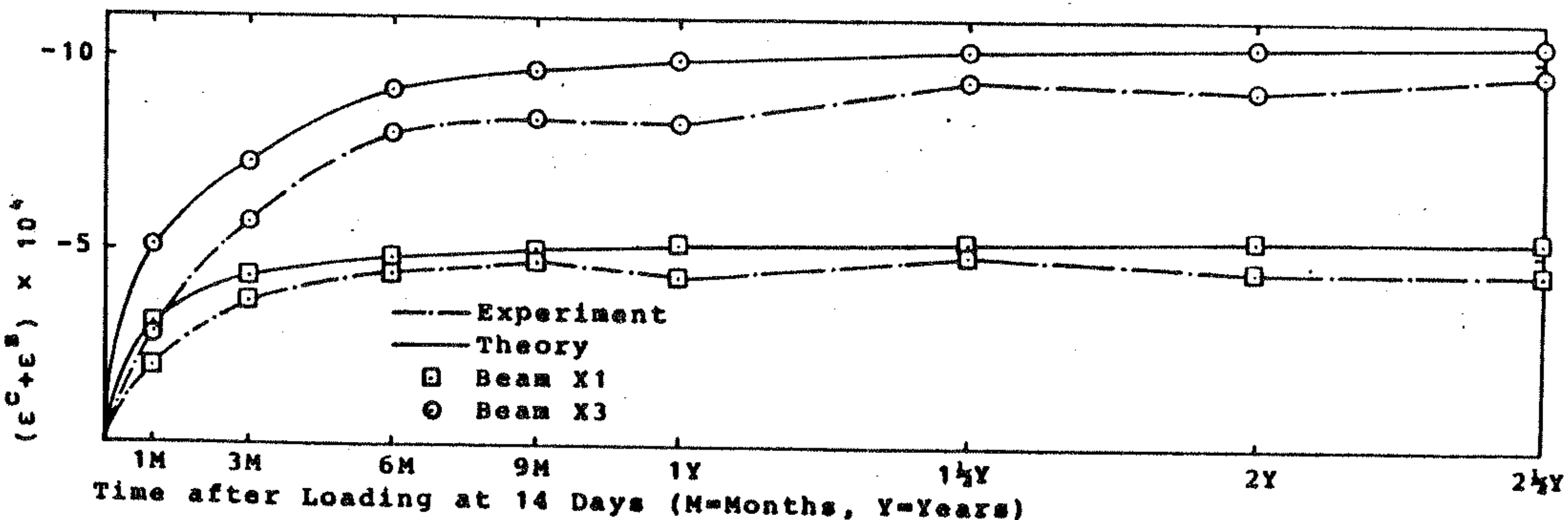

Fig. 8.5.e. Example 8.3.2 - Comparison of Strain Due to Creep and Shrinkage at Max. Positive Moment Location P at Compressive Steel Level

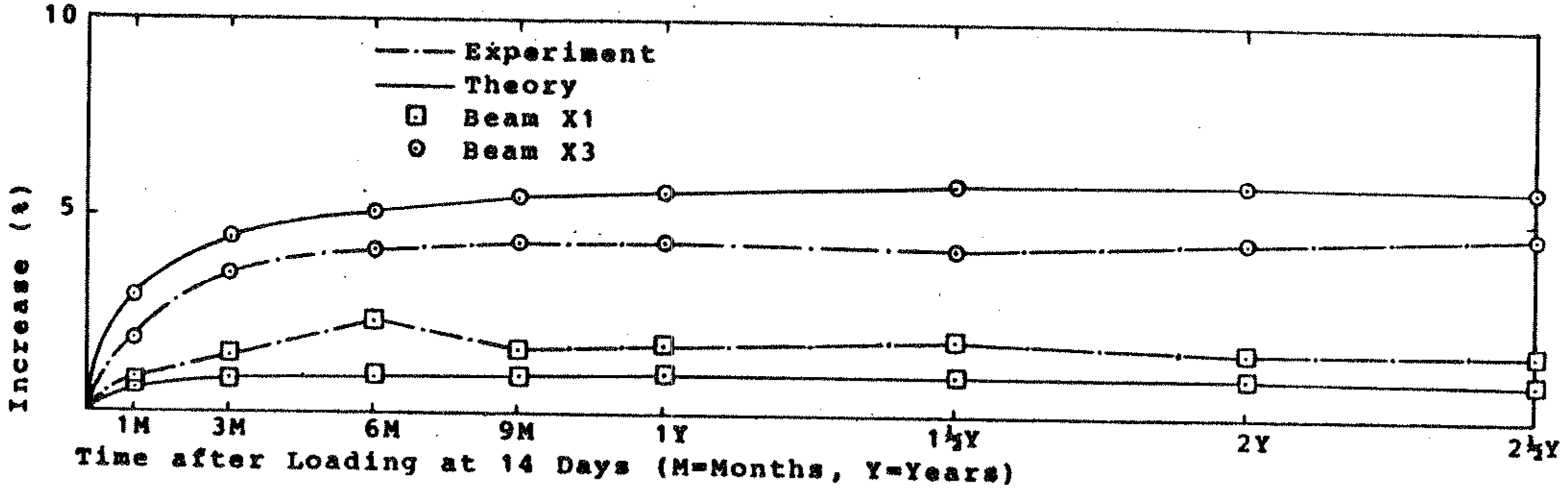

Fig. 8.5.f. Example 8.3.2 - Comparison of Increase in Midlength Reaction Due to Creep and Shrinkage

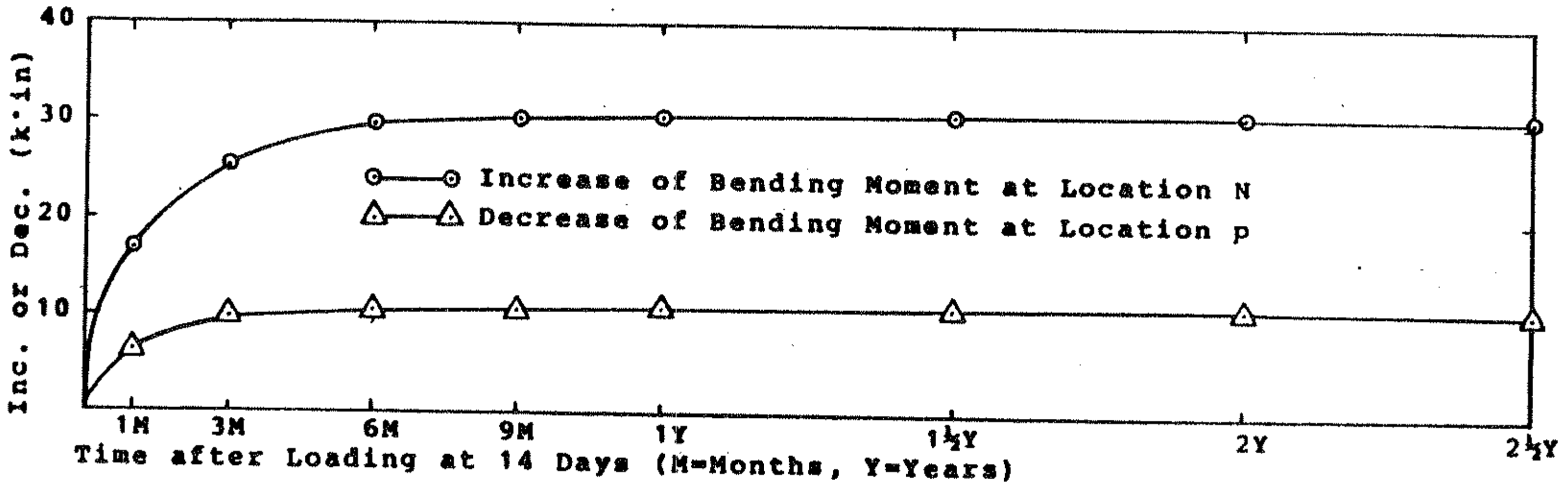

Fig. 8.5.g. Example 8.3.2 - Change in Bending Moment Due to Creep and Shrinkage for Beam X3 (Theoretical Results Only)

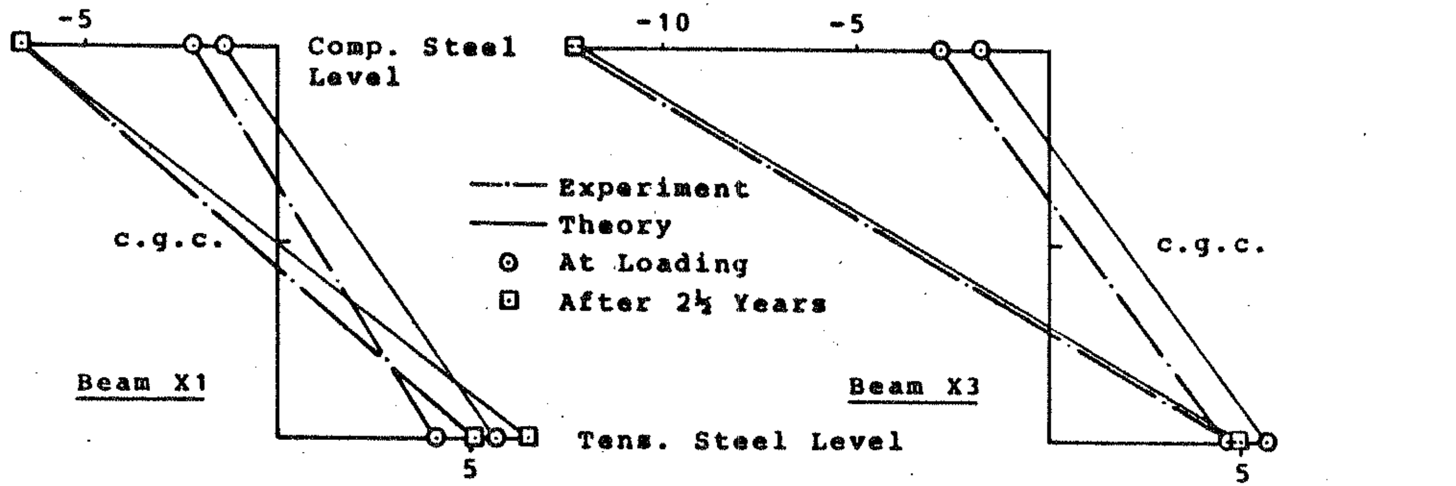

(a) Total Strain $\varepsilon \times 10^{4}$ at Maximum Positive Moment Location P

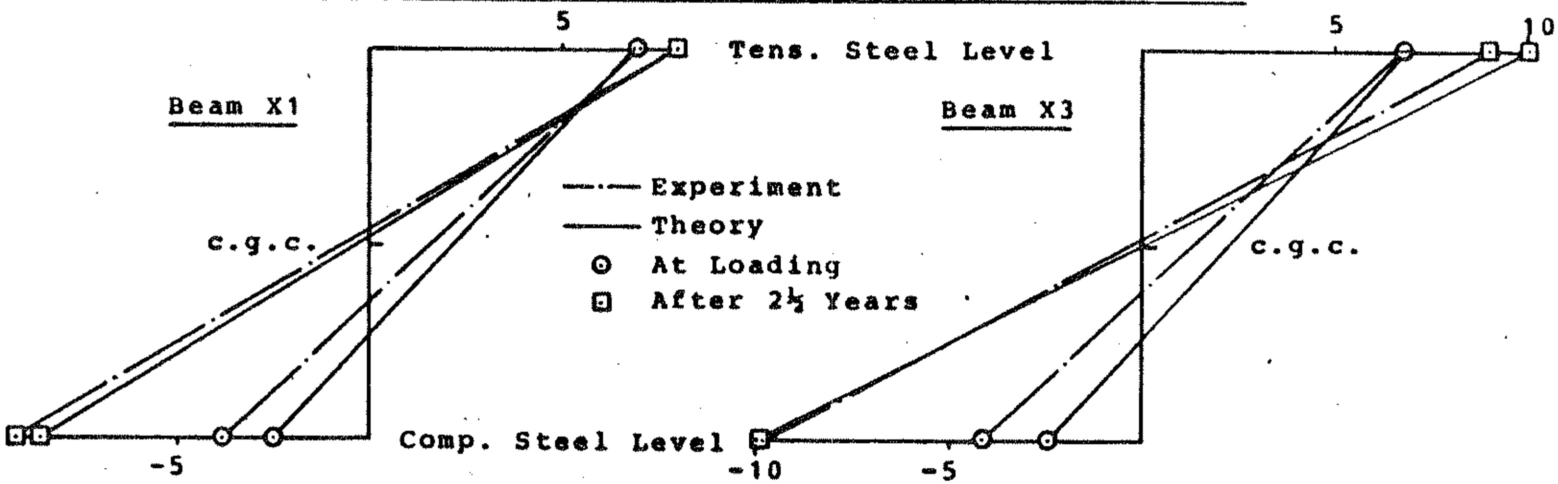

(b) Total Strain $\varepsilon \times 10^{4}$ at Maximum Negative Moment Location N

Fig. 8.5.h. Example 8.3.2 - Comparison of Experimental and Theoretical Strains

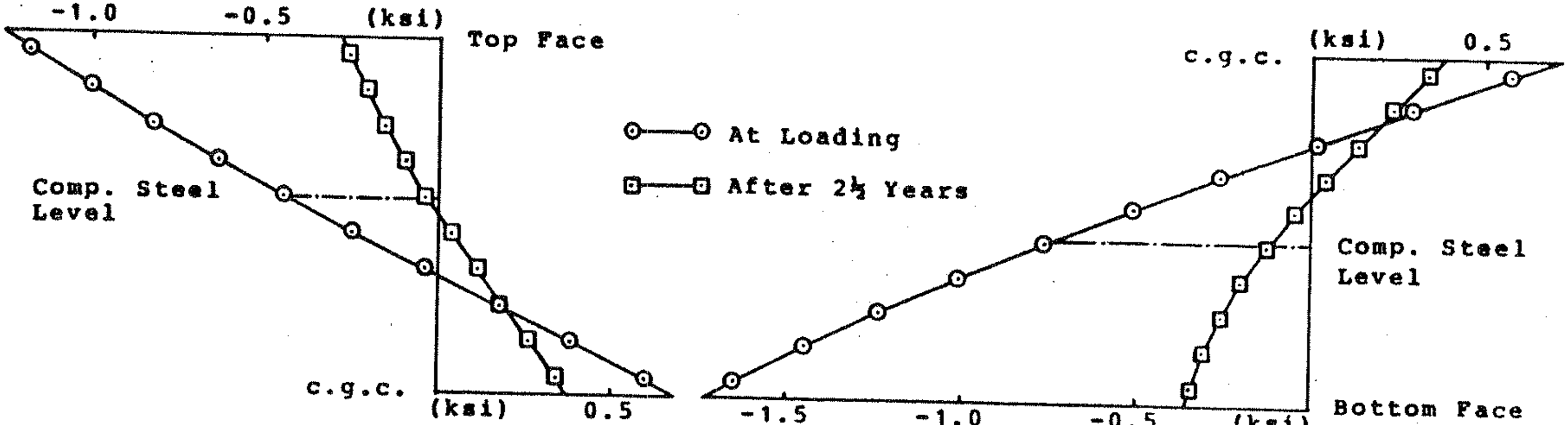

(a) Max. Positive Moment Location P

(b) Max. Negative Moment Location N

Fig. 8.5.i. Example 8.3.2 - Stress Distribution at Locations P and N for Beam X1 (Theoretical Values Only)

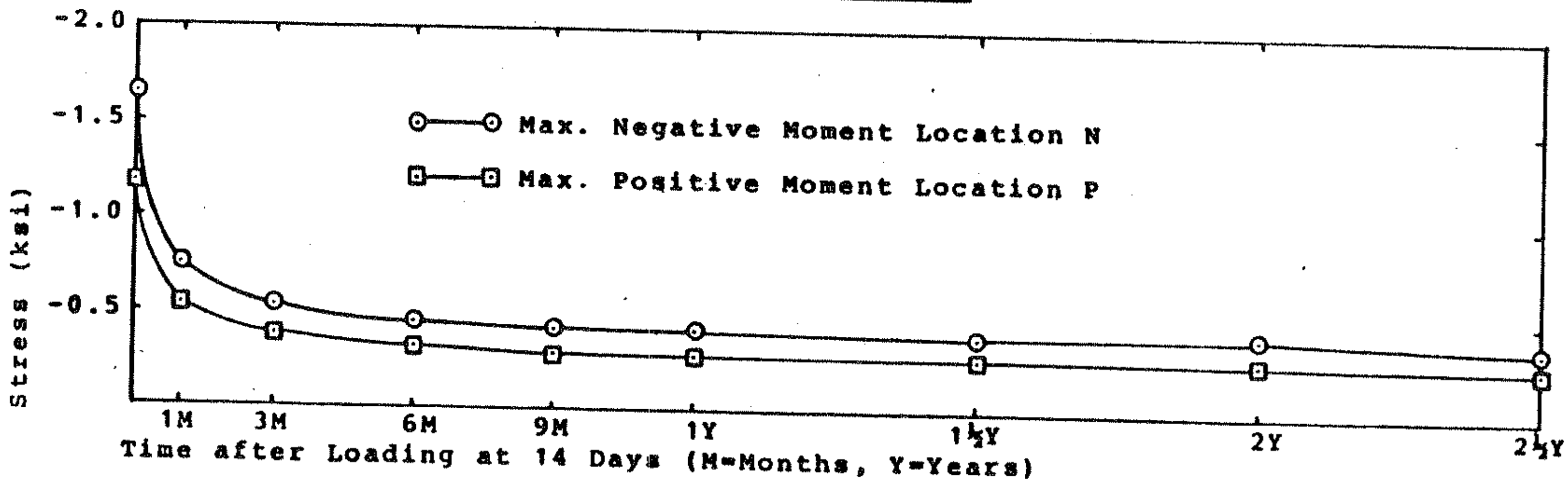

Fig. 8.5.j. Example 8.3.2 - History of Maximum Compressive Stress at Locations P and N for Beam X1 (Theoretical Results Only)

strains $\varepsilon^{nm}(t)$ which include the creep strain $\varepsilon^{c}(t)$ from the total strain $\varepsilon(t)$, as expressed in Eqs. (2.1) to (2.3). Since the creep strain increases at a higher rate with the increase of stress intensity, the corresponding mechanical strain and the stress is reduced at an increasing rate from the c.g.c. to the compression face of the cross section as shown in the figure.

8.3.3 England-Ross Beam - Temperature Dependent Creep and Shrinkage Analysis of a Flexurally Restrained Beam

Many reinforced concrete structures are subjected to thermal gradients. Chimneys, floor slabs under boilers, the biological shields of nuclear power stations are a few of the examples. Under the restraint of displacements or rotations thermal stresses develop in these structures, and the stresses undergo changes due to the creep and shrinkage of concrete. However, it has been widely reconized by engineers that the creep and shrinkage of concrete are temperature dependent. Creep and shrinkage generally increase with the increase of temperature, but the relationship is not linear.

One of the earliest experimental and analytical studies on the effects of temperature dependent creep and shrinkage on reinforced concrete structures was conducted by England and Ross (76). They tested flexurally restrained reinforced concrete beams subjected to a linear thermal gradient. They also obtained creep and shrinkage curves at different temperatures ranging from 20 deg C to 140 deg C.

Among the sealed and unsealed beams tested, the unsealed beam is selected for this study. The reinforced concrete beam, as shown in Fig. 8.6.a, is restrained against bending, but free to displace longitudinally. The beam is left unsealed at the laboratory temperature of 16 deg C until 80 days after casting of concrete, when the linear temperature gradient is applied by heating the top face of the beam to 110 deg C and the bottom face to 65 deg C. Since the strain remains constant along the length of the beam only one element is used in the analysis. The cross section is divided into 10 concrete layers.

The material properties used in the analysis are summarized in Fig. 8.6.a. ACI formulas for time dependent concrete properties are used. Temperature dependent experimental shrinkage data shown in the figure are used directly in the analysis. Uniform shrinkage throughout the depth of the beam is assumed. Temperature dependent creep is incorporated with the following specific creep function as described in detail in chapter 3.

$$c(\tau,t-\tau,T) = \sum_{i=1}^{3} a_i(\tau)[1 - e^{-10^{-i}\phi(T)(t-\tau)}] \qquad (8.2)$$

Temperature shift function $\phi(T)$ is approximated by the following function obtained from the specific creep versus logarithmic time curves for different temperatures shown in Fig. 8.6.b.

$$\phi(T) = e^{\psi(T)} \; ; \; \psi(T) = -T^2/2400 + 4T/30 - 8 \qquad (8.3)$$

where T is in deg C and the reference temperature is 80 deg C. We note the close resemblance of specific creep curves for different temperatures.

Experimental and theoretical results are summarized in table 8.5. Experimental steel stress, theoretical steel stress, concrete stress, strain and bending moment are tabulated up to 150 days after casting of concrete. In Fig. 8.6.c the history of steel stress is plotted. Results from experiment, present analysis and the analysis made by England and Ross are shown together for comparison. The result from the present analysis can be observed to be very close to the experimental result and it approximates the experimental result better than the analytical result obtained by England and Ross, in which they used a step-by-step method without considering the creep recovery and the effect of the concrete age on its specific creep. In Fig. 8.6.d, history of the concrete stress at 1 in. from the top face is plotted. Stress distributions at 80 days and 130 days after casting of concrete are shown in Fig. 8.6.e.

The behavior of the flexurally restrained beam subjected to temperature gradient will be briefly discussed. Up to 80 days after casting of concrete, shrinkage of concrete takes place. The effect is an equivalent compressive force acting on the beam. As a result compressive stress develops in the steel and tensile stress develops in the concrete since the net axial force is zero. When the temperature gradient is applied, the beam will bend concave downward if it was left free to bend. However, since the bending is restrained, tensile stress develops in the lower part of the beam and compressive stress develops in the upper part of the beam. As shown in Fig. 8.6.e, 2/5 of the beam on the lower part of the cross section is cracked as a result. The horizontal displacement of the beam is increased due to the overall increase of the temperature in the beam.

The stress distribution within the beam undergoes a drastic change due to the creep of concrete as time elapses. Fig. 8.6.e shows that compressive concrete stress is greatest at the top face of the beam, and the top face is subjected to the maximum temperature. Creep strain is proportion to stress intensity at low stress level as in this case, and it increases with the increase of temperature. Thus the compressive creep strain is greatest at the top face and decreases toward the c.g.c. If the beam was left free to bend, this creep strain distribution would produce an upward bending. As a result of the flexural restraint tensile stress develops in the upper part of the beam and compressive stress develops in the lower part of the beam. The amount of this stress redistribution due to creep is so great that the tensile steel stress becomes compressive as shown in Fig. 8.6.d. Shrinkage of concrete also contributes to the same effect as already mentioned. Note that tensile creep strain has little effect in this stress redistribution since tensile stresses

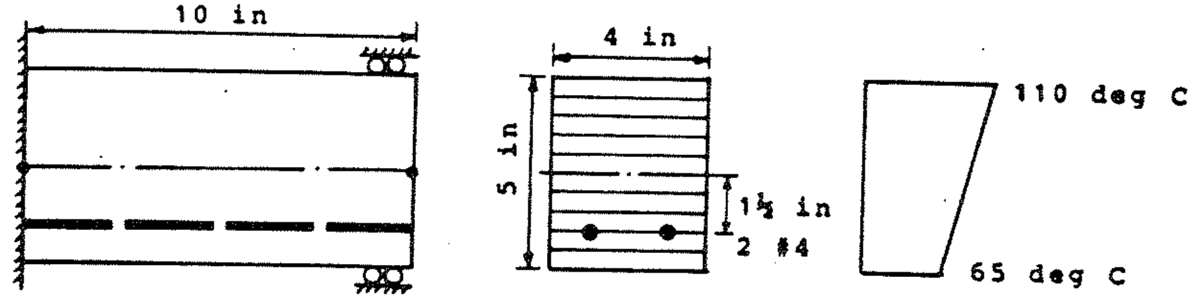

(a) Structure and Temperature Gradient Loading

(b) Concrete Properties

$$f'_c(\tau) = \frac{\tau}{a + b\tau} \cdot f'_c(28) \quad ; \quad f'_c(28) = 6246 \text{ psi}, \; a = 4., \; b = 0.85$$

$$E_i(\tau) = 33 \cdot w^{1.5} \sqrt{f'_c(\tau)} \text{ psi} \quad ; \quad w = 150 \text{ pcf}$$

$$f''_c(\tau) = f'_c(\tau) \quad ; \quad f'_t(\tau) = 0.7 \sqrt{w f'_c(\tau)}$$

$$\alpha = 12.1 \times 10^{-6} / \text{deg C}$$

$$c(\tau, t-\tau, T) = \sum_{i=1}^{3} a_i(\tau) [1 - e^{-10^{-i} \phi(T)(t-\tau)}]$$

$$a_i(\tau) = a_i(\tau_o) \cdot \frac{E_i(\tau_o)}{E_i(\tau)} \cdot \left(\frac{\tau}{\tau_o}\right)^{-0.118} \quad ; \quad \tau_o = 10 \text{ days}$$

$$\left. \begin{aligned} a_1(\tau_o) &= 5.8 \times 10^{-7} \\ a_2(\tau_o) &= 0.1 \times 10^{-7} \\ a_3(\tau_o) &= 4.0 \times 10^{-7} \end{aligned} \right\} \begin{array}{l} \text{Creep Coefficients per psi} \\ \text{at Reference Temperature} \\ T_o = 80 \text{ deg C} \end{array}$$

$$\phi(T) = e^{\psi(T)} \quad ; \quad \psi(T) = -T^2/2400 + 4T/30 - 8$$

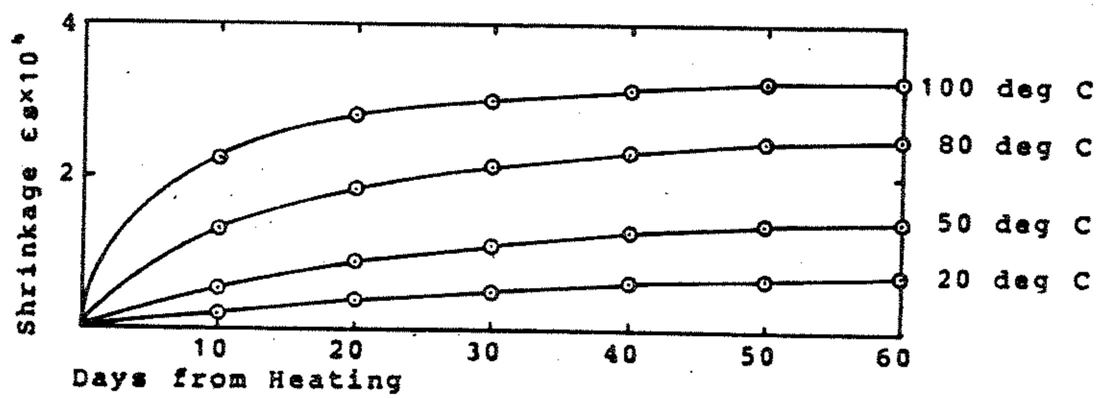

(c) Steel Properties

$$E_s = 30 \times 10^6 \text{ psi} \quad ; \quad A_s = 0.098 \text{ in}^2$$

$$\alpha = 11.7 \times 10^{-6} / \text{deg C}$$

Fig. 8.6.a. Example 8.3.3 - England-Ross Beam

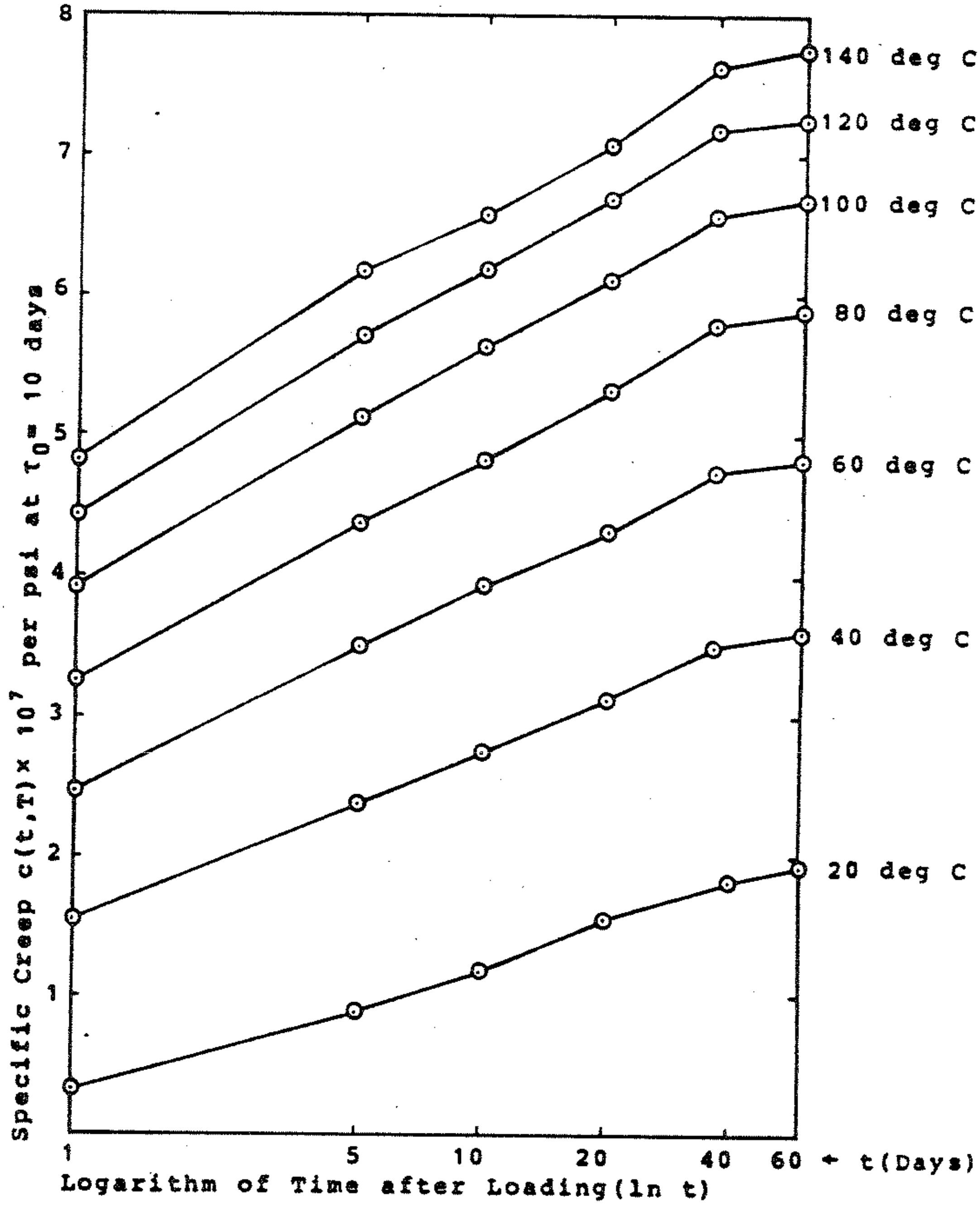

Fig. 8.6.b. <u>Example 8.3.3 - Temperature Dependent Specific Creep versus Logarithmic Time Curve</u>

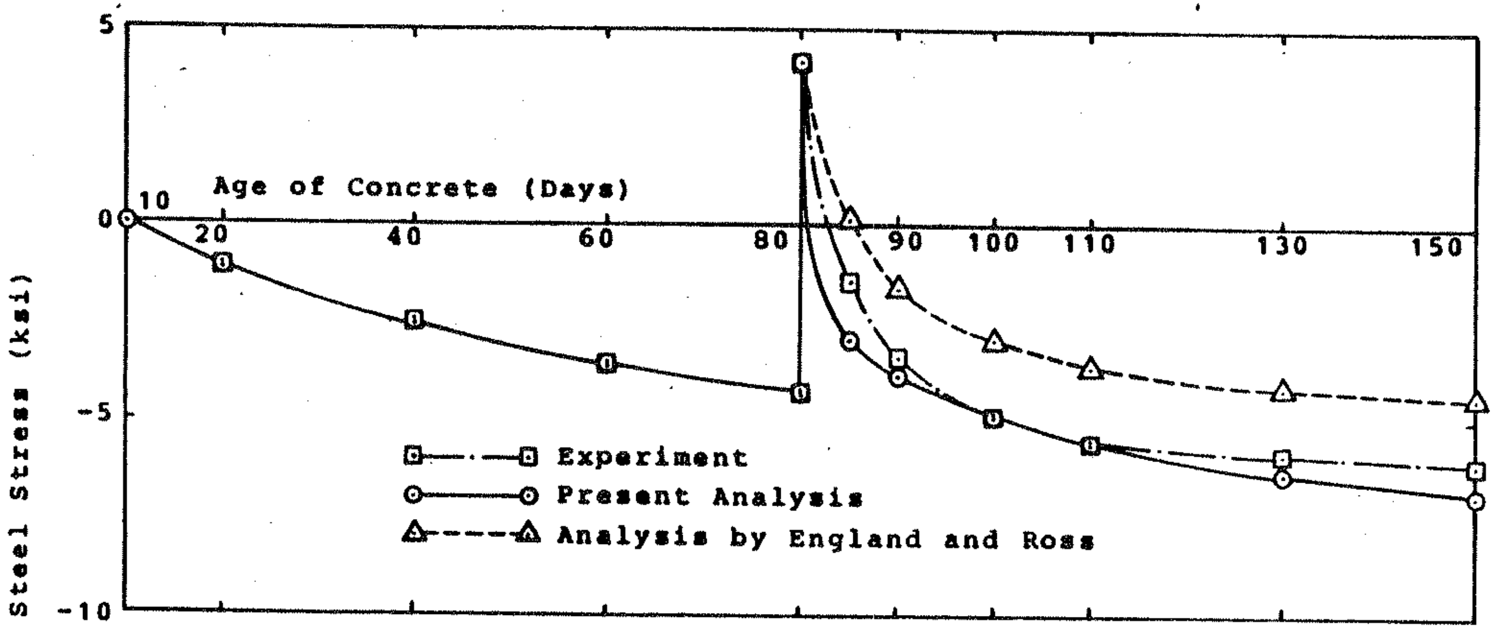

Fig. 8.6.c. Example 8.3.3 - History of Steel Stress

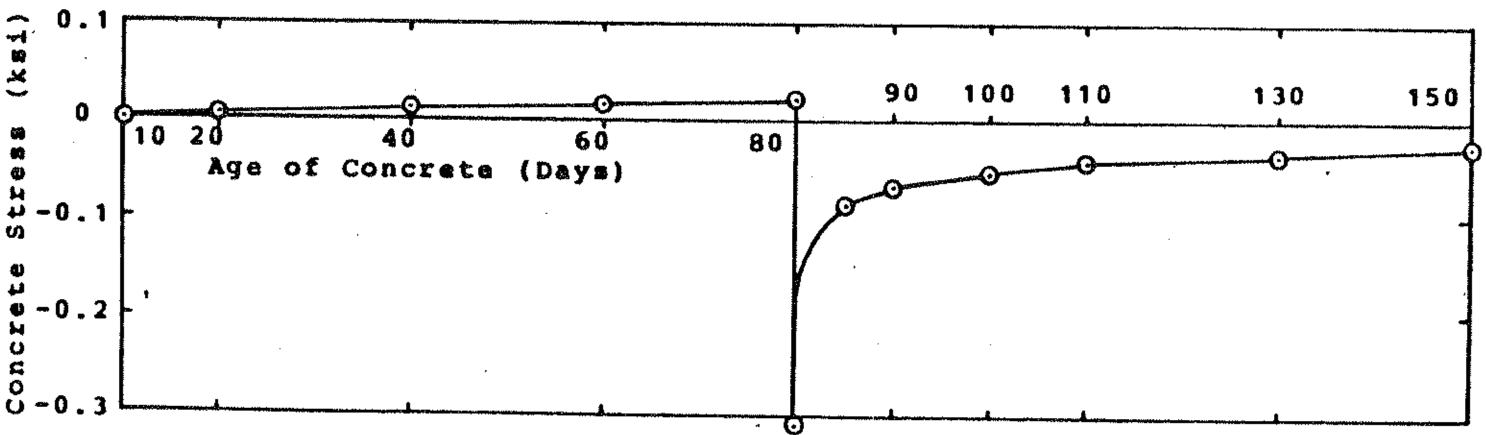

Fig. 8.6.d. Example 8.3.3 - History of Concrete Stress at 1 in. from Top Face (Present Analysis)

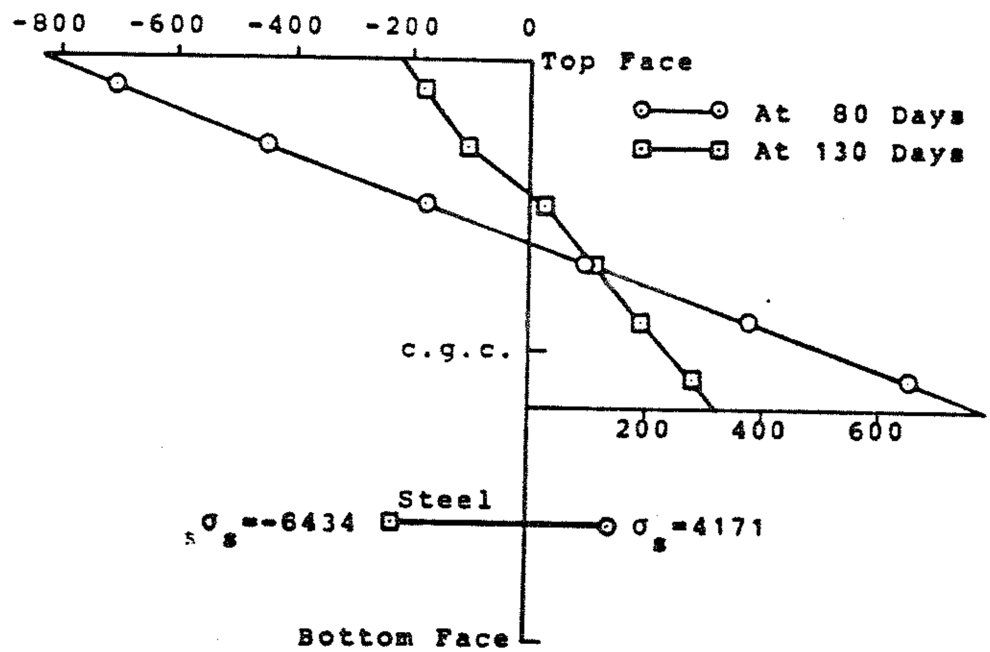

Fig. 8.6.e. Example 8.3.3 - Stress Distribution (psi) at 80 Days and 130 Days

Age (days)	σ_s(Exp) (psi)	σ_s(Th) (psi)	σ_c(Th) (psi)	ε(Th) $\times 10^6$	M(Th) (in·lb)
20	-1220	-1017	5	-34	-150
40	-2440	-2561	13	-85	-376
60	-3540	-3609	18	-120	-531
80	-4200	-4366	21	-146	-642
	4200	4171	-310	816	5775
85	-1460	-2886	-82	581	1051
90	-4310	-3819	-68	550	690
100	-4780	-4875	-53	515	404
110	-5490	-5565	-42	492	61
130	-5850	-6434	-38	463	65
150	-6100	-6992	-25	445	-565

* σ_c : Concrete Stress at 1 in from Top Face

* Temperature Gradient Applied at τ = 80 days

Table 8.5. Example 8.3.3 - Summary of Results

above and below the c.g.c. have comparable values when the temperature gradient is applied, as shown in Fig. 8.6.e, and their effects are more or less balanced.

The stress redistribution in concrete is shown in Fig. 8.6.e. Note that both compressive and tensile stresses are reduced. The reduction of stress is proportional to the amount of creep strain since the stress is a function of the mechanical strain which decreases as the creep strain increases. We also note in the figure that the ratio of the stress reduction is greatest on the top concrete fiber. Since the top fiber is subjected to the maximum temperature its creep strain is correspondingly magnified by the largest amount due to the temperature dependence of concrete creep.

8.4 Prestressed Concrete Frames

8.4.1 Lin Beam - Ultimate Load Analysis of a Post-tensioned Bonded Continuous Beam

Lin (114) tested a series of post-tensioned bonded continuous beams under static and repeated loads up to failure to determine their cracking and ultimate strengths. Two of the beams tested for static loads are selected for this study.

The structure and its material properties are shown in Fig. 8.7.a. The continuous beam is symmetric about its center support. The prestressing steel tendon has a concordant profile, and consists of a straight part which extends from the end of the beam to the point where the concentrated load is applied, and a curved part over the center support. The tendon consists of a 32 parallel wires of 0.196 in. diameter. Beam B is reinforced with mild steel bars while Beam A is not reinforced. One half of the beam is analyzed with 10 elements and the cross section is divided into 10 concrete layers. The prestressing steel tendon is also divided into 10 segments corresponding to each element.

At 14 days after casting of concrete the tensioning operation is performed with the initial prestress of 142 ksi and the beam is subjected to its dead load. Approximately two weeks thereafter, the concentrated load P is applied with increments up to failure. The analytical results after the tensioning operation and before the concentrated load is applied are summarized in table 8.6. The upward deflection at midspan, the end reaction and the stresses for each prestressing steel segment are tabulated. Due to friction and the anchorage slip, about 14% of the initial prestress is lost. Uneven distribution of prestress along the tendon due to friction can be noted. During the two week period before loading, a slight increase in the deflection and the reaction, and a decrease in the prestress take place due to the creep and shrinkage of concrete and the relaxation of prestress. Standard ACI creep and shrinkage data given in section 2.2.3 was used for the analysis.

In the analysis for the concentrated load, the aim is taken at studying the behavior of the prestressed concrete continuous beam as the load is applied up to failure, rather than determining the exact values of the cracking load and the ultimate load. Thus the structure is analyzed with a relatively crude mesh layout and large load increments are taken. With the average load increment of 5 kips, Beam A is analyzed up to P = 35 kips, and Beam B is analyzed up to P = 40 kips. The ultimate load measured in the experiment was 39.2 kips for Beam A and 45.8 kips for Beam B. The analysis showed failure of Beam A at 40 kips and Beam B at 45 kips. With the displacement increment ratio tolerance of 0.02, the average number of iterations per load step was 5.

In table 8.7.(a) the experimental and analytical values of the midspan deflection and the end reaction due to load are tabulated. These values are plotted in Fig. 8.7.b and 8.7.c. Although the analytical values are slightly stiffer than the experimental values, excellent comparison between two results can be noted. Due to the presence of the reinforcing steel, the results for Beam B are stiffer than those for Beam A, thus the addition of mild steel bars increases the load carrying capacity. After the cracking of concrete takes place, the internal forces are redistributed such that the rate of increase of the bending moment with the increase of the load in the positive moment region becomes greater compared to the rate prior to the cracking. In the negative moment region, the rate becomes smaller. Correspondingly, the ratio of the end reaction to the applied load increases after cracking, as shown in Fig. 8.7.c.

The analytical results for the increase of the stress in the prestressing steel due to load is tabulated in table 8.7.(b) and plotted in Fig. 8.7.d. Segments No. 5 and 10 represent the maximum positive and negative moment locations, respectively. Since the tendon is bonded with concrete the stress increases with the increase of the strain at the location of the tendon within the cross section. The increase of stress with the increase of load for segment No. 10 is greater than that for segment No. 5 since segment No. 10 is located farther apart from the c.g.c. and the absolute value of the maximum negative bending moment is greater than that of the maximum positive moment. The increase of beam stiffness due to mild steel bars for Beam B can also be noted.

The analytical stress distributions at maximum positive and negative moment locations at $P = 0$ and $P = 35$ kips are shown in Fig. 8.7.e for both beams. Prestressing and reinforcing steel stresses are plotted in different scale from concrete stresses. At $P = 0$, steeper concrete stress distribution can be noted at the maximum negative moment location due to greater eccentricity of the tendon compared to the maximum positive moment location. Total compressive forces are almost the same at both locations since the prestressing steel stresses are only slightly different. At $P = 35$ kips, both concrete and prestressing steel stresses are reduced for Beam B due to mild steel bars compared to Beam A although the magnitudes of the bending moment for two beams are comparable.

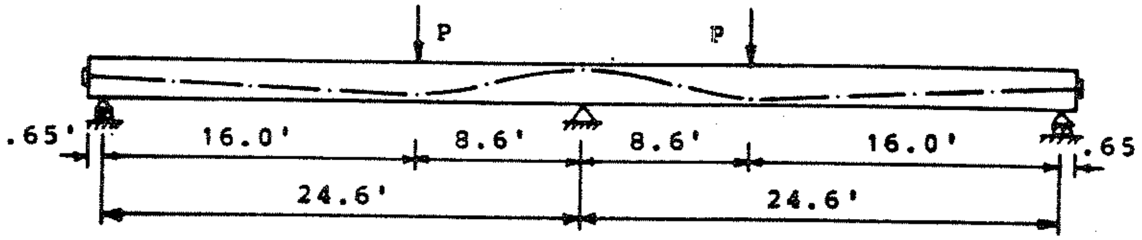

(a) Structure and Loading

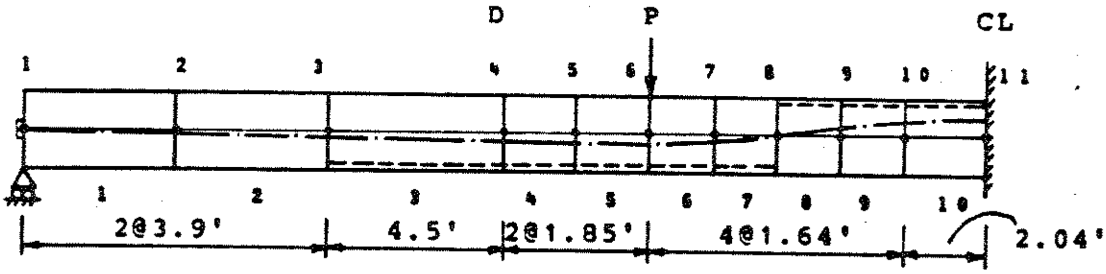

(b) Finite Element Mesh Layout

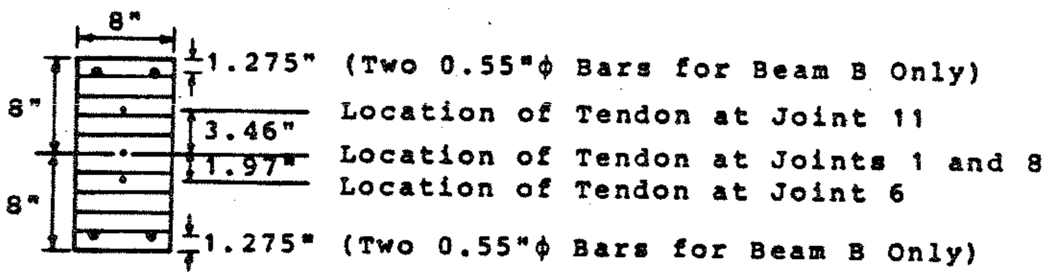

(c) Cross Section

(d) Concrete Properties

At 14 Days (Tensionong Operation)
f''_c=5428 psi, E_i=6.10×10^6 psi, f'_t=800 psi, ε_u=0.0034
At 28 Days (Application of the Load P)
f''_c=5990 psi, E_i=6.13×10^6 psi, f'_t=800 psi, ε_u=0.0034
w=155 pcf

(e) Reinforcing Steel Properties

f_{sy}=45.5 ksi, ε_{su}=0.16, E_{s1}=28.4×10^3 ksi, E_{s2}=104 ksi

(f) Prestressing Steel Properties

A=0.963 in^2, σ_o=142 ksi (P_o=136.746 kips)
Anchorage Slip : 2.01 in
Friction Coefficients : μ=0.3, K=5×10^{-4} rad/ft
Discrete Points in the Stress-Strain Curve
σ_1=208.8 ksi, ε_1=0.0072, E_1=29000 ksi
σ_2=227.8 ksi, ε_2=0.01, σ_3=244.4 ksi, ε_3=0.02
σ_4=250.0 ksi, ε_4=0.03, σ_5=256.0 ksi, ε_5=0.05

Fig. 8.7.a. Example 8.4.1 - Lin Beam

		Beam A		Beam B	
		14 Days*	28 Days*	14 Days*	28 Days*
δ (in)		-0.059	-0.099	-0.052	-0.086
R (k)		1.264	1.266	1.255	1.259
Stress (ksi) in P.S. Segments	1	121.90	121.85	121.90	121.85
	2	121.88	121.81	121.88	121.81
	3	121.86	121.69	121.86	121.78
	4	121.85	121.53	121.85	121.65
	5	121.84	121.38	121.84	121.53
	6	121.78	121.34	121.78	121.49
	7	121.68	121.53	121.68	121.62
	8	121.62	121.57	121.62	121.64
	9	121.58	121.01	121.58	121.18
	10	121.56	120.49	121.56	120.74

* At 14 days after casting of concrete the tensioning operation is performed.
* δ is the upward deflection at midspan.
* R is the upward end reaction.
* Prestressing steel segment numbers coincide with the element numbers in which they are embedded.

Table 8.6. Example 8.4.1 - Summary of Analytical Results Before Loading

Load P (kips)	Midspan Deflection (in)				End Reaction (kips)			
	Beam A		Beam B		Beam A		Beam B	
	Exp.	Th.	Exp.	Th.	Exp.	Th.	Exp.	Th.
10	0.11	0.11	0.11	0.10	1.61	1.62	1.61	1.61
15	0.18	0.16	0.18	0.15	2.39	2.43	2.39	2.42
20	0.26	0.22	0.26	0.22	3.35	3.34	3.34	3.33
25	0.38	0.33	0.36	0.30	4.43	4.49	4.43	4.40
30	0.62	0.59	0.50	0.46	5.43	5.34	5.37	5.29
35	1.00	0.96	0.70	0.67	6.35	6.17	6.22	6.12
37.5	—	—	0.85	0.82	—	—	6.74	6.59
40	—	—	1.00	0.99	—	—	7.26	7.15

(a) Comparison of Midspan Deflections and End Reactions

Load P (kips)	P.S. Segment 5				P.S. Segment 10			
	Beam A		Beam B		Beam A		Beam B	
	Stress (ksi)	Inc. (%)	Stress (ksi)	Inc. (%)	Stress (ksi)	Inc. (%)	Stress (ksi)	Inc. (%)
0	121.4		121.5		120.5		120.7	
10	122.3	0.7	122.3	0.7	122.9	2.0	123.0	1.9
15	122.7	1.1	122.7	1.0	124.1	3.0	124.1	2.8
20	123.2	1.5	123.1	1.3	126.4	4.9	126.3	4.6
25	125.9	3.7	124.4	2.4	134.3	11.3	131.4	8.8
30	138.6	14.2	130.9	7.7	153.6	27.2	142.2	17.7
35	154.8	27.5	137.6	13.2	178.9	48.0	153.6	27.1
37.5	—	—	140.9	15.9	—	—	163.9	35.5
40	—	—	145.0	19.3	—	—	173.5	43.4

(b) Variations of Prestressing Steel Stresses at Max. Positive and Negative Moment Locations

Table 8.7. Example 8.4.1 - Summary of Results Due to Loading

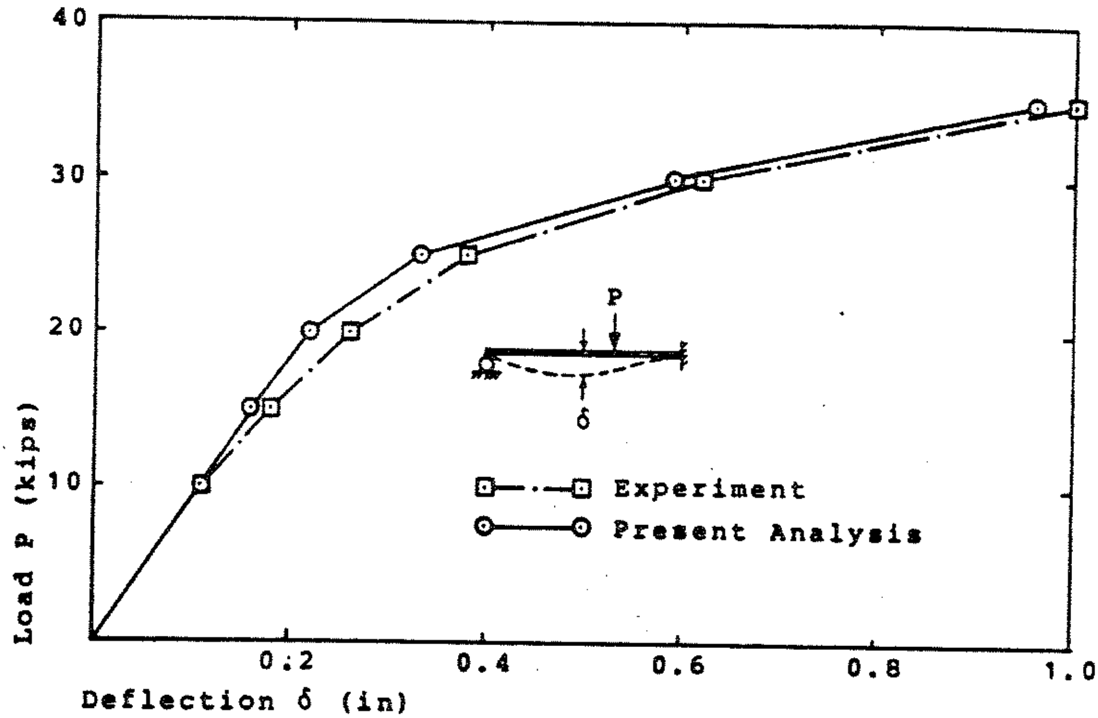

(a) Beam A (Without Mild Steel)

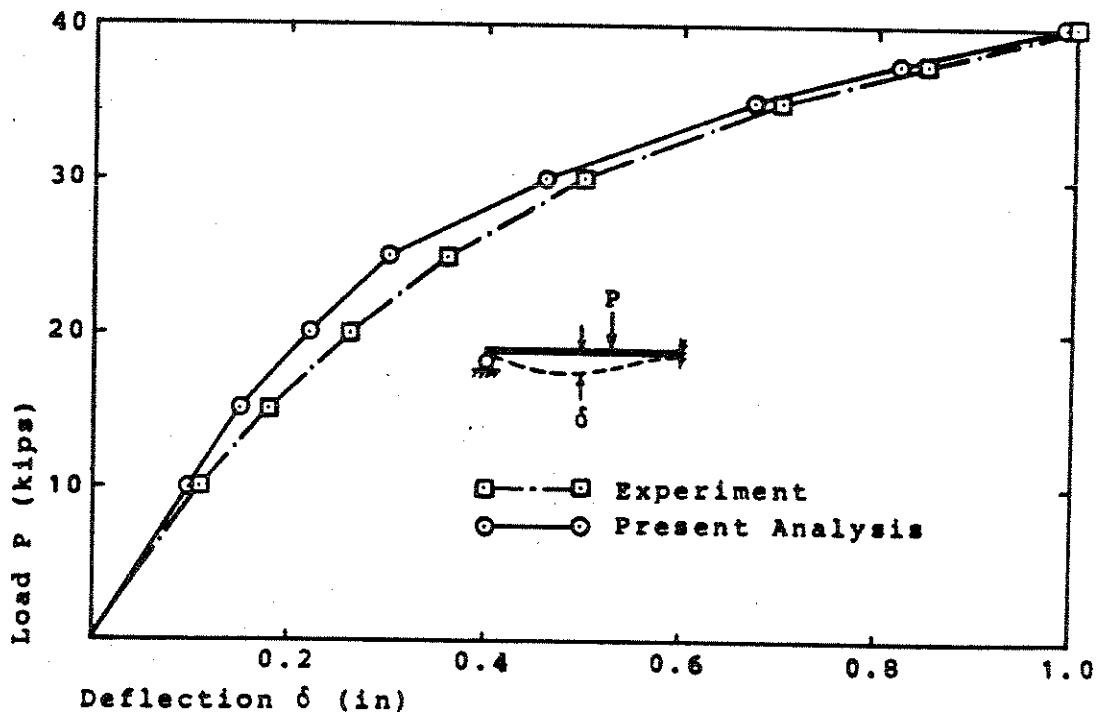

(b) Beam B (With Mild Steel)

Fig. 8.7.b. Example 8.4.1 - Comparison of Midspan Deflections

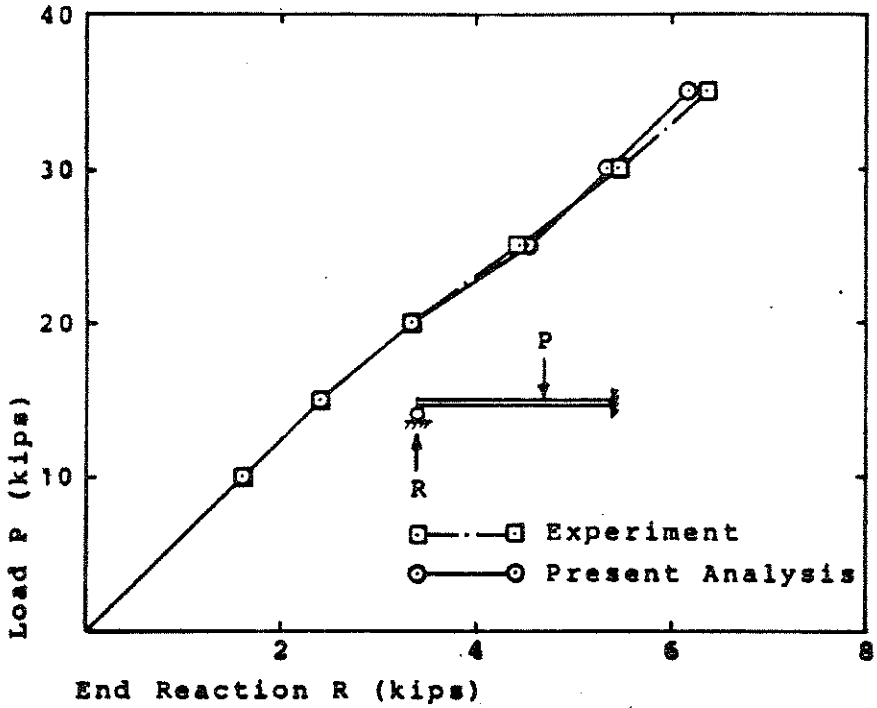

(a) Beam A (Without Mild Steel)

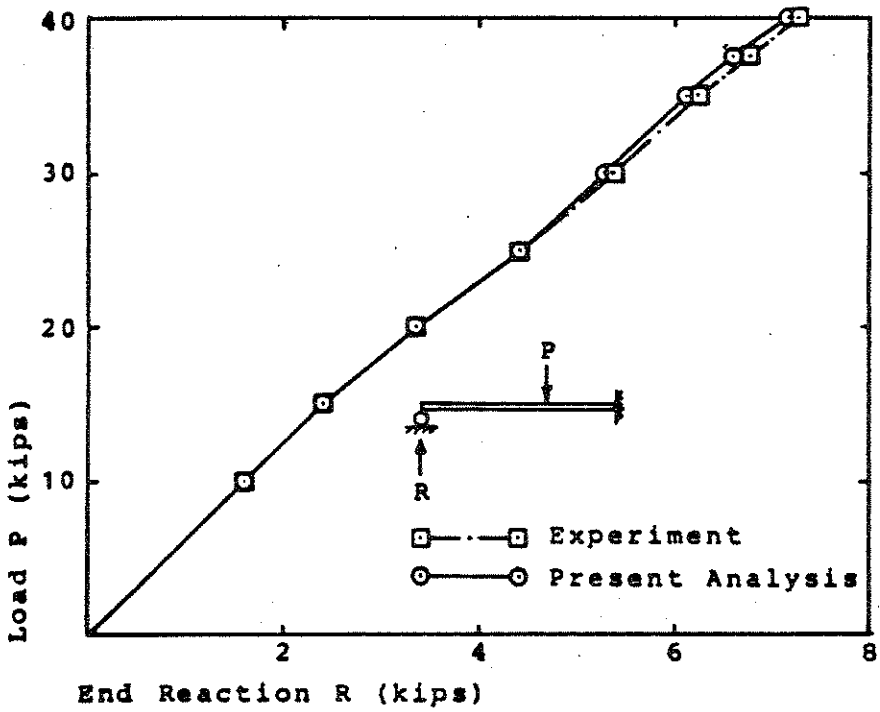

(b) Beam B (With Mild Steel)

Fig. 8.7.c. Example 8.4.1 - Comparison of End Reactions

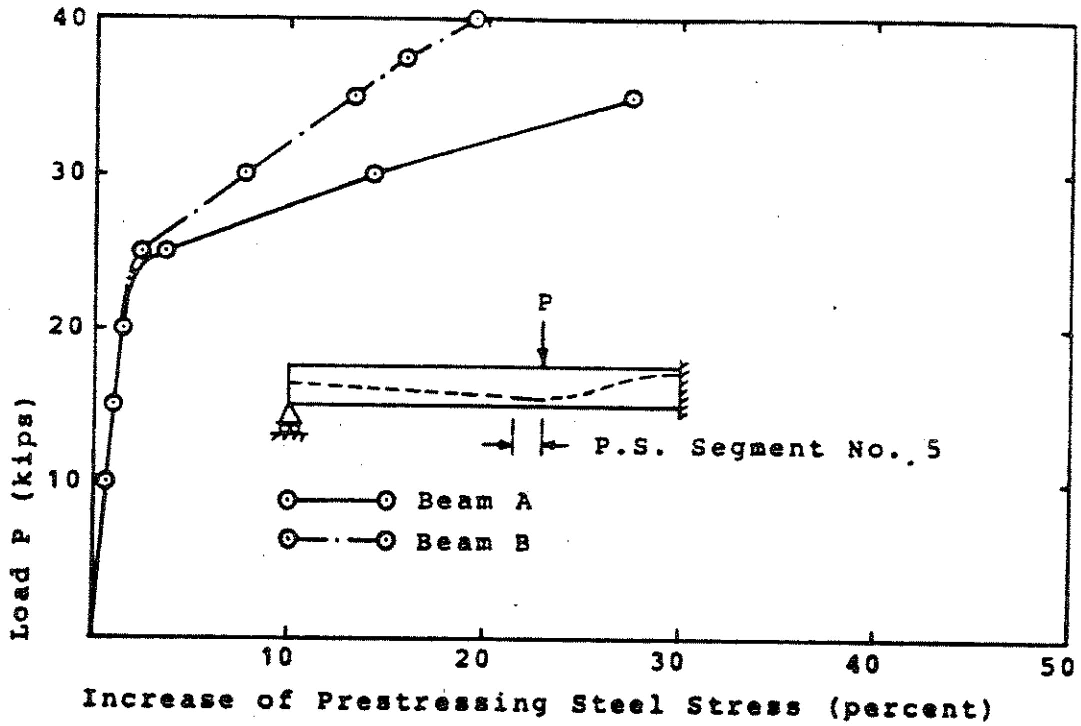

(a) Max. Positive Moment Region (P.S. Segment No. 5)

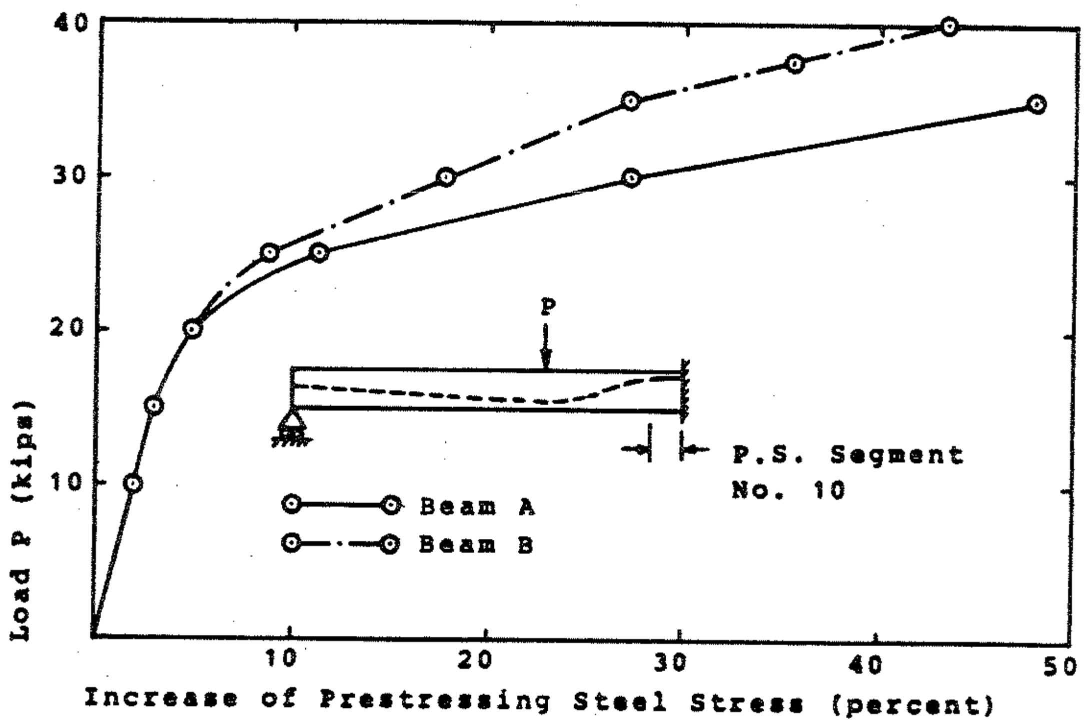

(b) Max. Negative Moment Region (P.S. Segment No. 10)

Fig. 8.7.6. Example 8.4.1 - Percent Increase of Prestressing Steel Stress Due to Load at Max. Positive and Negative Moment Regions

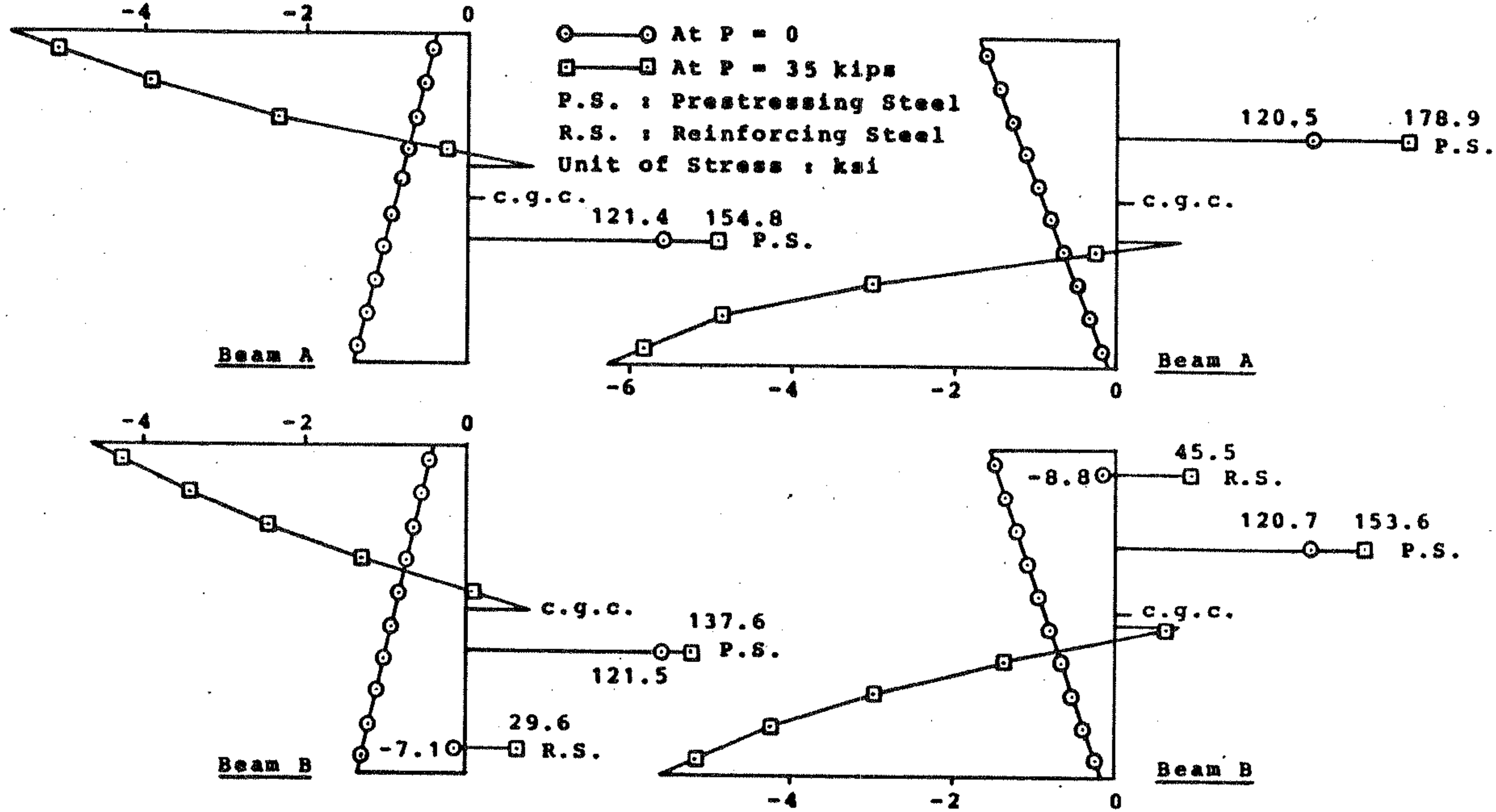

(a) Max. Positive Moment Location (Center of Element No. 5)

(b) Max. Negative Moment Location (Center of Element No. 10)

Fig. 8.7.e. Example 8.4.1 - Stress Distribution at Max. Positive and Negative Moment Locations (Center of Elements No. 5 and 10)

8.4.2 Sinno-Furr Beam - Camber Analysis of a Pre-tensioned Simple Beam

Sinno and Furr (115,116) tested a series of pre-tensioned simple beams to study the growth of camber and the prestress loss with time in the absence of live load after release. They also presented analytical methods to predict the amount of the increase of the camber and the prestress loss with time.

Among the beams tested, Beam L4-5 is selected for the present analytical study. The structure and its material properties are shown in Fig. 8.8.a. One half of the structure is divided into 10 elements. Closer element divisions are used for the three locations where strains were measured in the experiment. The I-shaped cross section is divided into 14 concrete layers.

The initial modulus of the lightweight concrete at 1 day after casting is computed by a procedure described in the section 8.3.1 based on the secant modulus $E = 2.95 \times 10^6$ psi at $0.5f'_c$. Creep coefficients are generated by the least-square method based on the given experimental creep curve. Experimental shrinkage values are also used, and its distribution is assumed to be uniform throughout the depth of the beam.

The prestressing steel tendon has a constant eccentricity in the midspan region, and the eccentricity decreases linearly toward supports. The prestress is released 1 day after casting of concrete with the initial prestressing force,

P_0 = 564.6 kips. In the analysis the relaxation of prestress with time is accounted for by Eq. (6.13). The dead load of the beam was 300.26 lb/ft.

Ten time steps were taken for the present analysis, i.e. at the release of the prestress, and 5, 10, 15, 20, 30, 40, 90, 180, 300 days after release. The experimental and analytical results for the camber, prestress loss and the total strain at midspan up to 300 days after release are tabulated in table 8.8. The predicted values represent the results obtained by Sinno and Furr by the rate of creep method. The midspan camber and the prestress loss at location B are plotted in Fig. 8.8.b and 8.8.c, respectively. The experimental and predicted values in the figures are taken from the figures in the reference 116 for Beam L4-5. Both analytical results can be observed to be in good agreement with the experimental results. Present analytical solution show better agreement with the experimental results at locations A and B compared to those at midspan.

Time dependent variations of the camber and the prestress due to the creep and shrinkage of concrete and the relaxation after release will be briefly discussed. When the prestress is released the beam is subjected the eccentric compression and its dead load. Some of the prestress is lost due to the shortening of concrete and the beam bends upward since the negative moment produced by the eccentric compression is bigger than the dead load moment. For the present example the experiment shows 11.7% loss of prestress, and the present analysis shows 12.2% loss at midspan. The loss at the midspan is greater than the loss at other locations due to the larger bending strain.

Due to the compressive creep of concrete the prestressed is decreased, which in turn decreases the camber. However, creep also increases the camber due to the uneven distribution of the compressive stress through the depth of the beam. The compressive stress is the smallest at the top face of the beam and the largest at the bottom face. Hence the creep strain also increases toward the bottom of the beam, which results in the increase of the camber. The net effect of the creep is an increase of the camber. Shrinkage of concrete and the relaxation of the prestress decreases the prestress, and the camber is decreased correspondingly.

The most dominant effect on the camber is the creep of concrete. This can be observed in the similarity of the camber curve with the creep curve in which large amount of the creep takes place at an earlier period and the rate of increase with time is decreasing. The shape of the prestress loss curve has similar properties since the shapes of the creep curve, shrinkage curve and the relaxation curve have above mentioned properties. Thus, most of the increase in the camber and the prestress loss after release can be observed to take place by 30 days after release. The ratio of the midspan camber increase at 30 days after release to the increase at 300 days after release is 0.87 in the experiment, and 0.92 by the present analysis. The experimental and analytical ratios for the prestress loss at midspan after release

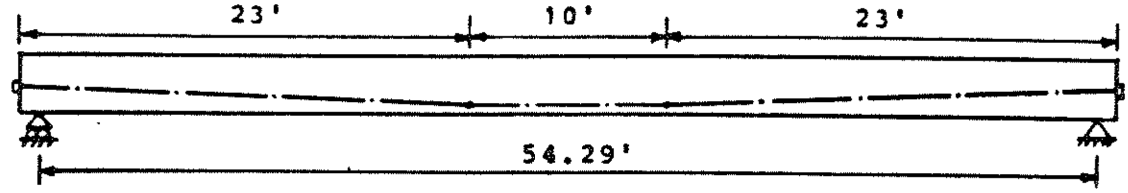

(a) Structure

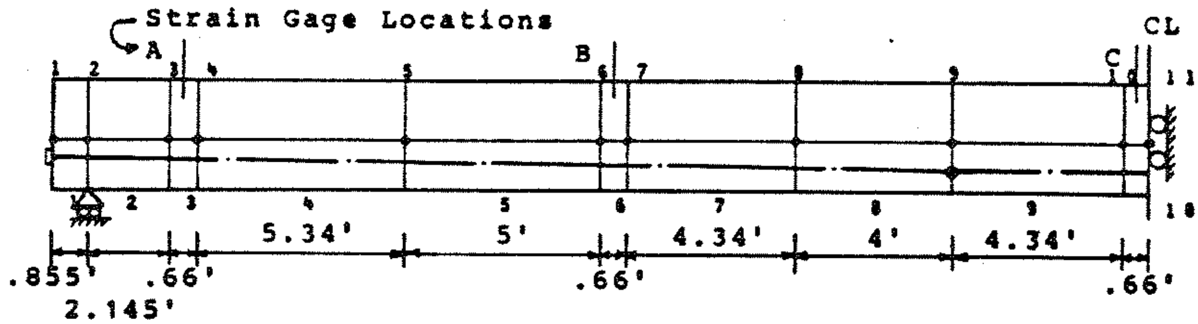

(b) Finite Element Mesh Layout

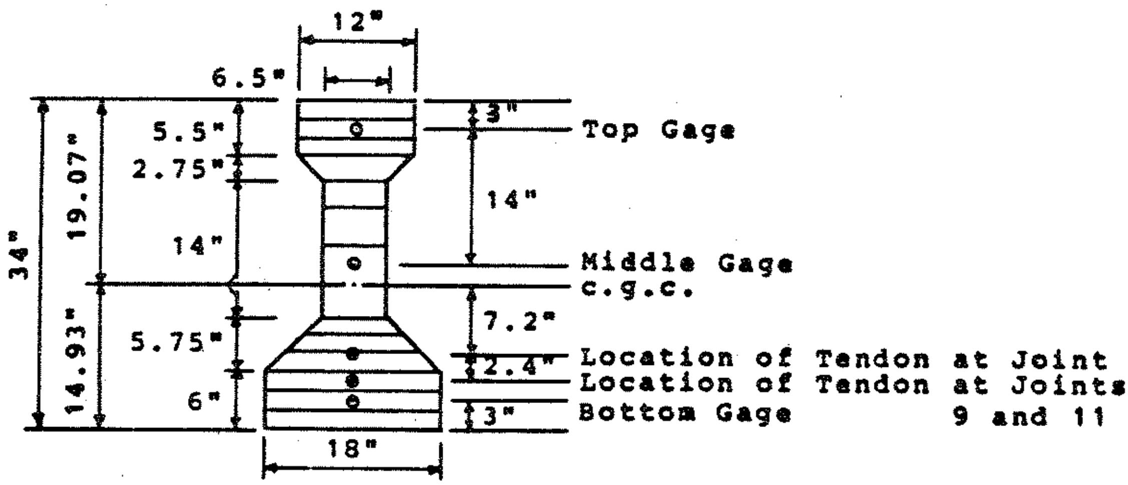

(c) Cross Section

(d) Concrete Properties

$f_c'=3430$ psi, $E_i=3.456\times10^6$ psi at 1 Day

$$c(\tau,t-\tau) = \sum_{i=1}^{3} a_i(\tau)[1 - e^{-10^{-i}(t-\tau)}]$$

Coefficients a_i per psi at 1 Day:
$a_1=3.1341\times10^{-7}$, $a_2=3.0730\times10^{-7}$, $a_3=0.7911\times10^{-7}$

$$\varepsilon^s(\tau) = \frac{-175\tau}{4+\tau} \times 10^{-6}, \quad \tau \text{ : Age of Concrete in Days}$$

(e) Prestressing Steel Properties

$A=3.27$ in^2, $E=28.5\times10^6$ psi, $P_o=564.6$ kips before Release
$f_y=230$ ksi in Eq. (6.13) for Relaxation

Fig. 8.8.a. Example 8.4.2 - Sinno-Furr Beam

Days After Release		Measured	Predicted		Present Analysis	
		Values	Values	% Error	Values	% Error
*Camber (in)	0	1.33	1.33	0.0	1.44	8.3
	10	1.82	2.06	13.2	2.04	12.1
	30	1.98	2.24	13.1	2.28	15.2
	90	2.06	2.32	12.6	2.31	12.1
	300	2.11	2.35	11.4	2.35	11.4
Prestress Loss (%)	0	11.73	11.99	2.2	12.24	4.3
	10	18.57	19.77	6.5	20.68	11.4
	30	20.43	21.81	6.8	23.59	15.5
	90	21.03	22.75	8.2	24.19	15.0
	300	22.65	23.11	2.0	24.64	8.8
Total Strain × 10^6 – Top Gage	0	75	40	-46.7	27	-64.0
	10	190	183	-3.7	195	2.6
	30	240	224	-6.7	251	4.6
	90	250	244	-2.4	270	8.0
	300	290	255	-12.1	280	-3.4
Total Strain × 10^6 – Middle Gage	0	415	413	-0.5	405	-2.4
	10	700	736	5.1	727	3.9
	30	780	823	5.5	843	8.1
	90	820	863	5.2	870	6.1
	300	900	881	-2.1	889	-1.2
Total Strain × 10^6 – Bottom Gage	0	770	783	1.7	784	1.8
	10	1210	1290	6.6	1259	4.0
	30	1315	1421	8.1	1435	9.1
	90	1380	1482	7.4	1470	6.5
	300	1470	1508	2.6	1498	1.9

* Measured and predicted values for camber represent the average of 5 beams.

Table 8.8. <u>Example 8.4.2 - Summary of Results at Midspan</u>

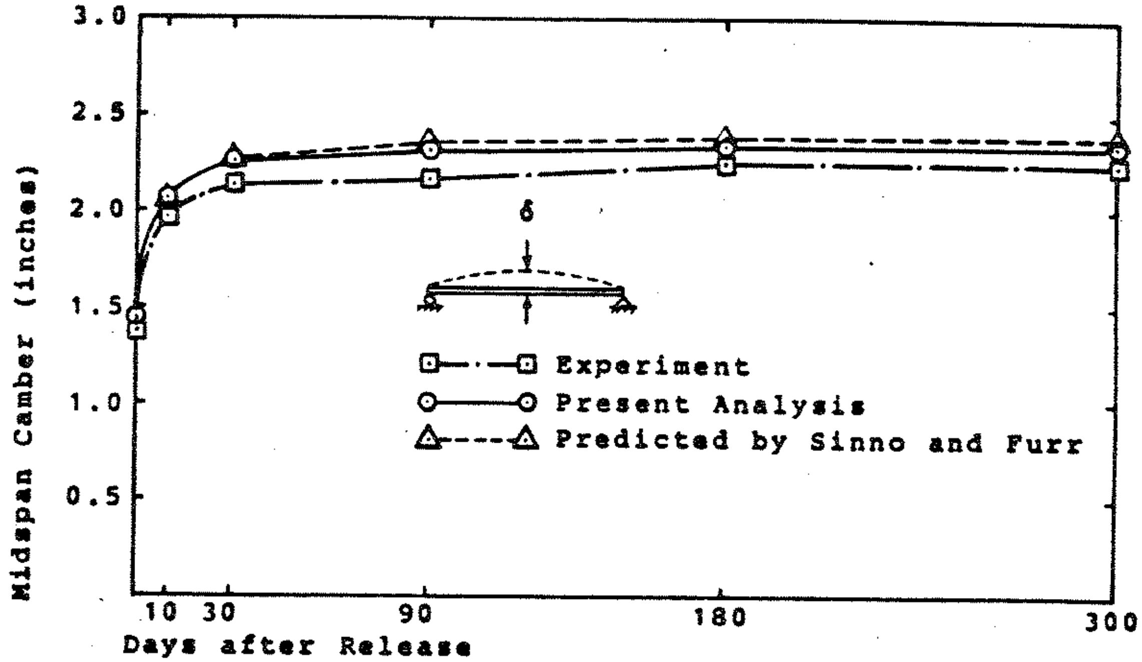

Fig. 8.8.b. Example 8.4.2 - Camber at Midspan

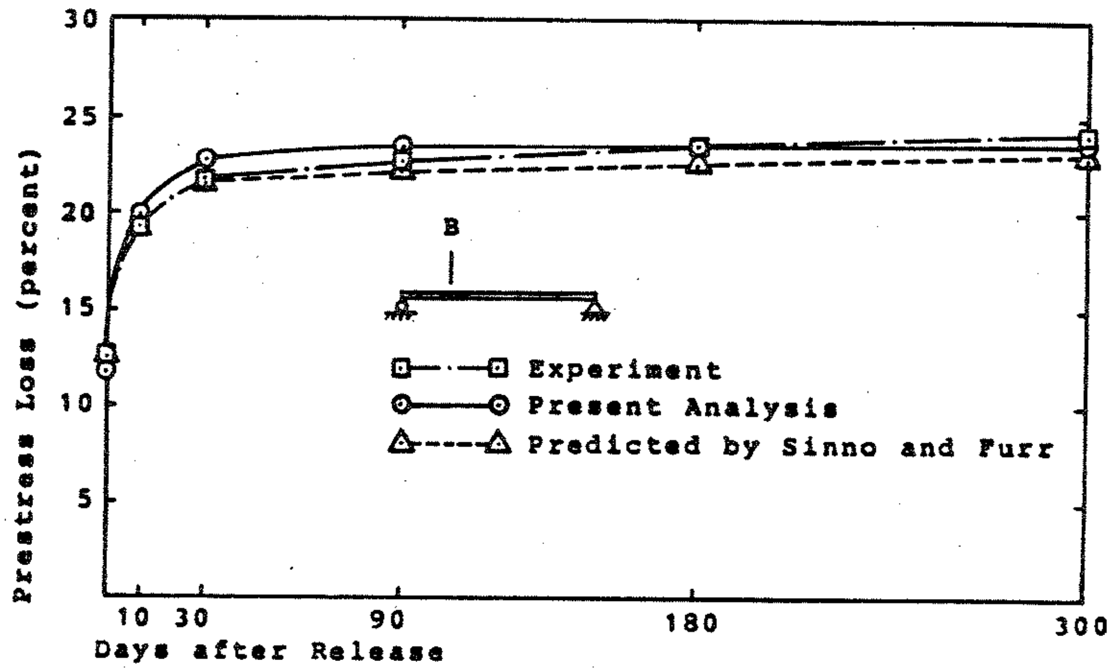

Fig. 8.8.c. Example 8.4.2 - Prestress Loss at Location B

are 0.80 and 0.91, respectively. It is also to be noted that the increases in the camber and the prestress loss at 300 days after release are comparable to the values at release.

8.4.3 Breckenridge-Bugg Beam - Time Dependent Analysis of Post-tensioned Bonded and Unbonded Simple Beams

Among a series of post-tensioned simple beams tested by Breckenridge and Bugg (117) up to 8 years after loading, bonded and unbonded beams having an I cross section and post-tensioned with two 1.25 inch diameter high-strength steel bars are analyzed for the present study.

The structure is shown in Fig. 8.9.a. One half of the 40 foot span beam is divided into 10 elements. The rectangular cross section at the support regions is divided into 10 concrete layers and the I cross section is divided into 15 concrete layers. 8 #3 bars are modeled by 3 reinforcing steel layers. Two prestressing steel tendons have a curved profile near the support region and they are straight with constant eccentricities elsewhere. Each tendon is divided into 10 prestressing steel segments. Segment numbers for the upper tendon correspond to the element numbers in which they are embedded. The segments for the lower tendon are numbered consecutively from 11 to 20, starting from the end support.

The material properties utilized in the analysis are summarized in Fig. 8.9.b. The variation of the compressive strength and the modulus of concrete with time is measured in the experiment. The tensile strength is assumed for the analysis. Since the experimental creep data is not given, the standard ACI creep data given in section 2.2.3 was used in the analysis. The ultimate creep coefficient C_u computed by Eqs. (2.19) and (2.20) was 2.01. The correction factors were computed based on the following experimental data ; average humidity H = 73%, slump S = 3.6 in, minimum thickness of the member T = 4 in. The specific creep curve for the loading age τ = 8 days, when the prestress was applied, was obtained by dividing Eq. (2.18) by $E_i(\tau)$. Then, the creep coefficients $a_i(\tau)$ shown in Fig. 8.9.a were computed by the least-square method. Eq. (3.44) was used for the creep coefficients for the loading age later than 8 days. Shrinkage was simulated by a hyperbolic function in which the ultimate shrinkage ε^{su} was assumed based on the average experimental shrinkage data for 3 years.

The beam was post-tensioned on 8 days after casting of concrete. The initial prestressing force P_o was 197 kip for the two tendons, and the total dead load of the beam was 9.47 kips. At 14 days after the transfer of prestress, the concentrated live load was applied at two quarter points of the beam.

The analysis was performed up to 7 years after the transfer of prestress with 13 time steps. Bonded beam was analyzed for three load cases ; 0P, 1.0P and 1.5P, where P = 15.2 kips Unbonded beam was analyzed for 1.0P. Since the shrinkage of bonded and unbonded beams were different an additional analysis was performed for the unbonded beam, in which the shrinkage data for the bonded beam was used, for comparison.

Summary of the midspan deflection and the comparison of some of the key values between the experiment and the analysis are given in table 8.9. For the bonded beam without the live load, the ratio of the 7-year camber to the initial camber is 1.96 for the experiment, and 1.91 for the analysis. For other cases, the ratio of the 7-year deflection to the instantaneous deflection due to loading is compared. The average of this ratio for different cases is 2.39 for both experiment and analysis. The experimental and analytical midspan deflection for the bonded beam is plotted in Fig. 8.9.c. A good agreement between the two results can be observed. With the same shrinkage data, analysis shows slightly larger deflection for the unbonded beam compared to the bonded beam.

Fig. 8.9.d shows the analytical results for the prestress loss with time in segments 3 and 20 for the bonded beam with LL = 1.0P. Fig. 8.9.e shows the results for the unbonded beam with the same shrinkage data as the bonded beam. Segment 3 is located near the support and close to the c.g.c., and segment 20 is located at midspan and has the largest eccentricity. Thus, the effect of bending on the variation of the prestress is negligible for segment 3 while the effect is maximum for segment 20 for the bonded beam. However, for the unbonded beam, the change in the prestress is evenly distributed along the length of each tendon. Thus, the results for segments 3 and 20 represent the average values for the upper

and lower tendon, respectively. Variations in the total strain and the stress at midspan for the bonded beam with LL = 1.0P are plotted in Fig. 8.9.f.

During the tensioning operation prestress is lost due to friction. The loss due to friction is larger for segment 20 compared to segment 3. But the positive moment due to the dead load increases the prestress for segment 20. The net effect is the smaller prestress loss for segment 20. The average initial prestress loss is 3.8%.

After the prestress is transferred the compressive strain increases due to creep and shrinkage, and consequently prestress loss takes place. The strain increase is larger for the bottom fiber compared to the top fiber due to the larger creep strain corresponding to the larger compressive stress. As a result the prestress loss for segment 20 becomes larger than that for segment 3 at 14 days after the transfer for the bonded beam. As the amount of the prestress is reduced, concrete stress is also reduced. A slight increase in the top fiber stress is the result of the reduction in the bending moment due to prestress.

When the live load is applied, the resulting upward bending increases the compressive strain and stress for the top fiber and decreases those for the bottom fiber. For the bonded beam, prestress loss for segment 20 is decreased correspondingly, but segment 3 is not affected by bending. For the unbonded beam the change is uniform along each tendon. The larger decrease of the prestress loss for the lower tendon is due to larger eccentricity.

After the loading the compressive strain for the top fiber is again increased due to creep and shrinkage. For the bottom fiber, the increase is neglible since the smaller increase of the compressive strain is counteracted by the increased positive bending. Prestress loss also increases accompanied by the decrease in the compressive stress. We note in the figures that the compressive strain for the bottom fiber and the prestress loss for segment 20 are both decreased up to 2 weeks after loading. This results from a large increase of the positive bending during this period due to the large increase of creep in the earlier period following loading. Afterwards, the net increase of the compressive strain due to creep and shrinkage and the relaxation increases the prestress loss.

At 7 years after the transfer of prestress the average prestress loss for all the segments is 19% for both bonded and unbonded beams. The average loss due to relaxation is 6.9%. Thus, subtracting the initial loss and the relaxation loss from the total loss, creep and shrinkage of concrete accounts for the loss of 8.3%. In the absence of the live load, the analysis shows the total loss of 28%. The loss due to creep and shrinkage is 19%.

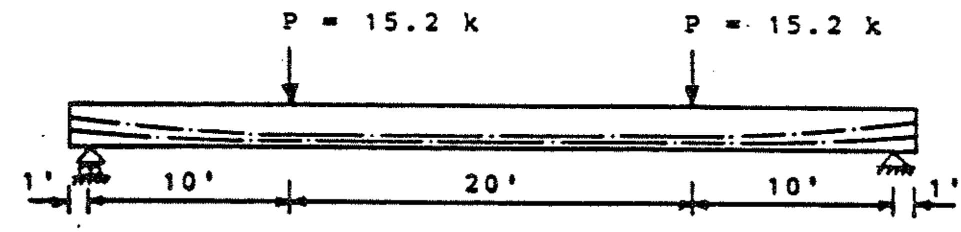

(a) Structure and Loading

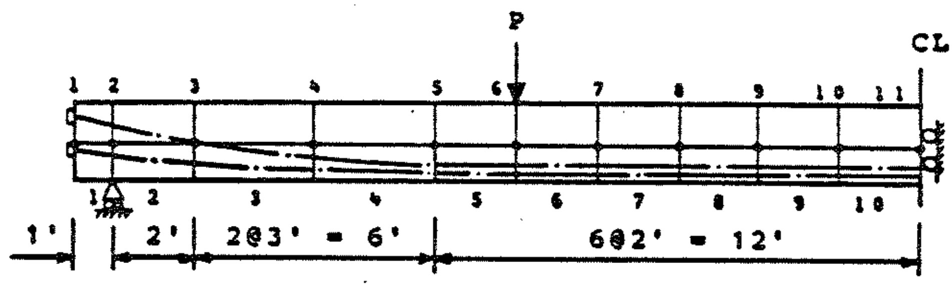

(b) Finite Element Mesh Layout

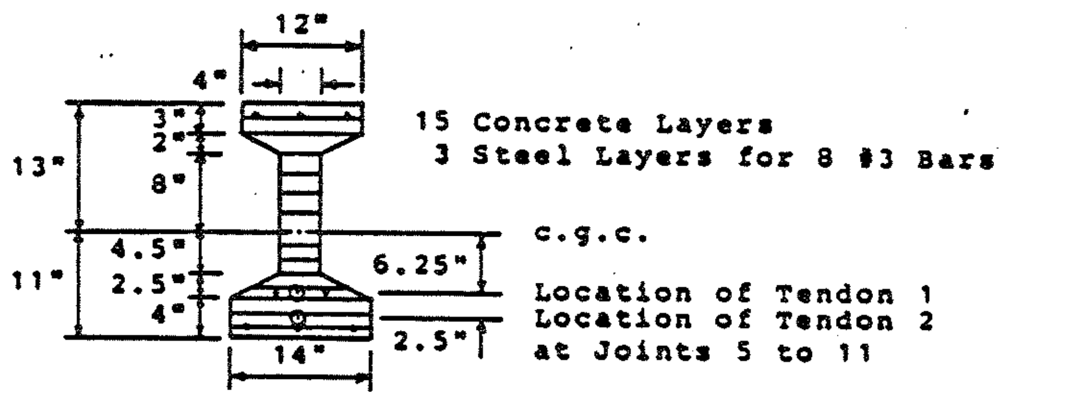

(c) Cross Section for Elements 3 to 10

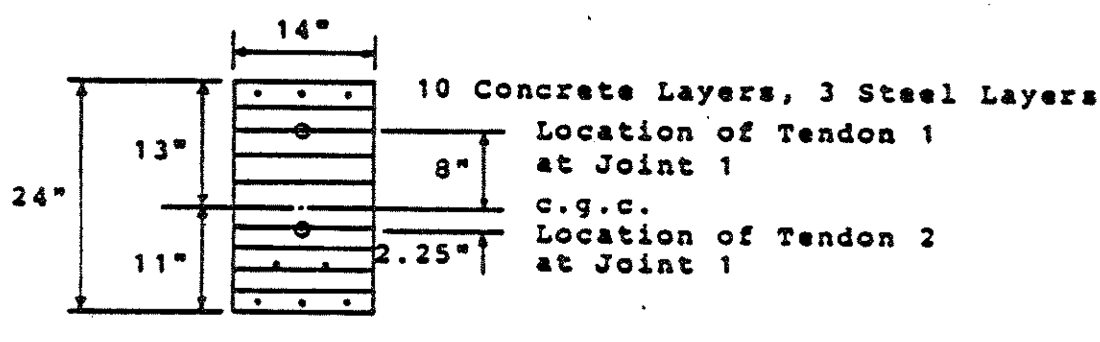

(d) Cross Section for Elements 1 and 2

Fig. 8.9.a. Example 8.4.3 - Breckenridge-Bugg Beam

(a) Concrete Properties

Time Step	t	$E_i \times 10^{-3}$ (ksi)	f_c^* (ksi)	f_t' (ksi)	ε_u
1	0	3.38	5.10	0.60	0.0038
2	7D	3.44	5.50	0.63	0.0038
3	14D	3.50	5.80	0.64	0.0038
4	21D	3.53	6.00	0.66	0.0038
5	1M	3.56	6.10	0.66	0.0038
6	2M	3.59	6.30	0.67	0.0038
7	4M	3.63	6.40	0.68	0.0038
8	8M	3.75	6.90	0.70	0.0038
9	1Y	3.81	7.10	0.71	0.0038
10	2Y	3.88	7.30	0.72	0.0038
11	3Y	3.94	7.40	0.73	0.0038
12	5Y	4.13	7.60	0.74	0.0038
13	7Y	4.25	7.80	0.75	0.0038

* t : Time after the Tensioning Operation at 8 Days after Casting of Concrete

Creep Coefficients $a_i \times 10^7$ per psi at τ_o=8 Days in Eq. (8.1) : a_1=2.7247, a_2=2.6202, a_3=1.6390
Eq. (3.44) for a_i's at Loading Ages Later Than τ_o.
r_1=0.35, r_2=1.865 in Eqs. (3.37) to (3.39)

$\varepsilon^s(\tau) = \frac{\tau}{35+\tau} \cdot \varepsilon^{su}$; $\varepsilon^{su}=366\times10^{-6}$ for Bonded Beam
$\varepsilon^{su}=258\times10^{-6}$ for Unbonded Beam

(b) Reinforcing Steel Properties (#3 Bars)

f_{sy}=45 ksi, ε_{su}=0.16, E_{s1}=29000 ksi, E_{s2}=100 ksi
Area(in^2) and the Distance from c.g.c. of 3 Steel Layers
A_{s1}=0.33, A_{s2}=0.22, A_{s3}=0.33
y_{s1}=11.3125, y_{s2}=-6.25, y_{s3}=-9.3125 (in inches)

(c) Prestressing Steel Properties (1.125"ϕ Bars)

A=0.994 in^2
P_o=197 kips (σ_o=99.09 ksi)
Friction Coefficients : μ=0.2, K=2.5×10^{-5} rad/in
f_y=130 ksi in Eq. (6.13) for Relaxation
Discrete Points in the Stress-Strain Curve :
σ_1=110.25 ksi, ε_1=0.0045, E_1=24500ksi
σ_2=130 ksi, ε_2=0.006, σ_3=146 ksi, ε_3=0.05

Fig. 8.9.b. Example 8.4.3 - Material Properties

Time Step	Time	Bonded Beams LL=0	Bonded Beams LL=1.0P	Bonded Beams LL=1.5P	Unbonded Beam (1)	Unbonded Beam (2)
1	0	0.70	0.70	0.70	0.70	0.70
2	7D	0.94	0.94	0.94	0.94	0.94
3	14D	1.03	1.03	1.03	1.04	1.04
			-0.03	-0.63	-0.03	-0.04
4	21D	1.07	-0.42	-1.32	-0.43	-0.44
5	1M	1.10	-0.65	-1.69	-0.67	-0.68
6	2M	1.15	-0.88	-2.07	-0.89	-0.91
7	4M	1.20	-1.02	-2.33	-1.04	-1.06
8	8M	1.25	-1.15	-2.61	-1.17	-1.20
9	1Y	1.26	-1.22	-2.68	-1.23	-1.26
10	2Y	1.30	-1.29	-2.86	-1.30	-1.34
11	3Y	1.31	-1.34	-2.96	-1.34	-1.38
12	5Y	1.33	-1.38	-3.23	-1.39	-1.43
13	7Y	1.34	-1.41	-3.33	-1.42	-1.46
δ_1	Exp.	0.69	1.01	1.81	1.03	—
	Th.	0.70	1.06	1.69	1.07	1.08
δ_2	Exp.	1.35	2.48	4.38	2.35	—
	Th.	1.34	2.44	4.36	2.46	2.50
$\frac{\delta_2}{\delta_1}$	Exp.	1.96	2.46	2.42	2.28	
	Th.	1.91	2.30	2.58	2.30	2.31

* Live load for both unbonded beams is 1.0P. Unbonded beam (2) is analyzed with the same shrinkage data as bonded beams.
* δ_1 and δ_2 represent the initial camber and the 7-year camber for LL=0. For other cases, they represent the instantaneous deflection and the 7-year deflection due to loading, respectively.

Table 8.9. Example 8.4.3 - Summary of Midspan Deflection

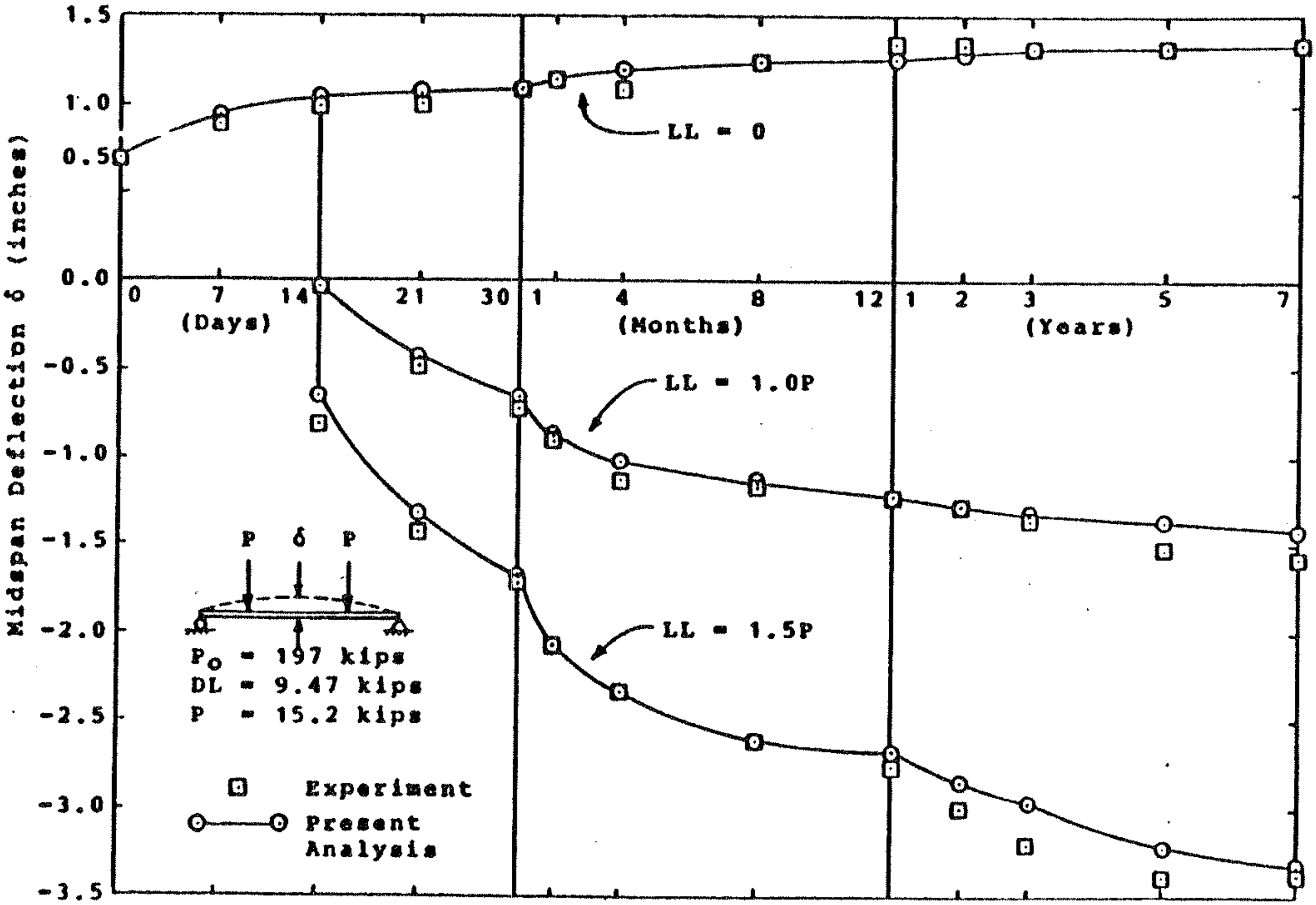

Fig. 8.9.c. Example 8.4.3 - Comparison of Midspan Deflection for Bonded Beams

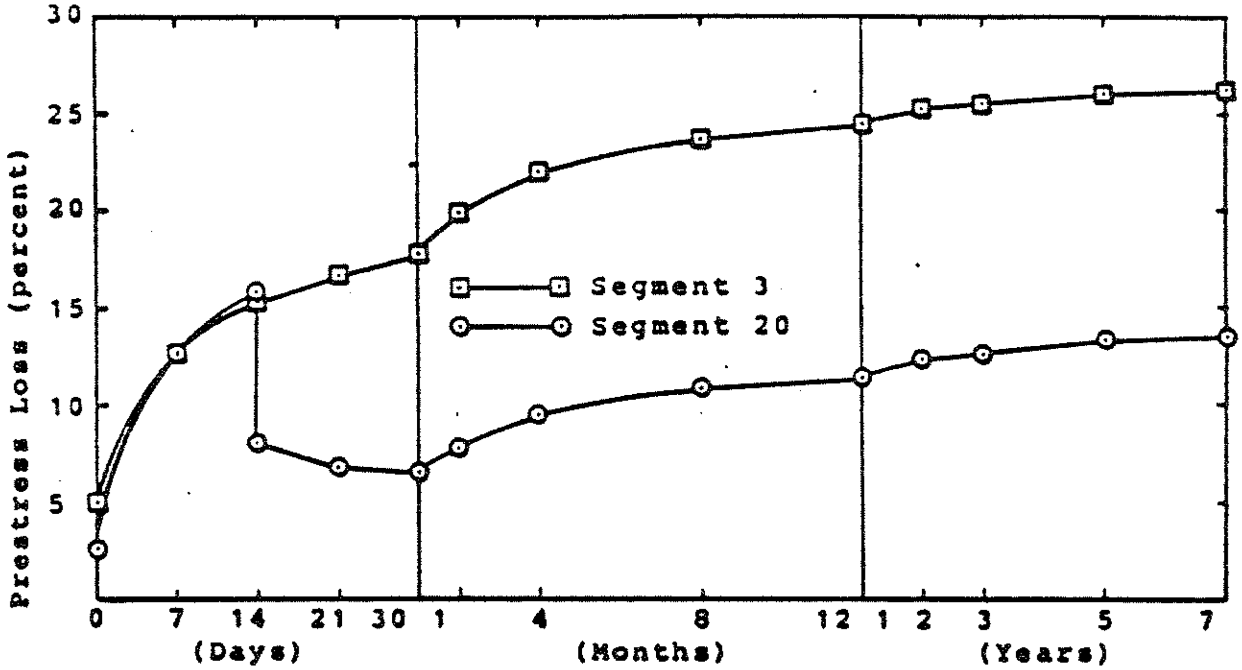

Fig. 8.9.d. Example 8.4.3 - Prestress Loss in Segments No. 3 (in Element 3, Upper Tendon) and No. 20 (in Element 10, Lower Tendon) for the Bonded Beam with LL = 1.0P

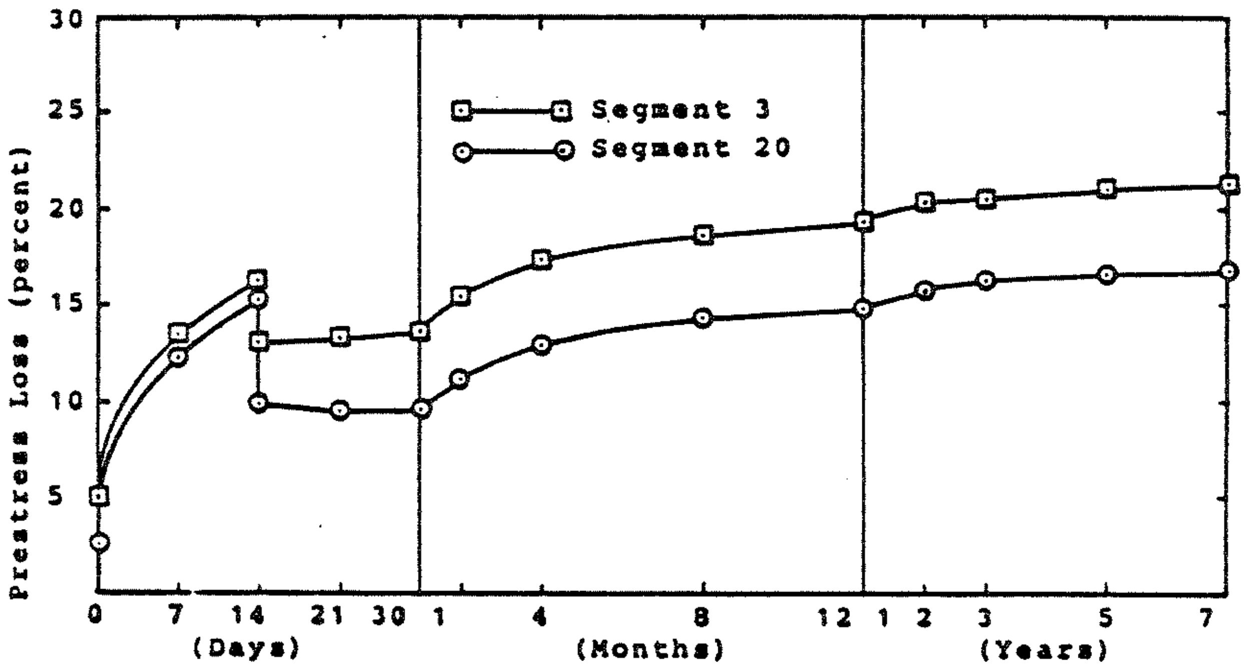

Fig. 8.9.e. Example 8.4.3 - Prestress Loss in Segments No. 3 and 20 for the Unbonded Beam with LL = 1.0P

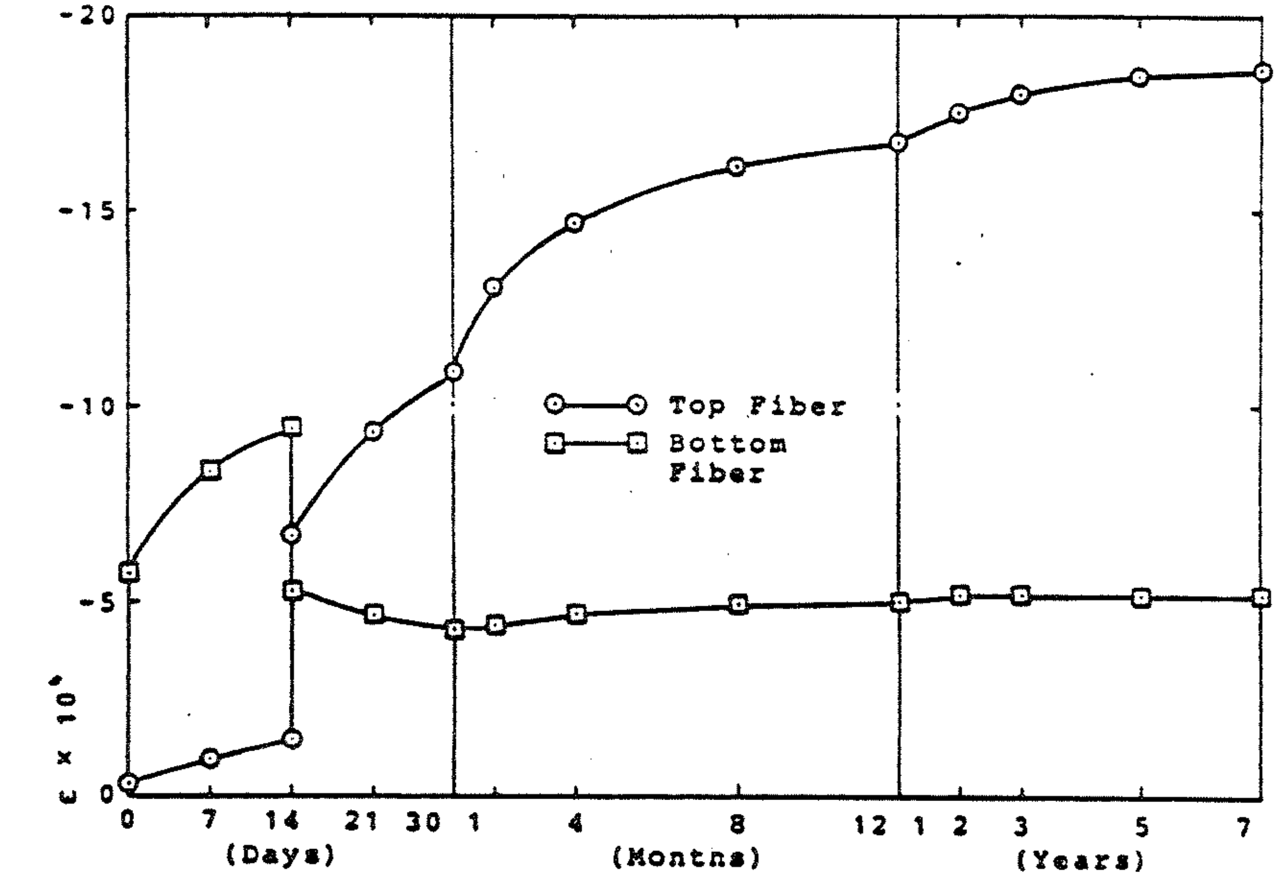

(a) Total Strain History

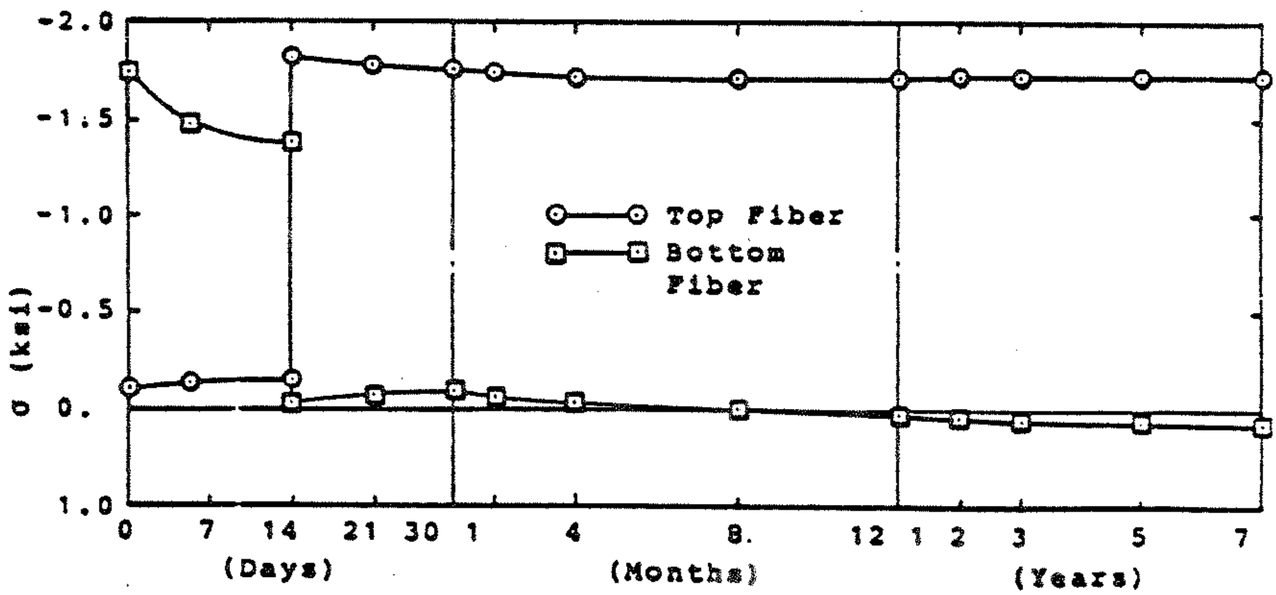

(b) Stress History

Fig. 8.9.f. Example 8.4.3 - History of the Total Strain and the Stress at Midspan for the Bonded Beam with LL = 1.0P

8.4.4 Aroni Column - Geometric and Material Nonlinear Analysis of a Pre-tensioned Column

Aroni (63,64) tested a series of eccentrically loaded pre-tensioned concrete columns to study their behavior under various conditions of eccentricity, slenderness and the amount of prestress. He also presented an analytical procedure to predict the strength of these columns. One of the columns, designated by $A_2$30c5, is analyzed to test the accuracy of the present geometric nonlinear analysis procedure.

The structure and its material properties are shown in Fig. 8.10.a. The 60 in. long column was axially pre-tensioned with four 0.198 in. diameter high tensile steel wires. The prestress was released at 14 days after casting of concrete, then cured under water until 28 days after casting, when the eccentric load was applied up to failure. The amount of initial prestress is not specified in the references. However, the initial compressive stress of 2265 psi for the concrete at loading was recorded in the experiment. Thus it is assumed in the analysis that the prestress was released when the load was applied with the initial prestress which would produce the recorded concrete stress. The initial prestressing force P_o is computed as follows considering the elastic shortening of concrete : $P_o = P/(1 - E_sA_s/E_cA_c) = 15600$ lbs, where P is the axial force of concrete after transfer.

One half of the column is analyzed with 10 elements. The eccentric compression is simulated by the equivalent concentric compression and the bending moment. The cross section

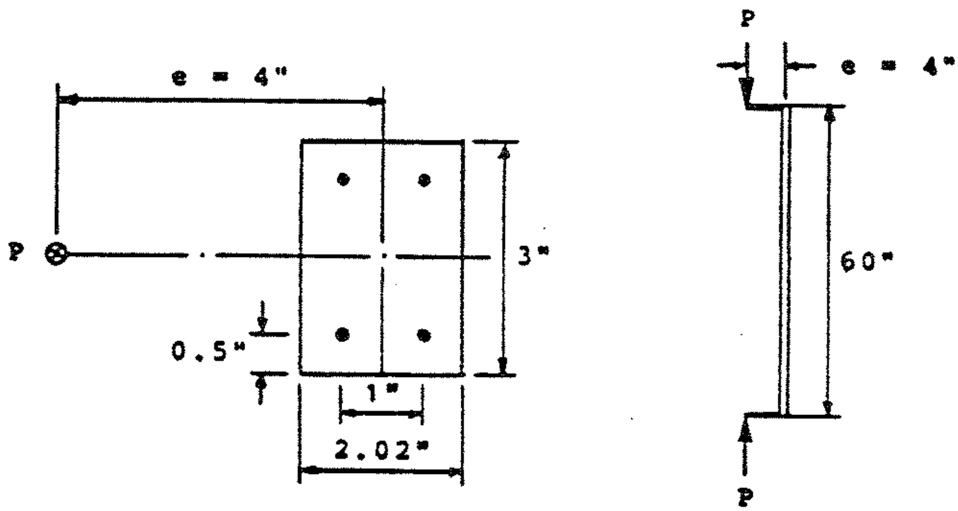

(a) Structure and Loading

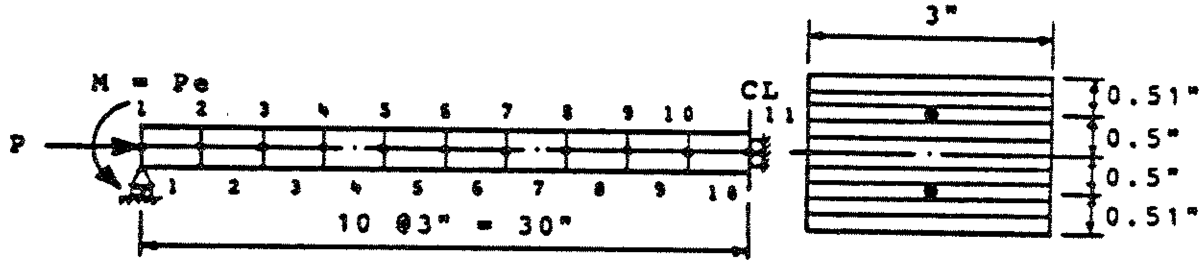

(b) Finite Element Mesh Layout

(c) Concrete Properties

$E_i = 4.94\times10^6$ psi ; $f_c'' = 5585$ psi

$\varepsilon_u = 0.006$; $f_t' = 558.5$ psi

(c) Prestressing Steel Properties (0.198"φ Wires)

Area = 0.0308 in^2 ; $E_1 = 29.34\times10^6$ psi

Discrete Points in the Stress-Strain Curve:

$\sigma_1 = 1.46\times10^5$ psi, $\varepsilon_1 = 4.976\times10^{-3}$

$\sigma_2 = 1.96\times10^5$ psi, $\varepsilon_2 = 6.900\times10^{-3}$

$\sigma_3 = 2.18\times10^5$ psi, $\varepsilon_3 = 8.630\times10^{-3}$

$\sigma_4 = 2.40\times10^5$ psi, $\varepsilon_4 = 3.000\times10^{-2}$

$\sigma_5 = 2.51\times10^5$ psi, $\varepsilon_5 = 5.600\times10^{-2}$

Fig. 8.10.a. Example 8.4.4 - Aroni Column

P (lbs)	Exp.	Aroni's Analysis	Present Analysis	*Present Analysis
400	0.06	0.09	0.08	0.08
700	0.11	0.17	0.14	0.14
1100	0.20	0.27	0.23	0.22
1500	0.34	0.39	0.34	0.31
1800	0.55	0.57	0.53	0.42
2000	—	0.84	0.79	0.53

* Present analysis neglecting geometric nonlinearity

Table 8.10. Example 8.4.4 - Midspan Deflections

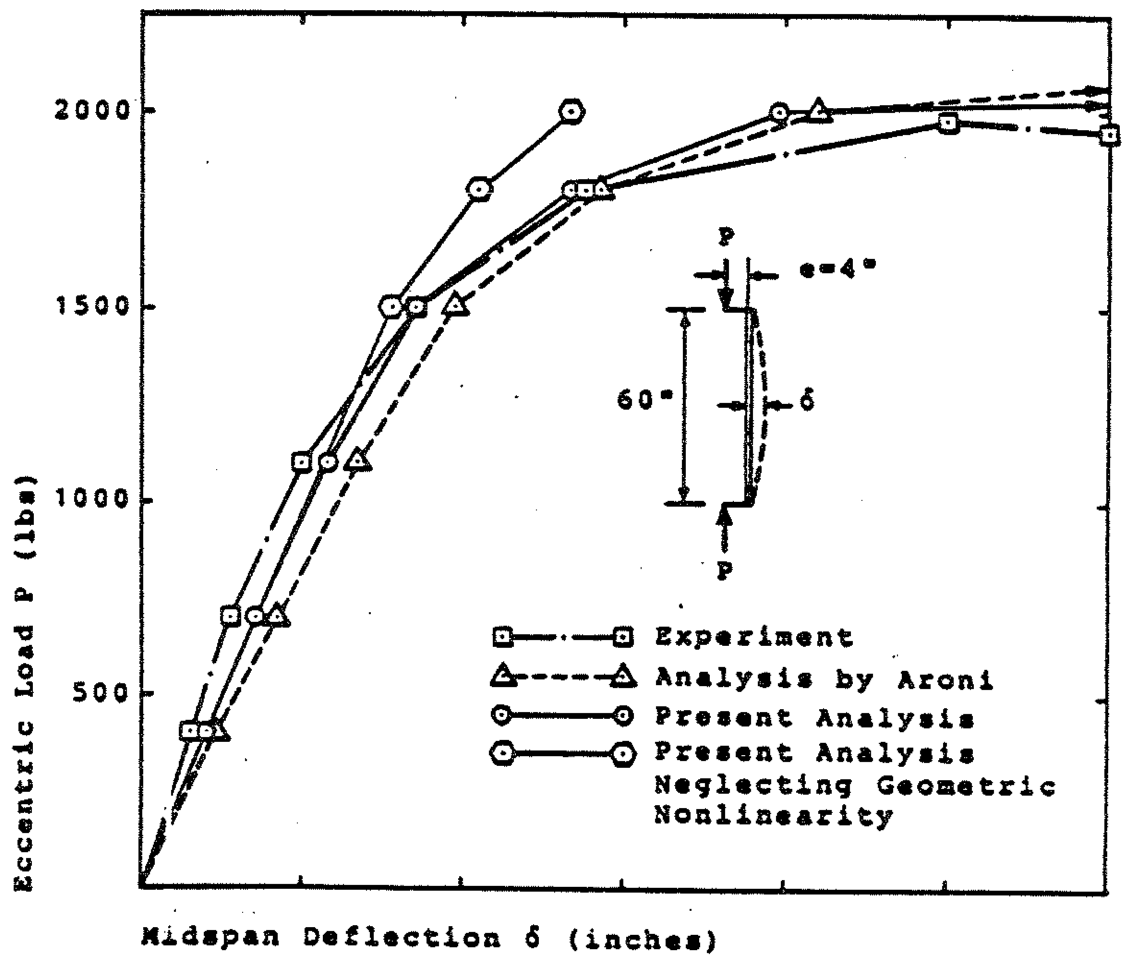

Fig. 8.10.b. Example 8.4.4 - Comparison of Midspan Deflections

is divided into 10 concrete layers. The prestressing steel wires are modeled by two prestressing steel tendons each of which is divided into 10 segments.

6 load steps are used to analyze the column up to P = 2000 lbs. The average number of iterations per load step with the displacement ratio tolerance of 0.01 is 4. To study the effect of the geometric nonlinearity the column is also analyzed with the material nonlinearity only. The experimental and analytical results for the midspan deflection are tabulated in table 8.10 and plotted in Fig. 8.10.b. Good agreement between the experimental result and the analytical results for both the present analysis and Aroni's analysis can be observed. The significance of the geometric nonlinearity for the column can be noted from the result obtained by considering the material nonlinearity only.

8.5. Summary of the Computer Time and Cost for the Examples

The examples presented in this chapter were run on the CDC 6400 computer at the University of California, Berkeley during the summer of 1976. In most cases, load modules produced from the FORTRAN source programs RCFRAME and PCFRAME described in chapter 7 were used. The central processor time, the peripheral processor time and the cost are tabulated in table 8.11 along with the parameters which affect the solution time.

Among the parameters listed in the table, the numbers of joints, elements and layers dictate the storage size, and the total number of iterations dictates the time required for the formation of the stiffness and the solution of equilibrium equations.

For the 10 examples presented in this chapter, the average central processor time was 30 seconds and the average cost was $4.5.

	(1)	(2)	(3)	(4)	(5)	(6)	(7)	(8)	(9)	(10)	(11)	(12)	(13)
Example	MN	GN	NJ	NE	NCL	NSL	NPS	NTS	NLS	NIT	CP(sec)	PP(sec)	COST($)
8.2.1	NO	YES	6	5	10	0	0	1	12	3.3	6.5	6.1	1.5
8.2.2	YES	YES	11	10	14	1	0	1	10	5.0	21.7	8.5	1.9
8.2.3	YES	NO	7	6	10	2	0	1	20	11.5	45.2	7.7	5.6
8.3.1	YES	NO	17	16	19	4	0	1	10	5.5	59.6	25.6	10.2
8.3.2	YES	NO	16	15	15	3	0	20	20	2.7	76.4	27.4	8.6
8.3.3	YES	NO	2	1	10	1	0	17	17	2.2	4.6	12.6	1.6
8.4.1	YES	NO	11	10	10	1	10	2	10	4.8	22.0	9.6	2.6
8.4.2	YES	NO	11	10	14	0	10	10	10	3.4	26.0	9.7	4.3
8.4.3	YES	NO	11	10	15	3	20	13	14	2.9	38.3	24.2	6.7
8.4.4	YES	YES	11	10	10	0	20	2	7	3.9	20.1	10.6	2.2

(1) MN : Material Nonlinearity
(2) GN : Geometric Nonlinearity
(3) NJ : Number of Joints
(4) NE : Number of Elements
(5) NCL: Number of Concrete Layers
(6) NSL: Number of Reinforcing Steel Layers
(7) NPS: Number of Prestressing Steel Segments
(8) NTS: Number of Time Steps
(9) NLS: Total Number of Load Step
(10) NIT: Number of Iterations per Load Step
(11) CP : Central Processor Time
(12) PP : Peripheral Processor Time

Table 8.11. Summary of the Computer Time and Cost for the Examples

9. CONCLUSIONS

9.1 Summary

An efficient numerical procedure for the material and geometric nonlinear analysis of planar reinforced and prestressed concrete frames including the time dependent effects due to load history, temperature history, creep, shrinkage and aging of concrete, relaxation of prestress has been presented. The method is capable of predicting the displacements, internal forces, stresses and strains of these structures throughout their service load history as well as throughout elastic, inelastic and ultimate load ranges.

For the quasi-static time dependent analysis a step forward integration is performed by dividing the time domain into a discrete number of intervals. For each time interval nonlinear equilibrium equations are set up and solved by the finite element method based on the displacement formulation. Total, incremental and tangential form of equilibrium equations which are valid for the current geometry and material properties at any instant of time are derived by the principle of virtual work. An incremental load method combined with the unbalanced load iterations for each load increment is utilized for the solution of the nonlinear equilibrium equations.

Time dependent variation of the concrete strength is recognized. Concrete strain is assumed to consist of the mechanical and non-mechanical components. The mechanical strain is the instantaneous strain due to short-time loading, and is the independent variable in the nonlinear stress-strain relationship. The non-mechanical strain is due to creep, shrinkage, aging and temperature variation. Stress-strain curve of concrete is approximated by a parabolic-linear function. Bilinear and multilinear forms of stress-strain curves are utilized for the reinforcing steel and the prestressing steel, respectively. Simple unloading and reloading models are incorporated in the stress-strain curves for the three materials to account for the load reversal.

An efficient numerical procedure for the evaluation of creep strain is developed with an integral formulation in which the history effect is accounted for by successively updating the values of only two variables instead of storing all the previous stress or strain histories. The effects of concrete age and temperature on creep is included. Nonlinear creep effect due to high stress intensity is also considered.

In order to account for varied material properties within a frame element, the element is divided into a discrete number of concrete and reinforcing steel layers which are assumed to be perfectly bonded together. The integrations required to evaluate the element properties such as the stiffness matrix or the internal resisting load vector, are then performed layer by layer through the depth of the element. Gaussian quatrature is used for the integration along the length of the element. By the use of the layer system non-uniform cross sections can be modeled.

Three distinct stages of loading are distinguished in the analysis of pre-tensioned and post-tensioned bonded and unbonded frames ; i.e. before, at and after the transfer of prestress. Prestressing steel tendons are divided into a discrete number of linear segments each of which is assumed to span an element and have a constant stress along its length. The contribution of the prestressing steel to the element properties are added directly. An iterative method is developed for the unbonded structures to account for the displacement incompatibility.

Finally, a series of numerical examples analyzed by the computer programs developed are presented to investigate the validity and applicability of the present method. The results are compared with experimental data and other theoretical results.

9.2 Conclusions

1. The present numerical procedure has been demonstrated to predict the response of planar reinforced and prestressed concrete frames subjected to both short-time and long-time load including the load due to environmental variations fairly accurately.

2. The present modelling of material properties is capable of capturing the dominant flexural behavior of reinforced and prestressed concrete frames in elastic, inelastic and ultimate load ranges.

3. The present time dependent analysis procedure including the efficient numerical formulation of creep predicts

the long-time behavior of concrete frames fairly well. Substantial redistribution of internal forces takes place due to time dependent loads. Temperature induced stresses are often damaging to structures and the effect of temperature on creep is substantial.

4. The accuracy of the present geometric nonlinear analysis procedure has been demonstrated.

5. The present method incorporates the prestressing steel as an integral part of the frame and the internal forces and deformations of both concrete and prestressing steel are determined in one complete analysis throughout various stages loading. Prestress loss is accurately predicted.

10. REFERENCES

1. Zienkiewicz, O.C., "The Finite Element Method in Engineering Science," McGraw-Hill Publishing Company, London, 1971.

2. Desai, C.S., and Abel, J.F., "Introduction to the finite Element Method, "Van Nostrand Rheinhold Company, 1972.

3. Gallagher, R.H., "Finite Element Analysis : Fundamentals," Prentice-Hall, Inc., 1975.

4. Scordelis, A.C., "Finite Element Analysis of Reinforced Concrete Structures," Proceedings of the Specialty Conference on Finite Element Methods in Civil Engineering, Montreal, June 1972.

5. Schnobrich, W.C., "Finite Element Determination of Nonlinear Behavior of Reinforced Concrete Plates and Shells," Proceedings of the Symposium on Nonlinear Techniques and Behavior in Structural Analysis, Transport and Road Research Laboratory, Department of environment, England, 1974.

6. Schnobrich, W.C., "Behavior of Reinforced Concrete Predicted by Finite Element Method, "Proceedings of the Second National Symposium on Computerized Structural Analysis and Design, George Washington University, Washington D.C., March 1976.

7. Wegner, R., "Finite Element Models for Reinforced Concrete," Preprint, Proceedings of the U.S. - Germany Symposium on Formulations and Computational Methods in Finite Element Analysis, Massachusetts Institute of Technology, Cambridge, August 1976.

8. Ngo, D., and Scordelis, A.C., "Finite Element Analysis of Reinforced Concrete Beams," ACI Journal, Vol. 64, No. 3, March 1967.

9. Ngo, D., Scordelis, A.C., and Franklin, H.A., "Finite Element Study of Reinforced Concrete Beams with Diagonal Tension Cracks," UC-SESM Report No. 70-19, Division of Structural Engineering and Structural Mechanics, University of California, Berkeley, December 1970.

10. Nilson, A.H., "Finite Element Analysis of Reinforced Concrete," Ph.D. Dissertation, Division of Structural Engineering and Structural Mechanics, University of California, Berkeley, March 1967.

11. Nilson, A.H., "Nonlinear Analysis of Reinforced Concrete by the Finite Element Method," ACI Journal, Vol. 65, No. 9, September 1968.

12. Franklin, H.A., "Nonlinear Analysis of Reinforced Concrete Frames and Panels," Ph.D. Dissertation, Division of Structural Engineering and Structural Mechanics, University of California, Berkeley, UC-SESM Report No. 70-5, March 1970.

13. Zienkiewicz, O.C., Valliappan, S., and King, I.P., "Stress Analysis of Rock as a 'No Tension' Material," Geotechnique, March 1968.

14. Zienkiewicz, O.C., Valliappan, S., and King, I.P., "Elasto-Plastic Solutions of Engineering Problems - Initial Stress - Finite Element Approach," International Journal for Numerical Methods in Engineering, Vol. I, 1969.

15. Cervenka, V., "Inelastic Finite Element Analysis of Reinforced Concrete Panels under In-Plane Loads," Ph.D. Dissertation, Department of Civil Engineering, University of Colorado, Boulder, 1970.

16. Cervenka, V., and Gerstle, K.H., "Inelastic Analysis of Reinforced Concrete Panels," Publication of International Association for Bridge and Structural Engineering, Vol. 31 - II, 1971.

17. Mufti, A.A., Mirza, M.S., McCutcheon, J.O., and Houde, J., "A Study of the Behavior of Reinforced Concrete Elements using Finite Elements," Structural Concrete Series No. 70-5, McGill University, Montreal, September 1970.

18. Mufti, A.A., Mirza, M.S., McCutcheon, J.O., and Spokowski, R.W., "A Finite Element Study of Reinforced Concrete Structures," Structural Concrete Series No. 71-8, McGill University, Montreal, October 1971.

19. Yuzugullu, O., and Schnobrich, W.C., "A Numerical Precedure for the Determination of the Behavior of a Shear Wall Frame System," ACI Journal, Vol. 70, No. 7, July 1973.

20. Darwin, D., and Pecknold, D.A., "Analysis of Reinforced Concrete Shear Panels under Cyclic Loading," Journal of the Structural Division, ASCE, Vol. 102, No. ST2, February 1976.

21. Valliappan, S., and Doolan, T.F., "Nonlinear Analysis of Reinforced Concrete," Journal of the Structural Division, ASCE, Vol. 98, No. ST4, April 1972.

22. Colville, J., and Abbasi, J., "Plane Stress Reinforced Concrete Finite Elements," Journal of the Structural Division, ASCE, Vol. 100, No. ST5, May 1974.

23. Nam, C.H., and Salmon, C.G., "Finite Element Analysis of Concrete Beams," Journal of the Structural Division, ASCE, Vol. 100, No. ST12, December 1974.

24. Melhorn, G., "Analysis of Plane Structures with Forces in Their Middle Plane Composed of Precast Concrete Panels," IASS Bulletin No. 58, August 1975.

25. Jofriet, J.C., and McNiece, G.M., "Finite Element Analysis of Reinforced Concrete Slabs," Journal of the Structural Division, ASCE, Vol. 97, No. ST3, March 1971.

26. Bell, J.C., and Elms, D., "Partially Cracked Finite Elements," Journal of the Structural Division, ASCE, Vol. 97, No. ST7, July 1971.

27. Bell, J.C., "A Complete Analysis of Reinforced Concrete Slabs and Shells," Ph.D. Dissertation, Department of Civil Engineering, University of Canterbury, Christchurch, New Zealand, 1970.

28. Dotroppe, J.C., Schnobrich, W.C., and Pecknold, D.A., "Layered Finite Element Procedure for Inelastic Analysis of Reinforced Concrete Slabs," IABSE Publication 33-11, 1973.

29. Berg, S., "Nonlinear Finite Element Analysis of Reinforced Concrete Plates," Report No. 73-1, Institutt for Statikk, Division of Structural Mechanics, University of Trondheim, Norway, February 1973.

30. Berg, S., Bergan, P.G., and Holand, I., "Nonlinear Finite Element Analysis of Reinforced Concrete Plates," Paper M3/5, 2nd International Conference on Structural Mechanics in Reactor Technology, Berlin, West Germany, September 1973.

31. Lin, C.S., "Nonlinear Analysis of Reinforced Concrete Slabs and Shells," Ph.D. Dissertation, Division of Structural Engineering and Structural Mechanics, University of California, Berkeley, UC-SESM Report No. 73-7, April 1973.

32. Lin, C.S., and Scordelis, A.C., "Nonlinear Analysis of Reinforced Concrete Shells of General Form," Journal of the Structural Division, ASCE, Vol. 101, No. ST3, March 1975.

33. Bell, J.C., and Elms, D.G., "A Finite Element Post Elastic Analysis of Reinforced Concrete Shells," Bulletin of the International Association for Shell and Spatial Structures, No. 54, April 1974.

34. Hand, F.R., Pecknold, D.A., and Schnobrich, W.C., "Nonlinear Layered Analysis of Reinforced Concrete Plates and Shells," Journal of the Structural Division, ASCE, Vol. 99, No. ST7, July 1973.

35. Suidan, M.T., and Schnobrich, W.C., "Finite Element Analysis of Reinforced Concrete," Journal of the Structural Division, ASCE, Vol. 99, No. ST10, October 1973.

36. Ngo, D., "A Network-Topological Approach to the Finite Element Analysis of Progressive Crack Growth in Concrete Members," UC-SESM Report No. 75-6, Division of Structural Engineering and Structural Mechanics, University of California, Berkeley, June 1975.

37. Sarne, Y., "Material Nonlinear Time Dependent Three-dimensional Finite Element Analysis for Reinforced and Prestressed Concrete Structures," Ph.D. Dissertation, Department of Civil Engineering, Massachusetts Institute of Technology, Cambridge, 1975.

38. Rashid, Y.R., "Ultimate Strength Analysis of Prestressed Concrete Pressure Vessels," Nuclear Engineering Design, Vol. 7, 1968.

39. Rashid, Y.R., and Rockenhauser, W., "Pressure Vessel Analysis by Finite Element Techniques," Conference on Prestressed Concrete Pressure Vessels, Institute of Civil Engineers, London, 1968.

40. Wahl, H.W., and Kasiba, R.J., "Design and Construction Aspects of Large Prestressed Concrete (PWR) Containment Vessels, ACI Journal, Vol. 77, No. 5, May 1969.

41. Zienkiewicz, O.C., Owen, D.R.J., Phillips, D.V., and Nayak, G.C., "Finite Element Methods in the Analysis of Reactor Vessels," Paper M5/1, 1st International Conference on Structural Mechanics in Reactor Technology, Berlin, West Germany, September 1971.

42. Argyris, J.H., et al., "Recent Developments in the Finite Element Analysis of Prestressed Concrete Reactor Vessels," Paper H1/1, 2nd International Conference on Structural Mechanics in Reactor Technology, Berlin, West Germany, September 1973.

43. Connor, J.J., and Sarne, Y., "Nonlinear Analysis of Prestressed Concrete Reactor Pressure Vessels," Paper H2/2, 3rd International Conference on Structural Mechanics in Reactor Technology, London, September 1975.

44. Selna, L.G., "Time-Dependent Behavior of Reinforced Concrete Structures," UC-SESM Report No. 67-19, Division of Structural Engineering and Structural Mechanics, University of California, Berkeley, 1967.

45. Selna, L.G., "Creep, Cracking and Shrinkage in Concrete Frame Structures," Journal of the Structural Division, ASCE, Vol. 95, No. ST12, December 1969.

46. Aas-Jackobsen, K., "Design of Slender Reinforced Concrete Frames," Bericht Nr. 48, Institut für Baustatik, ETH, Zürich, 1973.

47. Aldstedt, E., "Nonlinear Analysis of Reinforced Concrete Frames," Division of Structural Mechanics Institute of Technology, University of Trondheim, Norway, 1975.

48. Scanlon, A., "Time Dependent Deflections of Reinforced Concrete Slabs," Ph.D. Dissertation, Department of Civil Engineering, University of Alberta, Edmonton, Canada, December 1971.

49. Scanlon, A., and Murray, D.W., "Time Dependent Reinforced Concrete Slab Deflections," Journal of the Structural Division, ASCE, Vol. 100, No. ST9, September 1974.

50. Rashid, Y.R., "Nonlinear Analysis of Two-dimensional Problems in Concrete Creep," Journal of Applied Mechanics, Transactions of ASME, Paper No. 71-APMW-25, 1971.

51. Sandhu, R.S., Wilson, E.L., and Raphael, J.M., "Two-Dimensional Stress Analysis with Incremental Construction and Creep," UC-SESM Report No. 67-34, Division of Structural Engineering and Structural Mechanics, University of California, Berkeley, December 1967.

52. Wilhelm, W.J., and Zia, P., "Effects of Creep and Shrinkage on Prestressed Concrete Columns," Journal of the Structural Division, ASCE, Vol. 96, No. ST10, October 1970.

53. Bresler, B., edited, "Reinforced Concrete Engineering," Vol. I, John Wiley, 1974.

54. Rüsch, H., "Researches Toward a General Flexural Theory for Structural Concrete," ACI Journal, Proceeding, Vol. 32, July 1960.

55. Troxell, G.E., and Davis, H.E., "Composition and Properties of Concrete," McGraw-Hill Book Company, Inc., New York, 1956.

56. ACI Committee 209, "Prediction of Creep, Shrinkage and Temperature Effects in Concrete Structure," Paper SP 27-3 in ACI Special Publications SP-27, "Designing for Effects of Creep, Shrinkage, Temperature in Concrete Structures," April 1970.

57. Winter, G., Urquhart, L.C., O'Rourke, C.E., and Nilson, A.H., "Design of Concrete Structures," McGraw-Hill Book Company, Inc., 1964.

58. Popovics, S., "A Review of Stress-Strain Relationships for Concrete," ACI Journal, Vol. 66, No. 5, May 1969.

59. Comité Européen du Béton, "International Recommendation of Concrete Structures," English edition, Cement and Concrete Association, London, 1970.

60. Hognestad, E., "A Study of Combined Bending and Axial Load in Reinforced Concrete Members," University of Illinois Engineering Experiment Station, Bulletin Series No. 399, Bulletin No. 1, November 1951.

61. Kroenke, W.C., Gutzwiller, M.J., and Lee, R.H., "Finite Element for Reinforced Concrete Frame Study," Journal of the Structural Division, ASCE, Vol. 99, No. ST7, July 1973.

62. Goyal, B.B., and Jackson, N., "Slender Concrete Columns under Sustained Load," Journal of the Structural Division, ASCE, Vol. 97, No. ST11, November 1971.

63. Aroni, S., "Slender Prestressed Concrete Columns," UC-SESM Report No. 67-10, Division of Structural Engineering and Structural Mechanics, University of California, Berkeley, 1967.

64. Aroni, S., "Slender Prestressed Concrete Columns," Journal of the Structural Division, ASCE, Vol. 94, No. ST4, April 1968.

65. Neville, A.M., "Properties of Concrete," Pitman Publishing, Second edition, 1973.

66. Freyssinet, E., "The Deformation of Concrete," Magazine of Concrete Research, No. 8, 1951.

67. Vogt, F., "On the Flow and Extensibility of Concrete," Norges Tekniske Hoiskole, 1935.

68. Thomas, F.G., "Creep of Concrete under Load," International Association of Testing Materials, London Congress, April 1937.

69. Lynam, C.G., "Growth and Movement in Portland Cement Concrete," Oxford University Press, London, 1934.

70. Manuel, R.F., and McGregor, J.G., "Analysis of Restrained Concrete Columns Under Sustained Load," ACI Journal, Proc., Vol. 64, No. 1, January 1967.

71. Freudenthal, A.M., and Roll, F., "Creep and Creep Recovery of Concrete Under High Compressive Stress," ACI Journal, Vol. 54, No. 12, June 1958.

72. Roll, F., "Long-Time Creep Recovery of Highly Stressed Concrete Cylinders," ACI Special Publication SP-9, Symposium on Creep of Concrete, Paper No. 4, 1964.

73. Becker, J., and Bresler, B., "FIRES-RC, A Computer Program for the Fire Response of Structures - Reinforced Concrete Frames," Report No. UCB FRG 74-3, University of California, Berkeley, August 1974.

74. Davis, R.E., and Davis, H.E., "Flow of Concrete Under Sustained Compressive Stress," Proceedings ASTM, Part II, Vol. 30, 1930.

75. Hansen, T.C., and Mattock, A.H., "The Influence of Size and Shape of Member on the Shrinkage and Creep of Concrete," ACI Journal, Proc., Vol. 63, February 1966.

76. England, G.L., and Ross, A.D., "Reinforced Concrete Under Thermal Gradients," Magazine of Concrete Research, Vol. 14, No. 40, March 1962.

77. Ross, A.D., England, G.L., and Suan, R.H., "Prestressed Concrete Beams Under a Sustained Temperature Crossfall," Magazine of Concrete Research, Vol. 17, No. 52, September 1965.

78. Maréchal, J.C., "Le Fluage du Béton eu Fonction de la Temperature," Materials and Structures, Vol. 2, No. 8, March/April 1969.

79. Davis, R.E., Davis, H.E., and Brown, E.H., "Plastic Flow and Volume Changes in Concrete," Proc. ASTM, Vol. 37, Pt. II, 1937.

80. Troxell, G.E., Raphael, J.M., and Davis, R.E., "Long-Time Creep and Shrinkage Tests of Plain and Reinforced Concrete," Proc. ASTM, Vol. 58, 1958.

81. Glanville, W.H., "The Creep or Flow of Concrete Under Load," Department of Scientific and Industrial Research, Building Research Technical Paper, No. 12, 1930.

82. Philleo, R., "Some Physical Properties of Concrete at High Temperatures," ACI Journal, Proc., Vol. 54, April 1958.

83. Blakeley, R.W., and Park, R., "Prestressed Concrete Sections with Cyclic Flexure," Journal of the Structural Division, ASCE, Vol. 99, No. ST8, August 1973.

84. Bazant, Z.P., and Najjar, L.J., "Comparison of Approximate Linear Methods for Concrete Creep," Journal of the Structural Division, ASCE, Vol. 99, No.ST9, September 1973.

85. Ross, A.D., "Creep of Concrete Under Variable Stress," ACI Journal, Proc., Vol. 54, No. 9, March 1958.

86. England, G.L., "Numerical Creep Analysis Applied to Concrete Structures," ACI Journal, Proc., Vol. 64, No. 6, June 1967.

87. Faber, O., "Plastic Yield, Shrinkage, and Other Problems of Concrete and Their Effect on Design," Minutes of Proc. of Institution of Civil Engineers, London, Vol. 225, Part I, 1927.

88. Zienkiewicz, O.C., Watson, M., and King, I.P., "A Numerical Method of Visco-elastic Stress Analysis," Int. J. of Mech. Sci., Vol. 10, 1968.

89. McHenry, D., "A New Aspect of Creep in Concrete and Its Application to Design," Proc. ASTM, Vol. 43, 1943.

90. Arutyunyan, "Some Problems in the Theory of Creep in Concrete Structures," Perganon Press, New York, 1966.

91. Mukaddam, M.A., and Bresler, B., "Behavior of Concrete Under Variable Temperature and Loading," ACI Seminar on Concrete for Nuclear Reactors, SP-34, 1972.

92. Zienkiewicz, O.C., and Watson, M., "Some Creep Effects in Stress Analysis with Particular Reference to Concrete Pressure Vessels," Nuclear Engineering and Design, No. 4, 1966.

93. Browne, R., "Properties of Concrete in Reactor Vessels," Proc. of Conference on Prestressed Concrete Pressure Vessel, Group C, Paper 13, London, 1967.

94. Hannant, D., "Strain Behavior of Concrete up to 95 deg C Under Compressive Stresses," Proc. of Conference on Prestressed Concrete Pressure Vessel, Group C, Paper 17, London, 1967.

95. Pröberg, C.E., "Introduction to Numerical Analysis," 2nd Edition, Addison-Wesley Publishing Company, 1969.

96. Hildebrand, F.B., "Introduction to Numerical Analysis," McGraw-Hill Book Company, 1956.

97. Bathe, K.J., Ramm, E., and Wilson, E.L., "Finite Element Formulations for Large Displacement and Large Strain Analysis," UC-SESM Report No. 73-14, Division of Structural Engineering and Structural Mechanics, University of California, Berkeley, September 1973.

98. Bathe, K.J., Wilson, E.L., and Iding, R., "NONSAP - A Structural Analysis Program for Static and Dynamic Response of Nonlinear Systems," UC-SESM Report No. 74-3, Division of Structural Engineering and Structural Mechnics, University of California, Berkeley, February 1974.

99. Bathe, K.J., Ozdemir, H., and Wilson, E.L., "Static and Dynamic Geometric and Material Nonlinear Analysis," UC-SESM Report No. 74-4, Division of Structural Engineering and Structural Mechanics, University of California, Berkeley, February 1974.

100. Yeh, C.H., "Large Deflection Dynamic Analysis of Thin Shells Using the Finite Element Method," UC-SESM Report No. 70-18, Division of Structural Engineering and Structural Mechanics, University of California, Berkeley, October 1970.

101. Chi, H.M., and Powell, G.H., "Computational Procedure for Inelastic Finite Element Analysis," UC-SESM Report No. 73-2, Division of Structural Engineering and Structural Mechanics, University of California, Berkeley, January 1973.

102. Fung, Y.C., "Foundations of Solid Mechanics," Prentice-Hall Inc., New Jersey, 1965.

103. Przemieniecki, J.S., "Theory of Matrix Structural Analysis," McGraw-Hill Book Company, 1968.

104. Felippa, C.A., "Refined Finite Element Analysis of Linear and Nonlinear Two-Dimensional Structures," UC-SESM Report No. 66-22, Division of Structural Engineering and Structural Mechanics, University of California, Berkeley, October 1966.

105. Lin, T.Y., "Design of Prestressed Concrete Structures," Second Edition, John Wiley and Sons, Inc., 1963.

106. Magura, D.D., Sozen, M.A., and Siess, C.P., "A Study of Stress Relaxation in Prestressing Reinforcement," PCI Journal, Vol. 9, No. 2, April 1964.

107. Hernandez, H.D., and Gamble, W.L., "Time-Dependnet Prestress Losses in Pretensioned Concrete Construction," Structural Research Series No. 417, Civil Engineering Studies, University of Illinois, Urbana, May 1975.

108. Ghali, A., Sisodiya, R.G., and Tadros, G.S., "Displacements and Losses in Multistage Prestressed Members," Journal of the Structural Division, ASCE, Vol. 100, No. ST11, November 1974.

109. Timoshenko, S.P., and Woinowsky-Kreieger, S., "Theory of Plates and Shells," McGraw-Hill Book Company, Inc., 1959.

110. Bresler, B., and Scordelis, A.C., "Shear Strength of Reinforced Concrete Beams," Series 100, Issue 13, Structures and Materials Research, Department of Civil Engineering, University of California, Berkeley, June 1961.

111. Bresler, B., and Scordelis, A.C., "Shear Strength of Reinforced Concrete Beams," ACI Journal, Proc. Vol. 60, No. 1, January 1963.

112. Washa, G.W., and Fluck, P.G., "Plastic Flow (Creep) of Reinforced Concrete Continuous Beams," ACI Journal, Proc. Vol. 52, January 1956.

113. Washa, G.W., and Fluck, P.G., "Effect of Compressive Reinforcement on the Plastic Flow of Reinforced Concrete Beams," ACI Journal, Proc. Vol. 49, October 1952.

114. Lin, T.Y., "Strength of Continuous Prestressed Concrete Beams Under Static and Repeated Loads," ACI Journal, Vol. 26, No. 10, June 1955.

115. Sinno, R., and Furr, H.L., "Hyperbolic Functions for Prestress Loss and Camber," Journal of the Structural Division, ASCE, Vol. 96, No. ST4, April 1970.

116. Furr, H.L., and Sinno, R., "Creep in Prestressed Lightweight Concrete," Texas Transportation Institute, College Station, Texas, Research Report No. 69-2, October 1964.

117. Breckenridge, R.A., and Bugg, S.L., "Effects of Long-Time Loads on Prestressed Concrete Beams," PCI Journal, December 1964.

APPENDIX

Input Instructions for the Programs RCFRAME and PCFRAME

* The input data is key punched on cards as specified below. The sequential order of the input cards must be strictly adhered to and consistent units must be used throughout a problem. When ACI formulas for the time dependent concrete properties are used the pound-inch system must be used.

* Maximum allowed numbers of joints, members, etc. were set according to the minimum requirements for running the examples in chapter 8 to save the storage space. For bigger problems, the maximum allowed numbers can be easily increased in the source program.

RCFRAME Input Instructions

1. Title (8A10) - one card

   1-80 Title of the problem (HEAD)

2. Control Information (8I5,3F10.0) - one card

1- 5	No. of joints (NJ, max. 20)
6-10	No. of supported joints (NSJ, max. 5)
11-15	No. of members (NM, max. 20)
16-20	No. of different cross sections (NSEC, max. 10)
21-25	No. of load cases (NLC)
26-30	Concrete properties input code (KCNC) KCNC=0 if there is no concrete KCNC=1 if concrete properties are input according to ACI formulas KCNC=2 if concrete properties are input directly at each time step
31-35	No. of different concretes (NCNC, max. 5) Leave blank if there is no concrete.
36-40	No. of different steels (NSTL, max. 5) Leave blank if there is no steel.
41-50	Age of concrete in days at the time of initial loading (AGE)
51-60	Reference temperature (TZERO) USE 80°C FOR $\phi_T=1$
61-70	Coefficient of thermal expansion assumed to be

constant and equal for both concreteand steel (ALPHA)

3. Joint coordinates (I5,2F10.0) - One card for each joint

1- 5	Joint number (I)
6-15	X-coordinate of joint I (X(I))
15-25	Y-coordinate of joint I (Y(I))

4. Supported Joint Information (I5,4E10.0) - one card for each supported joint

1- 5	Joint number of Ith supported joint (JS(I))
6-15	Stiffness along A axis (SP(I,1))
16-25	Stiffness along B axis (SP(I,2))
26-45	Rotational Stiffness (SP(I,3))
36-45	Angle between X and A axes measured counterclockwise from X axis to A axis in degrees. A and B axes form a rectangular CArtesian coordinate system. (SP(I,4))

5. Material Properties

5.1. Concrete Properties - skip if NCNC=0

If KCNC=1 (4F10.0,4F5.0,F10.0) - one card for each different concrete

1-10	28 day strength in psi (FCP28(I)) Enter with negative sign.
11-20	Weight per unit volume in lb/cu.ft (WGT(I))
21-30	Coefficient a to compute $f_c'(t)$ (ACNC(I))
31-40	Coefficient b to compute $f_c'(t)$ (BCNC(I))
41-45	Ratio r_c in $f_c''=r_c \cdot f_c'$ (RCMP(I))
46-50	Ratio r_t in $f_t'=r_t \cdot \sqrt{wf_c'}$ (RTNS(I))
51-55	Ratio $r_1=f_c''/\sigma$ up to which $\sigma_e=\sigma$ in creep calculation (RCRP1(I))
56-60	Ratio $r_2=\sigma_e/\sigma$ when $\sigma=f_c''$ in creep calculation (RCRP2(I))
61-70	Ultimate compressive strain ε_u (ECU(I))

If KCNC=2 (6E10.0) - one card for each different concrete

1-10	Initial modulus E_i at the age of initial loading (ECI(I))
11-20	Compressive strength f_c'' (FCDP(I)) Enter with negative sign.
21-30	Tensile strength f_t' (FTP(I))
31-40	Ratio $r_1=f_c''/\sigma$ up to which $\sigma_e=\sigma$ in creep calculation (RCRP1(I))
41-50	Ratio $r_2=\sigma_e/\sigma$ when $\sigma=f_c''$ in creep calculation (RCRP2(I))
51-60	Ultimate compressive strain ε_u (ECU(I))

5.2. Steel Properties (4E10.0) - one card for each different steel, skip if NSTL=0

1-10 Yield stress f_{sy} (FSY(I))
11-20 Ultimate strain ε_{su} (ESU(I))
21-30 First modulus E_{s1} in the bilinear stress-strain curve (ES1(I))
31-40 Second modulus E_{s2} in the bilinear stress-strain curve (ES2(I))

6. Member data (4I5) - one card for each member

1- 5 Member number (I)
6-10 Node i of member I (NODI(I))
11-15 Node j of member I (NODJ(I))
16-20 Section number of member I (MSEC(I))

7. Section Data - The following data are input for each different cross section in section number order.

7.1. Section Information (4I5) - one card

1- 5 Section number (I)
6-10 No. of concrete layers (NCL(I)), max. 20) Leave blank if there is no concrete layer.
11-15 No. of steel layers (NSL(I), max. 5) Leave blank if there is no concrete layer.
16-20 Concrete material No. (MCNC(I)) Leave blank if there is no concrete layer.

7.2. Concrete Layer Data - skip if NCL(I) = 0

ACL (I,J);J=1,NCL(I)(8F10.0) - one or more cards
Areas of concrete layers J in layer No. order

YCL(I,J);J=1,NCL(I)(8F10.0) - one or more cards
Y coordinates of concrete layers J from member reference plane in layer No. order

7.3. Steel Layer Data - skip if NSL(I)=0

MSTL(I,J);J=1,NSL(I)(5I5) - one card
Steel numbers of steel layers J in layer No. order

ASL(I,J);J=1,NSL(I)(5F10.0) - one card
Areas of steel layers J in layer No. order

YSL(I,J);J=1,NSL(I)(5F10.0) - one card
Y coordinates of steel layers J from member reference plane in layer No. order

8. Load Control Data - The following data are input for each load case.

8.1. <u>Title (8A10)</u> - one card

```
 1-80  Title of the load case (HEAD)
```

8.2. <u>Control Data (9I5)</u> - one card

```
 1- 5  No. of time steps (NTIME)
       Enter 1 for short-time loading
 6-10  Output code for iterations (KOUT)
       KOUT=0 if output is given for each load step
       KOUT=1 if output is given for each iteration
11-15  Output code for layers (LOUT)
       LOUT=0 if layer output is not given
       LOUT=1 if output is given for each Gaussian
              quadrature point
       LOUT=2 if output is given only at the center of
              the member
16-20  Geometric nonlinearity code (KGN)
       KGN=0 if geometric nonlinearity is not considered
       KGN=1 if geometric nonlinearity is considered
21-25  Geometric stiffness code (KGS)
       KGS=0 if geometric stiffness is not included
       KGS=1 if geometric stiffness is included
26-30  Temperature code (KTEMP)
       KTEMP=0 if temperature variation is not considered
       KTEMP=1 if temperature is varied uniformly over
               the structure
       KTEMP=2 if temperature is varied unevenly for each
               member and layer
31-35  Shrinkage code (KSHRNK)
       KSHRNK=0 if no shrinkage is considered
       KSHRNK=1 if shrinkage occurs uniformly for concrete
       KSHRNK=2 if shrinkage occurs unevenly for each
                member and layer
36-40  Max. No. of iterations allowed for final load
       step (NITF)
41-45  Max. No. of iterations allowed for intermediate
       load steps (NITI)
```

8.3. <u>Tolerance Data (7F10.0)</u> - one card

Four kinds of convergence tolerances will be provided in addition to the number of iterations allowed for each load step.

The first is the maximum displacement ratio $|\Delta r_i/r_i|$ allowed for each load step where Δr_i is the displacement increment for the current iteration and r_i is the total displacement increment for the current load step up to previous iteration and i represents the component of displacement vector which has the maximum displacement increment at the first iteration of the current load step. The tolerance for the final load step is TOLF and that for intermediate load steps is TOLI.

The second is the maximum displacement ratio $|\Delta r_i/r_i|$

allowed for each iteration for changing stiffness (TOLC). If the displacement ratio is larger than TOLC the stiffness is updated for the next iteration and if the ratio is smaller than TOLC previously formed and reduced stiffness is used for the next iteration.

The third is the absolute value of displacement (TOLD) and rotation (TOLR) increment allowed for each iteration. These are provided in case of overshoot or load reversal. If maximum displacement increment exceeds this tolerance all the other components of displacement increment vector will be scaled down such that the maximum value is equal to TOLD or TOLR.

1-10	Displacement ratio tolerance for final load step (TOLF)
11-20	Displacement ratio tolerance for intermediate load steps (TOLI)
21-30	Displacement ratio tolerance for changing stiffness (TOLC)
31-40	Maximum allowed unbalanced load (TOLL)
41-50	Maximum allowed unbalanced moment (TOLM)
51-60	Maximum allowed displacement increment (TOLD)
61-70	Maximum allowed rotation increment (TOLR)

9. Load Data - The following data are input for each time step.

9.1. Control Data (3I5) - one card

1- 5	Time step No. (ITIME)
6-10	No. of load steps (NLS, max. 20)
11-15	No. of loaded joints (NLJ)

9.2. Load Step Data - two or more cards

FLSI(I);I=1,NLS (8F10.0) - one or more cards
Fraction of total loads due to non-mechanical strains during this time step for each load step in load step No. order

FLSJ(I);I=1,NLS (8F10.0) - one or more cards
Fraction of total joint loads during this time step for each load step in load step No. order

9.3. Joint Load Data (I5,3F10.0) - one card for each loaded joint, skip if NLJ=0

1- 5	Joint number (LJT)
6-15	X-load for the time step (BX)
16-25	Y-load for the time step (BY)
26-35	Moment for the time step (BM)

9.4. Time Increment (F10.0) - one card, skip for the first step

1-10 Time increment in days (DTIME, $t_n - t_{n-1}$)

9.5. Creep Data (3E10.0) - one card for each different concrete, skip if NCNC=0 or for the first time step

1-10 Creep coefficient a_1 for the time step t_{n-1} (XA1(I))
11-20 Creep coefficient a_2 for the time step t_{n-1} (XA2(I))
21-30 Creep coefficient a_3 for the time step t_{n-1} (XA3(I))

9.6. Current Concrete Properties (3E10.0) - one card for each different concrete, skip if KCNC=0 or 1 or for the first time step

1-10 Current E_i (ECI(I))
11-20 Current f_c'' (FCDP(I))
Enter with negative sign
21-30 Current f_t' (FTP(I))

9.7. Shrinkage Strain Increments - skip if NCNC=0 or NSHRNK=0

If KSHRNK=1 (E10.0) - one card

1-10 Shrinkage strain increment (DEPSS)

If KSHRNK=2 (8E10.0) - one or more cards for each member No. order
Shrinkage strain increments of concrete layers J in layer No. order, skip if JCL=0
DEPSS(I,J);J=1,JCL (JCL=NCL(K), K=MSEC(I))

9.8. Temperature Increments - skip if KTEMP=0

If KTEMP=1 (F10.0) - one card

1-10 Temperature increase (DTEMP)

If KTEMP=2 - The following cards are input for each member I in member No. order

DTEMPC(I,J);J=1,JCL (8F10.0) (JCL=NCL(K), K=MSEC(I))

Temperature increments of concrete layers J in layer No. order, skip if JCL=0

DTEMPS(I,J);J=1,JSL (8F10.0) (JSL=NSL(K),K=MSEC(I))

Temperature increments of steel layers J in layer No. order, skip if JSL=0

10. Next Problem

Following the data for this problem, the data for a new problem may be begun. Any number of problems may be entered. To terminate the data deck add two blank cards.

PCFRAME Input Instructions

The following informations are input in addition to those for the program RCFRAME

2.2. Prestress Control Information (4I5,3F10.0) - one card

1- 5	Prestressing type code (KPS) KPS=0 if pre-tensioned KPS=1 if post-tensioned
6-10	No. of prestressing steel tendons each of which has a given profile, initial tensioning force and a constant cross-rectional area along its length (NTND, max. 5)
11-15	No. of prestressing steel segments each of which is straight, spans a concrete member and has a constant force (NPS, max. 60)
16-20	No. of points used to specify stress-strain curve of prestressing steel excluding the origin (NPT, max. 5)
21-30	0.1% offset yield stress of prestressing steel (FPSY)
31-40	Time in days elapsed from initial tensioning operation until transfer for pre-tensioned case (AGEPS)
41-50	Coefficient for the calculation of relaxation loss (CRPS) Enter 10. for ordinary prestressing steels.

2.3. Post-tensioned Frame Information (2I5,2E10.0) - one card, skip if KPS=0

1- 5	Bond code (KBOND) KBOND=0 if unbonded KBOND=1 if bonded
6-10	Symmetry code (KSYM) KSYM=0 if the structure or loading is not symmetric KSYM=1 if the structure and loading are symmetric
11-20	Wobble friction coefficient K (CKPS)
21-30	Curvature friction coefficient μ (CMUPS)

2.4. <u>Prestressing Steel Tendon Information (3I5,3F10.0)</u>
<u>- one card for each prestressing tendon</u>

1- 5 Tendon No. (I)
6-10 Segment No. of the first prestressing steel segment of the tendon (NFRST(I))
11-15 Segment No. of the last prestressing steel segment of the tendon (NLAST(I))
16-25 Area of the tendon (ATND(I))
26-35 Initial tensioning force of the tendon (PZERO(I)) For symmetric post-tensioned case enter half of the total tensioning force since it is assumed that tensioning operation is performed symmetrically from both ends
36-45 Anchorage slip of the tendon (SLIP(I)) For symmetric post-tensioned case enter half of the total slip. Leave blank for pre-tensioned case.

5.3. <u>Prestressing Steel Properties (10E8.0)</u> - one card

1-80 Stress and strain values of each point in stress-strain curve in point No. order excluding the origin (PSF(I),PSE(I);I=1, NPT)

6.2. <u>Prestressing Steel Segment Data (3I5,3E10.0)</u> - one <u>card for each prestressing steel segment</u>

1- 5 Prestressing steel segment No. 9I0
6-10 No. of concrete member in which the segment is embedded (MPS(I))
11-15 No. of prestressing steel tendon to which the segment belongs (NTPS(I))
16-25 Eccentricity of the prestressing steel segment at joint i of the member MPS(I) in member coordinates, i.e. positive upward from member reference axis (ECCI(I))
26-35 Eccentricity at joint j (ECCJ(I))
36-45 Total angle change of the prestressing steel segment in radians. (THPS(I)) Leave blank for pre-tensioned case